INFORMATION TO USERS

This manuscript has been reproduced from the microfilm master. UMI films the text directly from the original or copy submitted. Thus, some thesis and dissertation copies are in typewriter face, while others may be from any type of computer printer.

The quality of this reproduction is dependent upon the quality of the copy submitted. Broken or indistinct print, colored or poor quality illustrations and photographs, print bleedthrough, substandard margins, and improper alignment can adversely affect reproduction.

In the unlikely event that the author did not send UMI a complete manuscript and there are missing pages, these will be noted. Also, if unauthorized copyright material had to be removed, a note will indicate the deletion.

Oversize materials (e.g., maps, drawings, charts) are reproduced by sectioning the original, beginning at the upper left-hand corner and continuing from left to right in equal sections with small overlaps.

Photographs included in the original manuscript have been reproduced xerographically in this copy. Higher quality 6" x 9" black and white photographic prints are available for any photographs or illustrations appearing in this copy for an additional charge. Contact UMI directly to order.

Bell & Howell Information and Learning
300 North Zeeb Road, Ann Arbor, MI 48106-1346 USA
800-521-0600

UMI®

Validation of a compartmental model of the kinetic behaviour of radiolabelled L-3,4-dihydroxyphenylalanine (L-dopa) in living brain

Paul Deep
McConnell Brain Imaging Center
Department of Neurology and Neurosurgery
McGill University, Montreal

Submitted: August, 1998

A Thesis submitted to the Faculty of Graduate Studies and Research in partial fulfilment of the requirements of the degree of M.Sc. in Neuroscience

To my beautiful and loving parents,
George and Georgette

TABLE OF CONTENTS

ACKNOWLEDGEMENTS

First and foremost, I wish to express my sincere gratitude to Dr. Paul Cumming, Assistant Professor in the Department of Neurology and Neurosurgery at McGill University, for accepting me as a graduate student, and supervising my research with competence and patience. I had the opportunity to benefit from a stimulating scientific environment that Paul generates by his exceptional enthusiasm for neuroscience. I would like to thank my co-supervisors, Dr. Albert Gjedde, Director of the PET Center at the Aarhus University Hospital in Aarhus, Denmark, and Dr. Alan Evans, Director of the McConnell Brain Imaging Center at McGill University, for their indispensable advice. I would also like to thank all the research students, post-doctoral fellows, technicians and administrative assistants in my department whose time and expertise led me through many difficult situations.

I would like to thank in advance the members of the Thesis committee for contributing their time and effort to the evaluation of this lengthy document.

Special appreciation is extended to Dr. Luis Oliva of the Lakeshore General Hospital in Pointe Claire, Quebec, for his last-minute corrections and insights into human pathobiology and wine tasting.

This work was made possible by the generous financial support of both the Fonds de Recherche en Santé du Québec, and the Montreal Neurological Institute.

CONTRIBUTION OF AUTHORS

I have chosen the option provided in the "Guidelines Concerning Thesis Preparation" which allows inclusion as chapters of the thesis the text of original papers concerning the thesis research project. The experimental parts of the thesis, Chapter II (Deep et al., 1997*a*) and Chapter III (Deep et al., 1997*b*), consist of two original articles that have been recently published. In these two studies, the original experimental work consisted of the development of computer algorithms which were subsequently used for data analysis and simulation studies. Some of the data so analyzed in Chapter III was acquired previously by Cumming et al. (1995*a*). Otherwise, I wrote the manuscripts, performed the calculations and statistical analyses, derived the equations, and drafted the figures, with supervision from Dr. P. Cumming and Dr. A. Gjedde. Together with my thesis supervisor and my co-authors, I have contributed to the design of the experiments, to the formulation of the working hypothesis, and to the interpretation of results.

INTRODUCTION

The subject of the present thesis is the validation of a nonlinear (or compartmental) model of the kinetic behaviour of radiolabelled L-3,4-dihydroxyphenylalanine (L-dopa) in living brain. Several such models describing the cerebral uptake and metabolism of radiolabelled L-dopa analogs, including [^{3}H]dopa and L-6-[^{18}F]fluorodopa, have been developed in recent years. Chromatographic identification of radiolabelled metabolites in brain tissue samples established qualitatively the biological accuracy of the models. However, the work presented in this thesis represents their first quantitative validation.

The article in Chapter II (Deep et al., 1997*a*) is the first comparison of radiolabelled L-dopa metabolite fractions calculated by a compartmental model with corresponding fractions measured analytically by chromatography in rat brain. The results of this study led to the development of a model describing the vesicular uptake of radiolabelled dopamine in vivo. Rate constants describing the distribution of radiolabelled dopamine between cytosolic and vesicular compartments are now estimated; previous models omitted vesicular storage.

Modelling of tissue radioactivities measured from a series of static cerebral autoradiograms in rats had been previously performed following injection of radiolabelled deoxyglucose (Sokoloff et al., 1977), but the article in Chapter III (Deep et al., 1997*b*) outlines the first attempt at modelling radioactivities derived from radiolabelled L-dopa in rat brain by an analogous autoradiographic technique. Furthermore, in comparing autoradiographic results from right cerebral hemispheres with corresponding analytic results obtained previously based on chromatographic fractionation of radiolabelled L-dopa metabolites in the left cerebral hemispheres of the same rats, we seek to establish the first direct empirical validation of compartmental modelling of autoradiographic data for quantitative assays of radiolabelled L-dopa uptake and metabolism in living brain.

A comprehensive general review of the pertinent literature is presented in Chapter I. The overall conclusions from the results of the different studies of this thesis are discussed in Chapter IV, while a complete set of references is listed alphabetically in Chapter V. An appendix containing the derivations of important equations and mathematical terms appearing in the two original articles is provided in Chapter VI. Finally, the thesis concludes with a second appendix that contains publisher reprints of these articles in Chapter VII.

ABSTRACT

This research details two experiments that together establish the legitimacy of a compartmental model which describes the cerebral uptake and metabolism of radiolabelled L-dopa in vivo. First, tissue radioactivities calculated with the model were compared with corresponding radioactivities measured previously by chromatographic fractionation of ^{18}F-labelled metabolites in striatal tissue extracts from rats given intravenous injections of L-6-[^{18}F]fluorodopa. Second, kinetic constants estimated by model fitting to measured radioactivities from combined metabolite pools in a time-series of static autoradiograms from right cerebral hemispheres of rats administered [^{3}H]dopa, were compared to corresponding previously published estimates based on analyses of measured radioactivities from individual metabolite pools separated by chromatographic fractionation of ^{3}H-labelled metabolites in the left cerebral hemispheres of the same rats. These comparisons confirmed quantitatively the biological accuracy of the model, thus validating the compartmental modelling of autoradiographic data for investigations of the kinetic behaviour of radiolabelled L-dopa in living brain.

RÉSUMÉ

Cette thèse détaille deux expérimentations effectuées pour établir la légitimité d'un modèle compartimental utilisé pour décrire la captation cérébrale et le métabolisme in vivo de la L-dopa marqueé avec un radioélément. Tout d'abord, les concentrations radioactives tissulaires calculées avec le modèle furent comparées aves les radioactivités correspondantes mesurées précédemment par fragmentation chromatographique des métabolites marqués au ^{18}F. Deuxièmement, les constantes cinétiques estimées par l'ajustement d'un modèle aux mesures radioactives faites à partir de pools combinées de métabolites d'autoradiogrammes statiques de l'hémisphère cérébral droit de rats administrés avec du [^{3}H]dopa, furent comparées avec les estimations correspondantes publiées basées sur la fractionation chromatographique de métabolites marqués au ^{3}H dans l'hémisphère gauche des mêmes rats. Ces comparaisons permirent de confirmer quantitativement la justesse biologique du modèle, validant ainsi la modélisation compartimentale de données autoradiographiques dans l'investigation du comportement cinétique in vivo de la L-dopa marquée avec un radioélément dans le cerveau humain.

REVIEW OF THE LITERATURE

1. Introduction

The present research is intended to validate quantitatively the biological accuracy of a nonlinear (or compartmental) model describing the kinetic behaviour of radiolabelled L-3,4-dihydroxyphenylalanine (L-dopa) in living brain. Analogs of the endogenous large neutral amino acid L-dopa incorporating positron-emitting isotopes (^{11}C and ^{18}F) have been used to obtain qualitative images of radiolabelled L-dopa uptake in the conscious human brain by positron emission tomography, a dynamic autoradiographic technique. The cerebral radioactivities so measured are analysed by compartmental modelling to yield estimates of kinetic constants that could otherwise only be assayed analytically in the autopsied brain. These constants define the rates of relevant physiological processes which are assumed to follow first-order kinetics, including the unidirectional transfer of radiolabelled L-dopa across the blood-brain barrier, and its subsequent in situ decarboxylation to radiolabelled dopamine by the cytosolic enzyme dopa decarboxylase. Of particular clinical importance is the measurement of dopa decarboxylase activity, since the magnitude of this value reflects the functional state of the nigrostriatal dopaminergic pathway; comparisons with corresponding mean values obtained in neurologically normal populations reveal the neurochemical basis of subcortical motor disorders such as Parkinson's disease. The present topic is introduced with a review of the literature describing the several techniques, chemical compounds, and mathematical models associated with the analysis of cerebral radioactivities measured in vivo by positron emission tomography following the peripheral administration of radiolabelled L-dopa analogs.

The review begins with an elucidation of the anatomical components of the striatum and the nigrostriatal dopaminergic pathway (section 2). The physiological steps involved in the synthesis, storage, and metabolism of dopamine in the striatum of living mammalian brain are detailed (section 3). This leads to a discussion of the etiology, neurochemical pathology, and pharmacological treatment of Parkinson's disease, a chronic and progressive disorder of the central nervous system caused by deficits in dopamine neurotransmission

(section 4). The physical and chemical characteristics of several radiolabelled analogs of the dopamine precursor, L-dopa, are then presented (section 5). The availability of these compounds permits in vivo studies of cerebral dopamine synthesis and metabolism, and led to the development of autoradiographic methods for external detection of radiotracer in brain, notably positron emission tomography (section 6). This is followed by an overview of the standard models, both linear and compartmental, that are applied to tissue radioactivities measured by autoradiography for the estimation of kinetic constants describing the cerebral uptake and metabolism of radiolabelled L-dopa in living brain (section 7). The review concludes with a brief summary of alternate tracers suitable for studying cerebral dopaminergic systems, such as radiolabelled analogs of *m*-tyrosine (section 8).

2. Dopamine in mammalian brain

2.1. *The detection of dopamine in nervous tissue*

The endogenous catecholamine 3,4-dihydroxyphenylethylamine (dopamine) is a chemical transmitter in many neuronal pathways of the mammalian central nervous system. Dopamine was first identified in situ nearly forty years ago. In post mortem studies on patients without neurological disorders, fractionation of the autopsied brains by liquid chromatography or alumina extraction, followed by fluorimetric analysis of the resulting tissue extracts, revealed significant concentrations (in the $\mu g\ g^{-1}$ range) of dopamine (Sano et al., 1959; Ehringer and Hornykiewicz, 1960; Bertler, 1961; Bernheimer et al., 1963; Hornykiewicz, 1963) and its major metabolite in humans, homovanillic acid (Bernheimer, 1963; Sharman, 1963; Hornykiewicz et al., 1968). Dopamine was similarly found in the brains of other mammals such as rats, guinea pigs, rabbits, cats, dogs, pigs, and sheep (Bertler and Rosengren, 1959). In all cases, the highest concentrations of dopamine and homovanillic acid were observed in the striatum, a component of the basal ganglia (see section 2.2). Dopamine is also widely distributed in peripheral tissues, but is localized mainly in chromaffin cells of the lung, liver, and small intestine (Bertler et al., 1959). Based on the oxidative potential of dopamine and its metabolites, the analysis of these compounds

in brain tissue has been facilitated by the availability of high-performance liquid chromatography with electrochemical detection (Felice et al., 1978; Cheng and Wooten, 1982).

The discovery of the detailed anatomical distribution of dopaminergic neurons and their terminals was facilitated by the development of the fluorescent histochemical method for the visualization of biogenic amines (Falck, 1962; Falck et al., 1962). This technique is based upon the conversion of biogenic amines in freeze-dried tissue sections to derivatives that fluoresce with a bright green colour after exposure to dry formaldehyde vapour at 60-80 °C. Swedish researchers used this method to identify several distinct groups of aminergic neurons in the brainstem and diencephalon (Dahlström and Fuxe, 1964; see Hillarp et al., 1966); they adopted the nomenclature A1-A12 for catecholaminergic groups and B1-B9 for serotonergic groups. Under the fluorescent microscope, all parts of the catecholaminergic neuron can be visualized; the concentration of dopamine is relatively low in cell bodies and axons, and high in terminals. Historically, this fluorescence method is very important because it represents one of the first tools for the demonstration of neurochemical heterogeneity of specific groups of neurons.

2.2. *The striatum: a component of the basal ganglia*

The basal ganglia consist of five extensively interconnected, subcortical gray matter nuclei located in the telencephalon: the caudate nucleus, putamen, globus pallidus, subthalamic nucleus, and substantia nigra (see Côté and Crutcher, 1991). In commenting that the basal ganglia have the "characteristics of basements, viz. darkness", the neurologist Kinnier Wilson was perhaps referring to the location of these structures deep beneath the outer layers of the cerebral cortex, or to the uncertainties still surrounding some of their functions, which include sensorimotor aspects of movement programming, conditional aspects of planning movements, program selection, and motor memory and retrieval (see Graybiel, 1990).

An important functional component of the basal ganglia is the neostriatum (or striatum), so named because of its stripy or striated appearance due to the presence of white

corticofugal fibres. The striatum serves as the input center for the basal ganglia. In the rodent the striatum is a single structure, but in primates (see Albin et al., 1989; see Netter, 1997) it consists of the caudate nucleus medially and the putamen laterally, divided by a cluster of fibres of the corona radiata called the internal capsule. There is also a ventral component of the striatum defined as the nucleus accumbens (Walaas, 1981; see Heimer et al., 1982) which is functionally and anatomically connected to limbic brain structures.

The majority of cells in the striatum are medium-sized neurons with dendrites that are densely covered with spines. These cells, first described by the anatomist Ramón y Cajal in 1911 using the Golgi staining method, were identified as the main projection neurons of the striatum with axons that discharge the inhibitory neurotransmitter gamma-amino-butyric acid (GABA) at terminals in the substantia nigra (Somogyi and Smith, 1979) and globus pallidus. The remaining striatal neurons are larger in size and do not have any axons that exit the striatum; these serve as local interneurons containing acetylcholine (see Groves, 1983), or peptides such as somatostatin or neuropeptide Y (Aosaki et al., 1995; Figueredo-Cardenas et al., 1997). A detailed description of the neuronal connections between the striatum and other components of the basal ganglia is provided in section 4.4.

2.3. *The nigrostriatal dopaminergic pathway*

Dopaminergic terminals in the striatum occur as a dense innervation of fibres from two specific groups of neurons in the brainstem (Dahlström and Fuxe, 1964; see Hillarp et al., 1966; see Fuxe et al., 1970); neurons with cell bodies in the ventral tegmentum (group A8) project to the nucleus accumbens and olfactory tubercle, while those with cell bodies in the pars compacta of the substantia nigra (group A9) project primarily to the putamen and the caudate. Together, the tegmental and nigral afferents constitute the nigrostriatal dopaminergic pathways. First identified in human brain, the presence of nigrostriatal dopaminergic pathways was similarly observed in rat brain (Andén et al., 1964, 1965). The substantia nigra, or 'black substance', is so named for its high concentration of neuromelanin, a black pigment derived from L-tyrosine, similar to the pigment found in hair and skin (see Zubay, 1993). Loss of these pigmented neurons was recognized as one of the two key

pathological findings in Parkinson's disease (see section 4.2); the other hallmark histological observation on microscopic analysis of the parkinsonian brain is the presence of Lewy bodies (Forno, 1969), described as eosinophilic, intracytoplasmic inclusions composed of fine filaments that are found primarily in surviving neurons of the substantia nigra and basal nucleus of Meynert (see Cotran et al., 1994).

Nigrostriatal dopaminergic neurons display two firing patterns with frequencies of approximately six spikes per second (Freeman et al., 1985): single spike activity, and a bursting mode with spikes of progressively decreasing amplitude within a burst. A quantitative study of nigrostriatal dopaminergic neurons counted about 3500 cell bodies on one side of the rat brain (Andén et al., 1966); the average amount of dopamine in each cell body was 2.5 μg with a concentration of approximately 200 μg/g striatum. Further calculations suggested that the terminal system of each dopaminergic neuron was about 65 cm in length and contained an average of 500,000 varicosities, illustrating the high degree of divergence in the innervation pattern. Functionally, this indicates that the activity in one nigrostriatal dopaminergic neuron can influence a large number of target nerve cells.

3. The metabolic pathway of dopamine in the striatum

3.1. *Rate constants measured in vitro*

The physiological steps involved in the metabolic pathway of striatal dopamine, from the synthesis and blood-brain uptake of its amino acid precursors to the clearance of its acidic metabolites into cerebrospinal fluid, have been extensively studied and characterized quantitatively. However, a more complete understanding of dopamine neurochemistry (or any other biochemical system) also requires quantitative kinetic information about the rates of relevant physiological processes. Therefore, the present discussion begins with a brief description of the fundamental concept of a rate constant, and the conventional method of its measurement in vitro.

According to classical Michaelis-Menten kinetics, and assuming first-order kinetic behaviour, the velocity of a chemical reaction (v) is given by,

$$v = \frac{V_{max}C}{(C + K_m)} \quad (1)$$

where C is the substrate concentration, V_{max} is the maximal reaction velocity, and K_m is the substrate concentration at which the reaction velocity is half-maximal. In vitro measurements of v are made under standard conditions of pH and temperature, and with the necessary enzymatic co-factors. A common method of estimating V_{max} and K_m is with a Lineweaver-Burk plot, also called a double-reciprocal plot, in which $1/v$ is plotted as a function of $1/C$. The resulting straight line has a slope of K_m/V_{max}, an ordinate intercept of $1/V_{max}$, and an abscissa intercept of $-1/K_m$. By definition, the fractional first-order rate constant (k, min^{-1}) is equal to v/C. Therefore, substitution of the expression for v (Eq. 1) yields k in terms of measurable parameters,

$$k = \frac{V_{max}}{(C + K_m)} \quad (2)$$

For reactions in which the substrate concentration is orders of magnitude lower than K_m (i.e. reactions involving an exogenously administered radiolabelled tracer compound such as [^{3}H]dopa or L-6-[^{18}F]fluorodopa; see section 5), then Eq. 2 reduces to,

$$k = \frac{V_{max}}{K_m} \quad (3)$$

3.2. *Enzymes that regulate the synthesis of striatal dopamine*

3.2.1. *Tyrosine hydroxylase*

The catecholamine pathway begins with the conversion of the essential amino acid L-phenylalanine to L-tyrosine, catalyzed by phenylalanine 4-monooxygenase (EC 1.14.16.1) in the liver. L-Tyrosine is subsequently converted to L-dopa by tyrosine hydroxylase (EC 1.14.13.2). This enzyme is found in catecholaminergic neurons and adrenal chromaffin cells. Tyrosine hydroxylase is stereospecific and has a high specificity for L-tyrosine, although L-

phenylalanine is also a substrate. D-Tyrosine, tyramine, and L-tryptophan are not substrates for this enzyme. Molecular O_2, Fe^{2+} ions, and a tetrahydrobiopterin co-factor are required for the oxidative activity of tyrosine hydroxylase. The apparent K_m value for the conversion of L-tyrosine to L-dopa is about 4 μM in a preparation of brain synaptosomes (see Cooper et al., 1991), while the steady-state concentration of L-tyrosine in rat brain is an order of magnitude larger (30 μM; Cumming et al., 1998*a*). This indicates that tyrosine hydroxylase is nearly saturated with L-tyrosine in vivo, and therefore may be rate-limiting with respect to catecholamine synthesis.

3.2.2. *Dopa decarboxylase*

The ultimate enzyme in the pathway for dopamine synthesis is dopa decarboxylase (EC 4.1.1.28), which decarboxylates L-dopa to form dopamine (Srinivasan and Awapara, 1978; Borri-Voltattorni et al., 1983). This stereospecific enzyme has a moderate affinity for several aromatic L-amino acids, including L-histidine, L-tyrosine, L-tryptophan and L-phenylalanine, and is therefore more properly referred to as aromatic L-amino acid decarboxylase. The activity of dopa decarboxylase requires pyroxidal phosphate (vitamin B_6, also known as co-decarboxylase) as a co-factor. Like many amino acid decarboxylases, this enzyme is found in the cytoplasm of certain peripheral tissues, with the highest activities in liver, kidney, and adrenal glands (Rahman et al., 1980). The efficient peripheral decarboxylation of L-dopa in the gastrointestinal tract contributes to a low concentration of circulating L-dopa in human blood (10^{-8} M; Hansson et al., 1978). The slightly higher concentrations of L-dopa in venous blood compared to arterial blood suggests that circulating L-dopa is not derived exclusively from the diet, but rather is released from sympathetic nerve endings, or the central nervous system, to reach the general circulation (Goldstein et al., 1987). In vitro assays of post mortem brain tissue samples from rats (Rahman et al., 1980), patients without neurological disorders (Lloyd and Hornykiewicz, 1972; Mackay et al., 1977), and patients with Parkinson's disease (Lloyd and Hornykiewicz, 1970; Lloyd et al., 1975*a*) revealed the highest concentrations of dopa decarboxylase in dopamine-rich regions, such as striatum and olfactory tubercle.

In rat brain, the apparent K_m value for the conversion of L-dopa to dopamine (100 μM; Cumming et al., 1988) is over two orders of magnitude larger than the steady-state concentration of L-dopa (< 1 μM; Cumming et al., 1998*a*). Therefore, dopa decarboxylase is far from saturated with L-dopa in vivo. The saturation of tyrosine hydroxylase coupled with the non-saturation of dopa decarboxylase has led to the suggestion that the activity of the latter enzyme does not contribute to the regulation of dopamine synthesis. In living brain, the decarboxylation of L-dopa in the axonal cytoplasm occurs in competition with at least two other processes: the elimination of L-dopa from brain to venous blood (Goldstein et al., 1987), and the methylation of L-dopa (see section 3.2.3), indicating that L-dopa in brain is not committed to dopamine synthesis (Cumming et al., 1998*a*). In this context, the fraction of L-dopa which is decarboxylated, rather than the fraction eliminated by other processes, influences the synthesis of dopamine in brain (Gjedde et al., 1993; see Opacka-Juffry and Brooks, 1995; see Gjedde, 1996).

It is unknown if optimal conditions for dopa decarboxylase activity prevail in vivo. The activities of dopa decarboxylase estimated in living brain of rat and primate (0.01-0.30 min^{-1}; see section 7.3) are much lower than the relative dopa decarboxylase activity predicted from in vitro measurements of Michaelis-Menten constants ($V_{max}/K_m = 3$ min^{-1}; Cumming et al., 1988), consistent with substantial inactivation of the enzyme in vivo. Indeed, much experimental evidence indicates that the activity of dopa decarboxylase is highly regulated. The activity of dopa decarboxylase in rat striatum measured ex vivo is regulated by dopamine receptors (Zhu et al., 1992; Hadjiconstantinou et al., 1993) and by glutamate receptors (Hadjiconstantinou et al., 1995). Similarly, dopamine receptor occupancy by antagonists (Cumming et al., 1997*a*) and possibly dopamine concentration (Cumming et al., 1995*a*) regulate the activity of dopa decarboxylase measured in living rat brain. In vitro, up-regulation of dopa decarboxylase gene expression in rat pheochromocytoma cells was observed following administration of the dopa decarboxylase inhibitor NSD-1015 (Li et al., 1993). Furthermore, the activation of adenylate cyclase in vitro transiently increased dopa decarboxylase activity, suggesting that dopa decarboxylase activity can be modulated by a cyclic AMP-dependent process (Young et al., 1993). Dopamine levels in the adult human

striatum decrease during aging, while dopa decarboxylase protein levels remain relatively constant, suggesting a compensatory up-regulation of dopa decarboxylase activity in surviving dopaminergic neurons (Kish et al., 1995).

3.2.3. *Catechol-O-methyltransferase*

In the periphery and in brain, L-dopa is also a substrate for catechol-*O*-methyltransferase (EC 2.1.1.6), which yields *O*-methyl-L-dopa (see Guldberg and Marsden, 1975; Gordonsmith et al., 1982). The formation of *O*-methyl-L-dopa, which can now be blocked by specific catechol-*O*-methyltransferase inhibitors (see section 4.5.2), reduces the rate of cerebral dopamine synthesis from exogenous L-dopa by decreasing the concentration of plasma L-dopa available for decarboxylation in brain. Catechol-*O*-methyltransferase is a relatively nonspecific enzyme; it catalyzes the transfer of methyl groups from a co-substrate, *S*-adenosyl methionine, to the *meta*-hydroxyl group of catecholamines and other catechol compounds. The activity of catechol-*O*-methyltransferase also requires Mg^{2+} as a co-factor. Like dopa decarboxylase, catechol-*O*-methyltransferase is found in the cytoplasm of several peripheral tissues, including even the blood vessel wall of human dental pulp (Nomura et al., 1996), with the highest concentrations in liver, kidney, and spleen (Rivett et al., 1983). Both membrane-bound and soluble forms of catechol-*O*-methyltransferase occur in brain, with the former displaying a 100-fold higher affinity for catecholamines (see Roth, 1992). In vitro assays of post mortem brain tissue samples from rats (Broch and Fonnum, 1972; Rivett et al., 1983; see Roth, 1992), patients without neurological disorders (Robinson et al., 1977), and patients with Parkinson's disease (Lloyd et al., 1975*a*), revealed that catechol-*O*-methyltransferase displays a relatively homogenous distribution throughout brain. Fluorescence immunohistochemical analysis of rat brain extracts indicates that this enzyme is not located in dopaminergic fibres, but is instead concentrated extraneuronally (Kaplan et al., 1979). This conclusion is supported by the finding that the activity of striatal catechol-*O*-methyltransferase is unchanged following electrolytic lesions of the substantia nigra in rats (Francis et al., 1987).

3.3. *Blood-brain uptake of L-dopa and dopamine*

The blood-brain transporter of large neutral amino acids is a hydrophillic molecule that occurs in the tight endothelium of the cerebrovascular bed that constitutes the blood-brain barrier. This compound has nine endogenous substrates, the affinities of which vary greatly. Overall, the carrier is 90% saturated with respect to its substrates in plasma (Gjedde and Bodsch, 1987). The transporter is Na^+-independent and functions by binding its substrate in a manner analogous to a receptor-ligand interaction. In this way, it is responsible for mediating the transport of L-tyrosine, L-dopa, and *O*-methyl-L-dopa into and out of brain by facilitated diffusion (Wade and Katzman, 1975; Oldendorf and Szabo, 1976; see Smith, 1991). The transport of L-dopa into brain occurs at a velocity of approximately 64 nM g^{-1} min^{-1}, with an apparent K_m value of 0.44 μM (Pardridge and Oldendorf, 1975). Since this transport process is passive as opposed to active, there exists no gradient for tissue uptake and hence the equilibrium distribution volumes of large neutral amino acids cannot in general exceed the ratio of water contents between brain tissue and plasma (close to unity); measurements in the rat confirm this postulate (Gjedde and Bodsch, 1987; Paetsch and Greenshaw, 1991). The stereoselectivity of the transporter is illustrated by the fact that concentrations of exogenous D-dopa are much lower than those of L-dopa in rat brain (Andén et al., 1972). Competition for transporter binding sites with *O*-methyl-L-dopa can decrease the rate of L-dopa entry intro brain (Wade and Katzman, 1975), and may in some circumstances contribute to limiting the rate of cerebral dopamine synthesis.

Unlike L-dopa, circulating monoamines do not enter the brain to an appreciable extent, except in regions lacking a morphological blood-brain barrier such as the choroid plexus, median eminence, and area postrema (Bertler et al., 1963, 1966; Fuxe and Owman, 1965). Indeed, fluorescence microscopy of rat brain extracts following the peripheral administration of large doses of dopamine (500 mg kg^{-1}) revealed intense fluorescence in the lumen of brain capillaries but little or no fluorescence in capillary walls (Bertler et al., 1963, 1966), indicating that dopamine is not transported from blood to the brain parenchyma. The presence of dopa decarboxylase in brain capillary walls (Owman and Rosengren, 1967; Hardebo et al., 1980) therefore acts as an enzymatic trapping mechanism for L-dopa. The

walls of mammalian brain microvessels also contain monoamine oxidase (Hardebo et al., 1980; Kalaria and Harik, 1987), the enzyme primarily responsible for dopamine metabolism (see section 3.5), such that the small fraction of dopamine that may pass from the lumen into endothelial cells is rapidly deaminated. Therefore, at the vascular level there exist both physical and enzymatic barriers that effectively regulate the concentration of neurotransmitter monoamines entering into mammalian brain (see Hardebo and Owman, 1980).

3.4. *Vesicular storage of striatal dopamine*

Dopamine formed in living striatal neurons by the decarboxylation of L-dopa is rapidly sequestered in synaptic storage vesicles (Buu, 1989; Leviel et al., 1989) at a concentration gradient of 10^4-10^5-fold, due to free energy derived from an ATP-driven proton pump that provides an acidic electrochemical gradient within the vesicle. It is speculated that L-dopa too undergoes vesicular storage and acts as a neurotransmitter (see Opacka-Juffrey and Brooks, 1995), but this remains unconfirmed. Vesicular dopamine is released exocytotically (Koshimura et al., 1992) in a quantal fashion (Pothos et al., 1996). The cytosolic concentration of dopamine is unknown in mammalian brain, but has been estimated at 2% of total dopamine in a giant dopaminergic neuron of the snail *Planorbis corneus* (Chien et al., 1990). The steady-state distribution of dopamine between cytosolic and vesicular pools in rat brain is investigated in Chapter II (Deep et al., 1997*a*) of the present thesis.

Centrifugation of rat brain homogenates revealed two distinct fractions of dopamine (Gutman and Weil-Malherbe, 1967): a dense particulate fraction (the pellet) in which dopamine is bound to subcellular structures, and a liquid soluble fraction (the supernatant). It seems reasonable that vesicular dopamine contributes to the former fraction, while dopamine in the cytosol may contribute to both fractions. The concentration of dopamine in the cytosol can be increased pharmacologically with the peripheral administration of reserpine, an alkaloid extracted primarily from the roots of trees and shrubs of the rauwolfia genus, that blocks the uptake of catecholamines into synaptic vesicles (see Carlsson, 1966; Guldberg and Broch, 1971). Dopamine not protected by vesicular storage is rapidly broken

down, as shown by the decreased dopamine concentrations and increased homovanillic acid concentrations measured in rat striatum following reserpine treatment (Guldberg and Broch, 1971).

3.5. *Metabolism of striatal dopamine*

Free dopamine in the striatum is a substrate for enzymatic degradation by catechol-*O*-methyltransferase and monoamine oxidase (EC 1.4.3.4), which yield 3-methoxytyramine and 3,4-dihydroxyphenylacetic acid (dopac), respectively. The two isoforms of the latter enzyme (A and B) have markedly different abundances and distributions in brain (Saura et al., 1992); in vitro studies indicate that the A form contributes significantly more to the deamination of dopamine (Fowler and Benedetti, 1983; Garrett and Soares-da-Silva, 1990). Both 3-methoxytyramine and dopac are precursors of homovanillic acid, but the majority of homovanillic acid is derived from the latter compound (80-95%; Westerink and Spaan, 1982*a*; see Westerink, 1985; Cumming et al., 1992). The concentrations of dopamine and its two acidic metabolites, dopac and homovanillic acid, in slices of rat striatum increase rostrocaudally (Widmann and Sperk, 1986), indicating that the striatum is not chemically homogenous with respect to dopamine metabolism.

The results of numerous pharmacological experiments indicate that 3-methoxytyramine is derived mainly from extraneuronal dopamine, while dopac is likely formed intraneuronally prior to the release of newly-formed dopamine or subsequent to re-uptake. For example, the dopamine re-uptake blockers quipazine and nomifensine increased the striatal concentration of 3-methoxytyramine, while a decrease in dopamine release induced by the dopamine agonist piribedil decreased 3-methoxytyramine concentrations (Ponzio et al., 1981). Local infusion of nomifensine into the striatum enhanced extracellular concentrations of dopamine, but did not change extracellular levels of dopac (Zetterström et al., 1988). Reductions in the firing of nigrostriatal dopaminergic neurons following treatment with reserpine and γ-butyrolactone, which blocks the impulse-dependant release of dopamine, decreased the concentration of 3-methoxytyramine but increased that of dopac in striatum (Westerink and Spaan, 1982*b*). The increase in striatal dopac concentration

following treatment with the dopamine antagonist sulpiride was not attenuated by the dopamine re-uptake blocker benztropine (Soares-da-Silva, 1987), suggesting that deamination occurs inside nigrostriatal dopaminergic neurons. Following inhibition of tyrosine hydroxylase with α-methyl-*p*-tyrosine, the rate of disappearance of dopac was faster than that of dopamine, indicating that most of the dopac originates from a newly-synthesized pool of dopamine that has not been released (Soares-da-Silva and Garrett, 1990). Furthermore, as mentioned above (see section 3.2.3), the enzyme responsible for the conversion of dopamine to 3-methoxytyramine, catechol-*O*-methyltransferase, is located extraneuronally. Therefore, the interstitial concentration of 3-methoxytyramine measured by cerebral microdialysis can be used as an index of dopamine release, while the synthesis of dopac is sensitive to the exposure of dopamine to an intraneuronal compartment containing monoamine oxidase.

Dopac and homovanillic acid diffuse out of living brain tissue into cerebrospinal fluid, as indicated by the significant concentrations of these compounds measured in samples of cerebrospinal fluid obtained by puncture of the cisterna magna in rats (Chung et al., 1993), sheep (Joseph and Walker, 1994), and monkeys (Ferguson et al., 1993), and by lumbar puncture in healthy human volunteers (Eklundh et al., 1996), patients with Parkinson's disease (Chia et al., 1993; Eldrup et al., 1995), patients with Huntington's disease (Garrett and Soares-da-Silva, 1992), patients with Menkes disease (Kaler et al., 1993), and patients with late onset and alcoholic ataxias (Kaakkola et al., 1993). Efflux of the acidic metabolites of dopamine out of brain occurs by sulfoconjugation catalyzed by phenolsulfotransferase (EC 2.8.2.1) and/or probenecid-sensitive transport (Dedek et al., 1979; Cumming et al., 1992), and is inhibited by a variety of centrally acting drugs (Moleman et al., 1978; Westerink and Kikkert, 1986). Therefore, steady-state concentrations of acidic metabolites in brain and cerebrospinal fluid are determined by the rate of decomposition of cytosolic dopamine, and by the rate of elimination of the metabolites from brain.

4. Parkinson's disease

4.1. *A brief history*

Parkinson's disease is a chronic and progressive disease of the central nervous system which afflicts over 500,000 people in Canada and the United States alone (see Youdim and Riederer, 1997). Parkinson's disease generally strikes late in life; the mean age of onset in a group of 270 patients from the McGill Movement Disorder Clinic was 58 ± 10 years (Gauthier and Gauthier, 1987). Individuals with Parkinson's disease display a characteristic triad of primary symptoms (see Hornykiewicz, 1975): (i) tremor of limbs at rest, which usually ceases when the affected limb is moved voluntarily, (ii) rigidity of the skeletal muscles, and (iii) akinesia, or difficulty in initiating movements or modifying ongoing motor activity. Secondary symptoms include subtle mask-like facies and autonomic disturbances, such as increased sweating. Individuals in the late stages of Parkinson's disease often experience psychological problems such as clinical depression or dementia. Symptoms of Parkinson's disease are readily observed in public figures such as Muhammad Ali and Pope John Paul II.

The recorded history of Parkinson's disease goes back nearly two centuries, when in 1817 the British physician James Parkinson, referring to the writings of the late-Roman physician Galen, documented the clinical manifestations of several patients with what he described as 'shaking palsy'. This term was subsequently translated to the Latin '*paralysis agitans*', and eventually given the name 'Parkinson's disease' by the French neurologist Charcot. The decade-long epidemic of von Economo's encephalitis that began in Vienna in 1917 was accompanied by a high incidence of parkinsonism, a syndrome resembling Parkinson's disease, among recovered patients (see Mizuno et al., 1997). This led to speculation that a virus was responsible for initiating the disease. In fact, cases of parkinsonism have been reported after other encephalitis infections, including Japanese B encephalitis, Western equine encephalitis, Coxsackie B type 2 encephalitis, and central European tick-borne encephalitis. However, the parkinsonism following these infections is usually non-progressive, in contrast to idiopathic Parkinson's disease. Furthermore, a pandemic of influenza occurred simultaneously with Economo's encephalitis from 1918 to

1919. These outbreaks prompted research into a possible relationship between viral infections and idiopathic Parkinson's disease, although none could be established. Therefore, it is unlikely that encephalitis or influenza play any etiologic role in Parkinson's disease.

4.2. *Neurochemical basis*

The nigrostriatal dopaminergic pathway has a critical role in the coordination of motor control. It follows that a deficit in the number of nigrostriatal dopaminergic neurons would disrupt the proper functioning of this system and therefore produce erratic motor behaviour in the affected individual. Indeed, a reduced neuronal count is characteristic of Parkinson's disease, as demonstrated by post mortem studies of parkinsonian brains which revealed depigmentation and loss of dopaminergic neurons in the pars compacta of the substantia nigra (Forno, 1966, 1969; Earle, 1968; Bernheimer et al., 1973). The direct consequences of this neuronal degeneration are concomitant reductions in the striatal concentrations of dopamine and homovanillic acid (Ehringer and Hornykiewicz, 1960; Bernheimer et al., 1963, 1973; Hornykiewicz, 1963; Bernheimer and Hornykiewicz, 1965; Hornykiewicz et al., 1968; Lloyd et al., 1975*a*). Within divisions of the parkinsonian striatum, there is regional heterogeneity with respect to the extent of dopamine depletion. Specifically, dopamine concentrations measured in vitro in brain tissue samples from eight patients with Parkinson's disease were reduced by 81% in caudate and 98% in putamen (Kish et al., 1988).

Another prominent neurochemical feature of Parkinson's disease is a massive reduction in the activities of the enzymes responsible for dopamine synthesis. A pair of studies by one group reported decreases in the activity of dopa decarboxylase activity of 85-91% in caudate and 94-96% in putamen of patients relative to neurologically normal controls (Lloyd and Hornykiewicz, 1970; Lloyd et al., 1975*a*), consistent with the striatal distribution of dopamine in Parkinson's disease; these in vitro results together indicate a more pronounced degeneration of the putamen in the pathological state. Conversely, the same group found the reduction in the activity of tyrosine hydroxylase to be homogenous throughout the parkinsonian striatum, with decreases of 83% in caudate and 82% in putamen

(Lloyd et al., 1975*a*).

It has been proposed that the activity of L-glutamic acid decarboxylase, the enzyme that converts L-glutamic acid to GABA, is decreased in the striatum of patients with Parkinson's disease. For example, one study based on in vitro analysis of post mortem brain tissue samples reported reductions in enzyme activity of 51% in caudate and 53% in putamen of patients relative to neurologically normal controls (Lloyd and Hornykiewicz, 1973), while a similar investigation by the same group reported less pronounced reductions of 25% in caudate and 30% in putamen (Lloyd et al., 1975*b*). However, both of these studies suffered from a small number of subjects (two and three, respectively), and thus it may be difficult to draw firm conclusions from their results. Furthermore, other in vitro studies noted no significant difference in striatal enzyme activity between patients and neurologically normal controls (Laaksonen et al., 1978; Perry et al., 1983). Therefore, it remains unclear whether the activity of L-glutamic acid decarboxylase is altered in the parkinsonian striatum.

The neurochemical changes associated with Parkinson's disease are not restricted to the components of the nigrostriatal dopaminergic pathway. Many areas of the brain degenerate during Parkinson's disease (see Jellinger, 1991), including (i) mesocortical dopaminergic systems of the ventral tegmental area, ventral mesencephalon, limbic areas, and neocortex, (ii) noradrenergic systems of the locus coeruleus, motor vagal nucleus, limbic areas, and neocortex, (iii) serotonergic systems of the dorsal raphe nuclei, striatum, and neocortex, (iv) cholinergic systems of the basal nucleus of Meynert, hippocampus, nucleus tegmenti pedunculopontinus, Edinger-Westphal nucleus, and neocortex, and (v) peptidergic systems of the striatum, medulla, hippocampus, brainstem, and cortex. The depletion of dopaminergic innervation to the motor cortex is laminar specific, with the most significant reductions observed in layers I and II; the innervation to layers V and VI is relatively spared (Gaspar et al., 1991). This result suggests the presence of two separate mesocortical dopaminergic pathways in humans, with the one projecting to the upper cortical layers being preferentially involved in Parkinson's disease. Patients with Parkinson's disease also display a selective reduction in the activity of complex I (NADH CoQ_1 reductase; EC 1.6.5.3) of the mitochondrial electron transport chain in platelets (Parker et al., 1989; Benecke et al., 1993)

and the substantia nigra (Schapira et al., 1990), suggesting that a breakdown of cellular respiration may contribute to the onset of Parkinson's disease. Therefore, Parkinson's disease displays an extremely complex pathology that affects numerous neurotransmitter and neuropeptide systems of the mammalian brain.

4.3. *MPTP: a model of Parkinson's disease*

Experimental models of Parkinson's disease can be produced by midbrain lesions resulting in degeneration of nigrostriatal dopaminergic neurons. Electrolytic lesions in cats cause neurochemical changes comparable to those observed in post mortem parkinsonian brains (Hockman et al., 1971). Selective neurotoxic lesions can also produce symptoms of Parkinson's disease. A compound displaying selective nigral toxicity was discovered under tragic circumstances in the summer of 1982, when several young adults in southern California mysteriously developed chronic and severe parkinsonism following repeated intravenous use of what they believed was the synthetic opiate meperidine (Langston et al., 1983; Langston and Ballard, 1984; Ballard et al., 1985). Analysis of the injected substance revealed primarily 1-methyl-4-phenyl-1,2,5,6-tetrahydropyridine (MPTP), a by-product in the synthesis of meperidine. Administration of MPTP in mice (Heikkila et al., 1984; Heikkila and Sonsalla, 1987) and monkeys (Langston et al., 1984; Bankiewicz et al., 1986; Brooks et al., 1987) produced cell loss in the pars compacta of the substantia nigra (group A9) and substantially decreased striatal concentrations of dopamine and its metabolites. Motor symptoms resulting from the neurotoxic effects of MPTP administration can be divided into distinct acute, subacute, and chronic phases (see Langston, 1984).

The selective neurotoxicity of MPTP results from its conversion in glia, serotonergic nerve terminals, or histaminergic nerve terminals to the ionic species 1-methyl-4-phenylpyridine (MPP^+) by monoamine oxidase B (Chiba et al., 1984; see Snyder and D'Amato, 1986). Nigrostriatal dopaminergic neurons actively accumulate MPP^+ (Chiba et al., 1985; Javitch et al., 1985*a*) since it is a substrate for the plasma membrane dopamine transporter (Ricaurte et al., 1985). Intraneuronally, MPP^+ appears to exert its toxic effects by inhibiting complex I of the mitochondrial electron transport chain (Mizuno et al., 1987*a*),

probably due to its structural similarity to the dehydrogenase co-factor NAD^+. The inhibition of mitochondrial respiration decreases the rate of oxidative phosphorylation and the cellular concentration of ATP (Mizuno et al., 1987*b*), which may be fatal to cells when ATP pools fall below a certain critical level. Energy crisis therefore appears to be one of the most important factors of neuronal degeneration in MPTP-induced parkinsonism. Therefore, MPTP is a potent and selective nigral neurotoxin that produces behavioural and neurochemical changes consistent with the pathophysiology of Parkinson's disease. Although MPTP is not implicated in the etiology of idiopathic Parkinson's disease, the elucidation of its mechanism of action has provided many insights into the degeneration of nigrostriatal dopaminergic neurons.

4.4. *Neuronal circuitry of the basal ganglia*

Having established the central role of dopamine in the presentation of Parkinson's disease, researchers investigated the apparent relationship between a decrease in striatal dopamine content and the associated loss of coordinated motor control. The explanation is provided by examining the major neuronal connections between the regions of the basal ganglia (see Albin et al., 1989; see Jellinger, 1991; see Heimer, 1995; see Wooten, 1997). In addition to dopamine, the striatum contains a high concentration of GABA, and acetylcholine, which is a transmitter of large striatal interneurons (see Groves, 1983). Dopaminergic projections from the pars compacta of the substantia nigra are inhibitory to striatal cholinergic interneurons, which themselves are excitatory to GABAergic neurons that project from the striatum to both the lateral globus pallidus and the pars reticulata of the substantia nigra. The lateral globus pallidus sends GABAergic projections to the subthalamic nucleus, which in turn sends excitatory glutamatergic projections to the medial globus pallidus and the pars reticulata of the substantia nigra. These two output nuclei of the basal ganglia project GABAergic connections to the ventrolateral thalamus, which in turn sends excitatory projections to motor regions of the cerebral cortex. Finally, the circuit closes with excitatory glutamatergic projections from the cortex back to the striatum. The striatum receives inputs from the entire cortical mantle, although inputs from specific cortical

regions are segregated with respect to target zones (see Côté and Crutcher, 1991). For example, the entorhinal cortex and amygdala project to the nucleus accumbens, while the prefrontal (motor) cortex projects to the dorsal striatum.

In Parkinson's disease, the loss of dopaminergic input to the striatum disinhibits striatal acetylcholine and so increases inhibitory output to the subthalamic nucleus. The ultimate result is increased activity of excitatory thalamocortical and corticostriatal projections, which manifest physically as parkinsonian symptoms. The proper functioning of the nigrostriatal dopaminergic pathway therefore requires a delicate balance between dopaminergic and cholinergic systems; the loss of dopamine in Parkinson's disease shifts this balance in favour of acetylcholine and disrupts coordinated motor control.

4.5. *Pharmacological treatments*

4.5.1. *Exogenous L-dopa*

The in vitro observation of decreased dopamine levels in the parkinsonian brain led to the logical hypothesis that replenishing lost stores of dopamine would alleviate the symptoms of Parkinson's disease. However, as discussed earlier (see section 3.3), direct administration of dopamine is not a viable method of treatment because it does not cross the blood-brain barrier. But L-dopa readily enters the brain, and so it could compensate for a deficiency of striatal dopamine. There nonetheless remained the question of how therapeutic doses of L-dopa could compensate for the massive reduction in striatal dopaminergic innervation that characterizes Parkinson's disease, if dopamine synthesis could occur only in the few remaining nigrostriatal dopaminergic neurons. Several lines of evidence provide a rationale for a potential anti-parkinsonian action of L-dopa. First, the turnover of dopamine, as measured by the ratio of homovanillic acid to dopamine concentrations, is increased in the parkinsonian striatum (Bernheimer and Hornykiewicz, 1965), suggesting that the activity of surviving nigrostriatal dopaminergic neurons is up-regulated as if to compensate for the reduced dopaminergic innervation. Second, the activity of dopa decarboxylase in the parkinsonian striatum, though reduced by 80%, is sufficient to account for the local formation of dopamine (Lloyd and Hornykiewicz, 1970). Third, the

pharmacologic effects of L-dopa are not solely related to striatal dopamine concentration; the turning behaviour induced by L-dopa therapy in rats with unilateral nigral lesions persisted long after striatal dopamine concentrations returned to control levels (Spencer and Wooten, 1984). Fourth, the high degree of divergence of the dopaminergic fibres projecting from the substantia nigra to the striatum (Andén et al., 1966) implies that only the loss of extensive portions of this innervation would prevent functional compensation by the surviving up-regulated nigrostriatal dopaminergic neurons. These factors together form the basis for the efficacy of L-dopa as the primary pharmacological therapy in the treatment of Parkinson's disease (see Hornykiewicz, 1974). Indeed, preliminary clinical trials revealed that the administration of L-dopa (Birkmayer and Hornykiewicz, 1961; Cotzias et al., 1969) and DL-dopa (Cotzias et al., 1967) relieves rigidity and tremor, but it nevertheless remains predominantly a symptomatic and transient treatment. The efficacy of L-dopa tends to decline with use, especially after a decade or more of treatment (Gauthier and Gauthier, 1987). Furthermore, chronic, high-dose use of L-dopa causes some undesirable side effects, such as nausea, vomiting, and choreiform hyperkinesias. One explanation for this latter effect is that high doses of exogenous L-dopa result in the accumulation of supra-optimal amounts of dopamine in the striatum, which may ultimately interfere with the proper functioning of the striatum as a coordinating center of extrapyramidal motor control.

Post mortem analysis revealed significantly higher tissue concentrations of dopamine and homovanillic acid in the striatum of patients with Parkinson's disease who were taking L-dopa prior to death (Davidson et al., 1971). In healthy rat striatum, the formation of dopamine from exogenous L-dopa occurs mainly in synaptic dopamine terminals, with a small contribution from striatal interneurons and efferent neurons (Hefti et al., 1981; Melamed et al., 1981). From this circumstantial evidence it was assumed that the clinical benefits of exogenous L-dopa in Parkinson's disease were in fact due, as initially postulated, to its enzymatic conversion to dopamine, a reaction which would partially compensate for the deficient neurotransmission in the nigrostriatal pathway. This was subsequently confirmed by demonstrating that pharmacologic blockade of cerebral dopa decarboxylase suppressed the L-dopa-induced circling response of rats with unilateral nigral lesions

(Melamed et al., 1984). Experiments such as these refuted the suggestion that L-dopa itself, and not its decarboxylated product, is responsible for alleviating parkinsonian symptoms, perhaps by direct stimulation of striatal dopamine receptors.

4.5.2. *Adjunct therapeutic agents*

L-Dopa is often administered adjunctly with a secondary therapeutic agent that either (i) potentiates the effects of L-dopa, or (ii) itself exhibits anti-parkinsonian properties. Important members of the first category are compounds designed to increase the bioavailability of L-dopa, such as inhibitors of dopa decarboxylase and catechol-*O*-methyltransferase. The plasma concentration of an exogenously administered dose of L-dopa is reduced by 50% within 5-30 min of oral intake (Nutt et al., 1985), due to the rapid redistribution of L-dopa from plasma to peripheral tissues. This initial phase of plasma clearance, combined with a second phase corresponding to metabolism, ultimately result in only a very small fraction of an oral dose of L-dopa reaching the brain unchanged. Co-administration of extracerebral dopa decarboxylase inhibitors such as carbidopa increase the amount of dopamine formed in brain by eliminating the peripheral decarboxylation of L-dopa. A mixture of L-dopa and carbidopa (commercially available as Sinemet®) was significantly more effective in alleviating tremor and rigidity in a group of 50 patients with Parkinson's disease than L-dopa alone (Lieberman et al., 1975). Carbidopa also reduced by 50% the infusion rate of L-dopa required to produce a clinical response (Nutt et al., 1985).

A series of catechol-*O*-methyltransferase inhibitors have been tested in combination with L-dopa, with varying degrees of success. The first such experiment was performed in a group of ten patients with Parkinson's disease using *N*-butyl gallate (GPA 1714; Ericsson, 1971). While this agent improved symptoms, including dyskinesias, and decreased the dose of L-dopa required for a clinical response, its use was discontinued due to toxicity. Nitecapone (OR-462), an inhibitor of peripheral catechol-*O*-methyltransferase, significantly improved markers of clinical disability in seven patients with Parkinson's disease but produced none of the side effects associated with *N*-butyl gallate (Teräväinen et al., 1990). Plasma concentrations of *O*-methyl-L-dopa were reduced by 40-60% following nitecapone

administration in monkeys (Cedarbaum et al., 1990) and healthy human volunteers (Gordin et al., 1990). In rats, the central catechol-*O*-methyltransferase inhibitor Ro 40-7592 increased striatal concentrations of dopac, but had no effect on dopamine concentration (Acquas et al., 1992). Another biochemical study with Ro 40-7592 found increased concentrations of both dopac and dopamine in rat striatum, coupled with significantly reduced concentrations of *O*-methyl-L-dopa (Kaakola and Wurtman, 1993). Therefore, compounds that inhibit the activities of dopa decarboxylase and catechol-*O*-methyltransferase alleviate parkinsonian symptoms by increasing the fraction of exogenous L-dopa that remains available for conversion to dopamine in the striatum.

Dopamine agonists are a class of compounds employed in the treatment of Parkinson's disease because of their ability to stimulate post-synaptic dopamine D_1 and D_2 receptors. One of the first such agents that proved clinically useful was bromocriptine (Parlodel®; Calne et al., 1974), an ergot derivative with a high affinity for D_2 receptors that was originally developed to treat certain endocrine disorders such as hyperprolactinemia. A six month study in 77 patients revealed that bromocriptine was as effective as L-dopa in alleviating functional and neurological deficits in Parkinson's disease (Riopelle, 1987), suggesting a role for bromocriptine as de novo therapy. A review of several previous clinical studies concluded that the optimum symptomatic control of Parkinson's disease was achieved with a mixture of L-dopa, carbidopa, and bromocriptine (see Bouchard, 1987).

The pharmacokinetic and clinical properties of several newer dopamine agonists have been reviewed (see Lang, 1987; see Obeso et al., 1987). Four such compounds, the D_2 agonists lergotrile, lisuride, and mesulergine, and the mixed D_1/D_2 agonist pergolide, were tested in a group of 278 patients with Parkinson's disease; all displayed levels of efficacy similar to that of bromocriptine, but individual patients often responded better to a particular agent (Lieberman et al., 1987). Oral administration of cabergoline, another ergot derivative that acts at D_2 receptors, to 18 patients resulted in a 50% decrease in Parkinson's disease severity ratings, and a reduction in the daily dose of Sinemet® from 1100 mg to 700 mg (see Lera et al., 1990). A similar long-term study in 36 patients with Parkinson's disease revealed increased dyskinesias in 23 patients after 17 months of daily cabergoline treatment (Lera et

al., 1993). The most common drawback associated with the administration of dopamine agonists is the induction of gastrointestinal disturbances resulting in anorexia, nausea, and vomiting (see Aminoff, 1998).

The earliest pharmacotherapy for Parkinson's disease was discovered by accident. Over a century ago, Ordenstein (1867) wrote in his doctoral thesis on Parkinson's disease that "M. Charcot prescrit chaque jour deux ou trois granules d'hyocyamine". This was the first published observation that compounds extracted from the belladonna plant eased certain parkinsonian symptoms. Later studies revealed that these belladonna alkaloids worked by inhibiting the activity of striatal cholinergic interneurons through blockade of post-synaptic muscarinic receptors; nicotinic receptors are not implicated in the etiology of Parkinson's disease (see Calne, 1970). This discovery led to the development of several potent anti-muscarinic agents; while these drugs have little effect on the akinetic symptoms of Parkinson's disease, they have proved beneficial in alleviating tremor and rigidity. Intravenous administration of biperidin (Akineton®) in ten patients with Parkinson's disease resulted in an acceleration of operating time and improvements of mood (Schneider et al., 1975). An investigation of the synthetic ester KR 339 (Sormodren®) in 44 patients revealed a selective action of the drug on tremor and the autonomic symptoms of Parkinson's disease (Ascher, 1976). However, the efficacy of muscarinic antagonists is tempered by several unpleasant and common side effects that manifest in a wide range of bodily systems, including sedation and delirium, dryness of the mouth, blurring of vision, urinary retention, nausea and vomiting, constipation, tachycardia, tachypnea, increased intraocular pressure, palpitations, and cardiac arrhythmias (see Aminoff, 1998).

Another drug that has gained acceptance in the treatment of Parkinson's disease is the tricyclic amine amantadine (Symmetrel®). The physiological mechanism underlying the therapeutic effects of amantadine in vivo remains elusive; a recent positron emission tomography study revealed that sub-chronic amantadine treatment does not result in significant up-regulation of dopa decarboxylase activity in living brain of healthy human volunteers (Deep et al., 1998). However, studies carried out in vitro suggest that the anti-parkinsonian properties of amantadine may be attributed to (i) enhanced release of dopamine

from central catecholamine nerve endings (Strömberg et al., 1970; Heikkila and Cohen, 1972; Jackisch et al., 1992; Stoof et al., 1992; Takahashi et al., 1996), (ii) inhibition of the re-uptake of dopamine by central catecholamine nerve endings (Fletcher and Redfern, 1970; Heikkila and Cohen, 1972; Mizoguchi et al., 1994), (iii) inhibition of the release of acetylcholine from central cholinergic nerve endings (Stoof et al., 1992; Feuerstein, 1994), or (iv) non-competitive antagonism of MK-801 binding sites at *N*-methyl-D-aspartate (NMDA)-receptor-gated cation channels of excitatory glutamatergic receptors (Kornhuber et al., 1991; Mizoguchi et al., 1994). The clinical efficacy of this latter mechanism of action is based on inhibition of the NMDA-evoked release of acetylcholine from striatal interneurons (see Starr, 1995), thereby re-establishing the balance between cholinergic and dopaminergic neurotransmission in the striatum (see section 4.4). Indeed, glutamate receptor antagonists such as amantadine and memantine are useful in the treatment of several conditions characterized by overactive corticostriatal glutamatergic projections, including akinetic hyperthermic parkinsonian crisis, neuroleptic malignant syndrome, and dopamine agonist withdrawal states (see Kornhuber et al., 1993).

The first clinical use of amantadine was as an anti-viral agent in the treatment of influenza A (100-300 mg, p.o.: Council on Drugs, 1967; Togo et al., 1968). Serendipitously, it was observed in April 1968 that a woman with Parkinson's disease experienced a marked remission in symptoms while taking amantadine to prevent the flu; this case led to controlled clinical trials of amantadine treatment in Parkinson's disease (Schwab et al, 1969; Dallos et al., 1970). Amantadine treatment has been shown recently to be an independent predictor of improved survival in Parkinson's disease (Uitti et al., 1996). Although minor side effects associated with its anti-cholinergic actions, such as dry mouth and constipation, are relatively common, the major side effects of amantadine use are due to its psychotomimetic properties. A healthy 35-year old woman was diagnosed with acute psychosis manifested by visual hallucinations and delirium following an overdose of amantadine (1.2 g over a 24-hour period; Snoey and Bessen, 1990). In patients with schizophrenia, amantadine treatment can exacerbate established psychotic symptoms (Nestelbaum et al., 1986; Kornhuber and Weller, 1993). Low doses of amantadine (200-300 mg, p.o.) induced visual hallucinations and

delirium in 13 elderly patients, 12 of whom had Parkinson's disease (Postma and van Tilburg, 1975). Treatment with amantadine for three weeks at doses ranging from 100-400 mg (p.o.) reduced dopa-dyskinesia scores by 60% in a group of 14 patients with advanced Parkinson's disease (Verhagen-Metman et al., 1998), but three of these patients experienced mild confusion or hallucinations at high doses. Therefore, the psychological state of patients should be carefully evaluated prior to administration of glutamate receptor antagonists such as amantadine.

5. Radiolabelled analogs of L-dopa

5.1. *Introduction*

In vitro studies provided important information on the distribution of dopamine in mammalian brain and the specific neurochemical mechanisms underlying its behaviour in situ; however, these results could not be automatically extrapolated to living brain. In vivo methods for studying dopamine synthesis and metabolism were developed using radiolabelled analogs (tracers) its brain-penetrating precursor, L-dopa. The concept of labelling L-dopa with a radioactive isotope is based on the assumption (and subsequent verification) that the analog behaves analogously to endogenous L-dopa in vivo. A tracer of L-dopa would therefore have to display the characteristics of reversible blood-brain transport, and decarboxylation and trapping in the striatum.

5.2. *^{3}H- and ^{14}C-labelled L-dopa: beta emitters*

Some of the first such tracers were prepared by replacing hydrogen atoms (^{2}H) on the catechol ring of L-dopa with radioactive tritium atoms (^{3}H). Tritium is produced by cosmic ray bombardment of water in the atmosphere (see Kotz and Purcell, 1987), and more recently from the testing of hydrogen bombs. Tritium emits beta particles (high-speed electrons) to form an isotope of helium (^{3}He) that has a half-life of 12.3 years (CRC Press, 1981). Another beta-emitter suitable for radiolabelling is the naturally occurring isotope ^{14}C. However, ^{14}C has a half-life of 5730 years (CRC Press, 1981), which puts limitations on the

specific radioactivity that can be attained during an in vivo experiment. Notwithstanding an excess of neutrons, both of these analogs are structurally identical to endogenous L-dopa.

Beta particles have extremely low penetrating power: a sheet of paper is sufficient to block their transit. Consequently, ^{3}H and ^{14}C injected into living subjects cannot pass through the body to be detected externally (see section 6.2). However, the radioactivities of these isotopes in dissected portions of brain tissue from experimental animals can be assayed by scintillation spectroscopy. Chemical fractionation of the radiolabelled compounds in these tissue samples by chromatographic techniques can then be used to identify individual metabolite fractions. This principle was used in the first studies with radiolabelled L-dopa in living mammals. Following intraperitoneal or intravenous injection of ^{3}H- and/or ^{14}C-labelled precursors of dopamine (L-phenylalanine, L-tyrosine, and L-dopa), the decline of specific radioactivity in dissected tissue samples was used to estimate the rate of turnover of catecholamines in the adrenal gland (Udenfriend and Wyngaarden, 1956), peripheral sympathetic organs (Burack and Draskóczy, 1964) and brain (Burack and Draskóczy, 1964; Iversen and Glowinski, 1966) of rats, and in the brain of guinea pigs (Udenfriend and Zaltzman-Nirenberg, 1963). Analogous experiments to investigate the peripheral and cerebral metabolism of [^{14}C]dopa were performed in mice (Wurtman et al., 1970) and rats (Bartholini and Pletscher, 1968; Guldberg and Broch, 1971). The disposition of dopamine in living rat brain was similarly studied with [^{3}H]dopa (Glowinski and Iversen, 1966); the preferential accumulation of radioactivity in the striatum confirmed the post mortem observation of high striatal dopamine content. The specific radioactivities of ^{3}H-labelled 3-methoxytyramine and dopac measured in rat striatum after administration of [^{3}H]tyrosine are much higher that those of their physiological precursor, suggesting a multiple compartmentalization of dopamine in nigrostriatal dopaminergic neurons (Groppetti et al., 1977).

5.3. *^{11}C- and ^{18}F-labelled L-dopa: positron emitters*

A dramatic breakthrough for in vivo studies of dopamine synthesis was achieved with the introduction of positron-emitting analogs of L-dopa. The short-lived isotope ^{11}C is

produced by thermal neutron bombardment of N_2 gas to yield $^{11}CO_2$; this compound served as a source of radiolabelled carbon that was incorporated into the *β*-position of the L-dopa catechol ring to yield [^{11}C]dopa (Reiffers et al., 1977). Like [^{3}H]dopa and [^{14}C]dopa, [^{11}C]dopa differs from the endogenous amino acid only in possible isotope effects, which are insignificant with respect to metabolic pathways. Another positron-emitting isotope is ^{18}F, first produced by neutron bombardment of enriched lithium carbonate, and subsequently incorporated into L-dopa to yield DL-5-[^{18}F]fluorodopa (Firnau et al., 1973*a*,*b*). A few years later, aromatic fluorination reactions with xenon difluoride (Firnau et al., 1980*a*, 1981) or [^{18}F]fluorine gas (Firnau et al., 1984; Chirakal et al., 1986) were used to produce L-6-[^{18}F]fluorodopa. Several other methods for the production of L-6-[^{18}F]fluorodopa have since been developed, and are reviewed elsewhere (see Firnau et al., 1986; see Luxen et al., 1992).

Like beta particles, positrons have low penetrating power and cannot themselves be detected externally. However, the high-energy photons produced by the collisions between emitted positrons and electrons in vivo do indeed pass through the body, and thus form the basis for the use of ^{11}C- and ^{18}F-labelled compounds in autoradiography with external detection of the signal (i.e. positron emission tomography; see section 6.3.1). The half-life of ^{11}C is short (20 min; CRC Press, 1981), and so the utility of [^{11}C]dopa for tracing processes near the end of the dopamine metabolic pathway, such as the clearance of acidic metabolites, may be compromised. However, the half-life of ^{18}F (110 min; CRC Press, 1981) is sufficiently long to permit L-6-[^{18}F]fluorodopa to trace all the steps involved in dopamine synthesis and metabolism.

5.4. *Qualitative validation of radiolabelled L-dopa analogs*

5.4.1. *Metabolism*

In vitro, DL-5-[^{18}F]fluorodopa is a substrate for dopa decarboxylase (Firnau et al., 1975), and radioactivity accumulates in brain following its intravenous injection in mice and baboons (Firnau et al., 1976) and monkeys (Garnett et al., 1980). Furthermore, decarboxylation of L-6-[^{18}F]fluorodopa yields 6-[^{18}F]fluorodopamine in vivo, as confirmed by chromatographic identification of ^{18}F-labelled metabolites in rat striatum (Cumming et

al., 1987*a*,*b*, 1988). Therefore, radiofluorinated L-dopa is not biochemically distinguished from the endogenous amino acid in the irreversible trapping step.

The introduction of the ^{18}F atom into the aromatic ring can alter the kinetic properties of the amino acid. The possible sites of ^{18}F-labelling of L-dopa are in the 2-, 5-, and 6-positions of the aromatic ring. In vitro, the *O*-methylation of the 6- isomer is decreased compared to that of unlabelled L-dopa, while the 2- and 5- isomers display an accelerated rate of methylation due to the electron-withdrawing effect of the electronegative ^{18}F atom on the adjacent hydroxyl group (Creveling and Kirk, 1985; Firnau et al., 1980*b*, 1988; see Firnau et al., 1986). Furthermore, the 2-isomer is a poor substrate for dopa decarboxylase in vitro and is not decarboxylated in living rat striatum (Cumming et al., 1988). These observations led to the use of L-6-[^{18}F]fluorodopa as the preferred radiofluorinated tracer of intracerebral dopamine.

Using high-performance liquid chromatography or solid phase alumina extraction techniques, chemical fractionation of radiolabelled compounds in plasma and brain extracts from rats (Cumming et al., 1987*a*,*b*, 1988, 1994*a*, 1995*a*; Melega et al., 1990*a*,*b*; J Reith et al., 1990) and monkeys (Melega et al., 1990*b*, 1991*a*,*b*), and plasma extracts from healthy human volunteers (Boyes et al., 1986; Firnau et al., 1987, 1988; Melega et al., 1990*b*, 1991*b*; Chan et al., 1992; Cumming et al., 1993) demonstrated unequivocally that L-6-[^{18}F]fluorodopa in vivo is metabolized in a manner analogous to endogenous L-dopa; its major metabolites are ^{18}F-labelled *O*-methyl-L-dopa, dopamine, dopac, and homovanillic acid. Chromatographic studies in rat brain yielded corresponding qualitative results for ^{3}H-labelled metabolites formed following intravenous injection of [^{3}H]tyrosine (Cumming et al., 1994*b*, 1997*a*, 1998) and [^{3}H]dopa (Cumming et al., 1995*a*,*b*), and for ^{11}C-labelled metabolites formed following intravenous injection of [^{11}C]dopa (Tsukada et al., 1994). Furthermore, L-6-[^{18}F]fluorodopa is transported into brain by the same carrier system as endogenous L-dopa, as demonstrated by the reduced uptake of L-6-[^{18}F]fluorodopa following peripheral administration of large neutral amino acids (Leenders et al., 1986*a*). Like endogenous dopac and homovanillic acid, the acidic metabolites of 6-[^{18}F]fluorodopamine are cleared from brain into cerebrospinal fluid (Hammerstad et al., 1993).

5.4.2. *Vesicular storage*

There is considerable evidence to suggest that, like endogenous dopamine, [^{3}H]dopamine and 6-[^{18}F]fluorodopamine are stored in synaptic vesicles. For example, dopaminergic nerve endings were visualized by electron microscopy after intracerebroventricular injection of [^{3}H]dopamine (Descarries et al., 1980). The apparent in vitro affinities of 6-[^{18}F]fluorodopamine for the pre-synaptic dopamine uptake transporter and chromaffin granule amine transporter (Endres et al., 1997), and [^{3}H]dopamine (MEA Reith et al., 1990) and 6-[^{18}F]fluorodopamine (Barrio et al., 1995) for the synaptic vesicle amine transporter, are similar to that of dopamine. An examination of nerve-ending microsacs, isolated from guinea pig striatum and incubated with fluorinated amines, by ^{19}F nuclear magnetic resonance spectroscopy detected a strong signal corresponding to 6-[^{18}F]fluorodopamine, with a minor signal corresponding to its deaminated metabolite (Diffley et al., 1983). Depolarization of dopaminergic nerve terminals by potassium releases 6-[^{18}F]fluorodopamine along with dopamine (Chiueh et al., 1983). Furthermore, reserpine treatment reduces striatal ^{18}F radioactivity, presumably derived from 6-[^{18}F]fluorodopamine, which has accumulated following L-6-[^{18}F]fluorodopa injection (Firnau et al., 1976; Garnett et al., 1983*a*). New evidence for the vesicular storage of 6-[^{18}F]fluorodopamine in vivo is also provided in Chapter II (Deep et al., 1997*a*) of the present thesis.

Based on this abundance of direct physical evidence, it is concluded that [^{3}H]dopa, [^{11}C]dopa, and L-6-[^{18}F]fluorodopa follow the same metabolic pathway as endogenous L-dopa, and are therefore accurate qualitative tracers of the amino acid in vivo (see Barrio et al., 1997).

6. Visualization of cerebral dopaminergic innervation in vivo

6.1. *Quantitative autoradiography*

Quantitative autoradiographic techniques, both static (see section 6.2) and dynamic (see section 6.3), measure the total radioactivity in living tissues due to regional accumulation over time of an injected tracer and its radiolabelled metabolites. The

radiochemical composition of this radioactivity is due to several product and precursor pools, the nature of which are not explicitly known unless tissue samples are available for chromatographic fractionation. Each metabolite pool is assumed to reflect an individual compartment, occupying a spatially homogenous region in brain.

6.2. *Static autoradiograms with radiolabelled L-dopa*

Autoradiograms made by exposing serial brain sections from experimental animals, together with autoradiographic standards on high-sensitivity film, measure the tissue radioactivity at a specific time following tracer injection, and therefore yield static images. This autoradiographic technique is suitable for weak beta-emitters such as ^{3}H and ^{14}C, the low penetrating power of which excludes their use in quantitative autoradiographic techniques with external detection of the signal (i.e. positron emission tomography; see section 6.3.1). The fact that static autoradiograms are produced following sacrifice of the animal means that the signals are subject to potential degradation due to post mortem changes in regional enzyme activities or receptor densities.

In rats, cerebral autoradiograms acquired following intravenous injection of [^{3}H]dopa (Liskowsky and Potter, 1985; Cumming et al., 1995*a*, 1997*b*) or [^{14}C]dopa (Wooten and Horne, 1982; Horne et al., 1984) revealed preferential uptake of radioactivity in the basal ganglia, due to trapping of the radiolabelled decarboxylated products in situ. Static autoradiograms have also been used to measure the concentrations of dopamine re-uptake sites, which represent a pre-synaptic marker of the integrity of dopaminergic innervations. The radiolabelled dopamine uptake inhibitors [^{3}H]mazindol (Javitch et al., 1985*b*) and [^{125}I]RTI-55 (Cumming et al., 1997*b*) revealed the highest concentrations of dopamine re-uptake sites in the target zones of the A8 and A9 neuron groups: the striatum, nucleus accumbens, and olfactory tubercle.

6.3. *Dynamic autoradiograms with radiolabelled L-dopa*

6.3.1. *Positron emission tomography*

Positron emission tomography measures tissue radioactivity concentrations over time following tracer injection, and therefore yields dynamic signals. It is an extremely sensitive autoradiographic technique which can detect concentrations of high specific radioactivity tracers in brain as low as the subpicomolar range (10^{-12} M; see Farde, 1996). The mechanism of detection is based upon the annihilation of emitted positrons with electrons in brain water, and the subsequent release of energy in the form of two high-energy photons (511 keV) at very nearly 180 degrees. Coincidence circuitry registers an annihilation (event) when photons simultaneously arrive at two diametrically opposed detectors. The accumulation of many millions of such coincidence events allows the reconstruction of dynamic images in two dimensions (2D) or three dimensions (3D). Specific cerebral structures in positron emission tomographic images are now accurately identified by aligning the reconstructed image to the same stereotaxic coordinates as the corresponding magnetic resonance image using a semi-automated computer registration algorithm (Woods et al., 1993).

The limited spatial resolution of tomographs results in measured signals that are contaminated by the spillover of radioactivity from and into adjacent tissues, phenomena which are known as partial volume effects. The result is a systematic under-estimation of radioactivities measured in gray matter regions such as caudate and putamen. However, a semi-automated computer method of correction for the recovery of true tissue radioactivities measured in 2D mode has been developed recently in this laboratory. Simulation studies using plastic brain phantoms filled with aqueous solutions of ^{11}C and ^{18}F have validated the correction algorithm for accuracy and precision, and demonstrated it to be independent of tracer levels (Rousset et al., 1993*a*,*b*, 1996, 1998*a*). Indeed, correction for partial volume effects greatly increases the amplitudes of time-activity curves recorded in the human basal ganglia and cerebral cortex following injection of [^{11}C]-(*S*)nicotine (Yokoi et al., 1997) and L-6-[^{18}F]fluorodopa (Rousset et al., 1998*b*), but at the cost of reduced signal-to-noise ratios. The magnitude of the partial volume effects is dependant on the size (Hoffman et al., 1979), shape (Mazziotta et al., 1981), and contrast (Kessler et al., 1984) of the region of interest.

All imaging systems experience quantitative measurement inaccuracies when object size is less than the spatial resolution of the tomograph (measured as full-width half-maximum of a line source); therefore, small, closely-spaced structures are particularly sensitive to contamination by spillover. Present 3D tomographs for use with primates, such as the ECAT HR+ (Seimens) at the McConnell Brain Imaging Centre of the Montreal Neurological Institute, have a resolution of 4 mm, while tomographs recently developed for studies in small animals achieve resolutions of 2-3 mm (Torres et al., 1995; Hume et al., 1996). Compared to 2D tomographs, the improved resolution of 3D tomographs may be expected to reduce the effects of partial volume phenomena, but the recovery of true radioactivities may be inhibited by the accentuation of positron scatter during acquisitions in 3D mode.

6.3.2. *Accumulation of radioactivity in the conscious primate brain*

The first visualization of the regional distribution of a neurotransmitter in the conscious primate brain was achieved with positron emission tomography; the neurotransmitter was dopamine. Radioactivity derived from L-6-[^{18}F]fluorodopa accumulates primarily in the striatum of monkeys (Garnett et al., 1983*a*), healthy human volunteers (Garnett et al., 1983*b*), patients with Parkinson's disease (Garnett et al., 1984, 1987; Nahmias et al., 1985; Leenders et al., 1986*b*), and patients with primary dystonia (Garnett et al., 1987) during positron emission tomography scans. These imaging studies also revealed significant accumulation of ^{18}F radioactivity in the anterior cingulate cortex and frontal cortex, with minimal uptake in the occipital cortex, consistent with the cortical distribution of dopamine measured in vitro in the post mortem primate brain (see Berger et al., 1991).

In patients with Parkinson's disease, the striatal accumulation of radioactivity is significantly reduced, with the putamen generally displaying less uptake than the caudate. This result is consistent with the post mortem observation of a more pronounced degeneration of the putamen, particularly its caudal portions, in the parkinsonian brain (Kish et al., 1988; see section 4.2). In ten cases of hemiparkinsonism, the reduction in radioactivity was greater in the striatum contralateral to the affected side of the body (Garnett et al., 1984),

as expected due to the crossing of corticospinal motor fibres at the level of the brainstem. Corresponding qualitative results were obtained with [^{11}C]dopa in living brain of monkeys (Tedroff et al., 1992*a*, 1997; Hartvig et al., 1993), healthy human volunteers (Hartvig et al., 1991), and patients with Parkinson's disease (Tedroff et al., 1992*b*). Therefore, positron emission tomography with radiolabelled L-dopa yields qualitative images of dopaminergic innervation which accurately reflect the extent and regional heterogeneity of dopamine depletion in the parkinsonian striatum.

7. Kinetic modelling of radiolabelled L-dopa autoradiographic data

7.1. *Introduction*

Autoradiography yields images of the distribution of tracer and its metabolites in vivo, but does not immediately yield quantitative kinetic data concerning tracer synthesis and metabolism. Such information can only be obtained by modelling the total cerebral radioactivities measured by static autoradiograms or dynamic positron emission tomograms. The process involves the development of a mathematical model that accurately describes the physiological behaviour of the tracer in living tissue. The model is then fit by least-squares regression to measured radioactivities to estimate a finite set of kinetic constants defining the rates of relevant physiological processes.

For the calculation of tissue radioactivities in a region of interest [$M(T)$], all models require an input function, which in most cases corresponds to the radioactivity of precursor in arterial plasma [$C_a(T)$]. For radiolabelled L-dopa, a power function derived empirically (see Appendix #1) has been shown to accurately describe arterial radioactivities as a function of circulation time (Wong et al., 1986; Cumming et al., 1997*a*, 1998); this function is of the form $C_a(T) = AT^{-b}$, where A is an arbitrary constant chosen to best fit the observed radioactivities, and b is a decay constant (see Chapter III, Deep et al., 1997*b*). To determine radiolabelled L-dopa radioactivities analytically, the total arterial curve must be corrected for the presence of brain-penetrating metabolites, such as radiolabelled *O*-methyl-L-dopa, by chromatographic fractionation of plasma samples (see section 8.1).

7.2. The plasma slope-intercept plot: a linear model

The plasma slope-intercept plot is a linear graphical method for measuring the net influx of tracer from blood to tissue (or net blood-tissue clearance) that is based on the assumption of irreversible trapping of radioactivity in situ (Gjedde 1981, 1982; Patlak et al., 1983; Patlak and Blasberg, 1985). The algebraic difference between the radioactivity measured in the region of interest and in a reference region devoid of specific accumulation [$M^{ref}(T)$] is assumed to equal the amount of product in the region of interest. The distribution volume of tissue product relative to plasma precursor radioactivity {$[M(T)-M^{ref}(T)]/C_a(T)$} is then plotted as a linear function of the normalized time-concentration integral of plasma precursor radioactivity [$\Theta(T)=\int C_a(t)dt/C_a(T)$]. Since the method is based on linear regression, it is computationally simple, and yields a single kinetic constant that is the composite of tracer influx, efflux, and trapping.

With respect to radiolabelled L-dopa, the region of interest is generally the striatum, while the reference region is one that displays negligible dopaminergic innervation, such as white matter, occipital cortex, or cerebellum (Tedroff et al., 1992*a*,*b*; Hartvig et al., 1993; Hoshi et al., 1993). Subtracting the reference radioactivity from that in the striatum partially corrects for the presence of radiolabelled *O*-methyl-L-dopa, which is nearly homogeneously distributed throughout brain following tracer injection (see section 8.3). The trapping process for radiolabelled L-dopa corresponds to decarboxylation. While decarboxylation is itself an irreversible step, the trapping of radioactivity is reversible since the radioactivity derived from radiolabelled dopamine is cleared from brain by efflux of its acidic metabolites. This fact accounts for the validity of the method over a limited temporal range (< 90 min), corresponding to times before significant clearance of acids from brain has occurred. Some deviation from linearity of the uptake plot at early times (< 15 min) may reflect initially greater unidirectional clearance of large neutral amino acids into the reference region.

The linear method has been used to estimate the net influx of L-6-[^{18}F]fluorodopa from blood to living brain (K_i^{FDOPA}, ml g^{-1} min^{-1}) of rats (Hume et al., 1996), healthy monkeys (Hoffman et al., 1992; Pate et al., 1993), monkeys on chronic amphetamine treatment (Melega et al., 1996*a*), monkeys with MPTP-induced hemiparkinsonism (Melega et al.,

1996*b*), healthy human volunteers (Martin et al., 1989; Gjedde et al., 1990; Sawle et al., 1990; Huang et al., 1991; Eidelberg et al., 1993; Shiraishi et al., 1996), healthy human volunteers administered subchronic levels of amantadine (Deep et al., 1998), patients with Parkinson's disease (Leenders et al., 1990; Hoshi et al., 1993; Snow et al., 1993; Sawle et al., 1994; Antonini et al., 1995; Eidelberg et al., 1995; Barrio et al., 1996; Boecker et al., 1996; Dhawan et al., 1996; Holden et al., 1996; Ishikawa et al., 1996*a*,*b*; Morrish et al., 1996; Vingerhoets et al., 1996), patients with multiple system atrophy (Antonini et al., 1997), patients with schizophrenia (Hietala et al., 1995), patients with Alzheimer's disease (Meguro et al., 1997), and patients with developmental stuttering (Wu et al., 1997). Comprehensive tables summarizing model estimates of K_i^{FDOPA} in living mammalian brain under various physiological and pathological conditions are presented elsewhere (see Cumming and Gjedde, 1998).

The significantly lower estimates of K_i^{FDOPA} observed in the living parkinsonian brain compared to neurologically normal controls is consistent with the reduced dopa decarboxylase activity associated with Parkinson's disease. The magnitude of K_i^{FDOPA} correlates with quantitative disease severity ratings (Ishikawa et al., 1996*a*), and is thus a useful clinical measure for detecting the stage of progression of disease. The magnitude of K_i^{FDOPA} also correlates with the number and size of nigrostriatal dopaminergic neurons, striatal levels of dopamine, total catecholamines, and the activities of tyrosine hydroxylase and dopa decarboxylase (Pate et al., 1993; Snow et al., 1993). It is therefore concluded that linear measurements using positron emission tomography with L-6-[^{18}F]fluorodopa provide a reliable index of the integrity of the nigrostriatal dopaminergic pathway.

7.3. *The compartmental model*

A major limitation of linear methods for the analysis of tracer uptake is that they are uninformative of the relative proportions of each radiolabelled metabolite compartment in brain. This information requires more complex, compartmental models that incorporate kinetic terms for the major physiological processes underlying tracer uptake, metabolism, and clearance. Fitting of these models to measured radioactivities yields a set of kinetic constants

describing the flux of mass between individual radiolabelled metabolite compartments. In general, these compartments are physically resolvable only through chromatographic fractionation of brain tissue samples.

A compartmental model describing the cerebral utilization of D-glucose was validated with radioactivities measured by autoradiograms in brains of rats administered [^{14}C]deoxyglucose (Sokoloff et al., 1977), a tracer which, like endogenous glucose (Gjedde et al., 1980; Gjedde, 1981), is transferred from blood to brain by facilitated diffusion. In this case, the accumulation of radioactivity in situ is due to trapping of the phosphorylated metabolite by hexokinase, the rate-limiting enzyme of the glycolytic pathway. Deoxyglucose, unlike D-glucose, is not further metabolized past the phosphorylation reaction, and so is essentially trapped irreversibly in brain as a function of the cerebral metabolic rate of D-glucose.

Methods for modelling the uptake and metabolism of radiolabelled L-dopa in living brain have been developed which, in formal terms, resemble the [^{14}C]deoxyglucose method. The systematic investigation of the validity of the several compartmental models for radiolabelled L-dopa (see Cumming et al., 1997*c*; see Cumming and Gjedde, 1998) is a major objective of the present thesis (see Chapter III, Deep et al., 1997*b*). These models differ with respect to the number and nature of the tissue compartments in brain; application of each distinct model to the same data set can therefore yield a unique set of results. For derivations of model equations, see Appendix #1.

Nonlinear regression of compartmental models to total cerebral radioactivities measured by positron emission tomography has yielded sets of blood-brain transfer coefficients for L-6-[^{18}F]fluorodopa and its *O*-methylated derivative, and regional activities of dopa decarboxylase with respect to L-6-[^{18}F]fluorodopa (k_3^{FDOPA}, min^{-1}), in living brain of pigs (Brust et al., 1997; Danielsen et al., 1997), monkeys (Garnett et al., 1980; Barrio et al., 1990, 1996; Doudet et al., 1991*a*; Guttman et al., 1992, 1993; Léger et al., 1998), healthy human volunteers (Huang et al., 1989, 1991; Gjedde et al., 1990, 1991, 1995; Yu et al., 1990; Léger et al., 1992; Kuwabara et al., 1992, 1993; Wahl et al., 1993, 1994; Vontobel et al., 1996), healthy human volunteers administered subchronic levels of amantadine (Deep et al.,

1998), patients with Parkinson's disease (Hoshi et al., 1992, 1993; Kuwabara et al., 1995; Dhawan et al., 1996; Ishikawa et al., 1996*a*,*b*; Wahl and Nahmias, 1996*a*,*b*), and patients with psychosis (Reith et al., 1994). Corresponding models for [^{3}H]dopa have been tested in the rat (Deep et al., 1996, 1997*c*; Reith et al., 1998). Comprehensive tables summarizing model estimates of k_3^{FDOPA} in living mammalian brain under various physiological and pathological conditions are presented elsewhere (see Cumming and Gjedde, 1998).

In agreement with post mortem in vitro assays of dopa decarboxylase activity, in vivo estimates of dopa decarboxylase activity were significantly lower in the parkinsonian brain than in neurologically normal controls. Conversely, estimates of dopa decarboxylase activity in living brain of psychotic individuals were increased relative to control values, indicating enzyme up-regulation consistent with the theory of suppressed tonic release of dopamine in striatum of patients with diseases displaying episodic psychosis such as schizophrenia (see Grace, 1991). Estimates of dopa decarboxylase activity in volunteers taking amantadine were not significantly different from control values, suggesting that the anti-parkinsonian action of amantadine (see section 4.5.2) is not due to a direct up-regulation of striatal dopa decarboxylase. Therefore, compartmental modelling of total cerebral radioactivities measured by positron emission tomography following L-6-[^{18}F]fluorodopa administration permits the quantification of dopa decarboxylase activity in living brain under various physiological and pathological conditions.

7.4. *Physiological constraints*

The presence of multiple fates in the metabolic pathway of radiolabelled L-dopa and its decarboxylated derivative require models with several compartments to account for all major metabolic products. Consequently, the compartmental models are sometimes defined in terms of more parameters than can be estimated in a single study in which only the total arterial and brain tissue radioactivities are known. This results in non-convergence of regression fits to measured data. Furthermore, the inherent problem of noisy data may interfere with the isolation of parameters. In principle, individual parameters could be estimated by separate experiments, but this process is not practical in terms of time, money,

or radiation dosimetry.

To reduce the number of model parameters to a dimension solvable in a single study, some groups have omitted certain compartments, such as that corresponding to the acidic metabolites of radiolabelled dopamine (Gjedde et al., 1991; Wahl and Nahmias, 1996*a*,*b*). The costs of such omissions are reduced biological accuracy of the model, and potential bias in estimates of kinetic constants. Alternatively, to preserve biological accuracy, a series of four physiological constraints have been incorporated into the models: i) a uniform value throughout brain of the tracer equilibrium distribution volume (V_e^{DOPA}, ml g^{-1}; Gjedde et al., 1991), defined as the ratio K_1^{DOPA}/k_2^{DOPA} where k_2^{DOPA} (min^{-1}) is the rate constant for the clearance of radiolabelled L-dopa from brain to plasma; ii) omission of cerebral catechol-*O*-methyltransferase activity (Gjedde et al., 1991); iii) a fixed ratio of the rate constants for the formation and clearance of the acidic metabolites of radiolabelled dopamine (Kuwabara et al., 1993); and iv) a fixed ratio of the unidirectional blood-brain clearances of radiolabelled L-dopa and *O*-methyl-L-dopa (J Reith et al., 1990). The validity of the last constraint is supported by arguments based on the permeability of large neutral amino acids (Crone, 1963; see Appendix #1). The omission of catechol-*O*-methyltransferase activity from brain is of particular concern because it might result in a significant and systematic underestimation of estimates of dopa decarboxylase activity, the measure of most interest in studies of striatal function. The mathematical and physiological justifiability of some of these constraints in the rat has been presented elsewhere (Deep et al., 1997*c*).

8. The presence in brain of radiolabelled *O*-methyl-L-dopa

8.1. *Methods of correction*

A major difficulty associated with using radiolabelled L-dopa as a tracer of dopa decarboxylase activity in vivo is the rapid formation in plasma of high concentrations of the brain-penetrating *O*-methylated metabolite, as observed in rats (Cumming et al., 1987*a*,*b*, 1988, 1994*a*, 1995*a*; Melega et al., 1990*a*,*b*; J Reith et al., 1990), monkeys (Melega et al., 1990*b*, 1991*a*,*b*), and healthy human volunteers (Boyes et al., 1986; Melega et al., 1990*b*,

1991*b*; Cumming et al., 1993). These same studies also revealed that the formation of other radiolabelled L-dopa metabolites, such as radiolabelled dopamine and dopac, in the periphery is of minor concern since their concentrations are negligible following pre-treatment with carbidopa.

The peripheral activity of catechol-*O*-methyltransferase reduces the availability of radiolabelled L-dopa for brain dopamine synthesis, and also requires correction of tissue radioactivities for the presence of the *O*-methylated compound, which does not contribute to dopamine synthesis. Accounting for radiolabelled *O*-methyl-L-dopa in plasma and brain requires fractionation of metabolites in samples of arterial plasma either by liquid chromatography or solid phase extraction. The solid phase separation of plasma radioactivities is based on the absorption of radiolabelled L-dopa, but not its methylated product, to basic alumina (Boyes et al., 1986; Chan et al., 1992). The main disadvantage of these techniques is the requirement of an invasive arterial catheter for the collection of blood samples. The temporal changes so measured in the arterial radioactivities of this amino acid pair can be used to estimate rate constants for (i) the peripheral *O*-methylation of radiolabelled L-dopa to *O*-methyl-L-dopa by catechol-*O*-methyltransferase, and (ii) the elimination of radiolabelled *O*-methyl-L-dopa from plasma, with a simple linear graphical method (Cumming et al., 1993; see Cumming et al., 1998*b*).

Various efforts have been directed towards eliminating the need to correct for the presence of brain-penetrating radiolabelled metabolites. The entry of radiolabelled *O*-methyl-L-dopa into monkey brain was blocked by saturating the transporter of large neutral amino acids with unlabelled L-phenylalanine, 15 min after L-6-[^{18}F]fluorodopa injection (Doudet et al., 1991*b*). This approach assumes that most of the radiolabelled dopamine synthesis in brain occurs within the first 15 min following tracer administration. Alternatively, based on the promising results of combining catechol-*O*-methyltransferase inhibition with exogenous L-dopa therapy (see section 4.5.2), specific enzyme inhibitors have been used to minimize the formation of radiolabelled *O*-methyl-L-dopa. In rats, the competitive catechol-*O*-methyltransferase inhibitor U-0521 increased the availability of L-6-[^{18}F]fluorodopa in plasma by 50% after 15 min, with a concomitant 50% increase in striatal

6-[^{18}F]fluorodopamine concentrations at 30-90 minutes following tracer injection (Cumming et al., 1987*b*); the concentration of fluorinated *O*-methyl-L-dopa in striatum was reduced by 30% during that time.

The effects of catechol-*O*-methyltransferase inhibitors on L-6-[^{18}F]fluorodopa metabolism have also been studied in living primate brain with positron emission tomography. Co-administration with L-6-[^{18}F]fluorodopa of peripherally acting compounds such as nitecapone (Comi et al., 1990; Léger et al., 1998), and centrally acting compounds such as entacapone (OR-611; Guttman et al., 1993; Sawle et al., 1994; Günther et al., 1995; Léger et al., 1998), and CGP 28014 and Ro 40-7592 (Günther et al., 1995), qualitatively improved the contrast between striatum and surrounding tissues in tomographic images. However, pre-treatment with entacapone resulted in 30-50% decreases in estimates of dopa decarboxylase activity, obtained by compartmental modelling, in the putamen of monkeys (Guttman et al., 1993; Léger et al., 1998) and patients with Parkinson's disease (Ishikawa et al., 1996*b*). This effect may be due to a direct action such as inhibition of cerebral dopa decarboxylase, or an indirect action such as activation of dopamine autoreceptor. Therefore, the full range of actions catechol-*O*-methyltransferase inhibitors in vivo must be elucidated before the results of such experiments can be interpreted with confidence.

8.2. *Radiolabelled analogs of L-m-tyrosine*

A promising new approach for positron emission studies of dopa decarboxylase activity is the use of dopa decarboxylase substrates which are not substrates for catechol-*O*-methyltransferase. Endogenous L-*m*-tyrosine lacks a catechol moiety and so is not methylated by catechol-*O*-methyltransferase (Guldberg and Marsden, 1975). However, like L-dopa, L-*m*-tyrosine is transported into brain and subsequently decarboxylated (Srinivasan and Awapara, 1978; Borri-Voltattorni et al., 1983) to yield *m*-tyramine, which can act as a false dopamine neurotransmitter by stimulating dopamine receptors (Ungerstedt et al., 1973).

These physiological characteristics of L-*m*-tyrosine provided the rationale for the preparation of several radiolabelled analogs, including L-6-[^{75}Br]bromo-*m*-tyrosine (DeJesus and Mukherjee, 1988), the 2-, 4-, and 6- isomers of L-[^{18}F]fluoro-*m*-tyrosine (Melega et al.,

1989; DeJesus et al., 1990*a*, 1997; Perlmutter et al., 1990; Chirakal et al., 1991; Firnau et al., 1991*a*,*b*; Namavari et al., 1993; Hayase et al., 1994; Nahmias et al., 1995; Barrio et al., 1996), and 6-[^{18}F]fluoro-β-fluoromethylene-*m*-tyrosine (DeJesus et al., 1990*b*, 1991*a*,*b*, 1992, 1997; Reddy et al., 1990; Holden et al., 1991; Murali et al., 1992). The decarboxylated product of 6-[^{18}F]fluoro-β-fluoromethylene-*m*-tyrosine, like that of its unlabelled counterpart (Palfreyman et al., 1985), is a suicide substrate of monoamine oxidase, a unique property among these tracers that further simplifies their metabolic pathway. All of these analogs enter the striatum and are decarboxylated, and consequently may be used as synaptic dopaminergic probes to estimate striatal dopa decarboxylase activity in living brain by positron emission tomography.

8.3. *Advantages and disadvantages of L-[^{18}F]fluoro-m-tyrosines*

The resistance of L-[^{18}F]fluoro-*m*-tyrosine compounds to *O*-methylation confers upon them, in principle, several advantages compared to L-6-[^{18}F]fluorodopa. First, L-[^{18}F]fluoro-*m*-tyrosines offer a non-pharmacological alternative to catechol-*O*-methyltransferase inhibitors, which themselves may alter the kinetic properties of L-6-[^{18}F]fluorodopa in vivo when administered adjunctly. Second, the metabolic pathways, and by extension the associated compartmental models, of L-[^{18}F]fluoro-*m*-tyrosines are markedly simpler (i.e. more linear) than that of L-6-[^{18}F]fluorodopa. Third, whereas significant quantities of radiofluorinated *O*-methyl-L-dopa are detected in plasma following L-6-[^{18}F]fluorodopa injection (Melega et al., 1991*a*,*b*), no methylated products are observed following injection of L-[^{18}F]fluoro-*m*-tyrosines.

The uptake of radiofluorinated *O*-methyl-L-dopa is nearly uniform throughout living brain of monkeys (Doudet et al., 1991*a*), healthy human volunteers (Wahl et al., 1994), and patients with Parkinson's disease (Wahl and Nahmias, 1996*a*,*b*), and thus contributes a homogenous layer of non-specific background radioactivity which contaminates the signal in regions of specific L-6-[^{18}F]fluorodopa uptake such as the striatum. Conversely, the major peripheral metabolite of L-[^{18}F]fluoro-*m*-tyrosines, [^{18}F]fluorohydroxyphenylacetic acid (Firnau et al., 1991*a*), does not cross the blood-brain barrier and consequently does not

contribute significantly to tissue radioactivities (Firnau et al., 1991*b*). Therefore, the lack of brain-penetrating peripheral metabolites associated with L-[^{18}F]fluoro-*m*-tyrosines results in increased availability of the tracer for tissue uptake, and reduced levels of background radioactivity in situ. Accordingly, the specific striatal radioactivity following administration of L-[^{18}F]fluoro-*m*-tyrosines is greater than that associated with L-6-[^{18}F]fluorodopa (Hayase et al., 1994; Nahmias et al., 1995), ultimately resulting in higher signal-to-noise ratios, improved contrast in positron emission tomography images, and more accurate delineation of the striatum and surrounding regions.

There remains some uncertainty regarding the fate of the metabolic products of L-[^{18}F]fluoro-*m*-tyrosines in living brain. In vitro, the decarboxylation product [^{18}F]fluoro-*m*-tyramine is a substrate for the synaptic vesicle amine transporter (Barrio et al., 1995), and the chromaffin granule amine transporter and pre-synaptic dopamine uptake transporter (Endres et al., 1997), but no such results have been demonstrated in vivo. For all three transporters, the transport rates for [^{18}F]fluoro-*m*-tyramine were significantly lower than those estimated for 6-[^{18}F]fluorodopamine, suggesting that the intravesicular and intraneuronal uptake of catecholamines is significantly dependant on the catechol moiety. Furthermore, the method of clearance of [^{18}F]fluorohydroxyphenylacetic acid, formed by the sequential actions of dopa decarboxylase and monoamine oxidase, across the neuronal membrane is unknown. The very slow clearance of [^{18}F]fluorohydroxyphenylacetic acid, which likely contributes to the trapping of ^{18}F radioactivity over the time frame of a positron emission tomography study, may result from a combination of slow brain egress, slow sulfoconjugation, and slow brain egress of the sulfoconjugate (DeJesus et al., 1997).

FIRST ARTICLE

The objective of this work was to investigate the biological accuracy of a compartmental model of the uptake and metabolism of L-6-[^{18}F]fluorodopa in living rat brain. The model consisted of a series of first-order differential equations, describing two plasma compartments and five brain tissue compartments. A simulated plasma L-6-[^{18}F]fluorodopa input function, along with kinetic constants previously estimated in rat following intravenous injection of L-6-[^{18}F]fluorodopa, were used as inputs to calculate the radioactivities of L-6-[^{18}F]fluorodopa and its several radiolabelled metabolites (*O*-methyl-L-6-[^{18}F]fluorodopa, 6-[^{18}F]fluorodopamine, L-3,4-dihydroxy-6-[^{18}F]fluorophenylacetic acid, and 6-[^{18}F]fluorohomovanillic acid) for tracer circulation times up to 120 min. Calculated metabolite radioactivities were expressed as fractions of total radioactivity to correct for individual variations in the amount of injected tracer. Calculated metabolite fractions were then compared with corresponding analytic measurements obtained in vivo in living rat brain based on chromatographic fractionation of radiolabelled metabolites in striatal tissue extracts. In so doing, we found evidence to suggest the sequestration of 6-[^{18}F]fluorodopamine in synaptic storage vesicles of living rat brain. We therefore attempted to model the distribution of 6-[^{18}F]fluorodopamine between the cytosol and a vesicular pool, a compartment hitherto absent from biological models of L-6-[^{18}F]fluorodopa metabolism.

This article, entitled "*On the accuracy of an [^{18}F]FDOPA compartmental model: evidence for vesicular storage of [^{18}F]fluorodopamine in vivo*" by Paul Deep, Albert Gjedde, and Paul Cumming, has been published in the Journal of Neuroscience Methods (76:157-165, 1997).

On the accuracy of an [^{18}F]FDOPA compartmental model: evidence for vesicular storage of [^{18}F]fluorodopamine in vivo

Paul Deep [a], Albert Gjedde [b], and Paul Cumming [a]

[a] *Montreal Neurological Institute, McGill University, 3801 University St., Montreal, Quebec H3A 2B4, Canada*
[b] *PET Center, Aarhus University Hospital, Aarhus, Denmark*

Abstract

The biological accuracy of a nonlinear compartmental model describing the in vivo kinetics of L-3,4-dihydroxy-6-[^{18}F]fluorophenylalanine ([^{18}F]FDOPA) metabolism was investigated. Tissue activities for [^{18}F]FDOPA and its labelled metabolites 3-*O*-methyl-[^{18}F]FDOPA ([^{18}F]OMFD), 6-[^{18}F]fluorodopamine ([^{18}F]FDA), L-3,4-dihydroxy-6-[^{18}F]fluorophenylacetic acid ([^{18}F]FDOPAC), and 6-[^{18}F]fluorohomovanillic acid ([^{18}F]FHVA) were calculated using a plasma [^{18}F]FDOPA input function, and kinetic constants estimated previously by chromatographic fractionation of ^{18}F-labelled compounds in plasma and brain extracts from rat. Present data accurately reflected the measured radiochemical composition in rat brain for tracer circulation times past 10 min. We formulated the hypothesis that the discrepancy between calculated and measured fractions of [^{18}F]FDOPA and the deaminated metabolite [^{18}F]FDOPAC at times earlier than 10 min reflected storage of [^{18}F]FDA in vesicles without monoamine oxidase. This hypothesis explained the initially rapid appearance of [^{18}F]FDOPAC in striatum by delayed transfer of [^{18}F]FDA from cytosol into vesicles. We conclude that the simpler model of [^{18}F]FDOPA compartmentation is accurate when the cytosolic and vesicular fractions of [^{18}F]FDA are at steady-state; the approach to equilibrium has a time constant of 15-30 min. The present model is valid for positron emission tomography studies of [^{18}F]FDOPA metabolism in living brain.

1. Introduction

Positron emission tomography (PET) following intravenous injection of L-3,4-dihydroxy-6-[^{18}F]fluorophenylalanine ([^{18}F]FDOPA), a radiolabelled analog of the endogenous amino acid L-3,4-dihydroxyphenylalanine (L-DOPA), reveals a time-dependent and specific accumulation of radioactivity in the basal ganglia (Garnett et al., 1983*b*). Models of tracer uptake and metabolism are fitted to measured activity data to estimate kinetic constants of physiological processes in vivo. Assuming irreversible trapping of radioactivity in brain, a unilinear graphical method (Gjedde, 1981, 1982; Patlak et al., 1983; Patlak and Blasberg, 1985) has been used to determine the net influx of [^{18}F]FDOPA into brain (Martin et al., 1989; Sawle et al., 1990). Alternatively, multilinear or nonlinear regression methods (Gjedde et al., 1991; Huang et al., 1991; Kuwabara et al., 1993; Wahl and Nahmias, 1996*a*) have yielded sets of blood-brain transfer coefficients for [^{18}F]FDOPA and 3-*O*-methyl-[^{18}F]FDOPA ([^{18}F]OMFD), and regional activities of L-DOPA decarboxylase (DDC; EC 4.1.1.28), the enzyme that converts [^{18}F]FDOPA to 6-[^{18}F]fluorodopamine ([^{18}F]FDA; Firnau et al., 1975).

Multilinear or nonlinear regression to [^{18}F]FDOPA activity data is computationally demanding but yields kinetic constants of several physiological processes. Conversely, the unilinear method is computationally simple, but valid only within certain times (~ 10-90 min) because of its unilinearity. It yields a single kinetic constant that is the composite of [^{18}F]FDOPA influx, efflux, and decarboxylation. The choice of method depends on the duration of tracer circulation and the desired kinetic information, but in all cases, the validity of the method can only be substantiated by the agreement between predicted and measured metabolite concentrations.

[^{18}F]FDOPA has metabolites analogous to those of the endogenous amino acid, as shown by high-performance liquid chromatography (HPLC) fractionation of ^{18}F-labelled compounds in plasma and brain extracts, from rat (Cumming et al., 1987*a*,*b*, 1988, 1994*a*, 1995*b*; Melega et al., 1990*a*,*b*; Reith et al., 1990) and primate (Boyes et al., 1986; Firnau et al., 1987, 1988; Melega et al., 1990*b*, 1991*a*,*b*; Cumming et al., 1993). Therefore, [^{18}F]FDOPA is a tracer of L-DOPA in vivo, whose tissue disposition can be predicted by

models which incorporate the major physiological processes responsible for L-DOPA uptake, metabolism and clearance.

The goal of this study is to test the validity of the present nonlinear compartmental model for kinetic analysis of [^{18}F]FDOPA activity data measured by PET in living brain, by demonstrating that it accurately predicts the concentrations of [^{18}F]FDOPA and its several labelled metabolites measured in vivo in rat by HPLC.

2. Materials and methods

2.1. [^{18}F]FDOPA compartmental Model

The in vivo metabolic pathway for [^{18}F]FDOPA, including the associated kinetic constants, is summarized in Fig. 1. Following injection into the venous circulation, [^{18}F]FDOPA is *O*-methylated (k_0^{FDOPA}, min^{-1}) by catechol-*O*-methyltransferase (COMT; EC 2.1.1.6) to form its principal metabolite [^{18}F]OMFD. Renal elimination clears [^{18}F]FDOPA and [^{18}F]OMFD from the circulation as a first-order process (k_{-1}^{FDOPA} and k_{-1}^{OMFD}, min^{-1}). The transporter of large neutral amino acids brings both tracers into brain (K_1^{FDOPA} and K_1^{OMFD}, ml g^{-1} per min) and out of brain (k_2^{FDOPA} and k_2^{OMFD}, min^{-1}) by facilitated diffusion. In brain, [^{18}F]FDOPA is *O*-methylated by COMT (k_5^{FDOPA}, min^{-1}) to form [^{18}F]OMFD, or decarboxylated by DDC (k_3^{FDOPA}, min^{-1}) to form [^{18}F]FDA, which is not directly cleared from brain. [^{18}F]FDA is sequestered in vesicles (circle) where it is protected from catabolism. In the cytosol, [^{18}F]FDA is deaminated (k_7^{FDA}, min^{-1}) by monoamine oxidase (MAO; EC 1.4.3.4) to yield L-3,4-dihydroxy-6-[^{18}F]fluorophenylacetic acid ([^{18}F]FDOPAC), which is *O*-methylated by COMT (k_{11}^{FDOPAC}, min^{-1}) to form 6-[^{18}F]fluorohomovanillic acid ([^{18}F]FHVA). The acidic metabolites [^{18}F]FDOPAC (k_{9a}^{FDOPAC}, min^{-1}) and [^{18}F]FHVA (k_{9b}^{FHVA}, min^{-1}) diffuse out of brain into cerebrospinal fluid (Hammerstad et al., 1993), and back into the venous circulation.

The present model thus identifies two plasma compartments ([^{18}F]FDOPA and [^{18}F]OMFD) and five brain compartments ([^{18}F]FDOPA, [^{18}F]OMFD, [^{18}F]FDA, [^{18}F]FDOPAC, and [^{18}F]FHVA). Estimates of brain kinetic constants (Table 1; Cumming

et al., 1994*a*) were obtained from striatum, since nigrostriatal dopaminergic terminals are the primary site of L-DOPA uptake and metabolism (Hefti et al., 1981; Melamed et al., 1981).

2.2. Plasma [^{18}F]FDOPA activity

The plasma [^{18}F]FDOPA activity [$C_a^{FDOPA}(T)$; dpm μl^{-1}] served as the input function for the subsequent calculation of metabolite activities in brain (see below). It was calculated as a single power function (Matlab, © The MathWorks, Natick, MA, USA),

$$C_a^{FDOPA}(T) = AT^{(\frac{1}{\alpha}-1)} \qquad (1)$$

where A is an arbitrary scaling constant (1000 dpm μl^{-1} min^{-1}), T is the tracer circulation time (min; defined as the time elapsed following tracer injection), and α is a dimensionless constant (2.2; Deep et al., 1997*b*) obtained as the linear regression slope of a plot of pharmacokinetic circulation time versus T for a population of rats administered [^{3}H]DOPA (Cumming et al., 1995*a*). A straight line between zero activity at injection time and peak activity at 0.5 min described the rapid increase in plasma [^{18}F]FDOPA concentration immediately after tracer injection.

2.3. Plasma [^{18}F]OMFD and brain tissue activities

Assuming first-order kinetics and instant equilibration between the sites of metabolite formation and clearance, the plasma [^{18}F]OMFD activity [$C_a^{OMFD}(T)$; dpm μl^{-1}] and the brain tissue activities (dpm mg^{-1}) of [^{18}F]FDOPA [$M^{FDOPA}(T)$], [^{18}F]OMFD [$M^{OMFD}(T)$], [^{18}F]FDA [$M^{FDA}(T)$], [^{18}F]FDOPAC [$M^{FDOPAC}(T)$], and [^{18}F]FHVA [$M^{FHVA}(T)$], all change with time according to the general compartmental equation,

$$\frac{d[Z_i(t)]}{dt} = \sum_1^m [k_{in}^m Z_{i-1}^m(t)] - [\sum_1^n k_{out}^n] Z_i(t) \qquad (2)$$

where $Z_i(t)$ is the time-activity curve of the metabolite, $Z_{i-1}^m(t)$ is the time-activity curve of the mth precursor compound, k_{in}^m is the kinetic constant of the process that converts the mth

precursor into metabolite, and k_{out}^{n} is the kinetic constant of the nth process that removes the metabolite from the compartment. Using $C_a^{FDOPA}(T)$ (Eq. (1)) as the input function, integration of Eq. (2) for each metabolite compartment yielded the following activities,

$$C_a^{OMFD}(T) = k_0^{FDOPA}\int_0^T C_a^{FDOPA}(t)e^{k_{-1}^{OMFD}(T-t)}dt \quad (3)$$

$$M^{FDOPA}(T) = K_1^{FDOPA}\int_0^T C_a^{FDOPA}(t)e^{-(k_2^{FDOPA}+k_3^{FDOPA}+k_5^{FDOPA})(T-t)}dt \quad (4)$$

$$M^{OMFD}(T) = K_1^{OMFD}\int_0^T C_a^{OMFD}(t)e^{-k_2^{OMFD}(T-t)}dt + k_5^{FDOPA}\int_0^T M^{FDOPA}(t)e^{-k_2^{OMFD}(T-t)}dt \quad (5)$$

$$M^{FDA}(T) = k_3^{FDOPA}\int_0^T M^{FDOPA}(t)e^{-k_7^{FDA'}(T-t)}dt \quad (6)$$

$$M^{FDOPAC}(T) = k_7^{FDA'}\int_0^T M^{FDA}(t)e^{-(k_{9a}^{FDOPAC}+k_{11}^{FDOPAC})(T-t)}dt \quad (7)$$

$$M^{FHVA}(T) = k_{11}^{FDOPAC}\int_0^T M^{FDOPAC}(t)e^{-k_{9b}^{FHVA}(T-t)}dt \quad (8)$$

Total activity in plasma [$C_a^{total}(T)$] was calculated as the sum of Eqs. (1) and (3),

$$C_a^{total}(T) = C_a^{FDOPA}(T) + C_a^{OMFD}(T) \quad (9)$$

The omission of plasma compartments for [^{18}F]FDA, [^{18}F]FDOPAC, and [^{18}F]FHVA is consistent with the results of HPLC fractionations of ^{18}F-labelled compounds in plasma extracts from rats (Cumming et al., 1987*a,b*, 1988, 1994*a*, 1995*b*; Melega et al., 1990*a,b*; Reith et al., 1990) and primates (Boyes et al., 1986; Melega et al., 1990*b*, 1991*a,b*; Cumming et al., 1993) treated with carbidopa, a peripheral DDC inhibitor, which failed to

detect significant amounts of these compounds.

Total activity in striatum [$M^{total}(T)$] was calculated as the sum of Eqs. 4-8,

$$M^{total}(T) = M^{FDOPA}(T) + M^{OMFD}(T) + M^{FDA}(T) + M^{FDOPAC}(T) + M^{FHVA}(T) + V_0^{FDOPA} C_a^{FDOPA}(T) + V_0^{OMFD} C_a^{OMFD}(T) \quad \textbf{(10)}$$

No brain compartment for labelled 3-methoxytyramine, a precursor of [^{18}F]FHVA formed by *O*-methylation of [^{18}F]FDA, was included because the majority of HVA in rat brain is derived from DOPAC (Westerink and Spaan, 1982*a*; Cumming et al., 1992). The final two terms in Eq. (10) account for the vascular components of tissue activity, where V_0^{FDOPA} and V_0^{OMFD} are the volumes of the vascular compartments of [^{18}F]FDOPA and [^{18}F]OMFD, respectively.

All metabolite activities were calculated for 120 min of tracer circulation, using the kinetic constants estimated for [^{18}F]FDOPA in rat (Cumming et al., 1994*a*; Table 1), with the following assumptions:

- V_0^{FDOPA} and V_0^{OMFD} were set to 0, since the rat brains were assumed to be devoid of blood prior to HPLC fractionation.
- k_{9a}^{FDOPAC} was assumed to be equal to the estimate of k_{9b}^{FHVA} (0.12 min^{-1}).
- k_5^{FDOPA} was assumed to be equal to the corresponding estimate for [^{3}H]DOPA in rat (0.06 min^{-1}; Cumming et al., 1995*a*), which was the average of estimates from five brain regions, assuming a homogenous distribution of COMT activity throughout rat brain (Broch and Fonnum, 1972; Rivett et al., 1983; Roth, 1992).

2.4. Fractional metabolite activities

The calculated plasma metabolite activities (Eqs. (1) and (3)) were expressed as fractions of total plasma activity by division by Eq. (9); the calculated striatal metabolite activities (Eqs. (4)-(8)) were expressed as fractions of total striatal activity by division by Eq. (10). The resulting metabolite fractions facilitated comparison of present estimates with literature results. Absolute metabolite activities could not be compared because of varying amounts of injected [^{18}F]FDOPA.

3. Results

The calculated metabolite activities and fractions in plasma and striatum are shown in Fig. 2. In striatum, the activities of [^{18}F]FDOPA, [^{18}F]OMFD, [^{18}F]FDA, [^{18}F]FDOPAC, and [^{18}F]FHVA peaked at 3, 89, 21, 28, and 39 min, respectively.

The present calculations predicted ^{18}F-labelled metabolite fractions to within 10% of those measured by HPLC in 83 out of 96 comparisons with the literature (Cumming et al., 1987*a,b*, 1988; Melega et al., 1990*a,b*; Table 2). The largest discrepancies between calculated and measured data occurred at early time points: the calculations over-estimated striatal [^{18}F]FDOPA by 33% at 5 min and 14% at 10 min, and under-estimated striatal [^{18}F]FDOPAC by 29% at 5 min.

4. Discussion

4.1. Model applicability

In the compartmental model, species differences between rat and human with respect to the handling of [^{18}F]FDOPA will be reflected in the magnitudes of kinetic constant estimates (Table 1). Since [^{18}F]FDOPA follows the same in vivo metabolic pathways (Fig. 1) in rat and primate, activity data measured in the two species reflect the same compartments, albeit of different sizes. Therefore, we propose that the present model can be used with equal accuracy in analyzing activity data from rat and human. We have confirmed this by successfully fitting the model to [^{3}H]DOPA autoradiographic data in rats (Deep et al., 1997*b*) and [^{18}F]FDOPA/PET data in humans (Gjedde et al., 1991; Kuwabara et al., 1993).

4.2. Comparison of calculated and measured data

In general, qualitative and quantitative profiles of [^{18}F]FDOPA metabolite fractions calculated by the present model were in close agreement with those measured by HPLC analyses of labelled plasma and brain extracts in rat, for circulation times past 10 min. The relative time of the peak activity of [^{18}F]OMFD does not reflect its formation in vivo before

[^{18}F]FDOPAC or [^{18}F]FHVA, since the striatal [^{18}F]OMFD activity (Eq. (4)) is the sum of two components: one originating in the transfer of plasma [^{18}F]OMFD into brain, and the other originating from COMT activity in brain. The time courses of metabolite fractions (Fig. 2) in plasma and striatum agreed excellently with corresponding measurements in rat (Cumming et al., 1987*a*; Melega et al., 1990*a*).

Uncertainty about the estimate of COMT activity in brain with respect to [^{18}F]FDOPA (k_5^{FDOPA}), which was set equal to the corresponding estimate for [^{3}H]DOPA (0.06 min^{-1}; Cumming et al., 1995*a*), may explain the consistent over-estimation of the calculated striatal [^{18}F]OMFD activities (Table 2). Fluorination of L-DOPA significantly reduces its affinity for COMT in vitro (Creveling and Kirk, 1985; Firnau et al., 1988), so k_5^{FDOPA} may be lower for [^{18}F]FDOPA than [^{3}H]DOPA. Other significant discrepancies (> 10%) between calculated and measured metabolite fractions likely reflect the simplicity of the biological model, compared to real brain. The present model excludes two known brain compartments, corresponding to (i) [^{18}F]FDA-sulfate, which has been detected at concentrations comparable to those of [^{18}F]FDOPAC and [^{18}F]FHVA in both rat (Melega et al., 1990*a*,*b*) and primate (Melega et al., 1990*b*, 1991*a*,*b*), and (ii) the vesicular fraction of [^{18}F]FDA. There is considerable evidence to suggest that [^{18}F]FDA, like endogenous dopamine (Leviel et al., 1989; Pothos et al., 1996) and perhaps L-DOPA (Opacka-Juffry and Brooks, 1995), is stored in vesicles. An ^{19}F nuclear magnetic resonance examination of nerve-ending microsacs, isolated from guinea pig striatum and incubated with fluorinated amines, detected a strong signal corresponding to [^{18}F]FDA, with a minor signal corresponding to [^{18}F]FDOPAC (Diffley et al., 1983). [^{18}F]FDA is released from dopaminergic nerve terminals along with dopamine following depolarization by potassium (Chiueh et al., 1983). Furthermore, depletion of striatal activity was observed by [^{18}F]FDOPA/PET in monkeys treated with reserpine (Garnett et al., 1983*a*), a drug known to discharge dopamine from pre-synaptic storage vesicles. We therefore attempted to model the vesicular fraction of [^{18}F]FDA in vivo.

4.3. Modelling the vesicular fraction of [^{18}F]FDA

By definition, the apparent MAO activity measured in vivo assuming a homogeneous distribution of [^{18}F]FDA in brain [$k_7^{FDA'}(T)$] is proportional to the fraction of [^{18}F]FDA in the cytosol (Cumming et al., 1995*a*),

$$k_7^{FDA'}(T) = \left[\frac{M_{cyt}^{FDA}(T)}{M_{cyt}^{FDA}(T) + M_{ves}^{FDA}(T)}\right] k_7^{FDA} \qquad \textbf{(11)}$$

where $M_{cyt}^{FDA}(T)$ is the concentration of [^{18}F]FDA in the cytosolic compartment, $M_{ves}^{FDA}(T)$ is the concentration of [^{18}F]FDA in the vesicular compartment, and k_7^{FDA} is the true MAO activity in vivo assuming a homogenous distribution of [^{18}F]FDA within the compartment containing MAO. Eq. (11) predicts that apparent MAO activity is not constant during a tracer experiment: at early times prior to vesicular trapping of [^{18}F]FDA, $k_7^{FDA'}(T)$ equals k_7^{FDA}. The magnitude of $k_7^{FDA'}(T)$ then declines as [^{18}F]FDA is sequestered in vesicles, until equilibrium between the cytosolic and vesicular compartments is reached.

According to Eq. (2), the activities of the cytosolic and vesicular [^{18}F]FDA compartments are given by,

$$\frac{d[M_{cyt}^{FDA}(t)]}{dt} = k_3^{FDOPA} M^{FDOPA} + k_{out}^{FDA} M_{ves}^{FDA} - (k_7^{FDA} + k_{in}^{FDA}) M_{cyt}^{FDA} \qquad \textbf{(12)}$$

$$\frac{d[M_{ves}^{FDA}(t)]}{dt} = k_{in}^{FDA} M_{cyt}^{FDA} - k_{out}^{FDA} M_{ves}^{FDA} \qquad \textbf{(13)}$$

where k_{in}^{FDA} is the rate constant for transfer of [^{18}F]FDA into vesicles, and k_{out}^{FDA} is the rate constant for release of [^{18}F]FDA from vesicles back into the cytosolic compartment. At late tracer circulation times, [^{18}F]FDA synthesis declines toward zero and the system approaches equilibrium (T=T_{eq}), in which case Eq. (13) reduces to,

$$\frac{k_{in}^{FDA}}{k_{out}^{FDA}} = \frac{M_{ves}^{FDA}(T_{eq})}{M_{cyt}^{FDA}(T_{eq})} \quad \textbf{(14)}$$

The magnitudes of k_{in}^{FDA} and k_{out}^{FDA} therefore determine the relative proportions of [^{18}F]FDA in the cytosolic and vesicular compartments in vivo at equilibrium. To our knowledge the only measurement of this ratio to date was made in vitro by Chien et al. (1990) in a giant dopamine neuron of the snail *Planorbis corneus*; voltametric techniques detected that at least 98% of intracellular dopamine is bound and not directly exchangeable with dopamine in the cytoplasm at equilibrium. It is currently unknown if a similar distribution occurs in dopamine neurons of the rat.

To obtain the first in vivo estimates of k_{in}^{FDA} and k_{out}^{FDA}, we integrated Eqs. 12-13,

$$M_{cyt}^{FDA}(T) = k_3^{FDOPA}\int_0^T M^{FDOPA}(t)e^{-(k_7^{FDA}+k_{in}^{FDA})(T-t)}dt + k_{out}^{FDA}\int_0^T M_{ves}^{FDA}(t)e^{-(k_7^{FDA}+k_{in}^{FDA})(T-t)}dt \quad \textbf{(15)}$$

$$M_{ves}^{FDA}(T) = k_{in}^{FDA}\int_0^T M_{cyt}^{FDA}(t)e^{-k_{out}^{FDA}(T-t)}dt \quad \textbf{(16)}$$

The sum of Eqs. (15) and (16), equal to total [^{18}F]FDA activity in brain, was fitted by least-squares nonlinear regression to [^{18}F]FDA activities measured in rat striatum (Cumming et al., 1987*a*; Table 2), with the striatal [^{18}F]FDOPA curve as the input function. To solve for k_3^{FDOPA}, k_{in}^{FDA}, and k_{out}^{FDA}, it was necessary to fix the magnitude of k_7^{FDA} to reduce parameterization. However, the magnitude of k_7^{FDA} in vivo in striatal dopamine neurons is unknown, so we varied k_7^{FDA} over a range of fixed input values. At $k_7^{FDA} > 0.6$ min^{-1}, fits did not converge; complete results of these analyses are summarized in Table 3.

Present estimates of k_{out}^{FDA} were not significantly different from zero. But transfer of dopamine from cytosol to vesicles in vivo is not irreversible (Leviel et al., 1989), so k_{out}^{FDA} must have a small positive value. With fixed k_7^{FDA} values between 0.1-0.4 min^{-1}, inclusion

of the vesicular compartment accounted for the large discrepancies between measured and calculated data at early times. In this range, estimates of DDC activity (k_3^{FDOPA}) were increased by 12-35%, relative to the HPLC estimate (0.17 min^{-1}; Cumming et al., 1994*a*). By under-estimating k_3^{FDOPA}, the exclusion of vesicular storage of [^{18}F]FDA from the present model may contribute to the over-estimation of [^{18}F]FDOPA concentrations in striatum at early times (Table 2). The magnitude of k_{in}^{FDA} suggests that newly-formed [^{18}F]FDA is transferred to the vesicular compartment with a half-life of 12-34 min (calculated as $0.693/k_{in}^{FDA}$). Therefore at early times, the majority of [^{18}F]FDA is in the cytosolic compartment and so unprotected from metabolism by MAO, accounting for the high proportion of [^{18}F]FDOPAC measured at 5 min (31%, Table 2). Previous estimates of apparent MAO activity (Table 1) are several-fold lower than the valid range of k_7^{FDA} input values, consistent with the initial under-estimation of [^{18}F]FDOPAC concentrations, which became insignificant at times after 10 min (Table 2).

5. Conclusion

The present study compared the time courses of [^{18}F]FDOPA metabolite fractions calculated by a compartmental model of [^{18}F]FDOPA blood-brain transfer and metabolism, with those measured in vivo by chromatographic fractionation of ^{18}F-labelled compounds in plasma and striatal tissue extracts in rat. Based on the general agreement between calculated and measured data, we conclude that the model is biologically accurate and therefore valid for analysis of [^{18}F]FDOPA activity data measured in living brain by PET. The large discrepancies between calculated and measured data at early times (< 10 min) could be explained by incorporation of a vesicular compartment for [^{18}F]FDA into the model, thereby providing indirect evidence for vesicular storage of [^{18}F]FDA in vivo. Present data and methods were insufficient to independently estimate all kinetic constants associated with the distribution of [^{18}F]FDA between the cytosol and vesicles. However, it is likely that the exclusion of vesicular storage from the model does not greatly alter the magnitudes of kinetic constants estimated by regression analysis of PET data, because the long duration of PET studies permits near-equilibration of cytosolic and vesicular [^{18}F]FDA.

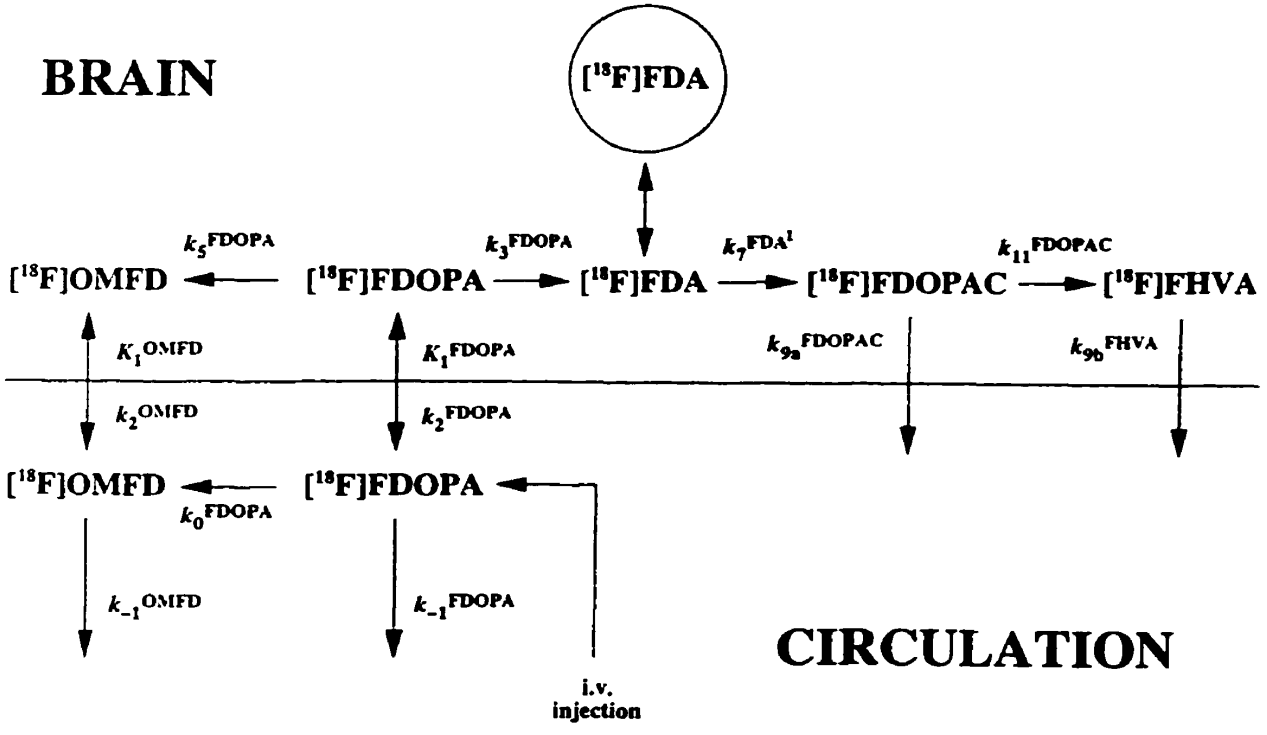

Fig. 1. Schematic summary of [^{18}F]FDOPA blood-brain transfer and metabolism, including the associated kinetic constants. [^{18}F]FDOPA injected intravenously into the circulation is *O*-methylated (k_0^{FDOPA}) by COMT to form [^{18}F]OMFD. Both tracers are subsequently cleared from circulation by renal elimination (k_{-1}^{FDOPA} and k_{-1}^{OMFD}). Both tracers are transferred into brain (K_1^{FDOPA} and K_1^{OMFD}) and out of brain (k_2^{FDOPA} and k_2^{OMFD}) by facilitated diffusion. [^{18}F]FDOPA in brain is *O*-methylated (k_5^{FDOPA}) by COMT to form [^{18}F]OMFD. In brain, [^{18}F]FDOPA is decarboxylated by DDC (k_3^{FDOPA}) to form [^{18}F]FDA, which is not cleared directly from brain. [^{18}F]FDA is sequestered in vesicles (circle) or undergoes oxidative deamination ($k_7^{FDA'}$) by MAO to form [^{18}F]FDOPAC, which is then *O*-methylated (k_{11}^{FDOPAC}) by COMT to yield [^{18}F]FHVA. Both [^{18}F]FDOPAC (k_{9a}^{FDOPAC}) and [^{18}F]FHVA (k_{9b}^{FHVA}) are cleared from brain into cerebrospinal fluid and then back into the circulation.

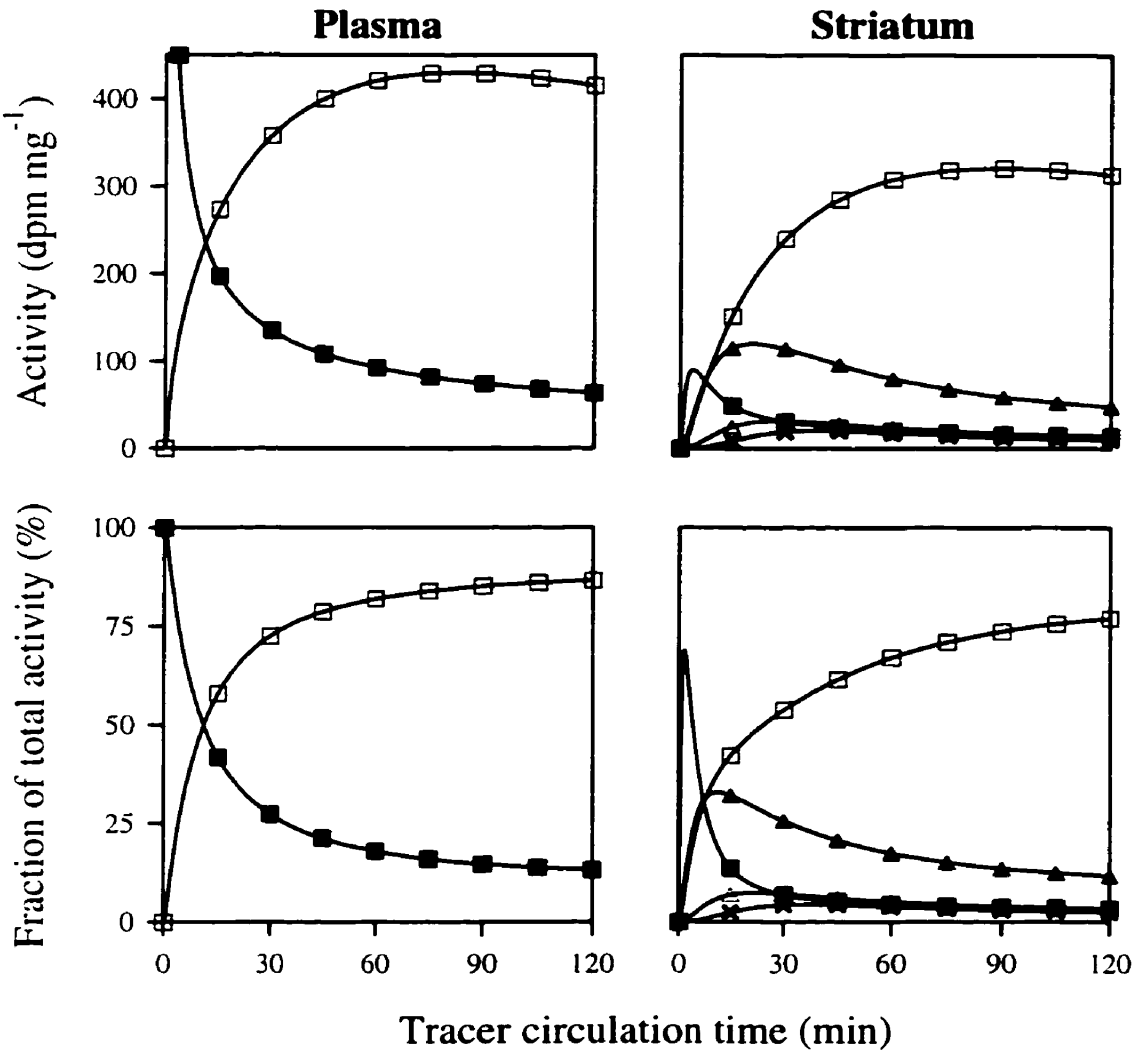

Fig. 2. Calculated activities and fractions in plasma and striatum for [^{18}F]FDOPA (■), [^{18}F]OMFD (□), [^{18}F]FDA (▲), [^{18}F]FDOPAC (Δ), and [^{18}F]FHVA (×) during 120 min of tracer circulation in rat. Plasma [^{18}F]FDOPA activities were calculated with a power function; all other activities were calculated by integration of first-order differential equations, with previous estimates of kinetic constants (Table 1) as inputs. Metabolite fractions were obtained by dividing calculated metabolite activities by total calculated activity.

Table 1
Estimates of [^{18}F]FDOPA kinetic constants in rat

Kinetic constant	Definition	Units	Estimate
V_0^{FDOPA}	Vascular volume of [^{18}F]FDOPA	ml g^{-1}	0.037[a]
V_0^{OMFD}	Vascular volume of [^{18}F]OMFD	ml g^{-1}	-
k_0^{FDOPA}	Rate constant for conversion of [^{18}F]FDOPA to [^{18}F]OMFD in plasma	min^{-1}	0.055
k_{-1}^{OMFD}	Rate constant for clearance of [^{18}F]OMFD from plasma	min^{-1}	0.01
K_1^{FDOPA}	Unidirectional blood-brain clearance of [^{18}F]FDOPA	ml g^{-1} per min	0.07
K_1^{OMFD}	Unidirectional blood-brain clearance of [^{18}F]OMFD	ml g^{-1} per min	0.08
k_2^{FDOPA}	Rate constant for clearance of [^{18}F]FDOPA from brain	min^{-1}	0.10
k_2^{OMFD}	Rate constant for clearance of [^{18}F]OMFD from brain	min^{-1}	0.11
k_3^{FDOPA}	Rate constant for conversion of [^{18}F]FDOPA to [^{18}F]FDA in brain	min^{-1}	0.17
k_5^{FDOPA}	Rate constant for conversion of [^{18}F]FDOPA to [^{18}F]OMFD in brain	min^{-1}	-
k_7^{FDA}	Rate constant for conversion of [^{18}F]FDA to [^{18}F]FDOPAC in brain	min^{-1}	0.055
k_{11}^{FDOPAC}	Rate constant for conversion of [^{18}F]FDOPAC to [^{18}F]FHVA in brain	min^{-1}	0.083
k_{9a}^{FDOPAC}	Rate constant for clearance of [^{18}F]FDOPAC from brain	min^{-1}	-
k_{9b}^{FHVA}	Rate constant for clearance of [^{18}F]FHVA from brain	min^{-1}	0.12

All kinetic constants were estimated by chromatographic fractionation of ^{18}F-labelled compounds in plasma extracts and striatal tissue following bolus i.v. injection of [^{18}F]FDOPA (Cumming et al., 1994*a*). Some estimates were unavailable (-); see Section 2 for explanations.

[a] Cumming et al., 1995*b*.

Table 2

[^{18}F]FDOPA metabolite fractions in plasma and striatum of rat

		Time (min)											
Metabolite	Reference	2.5	5	10	15	20	25	30	45	60	75	90	120
Plasma [^{18}F]FDOPA	present study	84	70	52	42	35	31	27	21	18	16	15	13
	Cumming et al., 1988	-	-	37	-	-	-	-	-	9	-	-	-
	Melega et al., 1990*a*	80	-	62	42	-	-	24	-	14	-	-	-
	Melega et al., 1990*b*	-	-	-	-	-	-	24	-	-	-	-	-
Plasma [^{18}F]OMFD	present study	16	30	48	58	65	69	73	79	82	84	85	87
	Cumming et al., 1988	-	-	45	-	-	-	-	-	72	-	-	-
	Melega et al., 1990*a*	20	-	38	58	-	-	72	-	81	-	-	-
	Melega et al., 1990*b*	-	-	-	-	-	-	70	-	-	-	-	-
Striatal [^{18}F]FDOPA	present study	62	42	22	14	10	8	7	5	4	4	4	3
	Cumming et al., 1987*a*	-	11	8	10	5	6	3	7	5	1	4	3
	Cumming et al., 1987*b*	-	-	-	-	-	-	4	-	4	-	4	-
	Cumming et al., 1988	-	-	12	-	-	-	-	-	3	-	-	-
	Melega et al., 1990*a*	-	-	-	7	-	-	2	-	2	-	-	-
	Melega et al., 1990*b*	-	-	-	-	-	-	2	-	-	-	-	-
Striatal [^{18}F]OMFD	present study	12	23	36	42	47	51	54	62	67	71	74	77
	Cumming et al., 1987*a*	-	18	32	37	36	41	45	50	50	49	58	69
	Cumming et al., 1987*b*	-	-	-	-	-	-	50	-	53	-	73	-
	Cumming et al., 1988	-	-	31	-	-	-	-	-	52	-	-	-
	Melega et al., 1990*a*		-	-	40	-	-	50	-	51	-	-	-
	Melega et al., 1990*b*	-	-	-	-	-	-	49	-	-	-	-	-
Striatal [^{18}F]FDA	present study	16	26	33	32	30	27	25	21	17	15	14	12
	Cumming et al., 1987*a*	-	23	24	25	20	19	21	18	21	17	15	7
	Cumming et al., 1987*b*	-	-	-	-	-	-	20	-	18	-	11	-
	Melega et al., 1990*a*	-	-	-	37	-	-	33	-	36	-	-	-
	Melega et al., 1990*b*	-	-	-	-	-	-	29	-	-	-	-	-
Striatal [^{18}F]FDOPAC	present study	1	2	5	7	7	7	7	6	5	4	4	3
	Cumming et al., 1987*a*	-	31	10	10	8	9	8	11	6	5	5	3
	Cumming et al., 1987*b*	-	-	-	-	-	-	6	-	5	-	4	-
	Melega et al., 1990*a*	-	-	-	5	-	-	5	-	4	-	-	-
	Melega et al., 1990*b*	-	-	-	-	-	-	7	-	-	-	-	-
Striatal [^{18}F]FHVA	present study	0	0	1	2	3	4	4	4	4	3	3	2
	Melega et al., 1990*a*	-	-	-	2	-	-	5	-	2	-	-	-
	Melega et al., 1990*b*	-	-	-	-	-	-	7	-	-	-	-	-

All results are percentages, determined as [(^{18}F metabolite activity) / (total regional ^{18}F activity) x 100]. A dash (-) indicates that the metabolite fraction was not given or could not be calculated with the given data at that time point.

Table 3

Estimates of rate constants (min^{-1}) for the distribution of cerebral [^{18}F]FDA between cytosolic and vesicular compartments, as a function of MAO activity (k_7^{FDA})

k_7^{FDA}	k_3^{FDOPA}	k_m^{FDA}	k_{out}^{FDA}
0.1	0.19 ± 0.01	0.02 ± 0.01	0.06 ± 0.07
0.2	0.24 ± 0.02	0.04 ± 0.02	0.05 ± 0.07
0.3	0.23 ± 0.03	0.05 ± 0.02	0.04 ± 0.05
0.4	0.20 ± 0.04	0.06 ± 0.02	0.03 ± 0.04
0.5	0.17 ± 0.04	0.07 ± 0.02	0.02 ± 0.03
0.6	0.14 ± 0.04	0.08 ± 0.02	0.01 ± 0.02
0.7	-	-	-

Results are best estimates ± 95% confidence intervals, obtained by nonlinear regression of the sum of Eqs. (15) and (16) to [^{18}F]FDA activities measured in rat striatum (Cumming et al., 1987*a*). To reduce model parameterization, the value of k_7^{FDA} was fixed as an input constant. Analyses were performed over a range of k_7^{FDA} values; fits did not converge for all $k_7^{FDA} > 0.6$ min^{-1}.

SECOND ARTICLE

In this study, we present an autoradiographic method for the assay of [^{3}H]dopa uptake and metabolism in living rat brain, based on the analysis of combined metabolite pools in a time-series of static autoradiograms. This approach is in contrast to previous methods for investigating the in vivo kinetics of radiolabelled L-dopa in the rat, which involved analyzing the radioactivities of individual metabolite pools separated by chromatographic fractionation of cerebral tissue samples following intravenous injection of tracer. We estimated the following kinetic constants in rat brain: (i) the blood-brain transfer coefficient of [^{3}H]dopa, (ii) dopa decarboxylase activity with respect to [^{3}H]dopa, and (iii) monoamine oxidase activity with respect to [^{3}H]dopamine, by compartmental modelling of total cerebral radioactivities in a time-series of autoradiograms from right cerebral hemispheres of rat. Present autoradiographic results were compared for the first time with previously published chromatographic estimates from the left hemispheres of the same rats. Furthermore, we tested three distinct [^{3}H]dopa compartmental models (based on the corresponding L-6-[^{18}F]fluorodopa models), to determine their suitability for corresponding assays of dopa decarboxylase activity in living human brain by positron emission tomography.

This article, entitled "*The kinetic behaviour of [^{3}H]dopa in living rat brain investigated by compartmental modelling of static autoradiograms*" by Paul Deep, Hiroto Kuwabara, Albert Gjedde, and Paul Cumming, has been published in the Journal of Neuroscience Methods (78:157-168, 1997).

The kinetic behaviour of [^{3}H]dopa in living rat brain investigated by compartmental modelling of static autoradiograms

Paul Deep [a], Hiroto Kuwabara [b], Albert Gjedde [c], and Paul Cumming [a]

[a] *Montreal Neurological Institute, McGill University, 3801 University St., Montreal, Quebec H3A 2B4, Canada*
[b] *Department of Neurosurgery, West Virginia University, Morgantown, West Virginia, U.S.A.*
[c] *PET Center, Aarhus University Hospital, Aarhus, Denmark*

Abstract

The kinetic behaviour of [^{3}H]dopa in living rat brain was investigated by compartmental modelling of measured activities from combined metabolite pools in a time-series (180 min) of static autoradiograms from right cerebral hemispheres. Two models of [^{3}H]dopa uptake and metabolism that incorporated the removal of the decarboxylation product, [^{3}H]dopamine, from brain were significantly more accurate than a model in which [^{3}H]dopamine accumulated irreversibly in situ. Present estimates of [^{3}H]dopa kinetic constants were compared to previously published results based on the analysis of measured activities from individual metabolite pools separated by chromatographic fractionation of [^{3}H]dopa metabolites in the left cerebral hemispheres of the same rats. Autoradiographic estimates of dopa decarboxylase activity with respect to [^{3}H]dopa in brain (k_3^{DOPA}) were under-estimated several-fold relative to chromatographic estimates; this discrepancy is explained by post-mortem enzyme activity and omission of biological compartments from the models. However, autoradiographic estimates of the unidirectional blood-brain clearance of [^{3}H]dopa (K_1^{DOPA}) and monoamine oxidase activity with respect to [^{3}H]dopamine in brain (k_7^{DA}) agreed with chromatographic estimates. This concordance represents the first empirical validation of compartmental modelling of autoradiographic data as a method for quantitatively investigating the kinetic behaviour of radiolabelled L-dopa in living mammalian brain.

1. Introduction

Static autoradiograms made from cryostat sections of brain have revealed that the cerebral accumulation of radioactivity in living rats following intravenous injection of [^{3}H]dopa (Liskowsky and Potter, 1985; Cumming et al., 1995*a*, 1997*b*) and [^{14}C]dopa (Horne et al., 1984) is greater in the basal ganglia than in structures containing little activity of dopa decarboxylase (EC 4.1.1.28), the ultimate enzyme in dopamine synthesis. The trapping of labelled decarboxylated metabolites in catecholamine fibres (Deep et al., 1997*a*) is the basis for similar qualitative results in living human brain, first observed by dynamic positron emission tomography with the exogenous dopa decarboxylase substrate L-6-[^{18}F]fluorodopa ([^{18}F]fluorodopa; Garnett et al., 1983*b*). With these autoradiographic techniques, the cerebral concentrations of individual radiolabelled metabolites cannot be measured directly, but are calculated by fitting compartmental models of tracer uptake and metabolism to a time-series of total observed cerebral activities.

Compartmental modelling of brain tissue activities measured by positron emission tomography in humans administered [^{18}F]fluorodopa (Gjedde et al., 1991; Huang et al., 1991; Kuwabara et al., 1993; Dhawan et al., 1996; Ishikawa et al., 1996*b*; Wahl and Nahmias, 1996*a*,*b*) has yielded in vivo estimates of equilibrium distribution volumes and blood-brain transfer coefficients for the tracer and its *O*-methylated derivative, and regional activities of dopa decarboxylase. In living rat, these same kinetic constants have been calculated for [^{3}H]dopa (Cumming et al., 1995*a*,*b*) and [^{18}F]fluorodopa (Cumming et al., 1994*a*, 1995*b*) from the temporal changes in the concentrations of product and precursor pools measured by chromatographic fractionation of labelled metabolites in brain tissue extracts. However, this chromatographic dopa decarboxylase assay has not hitherto been systematically compared with the corresponding assay based on compartmental modelling of total cerebral activities in labelled L-dopa autoradiograms.

The major metabolite of [^{3}H]dopa in circulation and brain is *O*-methyl-[^{3}H]dopa (Melega et al., 1990*a*; Cumming et al., 1995*a*,*b*), generated by catechol-*O*-methyltransferase (EC 2.1.1.6). [^{3}H]Dopa in brain is decarboxylated by dopa decarboxylase to form [^{3}H]dopamine, which is stored in synaptic vesicles (Descarries et al., 1980). Monoamine

oxidase (EC 1.4.3.4) further metabolizes [^{3}H]dopamine in the cytosol to yield 3,4-dihydroxy-[^{3}H]phenylacetic acid ([^{3}H]DOPAC), which is then *O*-methylated by catechol-*O*-methyltransferase to form [^{3}H]homovanillic acid. Whereas no transport mechanism is known to clear [^{3}H]dopamine directly from brain, the acidic metabolites [^{3}H]DOPAC and [^{3}H]homovanillic acid (collectively called [^{3}H]acids) are freely diffusible into cerebrospinal fluid. The total activity measured by [^{3}H]dopa autoradiography reflects the sum of all these physiological processes.

In the present study, we estimate [^{3}H]dopa kinetic constants in living rat brain by compartmental modelling of measured activities from combined metabolite pools in static autoradiograms from right cerebral hemispheres. To validate compartmental modelling of autoradiographic data as a method for investigating the kinetic behaviour of radiolabelled L-dopa in living mammalian brain, present results are compared with previously published results based on the analysis of measured activities from individual metabolite pools separated by chromatographic fractionation of [^{3}H]dopa metabolites in the left cerebral hemispheres of the same rats (Cumming et al., 1995*a*). The compartmental models of [^{3}H]dopa blood-brain clearance and metabolism described herein are based on the several distinct compartmental models used for the analysis of positron emission tomography studies with [^{18}F]fluorodopa in primates (for reviews, see Cumming et al., 1997*c*; Cumming and Gjedde, 1998). Therefore, we also test the influence of model choice on the estimation of [^{3}H]dopa kinetic constants previously defined by analytic methods.

2. Materials and methods

2.1. Autoradiography

In vivo studies were conducted in accordance with the requirements of the McGill Animal Ethics Committee, as described in detail previously (Cumming et al., 1995*a*). Briefly, male Wistar rats (Charles River, n=13) received polyethylene catheters (Clay Adams, 0.965 mm O.D.; Becton Dickenson and Co., Sparks, MD, USA) in the left femoral artery and vein. Rats were immobilized in a plaster body cast, and then administered carbidopa (5 mg

kg^{-1}, i.p.; MS&D, Kirkland, Quebec, Canada) 30 min prior to bolus injection (200 μCi/animal, i.v.) of L-3,4-dihydroxy-[*ring*-2,5,6-^{3}H]phenylalanine ([^{3}H]dopa, 80 Ci $mmol^{-1}$; New England Nuclear, Boston, MA, U.S.A.) to inhibit peripheral decarboxylation of tracer. Rats were decapitated at specific times after tracer injection (5, 10, 15, 30, 45, 60, 90, 120, 150, and 180 min); three rats were sacrificed at 30 min, two at 180 min, and one at all other times. Brains were removed and bisected; left cerebral hemispheres were further dissected and then fractionated by high-performance liquid chromatography to determine the radiochemical composition (Cumming et al., 1995*a*).

Right cerebral hemispheres were frozen, mounted with embedding matrix (Lipshaw, Pittsburgh, PA, U.S.A.), slowly warmed to -20°C in a refrigerated cryostat (HM 500 M, Zeiss), and then cut into a series of 20-μm-thick frontal sections. Each eighth section was placed on a glass coverslip. Tritium-sensitive film (Hyperfilm, Amersham, Oakville, Ontario, Canada) was exposed to these sections along with autoradiographic standards (Amersham) for 6 weeks before development by conventional means. Total regional activity was measured by quantitative densitometry (Imaging Systems, St. Catherines, Ontario, Canada) in (n) sections from the following 9 regions of rat brain: dorsal-medial caudate (10), central caudate (13), nucleus accumbens shell (5), nucleus accumbens body (5), olfactory tubercle (7), amygdala (4), hypothalamus (6), dorsal hippocampus (7), and ventral hippocampus (4). Boundaries between adjacent regions were determined by visual inspection. The regions of interest were circles approximately 2 mm in diameter. Anatomical coordinates of brain sections in the anterior-posterior axis were recorded relative to bregma (Paxinos and Watson, 1982).

To recalibrate the autoradiographic standards (nCi mg^{-1}) relative to plasma activity (dpm μl^{-1}), we measured the autoradiographic density in a reference region (occipital cortex). A portion of adjacent occipital cortex (30 mg) was then dissolved overnight in organic base (1 ml; NSC II, Amersham) and the radioactivity measured (dpm mg^{-1}) by scintillation spectroscopy following addition of scintillation fluid (10 ml; BCS, Amersham). A perchloric acid extract of another portion of occipital cortex was fractionated to determine the fraction of radioactivity due to [^{3}H]H_2O (10-20%). After correction for the presence of [^{3}H]H_2O

(which evaporated from the cryostat sections), the ratio of the activity measured by scintillation spectroscopy to the activity measured by autoradiography in the reference region gave a linear tissue cross-calibration factor (~1000 dpm nCi^{-1}). All autoradiographic densities were then multiplied by this factor to convert to dpm mg^{-1}, thus permitting the use of arterial activities (dpm μl^{-1}) as input functions for the calculation of brain tissue activities (dpm mg^{-1}).

Areas under the measured arterial [^{3}H]dopa curves were calculated for each rat. Corresponding areas under the common simulated arterial [^{3}H]dopa curve (Eq. (1), see below) were divided by the measured integrals to produce a linear plasma correction factor for each rat. Tissue activities in each rat were then multiplied by its respective factor. This normalization allowed the use of common arterial input curves for all rats, in order to (i) correct for scatter in measured data attributable to variations in the individual arterial curves, and (ii) approximate better the methodology of a positron emission tomography scan, in which all data points are measured from the same subject.

2.2. [^{3}H]Dopa compartmental models

The biological pathways traced by [^{3}H]dopa in circulation and brain tissue, including the associated kinetic constants, are illustrated in Fig. 1. In brain regions assumed to have low dopa decarboxylase activity, we used a 2-parameter 2-compartment model (M0) described by the unidirectional blood-brain clearance of [^{3}H]dopa (K_1^{DOPA}, ml g^{-1} per min) and the equilibrium distribution volume of [^{3}H]dopa (V_e^{DOPA}, ml g^{-1}). In brain regions assumed to have high dopa decarboxylase activity, we present three models extended to incorporate the presence of additional compartments. The first model (M1) is a 2-parameter 3-compartment model (Gjedde et al., 1991; Wahl and Nahmias, 1996*a*,*b*) described by K_1^{DOPA}, and the activity of dopa decarboxylase with respect to [^{3}H]dopa in brain (k_3^{DOPA}, min^{-1}); [^{3}H]dopamine is not metabolized or otherwise cleared from brain. The second model (M2) is a 3-parameter 3-compartment model (Huang et al., 1991) described by K_1^{DOPA}, k_3^{DOPA}, and the rate constant for the efflux of activity from brain ($k_{cl}^{DA+acids}$, min^{-1}); [^{3}H]dopamine and [^{3}H]acids are together cleared from brain into cerebrospinal fluid as a single compartment.

The third model (M3) is a 3-parameter 4-compartment model (Kuwabara et al., 1993) described by K_1^{DOPA}, k_3^{DOPA}, and the rate constant for the conversion of cerebral [^{3}H]dopamine to [^{3}H]acids by monoamine oxidase (k_7^{DA}, min^{-1}); [^{3}H]dopamine and [^{3}H]acids are in separate compartments, and only [^{3}H]acids are cleared from brain into cerebrospinal fluid. M1 was fitted to 60 min ($M1_{60}$) and 180 min ($M1_{180}$) of activity data; M2 and M3 were fitted to 180 min of activity data.

The model equations that define the individual metabolite compartments in arterial plasma and brain have been presented elsewhere (Cumming et al., 1995*a*; Deep et al., 1997*a*). Briefly, values of the normalized integral of plasma activity (Θ , min; Gjedde, 1981, 1982; Patlak et al., 1983) for [^{3}H]dopa were calculated for each rat. The linear regression slope of a plot of Θ versus tracer circulation time, defined as the dimensionless constant α (Wong et al., 1986), was then used to calculate the activity of arterial [^{3}H]dopa [$C_a^{DOPA}(T)$] as the single power function (Cumming et al., 1997*a*, 1998; Deep et al, 1997*a*),

$$C_a^{DOPA}(T) = AT^{(\frac{1}{\alpha}-1)} \qquad (1)$$

where A is an arbitrary scaling constant (dpm μl^{-1} min^{-1}), and T is the tracer circulation time (min). Using $C_a^{DOPA}(T)$ as the input function, the activities of arterial *O*-methyl-[^{3}H]dopa (dpm μl^{-1}) and all brain metabolites (dpm mg^{-1}) were calculated by the general compartmental equation,

$$Z_i(T) = \sum_1^m [k_{in}^m \int_0^T Z_{i-1}^m(t) e^{-\sum_1^n k_{out}^n (T-t)}] dt \qquad (2)$$

where $Z_i(T)$ is the instantaneous activity of the metabolite, $Z_{i-1}^m(t)$ is the time-activity curve of the mth precursor compound, k_{in}^m is the kinetic constant of the process that converts the mth precursor into metabolite, and k_{out}^n is the kinetic constant of the nth process that removes the metabolite from the compartment. Therefore, total brain activity was the sum of Eq. (2) for each metabolite compartment.

2.3. Constraints and assumptions

We applied the following assumptions and physiological constraints to the models to reduce parameterization:

1. Population means estimated previously from the same rats (Cumming et al., 1995*a*) for the rate constants for *O*-methylation of arterial [^{3}H]dopa (k_0^{DOPA}, 0.015 min^{-1}) and the elimination of arterial *O*-methyl-[^{3}H]dopa (k_{-1}^{OMD}, 0.013 min^{-1}) were used to calculate the activity of arterial *O*-methyl-[^{3}H]dopa.
2. By definition V_e^{DOPA} is equal to the ratio K_1^{DOPA}/k_2^{DOPA}, thus eliminating k_2^{DOPA}, the rate constant for clearance of [^{3}H]dopa from brain to plasma.
3. The magnitude of V_e^{DOPA} was estimated in posterior cingulate cortex and then assumed to be uniform throughout the rat brain (Gjedde et al., 1991).
4. The constant of proportionality (q; Reith et al., 1990) between the unidirectional blood-brain clearances of *O*-methyl-[^{3}H]dopa and [^{3}H]dopa (K_1^{OMD}/K_1^{DOPA}), also equal to the ratio of the rate constants of clearance from brain of *O*-methyl-[^{3}H]dopa and [^{3}H]dopa (k_2^{OMD}/k_2^{DOPA}), was fixed at a value of 1.5 based on previous measurements in the rat (Cumming et al., 1995*a*). Knowledge of this constant thus eliminates K_1^{OMD} and k_2^{OMD} from the models.
5. Cerebral *O*-methyl-[^{3}H]dopa originates from two sources: transfer of arterial *O*-methyl-[^{3}H]dopa into brain, and conversion of [^{3}H]dopa in brain to *O*-methyl-[^{3}H]dopa. However, the rate constant for *O*-methylation of [^{3}H]dopa in brain (k_5^{DOPA}) was set to zero (Gjedde et al., 1991). Therefore, arterial *O*-methyl-[^{3}H]dopa was assumed to be the only source of *O*-methyl-[^{3}H]dopa in brain.
6. No plasma compartments were defined for [^{3}H]dopamine or [^{3}H]acids, based on chromatographic studies in carbidopa-treated rats which failed to detect these compounds in plasma following injection of [^{3}H]dopa (Melega et al., 1990*a*; Cumming et al., 1995*a*).
7. The formation of homovanillic acid in rat brain proceeds by two pathways: *O*-methylation of DOPAC, and oxidative deamination of 3-methoxytyramine. However, the concentration of 3-methoxytyramine in striatum is low (Cheng and

Wooten, 1982) and the majority of homovanillic acid is derived from DOPAC (Westerink and Spaan, 1982*a*; Cumming et al., 1992), so the contribution of the labelled 3-methoxytyramine compartment to total activity in the autoradiograms was considered negligible.

8. In M3, [^{3}H]DOPAC and [^{3}H]homovanillic acid were assumed to occupy the same compartment in brain ([^{3}H]acids), thus eliminating one compartment and two rate constants from the model.

9. The rate constant $k_7^{DA'}$ indicates the apparent monoamine oxidase activity measured in vivo assuming a homogeneous distribution of [^{3}H]dopamine in brain. It is reduced relative to the true monoamine oxidase activity in vivo assuming a homogenous distribution of [^{3}H]dopamine within the compartment containing monoamine oxidase (k_7^{DA}), in proportion to the unknown ratio of cytosolic [^{3}H]dopamine to whole tissue [^{3}H]dopamine (Cumming 1995*a*; Deep et al., 1997*a*).

10. The rate constants for the formation ($k_7^{DA'}$) and clearance (k_9^{acids}) of [^{3}H]acids were fixed at a ratio of unity (Kuwabara et al., 1993), thus eliminating k_9^{acids} from M3.

11. The vascular component of brain tissue activity was omitted, since the rat brain sections were assumed to be devoid of significant plasma radioactivity during exposure to autoradiographic film.

2.4 Data analysis

Analyses were performed by least-squares nonlinear regression of compartmental models to the measured data (Matlab, © The MathWorks, Natick, MA, U.S.A.). We first estimated V_c^{DOPA} according to M0 in a section of posterior cingulate cortex, a brain region assumed to have negligible dopa decarboxylase activity. This value of V_c^{DOPA} was then used as a fixed input to estimate other kinetic constants in sections of brain regions with high dopa decarboxylase activity according to M1, M2, and M3.

The accuracy of a nonlinear regression fit to measured data was evaluated by the magnitude of the residual sum of squares. The mean value of multiple determinations was calculated for kinetic constant estimates in each brain region, and results were expressed as

mean ± SD. One-factor analysis of variance (ANOVA) tests were used for comparisons of mean regional values of residuals, K_1^{DOPA}, and k_3^{DOPA}, to identify a significant main effect of compartmental model. [^{3}H]Dopamine clearance rate constants ($k_{cl}^{DA+acids}$ and k_7^{DA}) were not compared statistically since they have different biological definitions. Tukey's test was used for post-hoc comparisons to identify specific differences in mean values between the models. The correlation between kinetic constant estimates and position along the anterior-posterior axis in each brain region was evaluated by linear regression analysis; the presence of a significant linear correlation was interpreted as signifying a regional gradient in the magnitude of that constant. For all tests a probability value (p) < 0.05 was considered significant.

3. Results

Linear regression of the normalized integral of plasma [^{3}H]dopa activity [$\Theta=\int C_a^{DOPA}(t)dt/C_a^{DOPA}(T)$] versus tracer circulation time for the population of rats (r=0.99, p<0.05; Fig. 2) yielded a slope α=2.2. The close agreement between the common simulated activities for arterial [^{3}H]dopa and *O*-methyl-[^{3}H]dopa, and measured activities of these compounds in arterial plasma of a carbidopa-treated rat following [^{3}H]dopa injection, is shown in Fig. 3. The fit of M0 to data measured in a section of posterior cingulate cortex (Fig. 4) yielded an estimate of V_e^{DOPA} of 0.75 ml g^{-1}. In Fig. 5 are plotted the fits of M1, M2, and M3 to data measured in a section of nucleus accumbens body. Tissue activities measured from autoradiograms clearly illustrate that regions of rat brain containing relatively high levels of dopa decarboxylase activity such as the basal ganglia (Fig. 5) retained more radioactivity following [^{3}H]dopa injection than regions with little or no dopa decarboxylase activity such as posterior cingulate cortex (Fig. 4).

In all brain regions, the mean residuals (data not shown) for fits with M2 and M3 were significantly lower than those for fits with $M1_{180}$; the mean residuals for M2 and M3 were equal. Estimates of the unidirectional blood-brain clearance of [^{3}H]dopa (K_1^{DOPA}; Table 1) ranged from 0.05-0.08 ml g^{-1} per min, and displayed little variation between the different

models. Estimates of dopa decarboxylase activity with respect to [^{3}H]dopa in brain (k_3^{DOPA}; Table 2) ranged from 0.01-0.09 min^{-1}, with the largest values in the basal ganglia. Estimates of k_3^{DOPA} for fits with $M1_{180}$ were significantly lower than those with all other models; k_3^{DOPA} estimates were not significantly different between $M1_{60}$ and M3. Estimates of the [^{3}H]dopamine clearance rate constants ($k_{cl}^{DA+acids}$ and $k_7^{DA'}$, Table 3) ranged from 0.02-0.04 min^{-1}. Results of post-hoc comparisons for mean estimates of K_1^{DOPA} and k_3^{DOPA} are summarized in Table 4.

Increasing posterior-anterior gradients were found for the magnitudes of K_1^{DOPA} in dorsal-medial caudate and hypothalamus, and [^{3}H]dopamine clearance rate constants ($k_{cl}^{DA+acids}$ and $k_7^{DA'}$) in nucleus accumbens body. Similar gradients for k_3^{DOPA} were observed in dorsal-medial caudate, olfactory tubercle, hypothalamus, dorsal hippocampus, and nucleus accumbens. Estimates of kinetic constant as functions of anatomical position in dorsal-medial caudate are plotted in Fig. 6.

4. Discussion

4.1. Estimates of [^{3}H]dopa kinetic constants

This study represents the first assay of [^{3}H]dopa kinetics in living rat brain by compartmental modelling of activities measured with quantitative autoradiography; the present technique is analogous to that of Sokoloff et al. (1977), who modelled cerebral glucose consumption in rats using [^{14}C]deoxyglucose autoradiograms. To validate compartmental modelling of autoradiographic data as a method for investigating the kinetic behaviour of radiolabelled L-dopa in living mammalian brain, we compared estimates of [^{3}H]dopa kinetic constants based on compartmental modelling of total cerebral activities from combined metabolite pools in a time-series of static autoradiograms from right cerebral hemispheres of rats, with corresponding estimates based on the analysis of measured activities from individual metabolite pools separated by chromatographic fractionation of [^{3}H]dopa metabolites in the left cerebral hemispheres of the same rats (Cumming et al., 1995*a*).

The present autoradiographic estimate of the equilibrium distribution volume of [^{3}H]dopa (V_e^{DOPA}) matched the corresponding chromatographic result in cortex (0.71 ml g^{-1}; Cumming et al., 1995*a*). Large neutral amino acids such as L-dopa are water-soluble, and are passively transferred from blood to brain by facilitated diffusion (Wade and Katzman, 1975; Oldendorf and Szabo, 1976; Smith, 1991); the same mechanism applies to [^{3}H]dopa. The fact that this transport process requires no energy indicates that the distribution volumes of large neutral amino acids cannot in general exceed the ratio of water contents between brain tissue and plasma (0.92 ml g^{-1}; Gjedde and Bodsch, 1987); amino acid concentrations measured in the rat clearly confirm this principle (Gjedde and Bodsch, 1987; Paetsch and Greenshaw, 1991). Indeed, the present autoradiographic estimate of V_e^{DOPA} is consistent with this postulate. Thus, there exists no gradient for the accumulation of [^{3}H]dopa in a specific region of brain, which is the basis of our assumption of a uniform distribution of [^{3}H]dopa throughout rat brain at equilibrium.

Autoradiographic estimates of the unidirectional blood-brain clearance of [^{3}H]dopa (K_1^{DOPA}; Table 1) showed excellent quantitative agreement with corresponding chromatographic results (0.04-0.06 ml g^{-1} per min; Cumming et al., 1995*a*). The small regional variation in brain uptake measured for [^{3}H]dopa, [^{18}F]fluorodopa (Cumming et al., 1994*a*), and [^{3}H]tyrosine (Cumming et al., 1994*b*), together suggest a relatively homogeneous concentration of the transporter of large neutral amino acids throughout the cerebral vasculature of rat forebrain.

Autoradiographic estimates of apparent monoamine oxidase activity with respect to [^{3}H]dopamine in brain ($k_7^{DA'}$; Table 3) agreed within the range of corresponding chromatographic results (0.01-0.15 min^{-1}; Cumming et al., 1995*a*). However, autoradiographic estimates of dopa decarboxylase activity with respect to [^{3}H]dopa in brain (k_3^{DOPA}; Table 2) were several-fold lower than chromatographic estimates, especially in striatum (0.26 min^{-1}; Cumming et al., 1995*a*). Several possible factors contributed to this discrepancy. First, analysis by chromatography could lead to systematic over-estimation of k_3^{DOPA} if dopa decarboxylase continued to consume cerebral [^{3}H]dopa in the post-mortem period: several minutes transpired between decapitation and extraction of brain samples in

perchloric acid, such that the true activity of [^{3}H]dopa at the time of death would be under-estimated. Indeed, the concentration of endogenous L-dopa in brain of rats killed by decapitation was over 2.5 times smaller than that measured in rats killed by microwave irradiation (Thiede and Kehr, 1981). Such irradiation causes thermal denaturation of enzymes, including dopa decarboxylase, and therefore prevents the rapid post-mortem degradation of L-dopa. Second, the omission of catechol-*O*-methyltransferase activity with respect to [^{3}H]dopa in brain (k_5^{DOPA}) from the present models over-estimated the amount of [^{3}H]dopa available for decarboxylation, thus under-estimating k_3^{DOPA}. Third, we have recently shown that the omission of the vesicular compartment of labelled dopamine further under-estimates k_3^{DOPA} (Deep et al., 1997*a*). Fourth, estimates of k_3^{DOPA} in rat decline rapidly with increasing V_e^{DOPA} (Deep et al., 1997*c*); if the magnitude of V_e^{DOPA} estimated in cortex was higher than the true magnitude in non-cortical regions, present estimates of k_3^{DOPA} would be further reduced relative to chromatographic estimates. The choice of q did not contribute to the discrepancy between present and chromatographic results. Values of k_3^{DOPA} previously estimated from this data set were relatively unaffected by input values of q between 0.5-3.0 (Deep et al., 1997*c*).

The regional distributions of enzyme activities measured in vivo by autoradiography (Tables 2-3) are consistent with those of dopa decarboxylase (Rahman et al., 1980) and monoamine oxidase (Saura et al., 1992) assayed in vitro in rat brain. Furthermore, we report gradients in the magnitudes of [^{3}H]dopa kinetic constant estimates within structures of the rat basal ganglia (Fig. 6), indicating that the striatum is chemically heterogeneous. A rostrocaudal gradient for dopa decarboxylase activity has been observed in vivo in the human striatum (Garnett et al., 1987). Present estimates of the activities of dopa decarboxylase in caudate nucleus and monoamine oxidase in nucleus accumbens also increased from posterior to anterior, in agreement with the distribution of endogenous dopamine, DOPAC, and homovanillic acid in divisions of rat striatum (Widmann and Sperk, 1986).

4.2. Comparison of compartmental models

The present modelling approach, in which a simulated arterial [^{3}H]dopa curve is used

as the input function, has been previously derived (Deep et al., 1997*a*). We now compare three different compartmental models of [^{3}H]dopa blood-brain clearance and metabolism (Fig. 1), each reflecting a different possible metabolic route available to [^{3}H]dopamine formed in brain. The present models are identical to those used for analysis of positron emission tomography studies with [^{18}F]fluorodopa in primates. M1 stipulates that [^{3}H]dopamine accumulates irreversibly in brain. Extrapolation of M1 fitted to 60 min of measured data (Fig. 5) predicted that activity would increase continuously in brain regions of nonzero dopa decarboxylase activity, due to accumulation of [^{3}H]dopamine in situ. Fits of M1 to 180 min of measured data greatly underestimated brain activity past 60 min. The absence of [^{3}H]acids in M1 indicates that all brain activity past 60 min (not including that due to [^{3}H]dopa and *O*-methyl-[^{3}H]dopa) must be due solely to [^{3}H]dopamine. The activity of [^{3}H]dopamine in M1 is therefore under-estimated, which leads to a consequent over-estimation of precursor [^{3}H]dopa, resulting in under-estimation of dopa decarboxylase activity. The omission of [^{3}H]dopamine clearance from compartmental models therefore explains the significant reductions in (i) accuracy, and (ii) the magnitude of k_3^{DOPA} estimates, in fits with M1 compared to fits with M2 and M3 (Table 2).

No difference was observed in kinetic constant estimates according to $M1_{60}$ and M3 (Table 4), indicating that significant clearance of [^{3}H]dopamine occurred only after 60 min of tracer circulation. This conclusion is consistent with the results of chromatographic assays of striatal tissue from rats administered [^{3}H]dopa (Melega et al., 1990*a*; Cumming et al., 1995*a*), and monkeys administered [^{18}F]fluorodopa (Firnau et al., 1987), in which labelled dopamine accounted for the majority of striatal activity during the first hour following tracer injection.

Several studies have omitted the clearance of ^{18}F-labelled dopamine from compartmental models of [^{18}F]fluorodopa metabolism in primate brain (Gjedde et al., 1991; Barrio et al., 1996; Dhawan et al., 1996; Ishikawa et al., 1996; Wahl and Nahmias, 1996*a*,*b*). However, there is considerable evidence to suggest that, for extended tracer studies (> 1 h), the clearance of labelled dopamine from brain cannot be ignored without prejudicing the results of model fits. Assuming that labelled dopamine accumulated irreversibly in brain

produced inaccurate fits to measured data (M1; Fig. 5), and influenced the magnitudes of kinetic constant estimates by 10-100% (Huang et al., 1991). Furthermore, independent estimates of the rate constants for the elimination of endogenous (Moleman et al., 1978; Dedek et al., 1979; Soares-da-Silva and Garrett, 1990; Cumming et al., 1992) and labelled (Cumming et al., 1994*a*, 1995*a*) acidic metabolites from brain of living rat are all in the range 0.04-0.10 min^{-1}. Therefore, most of the labelled acids formed during the first hour following tracer injection have been cleared into cerebrospinal fluid by the third hour, indicating that this process contributes significantly to activity signals measured during extended tracer studies.

Two of the compartmental models presented here account for the clearance of [^{3}H]dopamine from brain, either by direct transport into cerebrospinal fluid with [^{3}H]acids (M2, $k_{cl}^{DA+acids}$) or oxidative deamination by monoamine oxidase (M3, k_7^{DA}). Assuming that the net efflux of radioactivity from brain is the same for both models, then it may be shown that,

$$k_{cl}^{DA+acids}(T) = \frac{k_9^{acids} M^{acids}(T)}{M^{DA}(T) + M^{acids}(T)} \qquad (3)$$

Previous estimates of [^{3}H]dopa kinetic constants from four regions of rat brain (Cumming et al., 1995*a*) were used to calculate activities of [^{3}H]dopamine [$M^{DA}(T)$] and [^{3}H]acids [$M^{acids}(T)$] in brain according to Eq. (2), which were then substituted into Eq. (3). In all regions so simulated, the magnitude of $k_{cl}^{DA+acids}$ increased from nil at injection when the activity of [^{3}H]acids is nil, to a peak between 60-120 min when clearance of [^{3}H]acids from brain is well established (Fig. 7). During the rising portions of the curves, the apparent rate of formation of [^{3}H]acids is much greater than the apparent rate of clearance of [^{3}H]acids from brain. The plateau after 60 min thus corresponds to a state of transient equilibrium between the rates of these two processes. Therefore, in non-steady state, the magnitude of $k_{cl}^{DA+acids}$ (Huang et al., 1991) is time-dependent.

5. Conclusion

Excluding efflux of [^{3}H]dopa and *O*-methyl-[^{3}H]dopa, no significant elimination of activity from brain was detected by autoradiography before 60 min of tracer circulation. However, trapping of [^{3}H]dopamine is not irreversible; at circulation times greater than 60 min after tracer injection, compartmental modelling of autoradiograms failed to account for measured tissue activities unless the clearance of [^{3}H]dopamine from brain was included in the models.

The present autoradiographic method permits the analysis of discrete brain regions too small to be resolved by other in vivo techniques such as chromatography or positron emission tomography; small regions also better satisfy the compartmental definition of spatial homogeneity. Furthermore, unlike positron emission tomography, the present method is not influenced by partial volume effects (Mazziotta et al., 1981), which can significantly affect kinetic constant estimates (Rousset et al., 1993*a*). A disadvantage of the present autoradiographic method is the requirement of multiple subjects; in positron emission tomography studies all data are measured from a single subject. Notwithstanding efforts to normalize all animals to common arterial input curves, inter-subject variability contributed to the scatter observed in present data.

The general agreement of present autoradiographic estimates of [^{3}H]dopa kinetic constants based on compartmental modelling of total cerebral activities from combined metabolite pools in a time-series of static autoradiograms from right cerebral hemispheres of rats, with corresponding estimates based on the analysis of measured activities from individual metabolite pools separated by chromatographic fractionation of [^{3}H]dopa metabolites in the left cerebral hemispheres of the same rats (Cumming et al., 1995*a*), represents the first empirical validation of compartmental modelling of autoradiographic data as a method for quantitatively investigating the kinetic behaviour of radiolabelled L-dopa in living mammalian brain.

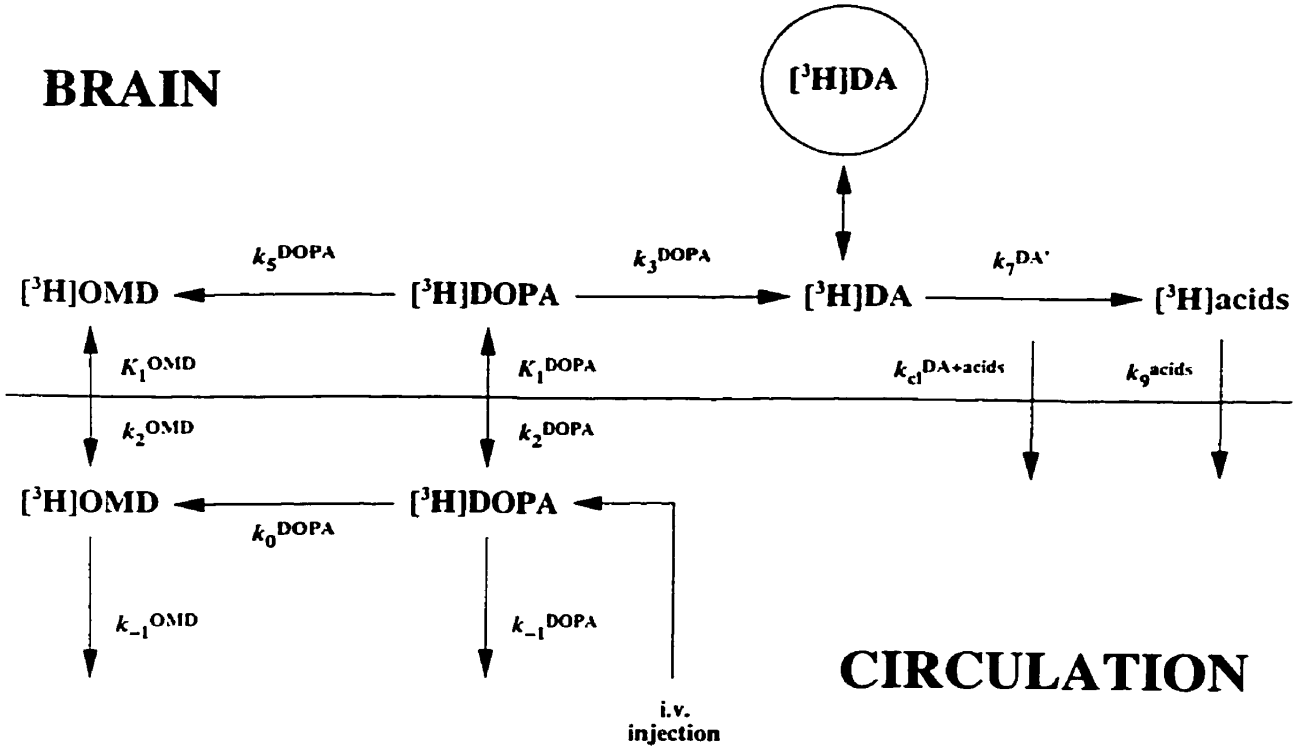

Fig. 1. Schematic summary of [^{3}H]dopa blood-brain transfer and metabolism, according to three different compartmental models. [^{3}H]Dopa in circulation is *O*-methylated (k_0^{DOPA}) by catechol-*O*-methyltransferase to form *O*-methyl-[^{3}H]dopa. Both tracers are subsequently cleared from circulation by renal elimination (k_{-1}^{DOPA} and k_{-1}^{OMD}). Both tracers are transferred into brain (K_1^{DOPA} and K_1^{OMD}) and out of brain (k_2^{DOPA} and k_2^{OMD}) by facilitated diffusion. [^{3}H]Dopa in brain is *O*-methylated (k_5^{DOPA}) by catechol-*O*-methyltransferase to form *O*-methyl-[^{3}H]dopa. In brain regions containing dopa decarboxylase, [^{3}H]dopa is decarboxylated (k_3^{DOPA}) to form [^{3}H]dopamine ([^{3}H]DA), most of which is rapidly sequestered in vesicles (circle) and so protected from deamination by monoamine oxidase. For M1, [^{3}H]DA is not metabolized or otherwise cleared from brain. For M2, [^{3}H]DA and [^{3}H]acids occupy the same compartment and are together cleared from brain ($k_{cl}^{DA+acids}$). For M3, [^{3}H]DA is not cleared from brain but is metabolized to form [^{3}H]acids ($k_7^{DA'}$), which are subsequently cleared from brain into cerebrospinal fluid (k_9^{acids}) and back into the venous circulation.

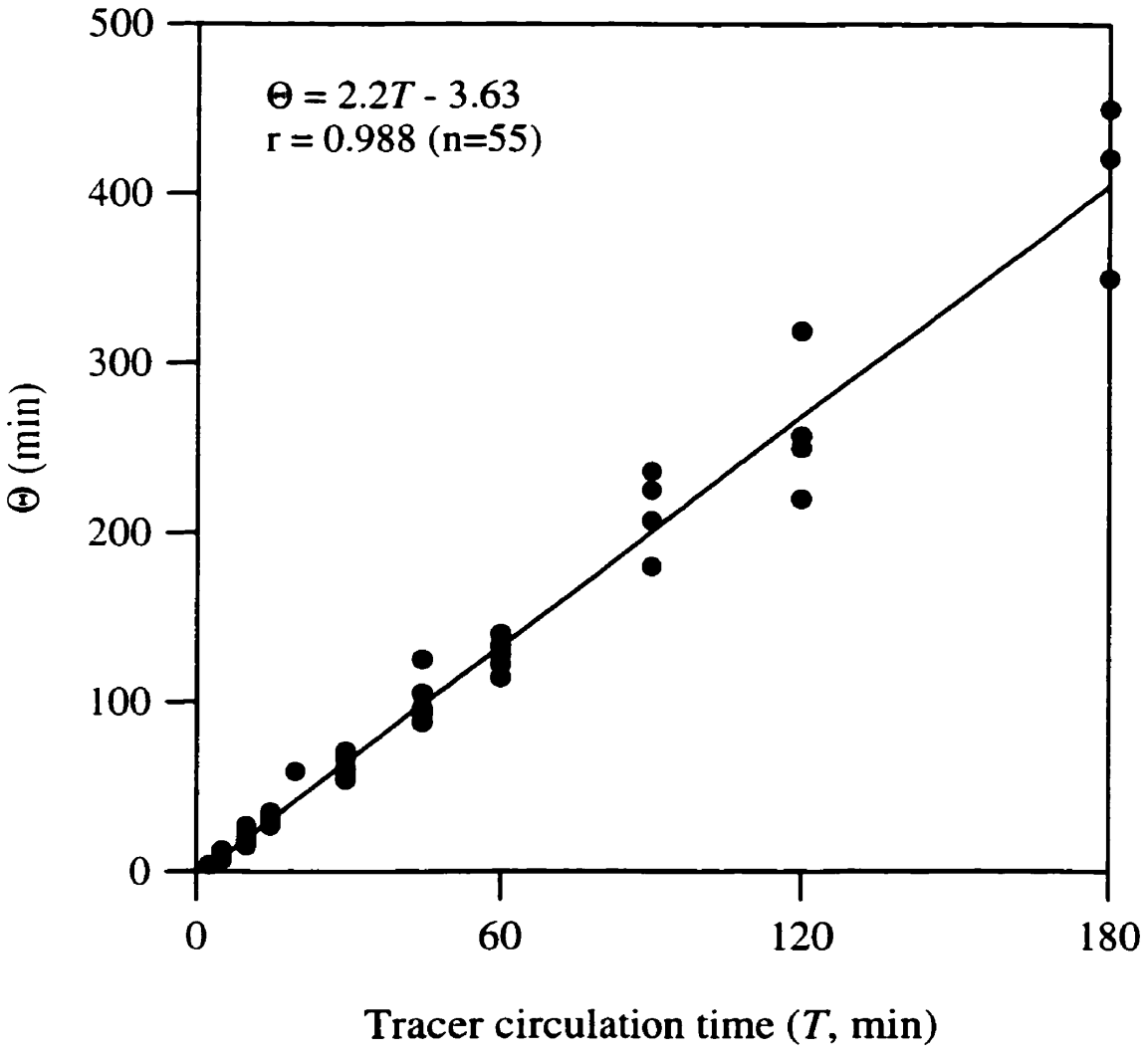

Fig. 2. Values of the normalized integral of plasma [^{3}H]dopa activity [$\Theta = \int C_a^{DOPA}(t)dt / C_a^{DOPA}(T)$; n=55] versus tracer circulation time in rat. A significant linear relationship is demonstrated by the line of regression (r=0.99, $p<0.05$) to the measured data (●). The regression slope α (2.2) was used to calculate the activity of arterial [^{3}H]dopa.

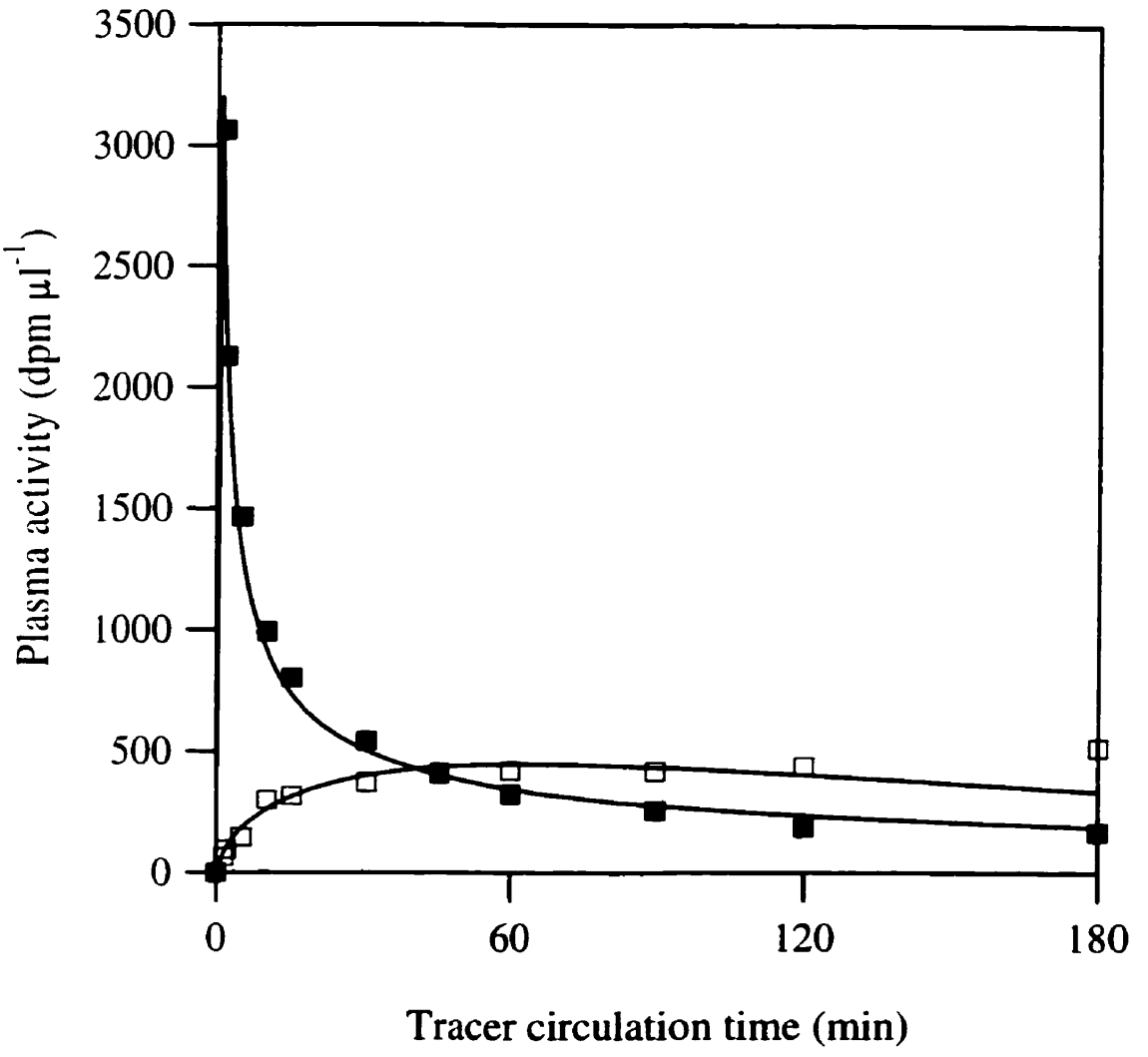

Fig. 3. Measured activities of [^{3}H]dopa (■) and *O*-methyl-[^{3}H]dopa (□) in arterial plasma of a single carbidopa-treated rat as a function of tracer circulation time following the injection of [^{3}H]dopa (200 µCi, i.v.; Cumming et al., 1995*a*). The smooth lines represent the calculated arterial activities of [^{3}H]dopa and *O*-methyl-[^{3}H]dopa. The arterial [^{3}H]dopa activities were calculated using a power function defined relative to the normalized arterial integral of [^{3}H]dopa. The arterial *O*-methyl-[^{3}H]dopa activities were calculated using population means for the rate constants for *O*-methylation of arterial [^{3}H]dopa (k_0^{DOPA}, 0.015 min^{-1}) and the elimination of arterial *O*-methyl-[^{3}H]dopa (k_{-1}^{OMD}, 0.013 min^{-1}), estimated previously in the same rats (Cumming et al., 1995*a*).

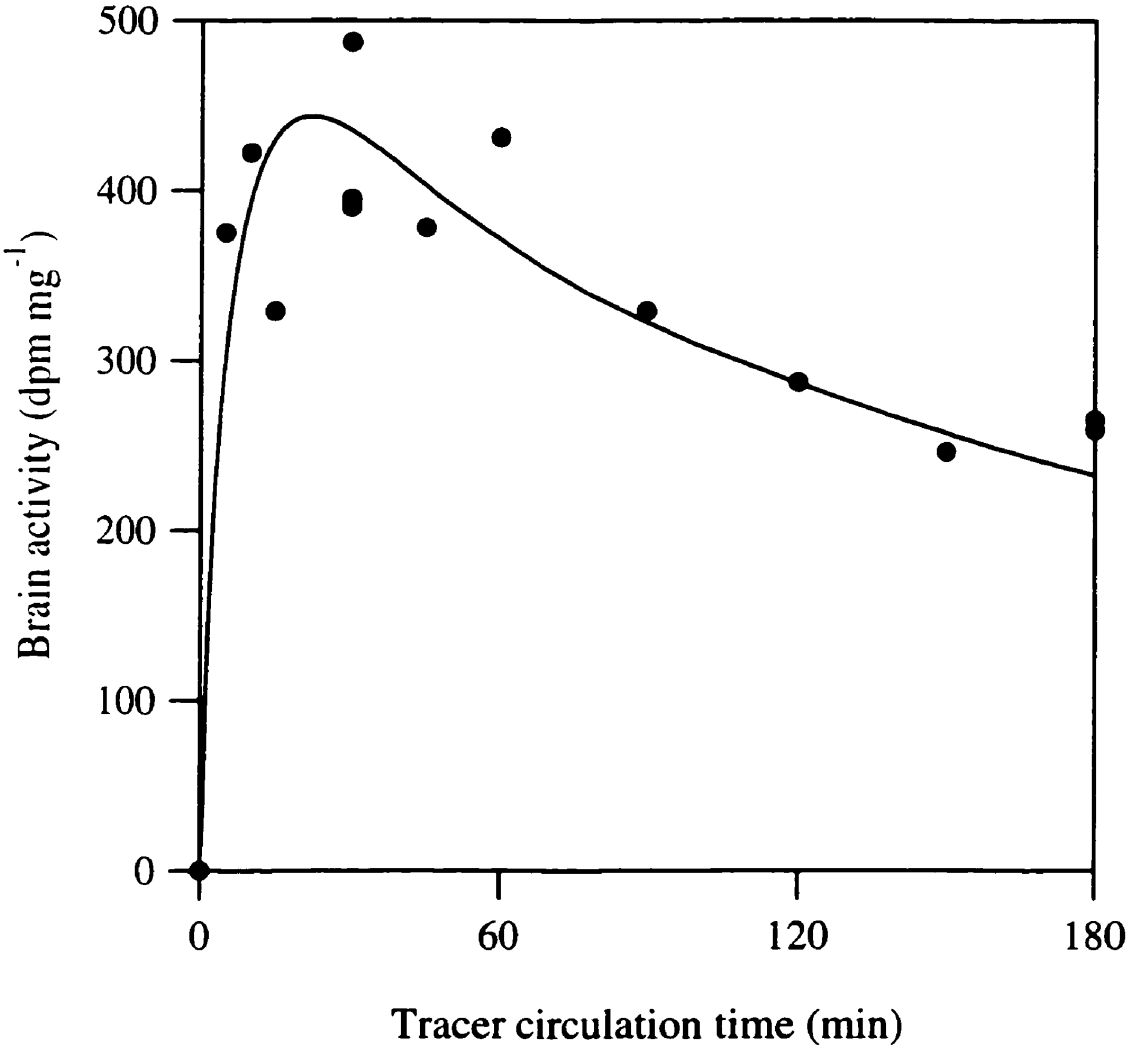

Fig. 4. Total activity measured in a section of posterior cingulate cortex during 180 min of [^{3}H]dopa circulation in rat (n=13). Tissue activities were scaled to common simulated [^{3}H]dopa and *O*-methyl-[^{3}H]dopa arterial curves. The smooth line is defined by least-squares nonlinear regression of a 2-parameter 2-compartment model (M0), in which [^{3}H]dopa is not decarboxylated to [^{3}H]dopamine, to the measured data (●). Each data point was measured in one rat.

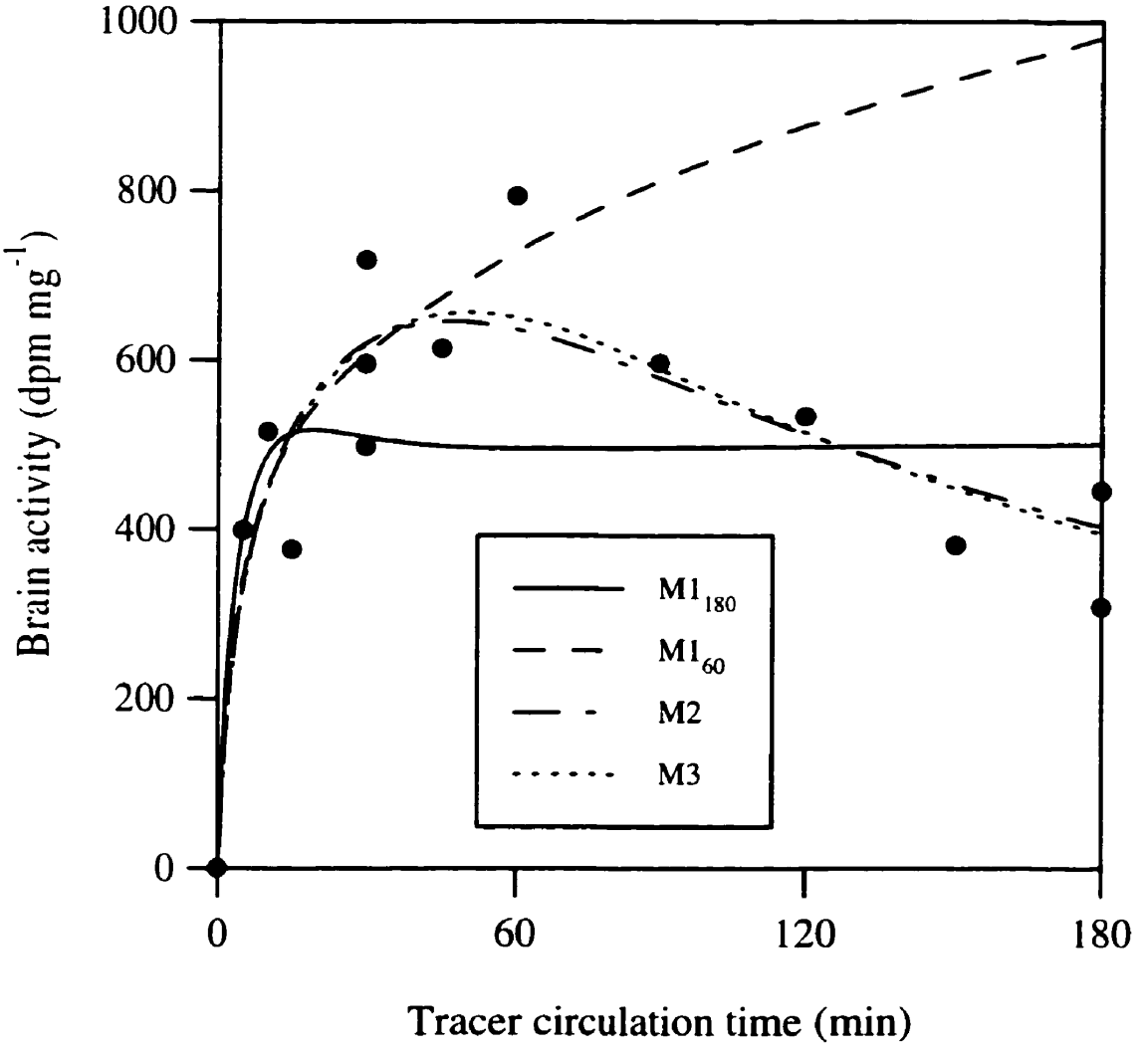

Fig. 5. Total activity measured in a section of nucleus accumbens body during 180 min of [^{3}H]dopa circulation in rat (n=13). Tissue activities were scaled to common simulated [^{3}H]dopa and *O*-methyl-[^{3}H]dopa arterial curves. The smooth lines are defined by least-squares nonlinear regression to the measured data (●) of a 2-parameter 3-compartment model (M1) in which [^{3}H]dopamine accumulates irreversibly in brain, a 3-parameter 3-compartment model (M2) in which [^{3}H]dopamine is cleared from brain with [^{3}H]acids as a single compartment, and a 3-parameter 4-compartment model (M3) in which [^{3}H]dopamine and [^{3}H]acids are assumed to occupy separate compartments. Model M1 was fitted to 60 min ($M1_{60}$) and 180 min ($M1_{180}$) of measured data; the curve fitted to 60 min has been extrapolated to 180 min. Each data point was measured in one rat.

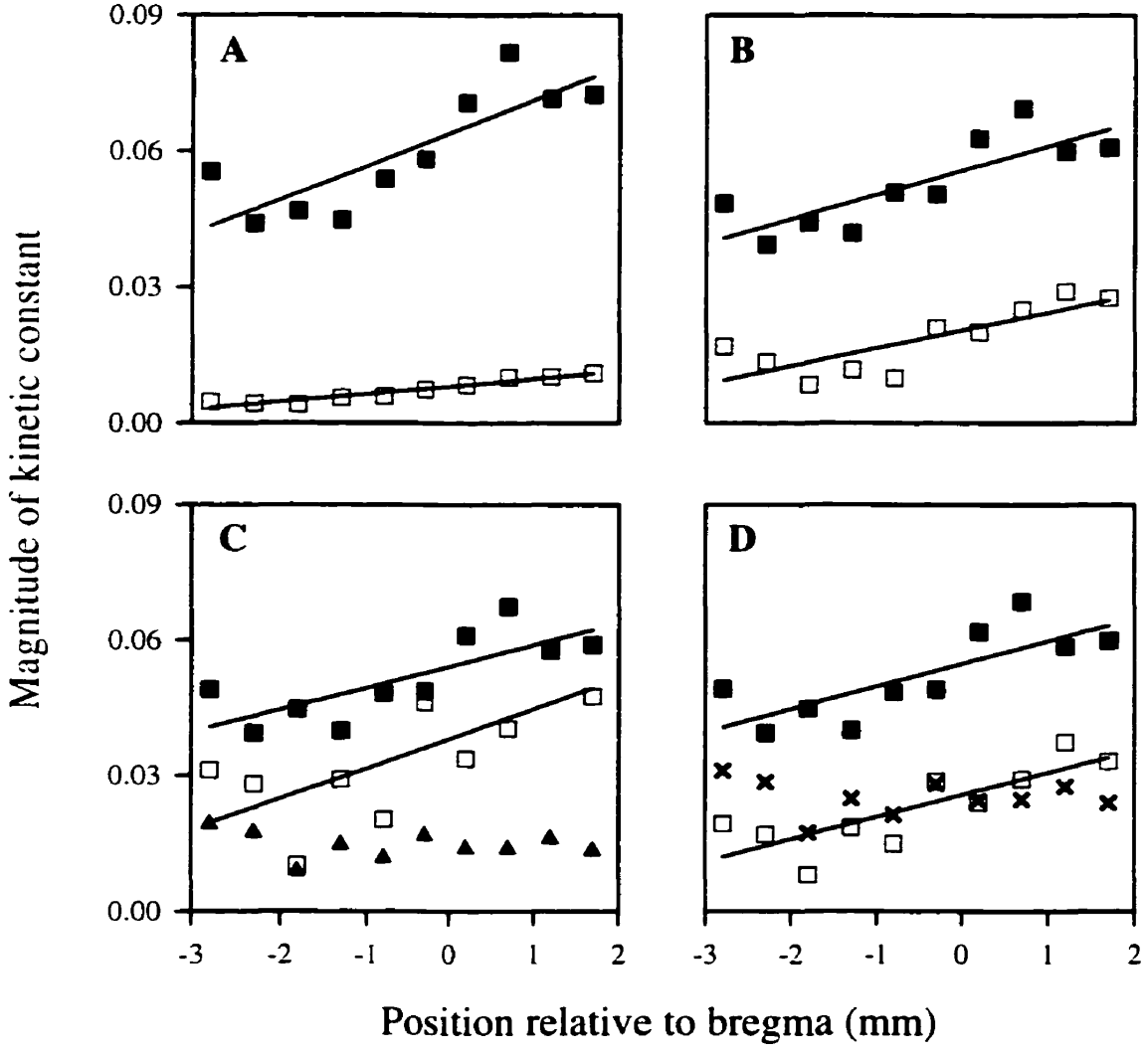

Fig. 6. Estimates of K_1^{DOPA} (■, ml g^{-1} per min), k_3^{DOPA} (□, min^{-1}), $k_{cl}^{DA+acids}$ (▲, min^{-1}), and k_7^{DA} (×, min^{-1}) as a function of anatomical position along the anterior-posterior axis of the rat dorsal-medial caudate, according to models $M1_{180}$ **(A)**, $M1_{60}$ **(B)**, M2 **(C)**, and M3 **(D)**. Positive abscissa points indicate positions anterior to bregma (recorded as 0 mm). Significant linear correlations ($p<0.05$), indicated by the lines of regression, between kinetic constant and position were found for K_1^{DOPA} ($M1_{180}$: r=0.83; $M1_{60}$: r=0.82; M2: r=0.77; M3: r=0.78), and k_3^{DOPA} ($M1_{180}$: r=0.93; $M1_{60}$: r=0.80; M2: r=0.72; M3: r=0.82).

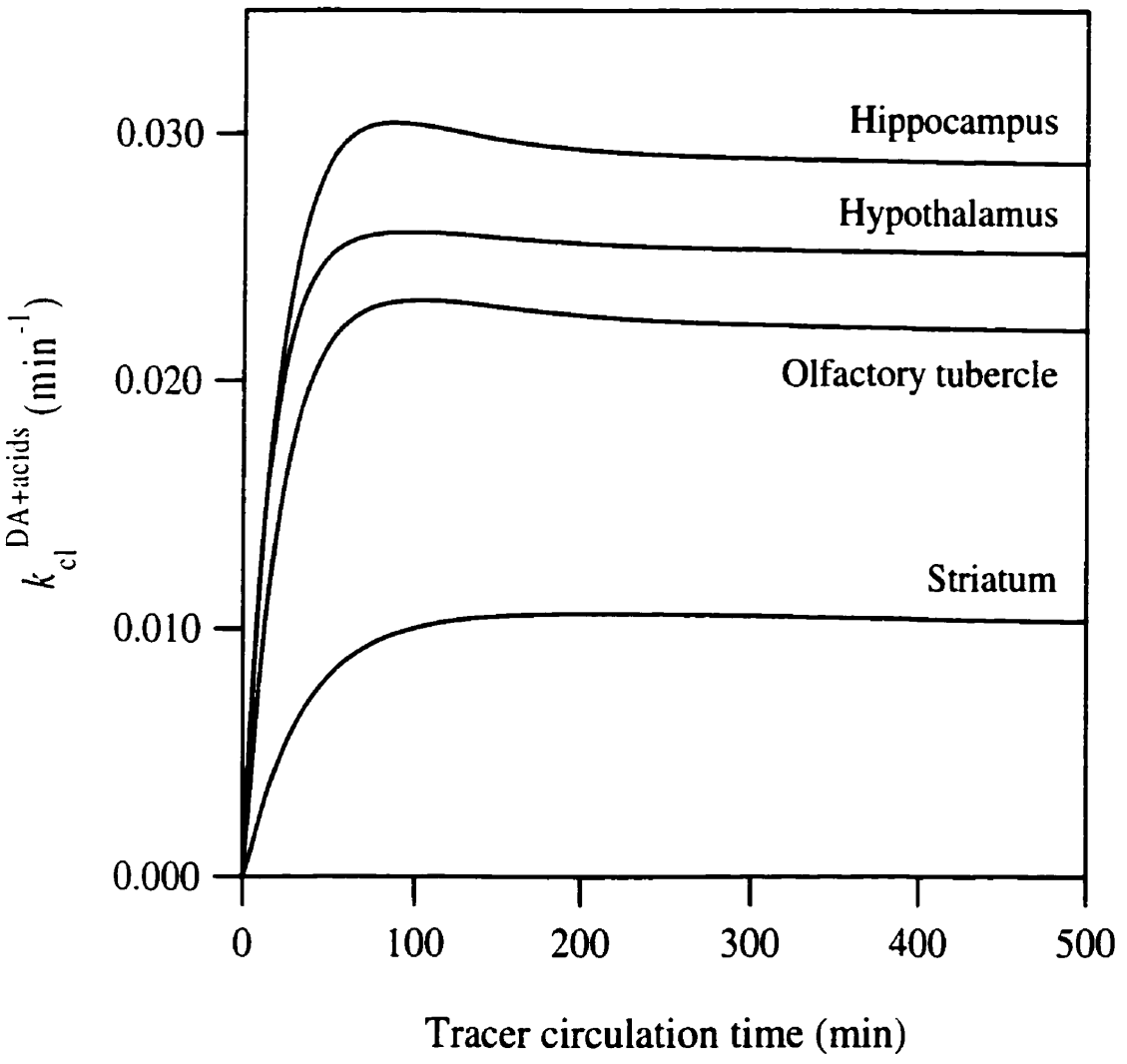

Fig. 7. The magnitude of $k_{cl}^{DA+acids}$ as a function of tracer circulation time, calculated in four regions of rat brain.

Table 1

Estimates of the unidirectional blood-brain clearance of [^{3}H]dopa (K_1^{DOPA}, ml g^{-1} per min)

Brain region	$M1_{180}$	$M1_{60}$	M2	M3	
dorsal-medial caudate (n=10)	0.060 ± 0.010	0.050 ± 0.010	0.052 ± 0.009	0.050 ± 0.010	
central caudate (n=13)	0.065 ± 0.005	0.056 ± 0.003	0.054 ± 0.003	0.054 ± 0.004	*
nucleus accumbens shell (n=5)	0.075 ± 0.007	0.063 ± 0.007	0.061 ± 0.007	0.061 ± 0.008	*
nucleus accumbens body (n=5)	0.073 ± 0.004	0.060 ± 0.004	0.057 ± 0.004	0.057 ± 0.004	*
olfactory tubercle (n=7)	0.076 ± 0.006	0.067 ± 0.005	0.064 ± 0.004	0.065 ± 0.004	*
amygdala (n=4)	0.053 ± 0.002	0.050 ± 0.004	0.052 ± 0.003	0.050 ± 0.004	
hypothalamus (n=6)	0.072 ± 0.006	0.069 ± 0.006	0.068 ± 0.005	0.068 ± 0.005	
dorsal hippocampus (n=7)	0.048 ± 0.002	0.046 ± 0.002	0.046 ± 0.002	0.046 ± 0.002	*
ventral hippocampus (n=4)	0.059 ± 0.002	0.056 ± 0.002	0.055 ± 0.002	0.055 ± 0.002	*

Results are mean ± SD values of separate determinations in (n) sections of rat brain region, obtained by nonlinear regression of compartmental models M1, M2, and M3 to total cerebral activities measured from a time-series (180 min) of autoradiograms from right cerebral hemispheres, obtained following i.v. injection of [^{3}H]dopa. One-factor ANOVA tests were performed on mean K_1^{DOPA} estimates: * indicates a significant main effect of compartmental model (p<0.05).

Table 2

Estimates of dopa decarboxylase activity with respect to [^{3}H]dopa in brain (k_3^{DOPA}, min^{-1})

Brain region	$M1_{180}$	$M1_{60}$	M2	M3	
dorsal-medial caudate (n=10)	0.007 ± 0.003	0.018 ± 0.007	0.030 ± 0.010	0.023 ± 0.009	*
central caudate nucleus (n=13)	0.009 ± 0.002	0.025 ± 0.006	0.060 ± 0.020	0.033 ± 0.009	*
nucleus accumbens shell (n=5)	0.008 ± 0.001	0.029 ± 0.002	0.070 ± 0.010	0.042 ± 0.006	*
nucleus accumbens body (n=5)	0.009 ± 0.001	0.032 ± 0.003	0.090 ± 0.010	0.050 ± 0.006	*
olfactory tubercle (n=7)	0.006 ± 0.001	0.025 ± 0.005	0.060 ± 0.020	0.040 ± 0.010	*
amygdala (n=4)	0.002 ± 0.001	0.010 ± 0.004	0.020 ± 0.010	0.013 ± 0.006	*
hypothalamus (n=6)	0.002 ± 0.001	0.010 ± 0.003	0.021 ± 0.009	0.013 ± 0.006	*
dorsal hippocampus (n=7)	0.002 ± 0.001	0.008 ± 0.001	0.017 ± 0.003	0.009 ± 0.002	*
ventral hippocampus (n=4)	0.003 ± 0.001	0.012 ± 0.002	0.028 ± 0.008	0.016 ± 0.003	*

Results are mean ± SD values of separate determinations in (n) sections of rat brain region, obtained by nonlinear regression of compartmental models M1, M2, and M3 to total cerebral activities measured from a time-series (180 min) of autoradiograms from right cerebral hemispheres, obtained following i.v. injection of [^{3}H]dopa. One-factor ANOVA tests were performed on mean k_3^{DOPA} estimates: * indicates a significant main effect of compartmental model ($p<0.05$).

Table 3

Estimates of rate constants (min^{-1}) for the clearance of cerebral [^{3}H]dopamine, either by direct removal from brain with [^{3}H]acids ($k_{cl}^{DA+acids}$) or oxidative deamination (k_7^{DA})

Brain region	M2 $k_{cl}^{DA+acids}$	M3 k_7^{DA}
dorsal-medial caudate (n=10)	0.015 ± 0.003	0.025 ± 0.004
central caudate (n=13)	0.017 ± 0.003	0.029 ± 0.004
nucleus accumbens shell (n=5)	0.023 ± 0.002	0.036 ± 0.002
nucleus accumbens body (n=5)	0.023 ± 0.002	0.036 ± 0.002
olfactory tubercle (n=7)	0.025 ± 0.003	0.039 ± 0.004
amygdala (n=4)	0.023 ± 0.006	0.040 ± 0.010
hypothalamus (n=6)	0.029 ± 0.004	0.043 ± 0.006
dorsal hippocampus (n=7)	0.024 ± 0.004	0.037 ± 0.005
ventral hippocampus (n=4)	0.027 ± 0.005	0.040 ± 0.007

[^{3}H]Dopamine clearance rate constants were explicitly set to 0 in M1. Results are mean ± SD values of separate determinations in (n) sections of rat brain region, obtained by nonlinear regression of compartmental models M2 and M3 to total cerebral activities measured from a time-series (180 min) of autoradiograms from right cerebral hemispheres, obtained following i.v. injection of [^{3}H]dopa.

Table 4

Summary of post-hoc comparisons for estimates of the unidirectional blood-brain clearance of [^{3}H]dopa (K_1^{DOPA}) and dopa decarboxylase activity with respect to [^{3}H]dopa in brain (k_3^{DOPA})

	$M1_{(4)}$	$M1_{(180)}$	M2	M3
$M1_{(4)}$		3	0	0
$M1_{(180)}$	6		4	4
M2	8	9		0
M3	1	9	8	

Results are number of brain regions (out of 9) in which a significant difference between compartmental models was found in mean estimates of K_1^{DOPA} (above the diagonal) and k_3^{DOPA} (below the diagonal), according to one-factor ANOVA followed by post-hoc comparison with Tukey's test.

GENERAL DISCUSSION

The assay of kinetic constants describing the behaviour of radiolabelled L-dopa in living brain by compartmental modelling of total cerebral radioactivities from autoradiography is a formidable problem. A confounding factor is the existence of several plausible compartmental models, each of which is based on the well-characterized metabolic pathway of L-dopa in vivo, but each slightly different with respect to the number of metabolite compartments and/or parameters to be estimated. This results in a confusing number of variants, sometimes yielding significantly different results when applied to the same data. Validation of a biologically accurate model was therefore a major challenge of this work, with the ultimate goal of establishing a "standard" model that could be used with confidence for positron emission tomography studies with L-6-[^{18}F]fluorodopa.

The present compartmental model can be used to estimate a maximum of three or four kinetic constants, within acceptable levels of confidence, in a single experiment. However, the nonlinearity of the L-dopa metabolic pathway requires knowledge of several additional parameters for a complete description of the kinetic behaviour of the amino acid in vivo. Consequently, it was necessary to constrain the compartmental model to dimensions solvable in a single experiment, by incorporating a series of physiological constraints. Of the constraints used (see Chapter III, Deep et al., 1997*b*), only the fixed ratio of the blood-brain transfer coefficients of L-dopa and *O*-methyl-L-dopa (q) can be justified mathematically (see Appendix #1). The use of a cortical value of the equilibrium distribution volume of radiolabelled L-dopa (V_e^{DOPA}) as a fixed input in regions of interest is not necessarily correct, and may slightly bias estimates of dopa decarboxylase activity. The choice of a fixed ratio of the rate constants for the formation and clearance of acidic metabolites (k_9^{acids}/k_7^{DA}) is arbitrary, but its magnitude has negligible effect on kinetic constant estimates. The omission of catechol-*O*-methyltransferase activity with respect to L-dopa in brain (k_5^{DOPA}) may result in significant under-estimation of dopa decarboxylase activity, but this is unavoidable since no estimates of catechol-*O*-methyltransferase activity in living brain are currently available. Despite lacking solid mathematical or biological justification in some cases, the

incorporation of physiological constraints into compartmental models of radiolabelled L-dopa uptake and metabolism is unavoidable if all major metabolite compartments of the model, and hence the accuracy of the model, is to be maintained. Without these constraints, model fits to measured radioactivities from extended tracer experiments (> 40 min) failed to converge. Nonetheless, caution is required when interpreting results obtained with a constrained model; for example, simulation studies clearly indicate that estimates of cerebral dopa decarboxylase activity are highly sensitive to the magnitudes of V_e^{DOPA} and k_5^{DOPA}.

The inherent biological accuracy of the model was validated quantitatively by two separate experiments that are, in effect, like two sides of the same coin. In the first study, it was shown that metabolite fractions predicted by the model, using as inputs previously published estimates of kinetic constants from rat, agreed excellently with corresponding metabolite fractions measured analytically by chromatographic separation of ^{18}F- labelled compounds in plasma and brain extracts of rats given intravenous injections of L-6-[^{18}F]fluorodopa. This work also demonstrated that omission of the vesicular storage of radiolabelled dopamine did not bias results of model fits for circulation times past 10 min, due to rapid equilibration of the cytosolic and vesicular fractions of radiolabelled dopamine in vivo. In the second study, the constrained model was used to estimate kinetic constants from total tissue radioactivities measured with static autoradiograms from right cerebral hemispheres of rats administered [^3H]dopa. By demonstrating agreement between model estimates based on combined metabolite pools and analytic estimates previously obtained on the basis of individual metabolite pools fractionated by chromatography in the left hemispheres of the same rats, we achieved the first direct empirical validation of a compartmental model describing the cerebral uptake and metabolism of radiolabelled L-dopa in living brain. The models used herein to analyze data in the rat are identical to those used with data from primates, thus validating the models for positron emission tomography studies.

Compared to the simplicity of linear methods for analyzing tracer uptake, the more complex approach of compartmental modelling offers the distinct advantage of isolating kinetic constants that describe individual physiological processes responsible for the blood-

brain transport and cerebral metabolism of radiolabelled L-dopa. The parameter of most interest is cerebral dopa decarboxylase activity, which defines the rate of endogenous dopamine formation from L-dopa. This rate constant is assumed to reflect the functional state of the nigrostriatal dopaminergic pathway. The present model seems to under-estimate the activity of dopa decarboxylase several-fold relative to the true value in living brain, most likely due to the omission of cerebral catechol-*O*-methyltransferase activity. In positron emission tomography studies, partial volume effects reduce the true radioactivity in gray matter structures such as the striatum and consequently may also contribute to under-estimation of dopa decarboxylase activity. Higher resolution tomographs and routine application of partial volume corrections are necessary for more accurate estimates of dopa decarboxylase activity in vivo. A method of correcting cerebral radioactivities for spillover was developed in our laboratory, and preliminary results suggest that the dopa decarboxylase activity in patients with Parkinson's disease may be nearly normal in caudate but greatly reduced in the putamen, entirely in agreement with post-mortem results that locate the major neurochemical pathology in the putamen.

Non-catechol substrates of dopa decarboxylase such as L-[^{18}F]fluoro-*m*-tyrosines offer significant advantages over L-6-[^{18}F]fluorodopa in terms of reduced peripheral metabolism, increased image contrast, and improved delineation of striatal regions of interest. Furthermore, the compartmental models associated with L-[^{18}F]fluoro-*m*-tyrosines are simpler since they do not include constants associated with methylated metabolites, such as q and k_5^{DOPA}. However, the lack of detailed kinetic information regarding relevant metabolic processes, such as the storage of [^{18}F]fluoro-*m*-tyramine and clearance of its deaminated derivative, inhibits the development of accurate compartmental models for L-[^{18}F]fluoro-*m*-tyrosines. Until these issues are resolved, L-[^{18}F]fluoro-*m*-tyrosines cannot supplant L-6-[^{18}F]fluorodopa as the preferred tracer for assays of dopa decarboxylase activity in living brain.

Positron emission tomography with L-6-[^{18}F]fluorodopa has yielded quantitative measures that are of clinical importance in distinguishing between patients with Parkinson's disease and healthy control subjects. However, it is unlikely that this autoradiographic

technique will ever become a standard clinical tool for neurological investigations due to its high cost and complexity of operation. Nonetheless, L-6-[^{18}F]fluorodopa remains an indispensable research tool for studying the underlying mechanisms of pathologies related to malfunctioning dopaminergic neuronal pathways. Application of the present compartmental model, in conjunction with a correction for partial volume effects, to total cerebral radioactivities measured by positron emission tomography permits the accurate and precise estimation of kinetic constants that reflect the rates of blood-brain uptake and decarboxylation of L-6-[^{18}F]fluorodopa, and by extension, the functional state of the biochemical pathway for nigrostriatal dopamine synthesis and metabolism in living brain.

REFERENCES

Acquas E, Carboni E, de Ree RHA, Da Prada M, Di Chiara G (1992) Extracellular concentrations of dopamine and metabolites in the rat caudate after oral administration of a novel catechol-*O*-methyltransferase inhibitor Ro 40-7592. *J Neurochem* 59:326-330.

Albin RL, Young AB, Penney JB (1989) The functional anatomy of basal ganglia disorders. [Review] *Trends Neurosci* 12:366-375.

Aminoff MJ (1998) Pharmacologic management of parkinsonism and other movement disorders. *In*: "Basic and Clinical Pharmacology" (Katzung BG, Ed.), 7th ed., pp. 450-463. Appleton & Lange, Connecticut.

Andén N-E, Carlsson A, Dahlström A, Fuxe K, Hillarp N-Å, Larsson K (1964) Demonstration and mapping out of nigro-neostriatal dopamine neurons. *Life Sci* 3:523-530.

Andén N-E, Dahlström A, Fuxe K, Larsson K (1965) Further evidence for the presence of nigro-neostriatal dopamine neurons in the rat. *Am J Anat* 116:329-334.

Andén N-E, Fuxe K, Hamberger B, Hökfelt T (1966) A quantitative study on the nigro-neostriatal dopamine neuron system in the rat. *Acta Physiol Scand* 67:306-312.

Andén N-E, Engel J, Rubenson A (1972) Central decarboxylation and uptake of L-DOPA. *Naunyn-Schmiedeberg's Arch Pharmacol* 273:11-26.

Antonini A, Vontobel P, Psylla M, Günther I, Maguire PR, Missimer J, Leenders KL (1995) Complementary positron emission tomography studies of the striatal dopaminergic system in Parkinson's disease. *Arch Neurol* 52:1183-1190.

Antonini A, Leenders KL, Vontobel P, Maguire P, Missimer J, Psylla M, Günther I (1997) Complementary PET studies of striatal neuronal function in the differential diagnosis between multiple system atrophy and Parkinson's disease. *Brain* 120:2187-2195.

Aosaki T, Kimura M, Graybiel AM (1995) Temporal and spatial characteristics of tonically active neurons of the primate's striatum. *J Neurophys* 73:1234-1252.

Ascher PW (1976) Das anticholinergische Behandlungsprinzip des Morbus Parkinson. *Wien Klin Wochenschr* 88:641-646.

Ballard PA, Tetrud JW, Langston JW (1985) Permanent human parkinsonism due to 1-methyl-4-phenyl-1,2,3,6-tetrahydropyridine (MPTP): seven cases. *Neurology* 35:949-956.

Bankiewicz KS, Oldfield EH, Chiueh CC, Doppman JL, Jacobowitz DM, Kopin IJ (1986) Hemiparkinsonism in monkeys after unilateral internal carotid artery infusion of 1-methyl-4-phenyl-1,2,3,6-tetrahydropyridine (MPTP). *Life Sci* 39:7-16.

Barrio JR, Huang S-C, Melega WP, Yu D-C, Hoffman JM, Schneider JS, Satyamurthy N, Mazziotta JC, Phelps ME (1990) 6-[^{18}F]Fluoro-L-DOPA probes dopamine turnover rates in central dopaminergic structures. *J Neurosci Res* 27:487-493.

Barrio JR, Nguyen QL, Svidler R, Namavari M, Edwards R, Lui Y, Peter D, Satyamurthy N, Phelps ME (1995). Intraneuronal vesicular transport and MAO A oxidation of 6-[^{18}F]-fluorodopamine and analogs. [Abstract] *J Cereb Blood Flow Metab* 15:S652.

Barrio JR, Huang S-C, Yu D-C, Melega WP, Quintana J, Cherry SR, Jacobson A, Namavari M, Satyamurthy N, Phelps ME (1996) Radiofluorinated L-*m*-tyrosines: new in-vivo probes for central dopamine biochemistry. *J Cereb Blood Flow Metab* 16:667-678.

Barrio JR, Huang S-C, Phelps ME (1997) Biological imaging and the molecular basis of dopaminergic diseases. [Review] *Biochem Pharmac* 54:341-348.

Bartholini G, Pletscher A (1968) Cerebral accumulation and metabolism of C^{14}-DOPA after selective inhibition of peripheral decarboxylase. *J Pharmacol Exp Ther* 161:14-20.

Benecke R, Strümper P, Weiss H (1993) Electron transfer complexes I and IV of platelets are abnormal in Parkinson's disease but normal in Parkinson-plus syndromes. *Brain* 116:1451-1463.

Berger B, Gaspar P, Verney C (1991) Dopaminergic innervation of the cerebral cortex: unexpected differences between rodents and primates. [Review] *Trends Neurosci* 14:21-27.

Bernheimer H (1963) Distribution of homovanillic acid in the human brain. *Nature* 204:587-588.

Bernheimer H, Birkmayer W, Hornykiewicz O (1963) Zur Biochemie des Parkinson-Sundroms des Menschen: Einflub der Monoaminoxydase-Hemmer-Therapie auf die Konzentration des Dopamins, Noradrenalins und 5-Hydroxytryptamins im Gehirn. *Klin Wochenschr* 41:465-469.

Bernheimer H, Hornykiewicz O (1965) Herabgesetzte Konzentration Derhomovanillinsäure im Gehirn von parkinsonkranken Menschen als Ausdruck der Störung des zentralen Dopaminstoffwechsels. *Klin Wochensch* 43:711-715.

Bernheimer H, Birkmayer W, Hornykiewicz O, Jellinger K, Seitelberger F (1973) Brain dopamine and the syndromes of Parkinson and Huntington. *J Neurol Sci* 20:415-455.

Bertler Å, Rosengren E (1959) Occurrence and distribution of dopamine in brain and other tissues. *Experientia* 15:10-11.

Bertler Å, Falck B, N-Å Hillarp, Rosengren E, Torp A (1959) Dopamine and chromaffin cells. *Acta Physiol Scand* 47:251-258.

Bertler Å (1961) Occurrence and localization of catechol amines in the human brain. *Acta Physiol Scand* 51:97-107.

Bertler Å, Falck B, Rosengren E (1963) The direct demonstration of a barrier mechanism in the brain capillaries. *Acta Pharmacol Toxicol* 20:317-321.

Bertler Å, Falck B, Owman CH, Rosengren E (1966) The localization of monoaminergic blood-brain barrier mechanisms. *Pharmacol Rev* 18:369-385.

Birkmayer W, Hornykiewicz O (1961) Der L-3,4-Dioxyphenylalanin (= DOPA)-Effekt bei der Parkinson-Akinese. *Wien Klin Wochenschr* 73:787-788.

Boecker H, Weindl A, Leenders K, Antonini A, Kuwert T, Kruggel F, Gräfin v Einseidel H, Conrad B (1996) Secondary parkinsonism due to focal substantia nigra lesions: a PET study with [^{18}F]FDG and [^{18}F]fluorodopa. *Acta Neurol Scand* 93:387-392.

Borri-Voltattorni C, Minelli A, Dominici P (1983) Interaction of aromatic amino acids in D and L forms with 3,4-dihydroxyphenylalanine decarboxylase from pig kidney. *Biochemistry* 22:2249-2254.

Bouchard S (1987) Optimum symptomatic control of Parkinson's disease with dopaminergic therapy. [Review] *Can J Neurol Sci* 14:460-465.

Boyes BE, Cumming P, Martin WRW, McGeer EG (1986) Determination of plasma [^{18}F]-6-fluorodopa during positron emission tomography: elimination and metabolism in carbidopa treated subjects. *Life Sci* 39:2243-2252.

Broch OJ Jr, Fonnum F (1972) The regional and subcellular distribution of catechol-*O*-methyl transferase in the rat brain. *J Neurochem* 19:2049-2055.

Brooks BA, Eidelberg E, Morgan WW (1987) Behavioral and biochemical studies in monkeys made hemiparkinsonian by MPTP. *Brain Res* 419:329-332.

Brust P, Bauer R, Walter B, Bergmann R, Vorwieger G, Steinbach J, Füchtner F, Will E, Linemann H, Johannsen B (1997) Simultaneous measurement of cerebral blood flow and [^{18}F]DOPA metabolism in newborn piglets. [Abstract] *Neuroimage* 5:A25.

Burack WR, Draskóczy PR (1964) The turnover of endogenously labeled catecholamine in several regions of the sympathetic nervous system. *J Pharmacol Exp Ther* 144:66-75.

Buu NT (1989) Vesicular accumulation of dopamine following L-DOPA administration. *Biochem Pharmacol* 38:1787-1792.

Calne DB (1970) Parkinsonism: physiology, pharmacology and treatment, 1st ed., pp. 49-50. Edward Arnold Publishers, London.

Calne DB, Teychenne PF, Claveria LE, Eastman R, Greenacre JK, Petrie A (1974) Bromocriptine in parkinsonism. *Brit Med J* 4:442-444.

Carlsson A (1966) Pharmacological depletion of catecholamine stores. [Review] *Pharmacol Rev* 18:541-549.

Cedarbaum JM, Guttman M, Leblanc C, Léger G, Reches A (1990) OR-462 inhibits 3-*O*-methyldopa formation in monkeys. [Abstract] *Neurology* 40 (Suppl 1):270.

Chan GL-Y, Hewitt KA, Pate BD, Schofield P, Adam MJ, Ruth TJ (1992) Routine determination of [^{18}F]-L-6-fluorodopa and its metabolites in blood plasma is essential for accurate positron emission tomography studies. *Life Sci* 50:309-318.

Cheng CH, Wooten GF (1982) Dopamine turnover estimated by simultaneous LCEC assay of dopamine and dopamine metabolites. *J Pharmacol Methods* 8:123-133.

Chia L-G, Cheng F-C, Kuo J-S (1993) Monoamines and their metabolites in plasma and lumbar cerebrospinal fluid of Chinese patients with Parkinson's disease. *J Neurol Sci* 116:125-134.

Chiba K, Trevor AJ, Castagnoli N Jr (1984) Metabolism of the neurotoxic tertiary amine, MPTP, by brain monoamine oxidase. *Biochem Biophys Res Commun* 120:574-578.

Chiba K, Trevor AJ, Castagnoli N Jr (1985) Active uptake of MPP^+, metabolite of MPTP, by brain synaptosomes. *Biochem Biophys Res Commun* 128:1228-1232.

Chien JB, Wallingford RA, Ewing AG (1990) Estimation of free dopamine in the cytoplasm of the giant dopamine cell of *Planorbis corneus* by voltammetry and capillary electrophoresis. *J Neurochem* 54:633-638.

Chirakal R, Firnau G, Garnett ES (1986) High yield synthesis of 6-[^{18}F]fluoro-L-dopa. *J Nucl Med* 27:417-421.

Chirakal R, Schrobilgen GJ, Firnau G, Garnett S (1991) Synthesis of ^{18}F labelled fluoro-*m*-tyrosine, fluoro-*m*-tyramine and fluoro-3-hydroxyphenylacetic acid. *Appl Radiat Isot* 42:113-119.

Chiueh CC, Zukowska-Grojec Z, Kirk KL, Kopin IJ (1983) 6-Fluorocatecholamines as false neurotransmitters. *J Pharmacol Exp Ther* 225:529-533.

Chung MY, Kim DG, Yoo KJ, Hong SS (1993) Regional differences in the levels of biogenic amines and their metabolites in rat brain after tricyclic antidepressant treatments. *Yonsei Med J* 34:266-277.

Comi G, Miletich RS, Kopin I, Bankiewicz K, Plunkett R, Adams R, Dunn B, Di Chiro G (1990) Metabolism and PET imaging of 6-[F-18]fluoro-L-dopa after catechol-*O*-methyltransferase inhibition in normal and hemiparkinsonian monkeys. [Abstract] *Neurology* 40 (Suppl 1):270-271.

Cooper JR, Bloom FE, Roth RH (1991) The Biochemical Basis of Neuropharmacology, 6th ed., p. 228. Oxford University Press, New York.

Côté L, Crutcher MD (1991) The basal ganglia. *In*: "Principles of Neural Science" (Kandel ER, Schwartz JH, Jessell TM, Eds.), 3rd ed., pp. 647-659. Elsevier Science Publishing, New York.

Cotran RS, Kumar V, Robbins SL (1994) Robbins Pathologic Basis of Disease, 5th ed., p.1332. WB Saunders Co., Philadelphia.

Cotzias GC, Van Woert MH, Schiffer LM (1967) Aromatic amino acids and modification of parkinsonism. *N Eng J Med* 276:374-379.

Cotzias GC, Papavasiliou PS, Gellene R (1969) Modification of parkinsonism: chronic treatment with L-DOPA. *New Eng J Med* 280:337-345.

Council on Drugs (1967) Evaluation of a new antiviral agent: amantadine hydrochloride (Symmetrel). *JAMA* 201:114-115.

CRC Press (1981) CRC Handbook of Chemistry and Physics (Weast RC and Astle MJ, Eds.), 62nd ed., pp. B256-B339. CRC Press, Florida.

Creveling CR, Kirk KL (1985) The effect of ring-fluorination on the rate of *O*-methylation of dihydroxyphenylalanine (DOPA) by catechol-*O*-methyltransferase: significance in the development of ^{18}F-PETT scanning agents. *Biochem Biophys Res Commun* 130:1123-1131.

Crone C (1963) The permeability of capillaries in various organs as determined by the use of 'the indicator diffusion' method. *Acta Physiol Scand* 58:292-305.

Cumming P, Boyes BE, Martin WRW, Adam M, Grierson J, Ruth T, McGeer EG (1987*a*) The metabolism of [^{18}F]6-fluoro-L-3,4-dihydroxyphenylalanine in the hooded rat. *J Neurochem* 48:601-608.

Cumming P, Boyes BE, Martin WRW, Adam M, Ruth TJ, McGeer EG (1987*b*) Altered metabolism of [^{18}F]6-fluorodopa in the hooded rat following inhibition of catechol-*O*-methyltransferase with U-0521. *Biochem Pharmacol* 36:2527-2531.

Cumming P, Häusser M, Martin WRW, Grierson J, Adam MJ, Ruth TJ, McGeer EG (1988) Kinetics of in vitro decarboxylation and the in vivo metabolism of 2-^{18}F and 6-^{18}F-fluorodopa in the hooded rat. *Biochem Pharmacol* 37:247-250.

Cumming P, Brown E, Damsma G, Fibiger H (1992) Formation and clearance of interstitial metabolites of dopamine and serotonin in the rat striatum: an in vivo microdialysis study. *J Neurochem* 59:1905-1914.

Cumming P, Léger GC, Kuwabara H, Gjedde A (1993) Pharmacokinetics of plasma 6-[^{18}F]fluoro-L-3,4-dihydroxyphenylalanine ([^{18}F]FDOPA) in humans. *J Cereb Blood Flow Metab* 13:668-675.

Cumming P, Kuwabara H, Gjedde A (1994*a*) A kinetic analysis of 6-[^{18}F]fluoro-L-dihydroxyphenylalanine metabolism in the rat. *J Neurochem* 63:1675-1682.

Cumming P, Venkatachalam TK, Rajagopal S, Diksic M, Gjedde A (1994*b*) Brain uptake of α-[^{14}C]methyl-*para*-tyrosine in the rat. *Synapse* 17:125-128.

Cumming P, Kuwabara H, Ase A, Gjedde A (1995*a*) Regulation of DOPA decarboxylase activity in brain of living rat. *J Neurochem* 65:1381-1390.

Cumming P, Ase A, Diksic M, Harrison J, Jolly D, Kuwabara H, Laliberté C, Gjedde A (1995*b*) Metabolism and blood-brain clearance of L-3,4-dihydroxy-[^{3}H]phenylalanine ([^{3}H]DOPA) and 6-[^{18}F]fluoro-L-DOPA in the rat. *Biochem Pharmacol* 50:943-946.

Cumming P, Ase A, Laliberté C, Kuwabara H, Gjedde A (1997*a*) In vivo regulation of DOPA decarboxylase by dopamine receptors in rat brain. *J Cereb Blood Flow Metab* 17:1254-1260.

Cumming P, Ljubic-Thibal V, Laliberté C, Diksic M (1997*b*) The effect of unilateral neurotoxic lesions to serotonin fibres in the medial forebrain bundle on the metabolism of [^{3}H]DOPA in the telencephalon of the living rat. *Brain Res* 747:60-69.

Cumming P, Deep P, Rousset O, Evans A, Gjedde A (1997*c*) On the rate of decarboxylation of dopa to dopamine in living mammalian brain. *In*: "Frontiers of Neurology - A Symposium in Honour of Fred Plum." (Reis DJ, Posner J, Eds.), vol. 835, pp. 274-308. New York Academy of Sciences Press, New York.

Cumming P, Gjedde A (1998) Compartmental analysis of dopa decarboxylation in living brain from dynamic positron emission tomograms. [Review] *Synapse* 29:37-61.

Cumming P, Ase A, Kuwabara H, Gjedde A (1998*a*) [^{3}H]DOPA formed from [^{3}H]tyrosine in living rat brain is not committed to dopamine synthesis. *J Cereb Blood Flow Metab* 18:491-499.

Cumming P, Yokoi F, Chen A, Deep P, Dagher A, Reutens D, Gjedde A, Wong D (1998*b*) Pharmacokinetics of radiotracers in human plasma during positron emission tomography. *Synapse*, submitted.

Dahlström A, Fuxe K (1964) Evidence for the existence of monoamine-containing neurons in the central nervous system. *Acta Physiol Scand* 62 (Suppl 232):1-55.

Dallos V, Heathfield K, Stone P, Allen FAD (1970) Use of amantadine in Parkinson's disease: results of a double-blind trial. *Brit Med J* 4:24-26.

Danielsen EH, Smith DF, Gee AD, Venkatachalam TK, Hansen SB, Gjedde A (1997) The metabolism of [^{18}F]-DOPA in pigs estimated by PET. [Abstract] *Brain-PET '97*, Washington D.C., USA.

Davidson L, Lloyd K, Dankova J, Hornykiewicz O (1971) L-DOPA treatment in Parkinson's disease: effect on dopamine and related substances in discrete brain regions. *Experientia* 27:1048-1049.

Dedek J, Baumes R, Tien-Duc N, Gomeni R, Korf J (1979) Turnover of free and conjugated (sulphonyloxy)-dihydroxyphenylacetic acid and homovanillic acid in rat striatum. *J Neurochem* 33:687-695.

Deep P, Kuwabara H, Gjedde A, Reith J, Cumming P (1996) A parametric atlas of the metabolism of [^{3}H]DOPA in brain of living rat. [Abstract] *Society for Neuroscience 26th Annual Meeting*, Washington D.C., U.S.A.

Deep P, Gjedde A, Cumming P (1997*a*) On the accuracy of an [^{18}F]FDOPA compartmental model: evidence for vesicular storage of [^{18}F]fluorodopamine in vivo. *J Neurosci Methods* 76:157-165.

Deep P, Kuwabara H, Gjedde A, Cumming P (1997*b*) The kinetic behaviour of [^{3}H]dopa in living rat brain investigated by compartmental modelling of static autoradiograms. *J Neurosci Methods* 78:157-168.

Deep P, Kuwabara H, Gjedde A, Cumming P (1997*c*) Modelling the cerebral kinetics of [^{3}H]DOPA. [Abstract] *Neuroimage* 5:A24.

Deep P, Dagher A, Sadikot A, Gjedde A, Cumming P (1998) Amantadine at low dose stimulates slightly the metabolism of 6-[^{18}F]fluoro-L-dopa (FDOPA) in healthy human brain. *Synapse*, submitted.

DeJesus OT, Mukherjee J (1988) Radiobrominated *m*-tyrosine analog as potential CNS L-dopa PET tracer. *Biochem Biophys Res Commun* 150:1027-1031.

DeJesus OT, Sunderland JJ, Nickles JR, Mukherjee J, Appelman EH (1990*a*) Synthesis of radiofluorinated analogs of *m*-tyrosine as potential L-DOPA tracers via direct reaction with acetylhypofluorite. *Appl Radiat Isot* 41:433-437.

DeJesus OT, Murali D, Sunderland JJ, Chen C-A, Weiler M, Nickles RJ (1990*b*) [F-18]-Fluoro-MDL 72394, a potentially trappable tracer for presynaptic dopamine neurons. [Abstract] *J Nucl Med* 31:902.

DeJesus OT, Holden JE, Murali D, Uno H, Shelton S, Freund L, Houser WD, Nickles RJ (1991*a*) Validation of [F-18]-6-fluoro-MDL-72394 as optimal probe for dopamine nerve terminals: metabolism in rats and monkeys. [Abstract] *J Nucl Med* 32:1096.

DeJesus OT, Murali D, Chen C-A, Sunderland JJ, Weiler M, Nickles RJ (1991*b*) F-18 Labelled PET tracers for CNS presynaptic dopamine neurons. [Abstract] *J Labelled Com Radiopharm* 30:272-273.

DeJesus OT, Holden JE, Endres C, Murali D, Oakes TR, Shelton S, Uno H, Houser D, Freund L, Perlman SB, Nickles RJ (1992) Visualization of dopamine nerve terminals by positron tomography using [^{18}F]fluoro-β-fluoromethylene-*m*-tyrosine. *Brain Res* 597:151-154.

DeJesus OT, Endres CJ, Shelton SE, Nickles RJ, Holden JE (1997) Evaluation of fluorinated *m*-tyrosine analogs as PET imaging agents of dopamine nerve terminals: comparison with 6-fluorodopa. *J Nucl Med* 38:630-636.

Descarries L, Bosler O, Berthelet F, Des Rosiers MH (1980) Dopaminergic nerve endings visualized by high-resolution autoradiography in adult rat neostriatum. *Nature* 284:620-622.

Dhawan V, Ishikawa T, Patlak C, Chaly T, Robeson W, Belakhlef A, Margouleff C, Mandel F, Eidelberg D (1996) Combined FDOPA and 3OMFD PET studies in Parkinson's disease. *J Nucl Med* 37:209-216.

Diffley DM, Costa JL, Sokoloski EA, Chiueh CC, Kirk KL, Creveling CR (1983) Direct observation of 6-fluorodopamine in guinea pig nerve microsacs by ^{19}F NMR *Biochem Biophys Res Commun* 110:740-745.

Doudet DJ, McLellan CA, Carson R, Adams HR, Miyake H, Aigner TG, Finn RT, Cohen RM (1991*a*) Distribution and kinetics of 3-*O*-methyl-6-[^{18}F]fluoro-L-DOPA in the rhesus monkey brain. *J Cereb Blood Flow Metab* 11:726-734.

Doudet DJ, McLellan CA, Aigner TG, Wyatt R, Adams HR, Miyake H, Finn RT, Cohen RM (1991*b*) Postinjection L-phenylalanine increases basal ganglia contrast in PET scans of 6-^{18}F-DOPA. *J Nucl Med* 32:1408-1413.

Earle KM (1968) Studies of Parkinson's disease including x-ray fluorescent spectroscopy of formalin fixed brain tissue. *J Neuropath Exp Neurol* 27:1-14.

Ehringer H, Hornykiewicz O (1960) Verteilung von Noradrenalin und Dopamin (3-hydroxytyramin) im Gehirn des Menschen und ihr Verhalten bei Erkrankungen des extrapyramidalen Systems. *Klin Wochenschr* 38:1236-1239.

Eidelberg D, Takikawa S, Dhawan V, Chaly T, Robeson W, Dahl R, Margouleff D, Moeller JR, Patlak CS, Fahn S (1993) Striatal ^{18}F-DOPA uptake: absence of an aging effect. *J Cereb Blood Flow Metab* 13:881-888.

Eidelberg D, Moeller JR, Ishikawa T, Dhawan V, Spetsieris P, Chaly T, Belakhlef A, Mandel F, Przedborski S, Fahn S (1995) Early differential diagnosis of Parkinson's disease with ^{18}F-fluorodeoxyglucose and positron emission tomography. *Neurology* 45:1995-2004.

Eklundh T, Eriksson M, Sjöberg S, Nordin C (1996) Monoamine precursors, transmitters and metabolites in cerebrospinal fluid: a prospective study in healthy male subjects. *J Psychiat Res* 30:201-208.

Eldrup E, Mogensen P, Jacobsen J, Pakkenberg H, Christensen NJ (1995) CSF and plasma concentrations of free norepinephrine, dopamine, 3,4-dihydroxyphenylacetic acid (DOPAC), 3,4-dihydroxyphenylalanine (DOPA), and epinephrine in Parkinson's disease. *Acta Neurol Scand* 92:116-121.

Endres CJ, Swaminathan S, DeJesus OT, Sievert M, Ruoho AE, Murali D, Rommelfanger SG, Holden JE (1997) Affinities of dopamine analogs for monoamine granular and plasma membrane transporters: implications for PET dopamine studies. *Life Sci* 60:2399-2406.

Ericsson AD (1971) Potentiation of the L-dopa effect in man by the use of catechol-*O*-methyltransferase inhibitors. *J Neurol Sci* 14:193-197.

Falck B (1962) Observations on the possibilities of the cellular localization of monoamines by a fluorescence method. *Acta Physiol Scand* 56 (Suppl 197):1-26.

Falck B, Hillarp N-Å, Thieme G, Torp A (1962) Fluorescence of catechol amines and related compounds condensed with formaldehyde. *J Histochem Cytochem* 10:348-354.

Farde L (1996) The advantage of using positron emission tomography in drug research. [Review] *Trends Neurosci* 19:211-214.

Felice LJ, Felice JD, Kissinger PT (1978) Determination of catecholamines in rat brain parts by reverse-phase ion-pair liquid chromatography. *J Neurochem* 31:1461-1465.

Ferguson SA, Kraemer GW, Bowman RE, Schmidt DE, Ebert MH (1993) Lack of effect of chronic developmental lead treatment on biogenic amines and metabolites in monkey cerebrospinal fluid. *Neurotox Teratol* 15:229-235.

Feuerstein TJ (1994) Ketamin hemmt die *N*-Methyl-D-Aspartat (NMDA)-Rezeptor vermittelte Azetylcholinfreisetzung aus N. caudatus-Schnitten des Kaninchens. *Anaesthesist* 43 (Suppl 2):S48-S51

Figueredo-Cardenas G, Chen Q, Reiner A (1997) Age-dependent differences in survival of striatal somatostatin-NPY-NADPH-diaphorase-containing interneurons versus striatal projection interneurons after interstriatal injection of quinolinic acid in rats. *Exp Neurol* 146:444-457.

Firnau G, Nahmias C, Garnett S (1973*a*) The preparation of [^{18}F]5-fluoro-DOPA with reactor-produced fluorine-18. *Int J Appl Radiat Isot* 24:182-184.

Firnau G, Nahmias C, Garnett S (1973*b*) Synthesis of 3,4-dihydroxy-5-fluoro-DL-phenylalanine and 3,4-dihydroxy-5-[^{18}F]fluoro-DL-phenylalanine. *J Med Chem* 16:416-418.

Firnau G, Garnett ES, Sourkes TL, and Missala K (1975) [^{18}F]Fluoro-dopa: a unique gamma emitting substrate for dopa decarboxylase. *Experientia* 31:1254-1255.

Firnau G, Garnett ES, Chan PHK, Belbeck LW (1976) Intracerebral dopamine metabolism studied by a novel radioisotope technique. *J Pharm Pharmacol* 28:584-585.

Firnau G, Chirakal R, Sood S, Garnett S (1980*a*) Aromatic fluorination with xenon difluoride: L-3,4-dihydroxy-6-fluoro-phenylalanine. *Can J Chem* 58:1449-1450.

Firnau G, Sood S, Pantel R, Garnett S (1980*b*) Phenol ionization in dopa determines the site of methylation by catechol-*O*-methyltransferase. *Molec Pharmac* 19:130-133.

Firnau G, Chirakal R, Sood S, Garnett ES (1981) Radiofluorination with xenon difluoride: L-6[F-18]fluoro-dopa. *[Abstract] J Labelled Com Radiopharm* 18:7-8.

Firnau G, Chirakal R, Garnett ES (1984) Aromatic radiofluorination with [^{18}F]fluorine gas: 6-[^{18}F]fluoro-L-dopa. *J Nucl Med* 25:1228-1233.

Firnau G, Garnett ES, Chirakal R, Sood S, Nahmias C, Schrobilgen G (1986) [^{18}F]Fluoro-L-dopa for the in vivo study of intracerebral dopamine. [Review] *Appl Radiat Isot* 37:669-675.

Firnau G, Sood S, Chirakal R, Nahmias C, Garnett ES (1987) Cerebral metabolism of 6-[^{18}F]fluoro-L-3,4-dihydroxyphenylalanine in the primate. *J Neurochem* 48:1077-1082.

Firnau G, Sood S, Chriakal R, Nahmias C, Garnett ES (1988) Metabolites of 6-[^{18}F]fluoro-L-dopa in human blood. *J Nucl Med* 29:363-369.

Firnau G, Chirakal R, Nahmias C, Garnett ES (1991*a*) [F-18]Fluoro-*meta*-L-tyrosine is a better PET tracer than [F-18]fluoro-L-dopa for the delineation of dopaminergic structures in the human brain. [Abstract] *J Labelled Com Radiopharm* 30:266-268.

Firnau G, Chirakal R, Nahmias C, Garnett ES (1991*b*) Do the metabolites of [F-18]fluoro-*meta*-L-tyrosine contribute to the F-18 accumulation in the human brain? [Abstract] *J Labelled Com Radiopharm* 30:293-294.

Fletcher EA, Redfern PH (1970) The effect of amantadine on the uptake of dopamine and noradrenaline by rat brain homogenates. *J Pharm Pharmacol* 22:957-959.

Forno LS (1966) Pathology of parkinsonism: a preliminary report of 24 cases. *J Neurosurg* 24:266-271.

Forno LS (1969) Concentric hyalin intraneuronal inclusions of Lewy type in the brains of elderly persons (50 incidental cases): relationship to parkinsonism. *J Amer Geriat Soc* 17:557-575.

Fowler CJ, Benedetti MS (1983) The metabolism of dopamine by both forms of monoamine oxidase in the rat brain and its inhibition by cimoxatone. *J Neurochem* 40:1534-1541.

Francis A, Whittemore R, Jeffery DR, Pearce LB, Roth JA (1987) Catecholamine-metabolizing enzyme activity in the nigrostriatal system. *Biochem Pharmacol* 36:2229-2231.

Freeman AS, Meltzer LT, Bunney BS (1985) Firing properties of substantia nigra dopaminergic neurons in freely moving rats. *Life Sci* 36:1983-1994.

Fuxe K, Owman C (1965) Cellular localization of monoamines in the area postrema of certain mammals. *J Comp Neurol* 125:337-354.

Fuxe K, Hökfelt T, Ungerstedt U (1970) Morphological and functional aspects of central monoamine neurons. [Review] *Int Rev Neurobiol* 13:93-126.

Garnett ES, Firnau G, Nahmias C, Sood S, Belbeck L (1980) Blood-brain barrier transport and cerebral utilization of dopa in living monkeys. *Am J Physiol* 238:R318-R327.

Garnett S, Firnau G, Nahmias C, Chirakal R (1983*a*) Striatal dopamine metabolism in living monkeys examined by positron emission tomography. *Brain Res* 280:169-171.

Garnett ES, Firnau G, Nahmias C (1983*b*) Dopamine visualized in the basal ganglia of living man. *Nature* 305:137-138.

Garnett ES, Nahmias C, Firnau G (1984) Central dopaminergic pathways in hemiparkinsonism examined by positron emission tomography. *Can J Neurol Sci* 11:174-179.

Garnett ES, Lang AE, Chirakal R, Firnau G, Nahmias C (1987) A rostrocaudal gradient for aromatic acid decarboxylase in the human striatum. *Can J Neurol Sci* 14:444-447.

Garrett MC, Soares-da-Silva P (1990) Role of type A and B monoamine oxidase on the formation of 3,4-dihydroxyphenylacetic acid (DOPAC) in tissues from the brain of the rat. *Neuropharmacology* 29:875-879.

Garrett MC, Soares-da-Silva P (1992) Increased cerebrospinal fluid dopamine and 3,4-dihydroxyphenylacetic acid levels in Huntington's disease: evidence for an overactive dopaminergic brain transmission. *J Neurochem* 58:101-106.

Gaspar P, Duyckaerts C, Alvarez C, Javoy-Agid F, Berger B (1991) Alterations of dopaminergic and noradrenergic innervations in motor cortex in Parkinson's disease. *Ann Neurol* 30:365-374.

Gauthier S, Gauthier L (1987) Current status of levodopa therapy in idiopathic Parkinson's disease. *Can J Neurol Sci* 14:452-454.

Gjedde A, Hansen AJ, Siemkowicz E (1980) Rapid simultaneous determination of regional blood flow and blood-brain glucose transfer in brain of rat. *Acta Physiol Scand* 108:321-330.

Gjedde A (1981) High- and low-affinity transport of D-glucose from blood to brain. *J Neurochem* 36:1463-1471.

Gjedde A (1982) Calculation of glucose phosphorylation from brain uptake of glucose analogs in vivo: a re-examination. [Review] *Brain Res Rev* 4:237-274.

Gjedde A, Bodsch W (1987) Facilitated diffusion across the blood-brain barrier: interactions between receptors and transporters. *Wissenschaftl Z Karl Marx Univ (Leipzig)* 36:67-71.

Gjedde A, Reith J, Kuwabara H, Dyve S (1990) Determining dopa decarboxylase activity in the human brain in vivo: the complete fluoro-dopa model. [Abstract] *J Nucl Med* 31:720-721.

Gjedde A, Reith J, Dyve S, Léger G, Guttman M, Diksic M, Evans A, Kuwabara H (1991) Dopa decarboxylase activity of the living human brain. *Proc Natl Acad Sci USA* 88:2721-2725.

Gjedde A, Léger GC, Cumming P, Yasuhara Y, Evans AC, Guttman M, Kuwabara H (1993) Striatal L-DOPA decarboxylase activity in Parkinson's disease in vivo: implications for the regulation of dopamine synthesis. *J Neurochem* 61:1538-1541.

Gjedde A, Reith J, Léger G, Cumming P, Yasuhara Y, Guttman M, Kuwabara H (1995) Brain-blood barrier removal of DOPA: role in regulation of dopamine synthesis and treatment in Parkinson's disease. *In*: "New Concepts of a Blood-Brain Barrier" (Greenwood J, Ed.), 1st ed., pp. 103-109. Plenum Press, New York.

Gjedde A (1996) DOPA decarboxylase [Letter] *Move Disord* 11:462-463.

Glowinski J, Iversen LL (1966) Regional studies of catecholamines in the rat brain - I: the disposition of [^{3}H]norepinephrine, [^{3}H]dopamine, and [^{3}H]DOPA in various regions of the brain. *J Neurochem* 13:655-669.

Goldstein DS, Udelsman R, Eisenhofer G, Stull R, Keiser HR, Kopin IJ (1987) Neuronal source of plasma dihydroxyphenylalanine. *J Clin Endocrinol Metab* 64:856-861.

Gordin A, Järvinen M, Kaakola S, Wikberg T, Pohto P (1990) Effect of nitecapone, a novel COMT inhibitor, on the metabolism of L-dopa after single and multiple dosing. [Abstract] *Neurology* 40 (Suppl 1):271.

Gordonsmith RH, Raxworthy MJ, Gulliver PA (1982) Substrate specificity and selectivity of catechol-*O*-methyltransferase for DOPA, DOPA derivatives and α-substituted catecholamines. *Biochem Pharmacol* 31:433-437.

Grace AA (1991) Phasic versus tonic dopamine release and the modulation of dopamine system responsivity: a hypothesis for the etiology of schizophrenia. [Review] *Neuroscience* 41:1-24.

Graybiel AM (1990) Neurotransmitters and neuromodulators in the basal ganglia. [Review] *Trends Neurosci* 13:244-254.

Groppetti A, Algeri S, Cattabeni F, Di Giulio AM, Galli CL, Ponzio F, Spano PF (1977) Changes in specific activity of dopamine metabolites as evidence of a multiple compartmentation of dopamine in striatal neurons. *J Neurochem* 28:193-197.

Groves PM (1983) A theory of the functional organization of the neostriatum and the neostriatal control of voluntary movement. [Review] *Brain Res Rev* 5:109-132.

Guldberg HC, Broch OJ Jr (1971) On the mode of action of reserpine on dopamine metabolism in the rat striatum. *Eur J Pharmacol* 13:155-167.

Guldberg HC, Marsden CA (1975) Catechol-*O*-methyltransferase: pharmacological aspects and physiological role. [Review] *Pharmacol Rev* 27:135-206.

Günther I, Psylla M, Reddy GN, Antonini A, Vontobel P, Reist HW, Zollinger A, Nickles RJ, Beer H-F, Schubiger PA, Leenders KL (1995) Positron emission tomography in drug evaluation: influence of three different catechol-*O*-methyltransferase inhibitors on metabolism of [NCA] 6-[^{18}F]fluoro-L-dopa in rhesus monkey. *Nucl Med Biol* 22:921-927.

Gutman Y, Weil-Malherbe H (1967) The intracellular distribution of brain catecholamines. *J Neurochem* 14:619-625.

Guttman M, Léger G, Cedarbaum JM, Reches A, Woodward W, Evans A, Diksic M, Gjedde A (1992) 3-*O*-Methyldopa administration does not alter fluorodopa transport into the brain. *Ann Neurol* 31:638-643.

Guttman M, Léger G, Reches A, Evans A, Kuwabara H, Cedarbaum JM, Gjedde A (1993) Administration of the new COMT inhibitor OR-611 increases striatal uptake of fluorodopa. *Move Disord* 8:298-304.

Hadjiconstantinou M, Wemlinger TA, Sylvia CP, Hubble JP, Neff NH (1993) Aromatic L-amino acid decarboxylase of mouse striatum is modulated via dopamine receptors. *J Neurochem* 60:2175-2180.

Hadjiconstantinou M, Rossetti ZL, Wemlinger TA, Neff NH (1995) Dizocilpine enhances striatal tyrosine hydroxylase and aromatic L-amino acid decarboxylase activity. *Eur J Pharmacol* 289:97-101.

Hammerstad JP, Pate BD, Hewitt KA, Chan GL-Y, Ruth TJ, Calne DB (1993) The transport of L-6-fluorodopa and its metabolites from blood to cerebrospinal fluid and brain. *Ann Neurol* 34:604-608.

Hansson C, Edholm L-E, Agrup G, Rorsman H, Rosengren A-M, Rosengren E (1978) The quantitative determination of 5-*S*-cysteinyldopa and dopa in normal serum and in serum from patients with malignant melanoma by means of high-pressure liquid chromatography. *Clin Chim Acta* 88:419-427.

Hardebo JE, Owman C (1980) Barrier mechanisms for neurotransmitter monoamines and their precursors at the blood-brain interface. [Review] *Ann Neurol* 8:1-11

Hardebo JE, Emson PC, Falck B, Owman C, Rosengren E (1980) Enzymes related to monoamine transmitter metabolism in brain microvessels. *J Neurochem* 35:1388-1393.

Hartvig P, Ågren H, Reibring L, Tedroff J, Bjurling P, Kihlberg T, Långström B (1991) Brain kinetics of L-[β-^{11}C]DOPA in humans studied by positron emission tomography. *J Neural Transm (Gen Sect)* 86:25-41.

Hartvig P, Tedroff J, Lindner KJ, Bjurling P, Chang C-W, Tsukada H, Watanabe Y, Långström B (1993) Positron emission tomographic studies on aromatic L-amino acid decarboxylase activity in vivo for L-dopa and 5-hydroxy-L-tryptophan in the monkey brain. *J Neural Transm (Gen Sect)* 94:127-135.

Hayase N, Tomiyoshi K, Watanabe K, Horikoshi S, Hirato M, Shibasaki T, Ohye C (1994) Visualization of dopamine nerve terminals in monkey by positron emission tomography using 4-[^{18}F]fluoro-L-m-tyrosine. *Stereotact Funct Neurosurg* 62:191-196.

Hefti F, Melamed E, Wurtman RJ (1981) The site of dopamine formation in rat striatum after L-dopa administration. *J Pharmacol Exp Ther* 217:189-197.

Heikkila RE, Cohen G (1972) Evaluation of amantadine as a releasing agent or uptake blocker for H^3-dopamine in rat brain slices. *Eur J Pharmacol* 20:156-160.

Heikkila RE, Hess A, Duvoisin RC (1984) Dopaminergic neurotoxicity of 1-methyl-4-phenyl-1,2,5,6-tetrahydropyridine in mice. *Science* 224:1451-1453.

Heikkila RE, Sonsalla PK (1987) The use of the MPTP-treated mouse as an animal model of parkinsonism. *Can J Neurol Sci* 14:436-440.

Heimer L, Switzer RD, Van Hoesen GW (1982) Ventral striatum and ventral pallidum: components of the motor system? [Review] *Trends Neurosci* 5:83-87.

Heimer L (1995) The Human Brain and Spinal Cord: Functional Neuroanatomy and Dissection Guide, 2nd ed., pp. 337-360. Springer-Verlag, New York.

Hietala J, Syvälahti E, Vuorio K, Räkköläinen V, Bergman J, Haaparanta M, Solin O, Kuoppamäki M, Kirvelä O, Ruotsalainen U, Salokangas RKR (1995) Presynaptic dopamine function in striatum of neuroleptic-naive schizophrenic patients. *Lancet* 346:1130-1131.

Hillarp N-Å, Fuxe K, Dahlström A (1966) Demonstration and mapping of central neurons containing dopamine, noradrenaline, and 5-hydroxytryptamine and their reactions to psychopharmaca. [Review] *Pharmacol Rev* 18:727-741.

Hockman CH, Lloyd KG, Farley IJ, Hornykiewicz O (1971) Experimental midbrain lesions: neurochemical comparison between the animal model and Parkinson's disease. *Brain Res* 35:613-618.

Hoffman EJ, Huang S-C, Phelps ME (1979) Quantitation in positron emission computed tomography: 1. Effect of object size. *J Comput Assist Tomogr* 3:299-308.

Hoffman JM, Melega WP, Hawk TC, Grafton SC, Luxen A, Mahoney DK, Barrio JR, Huang S-C, Mazziotta JC, Phelps ME (1992) The effects of carbidopa administration on 6-[^{18}F]fluoro-L-DOPA kinetics in positron emission tomography. *J Nucl Med* 33:1472-1477.

Holden JE, DeJesus OT, Nickles RJ, Shelton S, Houser WD, Uno H, Freund L, Perlman SB (1991) PET study of *β*-fluoromethylene-*m*-tyrosine (MDL 72394), a non-catechol probe of striatal dopamine nerve terminals, in primate. [Abstract] *J Nucl Med* 32:1070.

Holden JE, Vingerhoets FJG, Snow BJ, Chan GL-Y, Legg B, Morrison S, Adam M, Jivan S, Sossi V, Buckley KR, Ruth TJ (1996) Links between 6-fluorodopa and 6-fluoro-3-O-methyldopa kinetics. *In*: "Quantification of Brain Function Using PET." (Myers R, Cunningham V, Bailey D, Jones T, Eds.), 1st ed., pp. 227-231. Academic Press, San Diego.

Horne MK, Cheng CH, Wooten GF (1984) The cerebral metabolism of L-dihydroxyphenylalanine: an autoradiographic and biochemical study. *Pharmacology* 28:12-26.

Hornykiewicz O (1963) Die topische Lokalisation und das Verhalten von Noradrenalin und Dopamin (3-Hydroxytyramin) in der Substantia nigra des normalen und Parkinson-kranken Menschen. *Wien Klin Wochenschr* 75:309-312.

Hornykiewicz O, Lisch H-J, Springer A (1968) Homovanillic acid in different regions of the human brain: attempt at localizing central dopamine fibres. *Brain Res* 11:662-671.

Hornykiewicz O (1974) The mechanisms of action of L-DOPA in Parkinson's disease. [Review] *Life Sci* 15:1249-1259.

Hornykiewicz O (1975) Parkinson's disease and its chemotherapy. [Review] *Life Sci* 24:1061-1065.

Hoshi H, Kuwabara H, Gjedde A (1992) Uptake of 6-[F-18]fluoro-L-dihydroxyphenylalanine (FDOPA) in human brain in vivo: a comparison of six analytical methods. *J Nucl Med* 33:916-917.

Hoshi H, Kuwabara H, Léger G, Cumming P, Guttman M, Gjedde A (1993) 6-[^{18}F]fluoro-L-DOPA metabolism in living human brain: a comparison of six analytical methods. *J Cereb Blood Flow Metab* 13:57-69.

Huang S-C, Barrio JR, Hoffman JM, Mahoney DK, Hawk TC, Melega WP, Luxen A, Grafton S, Mazziotta JC, Phelps ME (1989) A compartmental model for 6-[F-18]fluoro-L-DOPA kinetics in cerebral tissues. [Abstract] *J Nucl Med* 30:735.

Huang S-C, Yu D-C, Barrio JR, Grafton S, Melega WP, Hoffman JM, Satyamurthy N, Mazziotta JC, Phelps ME (1991) Kinetics and modelling of L-6-[^{18}F]fluoro-DOPA in human positron emission tomographic studies. *J Cereb Blood Flow Metab* 11:898-913.

Hume SP, Lammertsma AA, Myers R, Rajeswaran S, Bloomfield PM, Ashworth S, Fricker RA, Torres EM, Watson I, Jones T (1996) The potential of high-resolution positron emission tomography to monitor striatal dopaminergic function in rat models of disease. *J Neurosci Methods* 67:103-112.

Ishikawa T, Dhawan V, Chaly T, Margouleff C, Robeson W, Dahl JR, Mandel F, Spetsieris P, Eidelberg D (1996*a*) Clinical significance of striatal DOPA decarboxylase activity in Parkinson's disease. *J Nucl Med* 37:216-222.

Ishikawa T, Dhawan V, Chaly T, Robeson W, Belakhlef A, Mandel F, Dahl R, Margouleff C, Eidelberg D (1996*b*) Fluorodopa positron emission tomography with an inhibitor of catechol-*O*-methyltransferase: effect of the plasma 3-*O*-methyldopa fraction on data analysis. *J Cereb Blood Flow Metab* 16:854-863.

Iversen LL, Glowinski J (1966) Regional studies of catecholamines in the rat brain - II: rate of turnover of catecholamines in various brain regions. *J Neurochem* 13:671-682.

Jackisch R, Link T, Neufang B, Koch R (1992) Studies on the mechanism of action of the antiparkinsonian drugs memantine and amantadine: no evidence for direct dopaminomimetic or antimuscarinic properties. *Arch Int Pharmacodyn* 320:21-42.

Javitch JA, D'Amato RJ, Strittmatter SM, Snyder SH (1985*a*) Parkinsonism-inducing neurotoxin, *N*-methyl-4-phenyl-1,2,3,6-tetrahydropyridine: uptake of the metabolite *N*-methyl-4-phenylpyridine by dopamine neurons explains selective neurotoxicity. *Proc Natl Acad Sci USA* 82:2173-2177.

Javitch JA, Strittmatter SM, Snyder SH (1985*b*) Differential visualization of dopamine and norepinephrine uptake sites in rat brain using [^{3}H]mazindol autoradiography. *J Neurosci* 5:1513-1521.

Jellinger KA (1991) Pathology of Parkinson's disease: changes other than the nigrostriatal pathway. [Review] *Molec Chem Neuropathol* 14:153-197.

Joseph SA, Walker DW (1994) Monoamine concentrations in cerebrospinal fluid of fetal and newborn sheep. *Am J Physiol* 266:R472-R480.

Kaakkola S, Wurtman RJ (1993) Effects of catechol-*O*-methyltransferase inhibitors and L-3,4-dihydroxyphenylalanine with or without carbidopa on extracellular dopamine in rat striatum. *J Neurochem* 60:137-144.

Kaakkola S, Tuomainen P, Männistö PT, Palo J (1993) Biogenic amine metabolites in the CSF of patients with late onset and alcoholic ataxias. *Acta Neurol Scand* 87:309-311.

Kalaria RN, Harik SI (1987) Blood-brain barrier monoamine oxidase: enzyme characterization in cerebral microvessels and other tissues from six mammalian species, including human. *J Neurochem* 48:856-864.

Kaler SG, Goldstein DS, Holmes C, Salerno JA, Gahl WA (1993) Plasma and cerebrospinal fluid neurochemical pattern in Menkes disease. *Ann Neurol* 33:171-175.

Kaplan GP, Hartman BK, Creveling CR (1979) Immunohistochemical demonstration of catechol-*O*-methyltransferase in mammalian brain. *Brain Res* 167:241-250.

Kessler RM, Ellis JR Jr, Eden M (1984) Analysis of emission tomographic scan data: limitations imposed by resolution and background. *J Comput Assist Tomogr* 8:514-522.

Kish SJ, Shannak K, Hornykiewicz O (1988) Uneven pattern of dopamine loss in the striatum of patients with idiopathic Parkinson's disease: pathophysiologic and clinical implications. *New Eng J Med* 318:876-880.

Kish SJ, Zhong XH, Hornykiewicz O, Haycock JW (1995) Striatal 3,4-dihydroxyphenylalanine decarboxylase in aging: disparity between postmortem and positron emission tomography studies? *Ann Neurol* 38:260-264.

Kornhuber J, Bormann J, Hubers M, Rusche K, Riederer P (1991) Effects of the 1-amino-adamantanes at the MK-801 binding site of the NMDA-receptor-gated ion channel: a human postmortem brain study. *Eur J Pharmacol* 206:297-300.

Kornhuber J, Weller M (1993) Amantadine and the glutamate hypothesis of schizophrenia: experiences in the treatment of neuroleptic malignant syndrome. *J Neural Transm (Gen Sect)* 92:57-65.

Kornhuber J, Weller M, Riederer P (1993) Glutamate receptor antagonists for neuroleptic malignant syndrome and akinetic hyperthermic Parkinsonian crisis. [Review] *J Neural Transm (PD Sect)* 6:63-72.

Koshimura K, Ohue T, Akiyama Y, Itoh A, Miwa S (1992) L-DOPA administration enhances exocytotic dopamine release in vivo in the rat striatum. *Life Sci* 51:747-755.

Kotz JC, Purcell KF (1987) Chemistry and Chemical Reactivity, p. 749. Saunders College Publishing, Philadelphia

Kuwabara H, Cumming P, Léger G, Gjedde A (1992) Loss of 6-[^{18}F]fluoro-L-dihydroxyphenylalanine (FDOPA) metabolites from human striatum. [Abstract] *J Nucl Med* 33:916.

Kuwabara H, Cumming P, Reith J, Léger G, Diksic M, Evans AC, Gjedde A (1993) Human striatal L-DOPA decarboxylase activity estimated in vivo using 6-[^{18}F]fluoro-DOPA and positron emission tomography: error analysis and application to normal subjects. *J Cereb Blood Flow Metab* 13:43-56.

Kuwabara H, Cumming P, Yasuhara Y, Léger GC, Guttman M, Diksic M, Evans AC, Gjedde A (1995) Regional striatal DOPA transport and decarboxylase activity in Parkinson's disease. *J Nucl Med* 36:1226-1231.

Laaksonen H, Rinne UK, Sonninen V, Riekkinen P (1978) Brain GABA neurons in Parkinson's disease. [Abstract] *Acta Neurol Scand* 57:282-283.

Lang AE (1987) Update on dopamine agonists in Parkinson's disease: "beyond bromocriptine". [Review] *Can J Neurol Sci* 14:474-482.

Langston JW, Ballard PA, Tetrud JW, Irwin I (1983) Chronic parkinsonism in humans due to a product of meperidine-analog synthesis. *Science* 219:979-980.

Langston JW (1984) MPTP neurotoxicity: an overview and characterization of phases of toxicity. *Life Sci* 34:201-206.

Langston JW, Ballard P (1984) Parkinsonism induced by 1-methyl-4-phenyl-1,2,3,6-tetrahydropyridine (MPTP): implications for treatment and the pathogenesis of Parkinson's disease. *Can J Neurol Sci* 11:160-165.

Langston JW, Forno LS, Rebert CS, Irwin I (1984) Selective nigral toxicity after systemic administration of 1-methyl-4-phenyl-1,2,5,6-tetrahydropyrine (MPTP) in the squirrel monkey. *Brain Res* 292:390-394.

Leenders KL, Poewe WH, Palmer AJ, Brenton DP, Frackowiak RSJ (1986*a*) Inhibition of L-[^{18}F]fluorodopa uptake into human brain by amino acids demonstrated by positron emission tomography. *Ann Neurol* 20:258-262.

Leenders KL, Palmer AJ, Quinn N, Clark JC, Firnau G, Garnett ES, Nahmias C, Jones T, Marsden CD (1986*b*) Brain dopamine metabolism in patients with Parkinson's disease measured with positron emission tomography. *J Neurol Neurosurg Psychiat* 49:853-860.

Leenders KL, Salmon EP, Tyrrell P, Perani D, Brooks DJ, Sager H, Jones T, Marsden D, Frackowiak RSJ (1990) The nigrostriatal dopaminergic system assessed in vivo by positron emission tomography in healthy volunteer subjects and patients with Parkinson's disease. *Arch Neurol* 47:1290-1298.

Léger GC, Kuwabara H, Gjedde AH (1992) Parametric dopa decarboxylase imaging in vivo. [Abstract] *J Nucl Med* 33:879-880.

Léger G, Cumming P, Kuwabara H, Guttman M, Gjedde A (1998) Effect of catechol-*O*-methyltransferase inhibition on brain uptake of [^{18}F]fluorodopa: implications for compartmental modelling and clinical usefulness. *Synapse* 30:351-361.

Lera G, Vaamonde J, Muruzabal J, Obeso JA (1990) Cabergoline: a long-acting dopamine agonist in Parkinson's disease. [Letter] *Ann Neurol* 28:593-594.

Lera G, Vaamonde J, Rodriguez M, Obeso JA (1993) Cabergoline in Parkinson's disease: long-term follow-up. *Neurology* 43:2587-2590.

Leviel V, Gobert A, Guilbert B (1989) Direct observation of dopamine compartmentation in striatal nerve terminal by 'in vivo' measurement of the specific activity of released dopamine. *Brain Res* 499:205-213.

Li X-M, Juorio AV, Boulton AA (1993) NSD-1015 alters the gene expression of L-amino acid decarboxylase in rat PC12 pheochromocytoma cells. *Neurochem Res* 18:915-919.

Lieberman A, Goodgold A, Jonas S, Leibowitz M (1975) Comparison of dopa decarboxylase inhibitor (carbidopa) combined with levodopa and levodopa alone in Parkinson's disease. *Neurology* 25:911-916.

Lieberman AN, Goldstein M, Gopinathan G, Neophytides A (1987) D-1 and D-2 agonists in Parkinson's disease. *Can J Neurol Sci* 14:466-473.

Liskowsky DR, Potter LT (1985) A pre-positron emission tomography study of L-3,4-dihydroxy-[^{3}H]phenylalanine distribution in the rat. *Neurosci Lett* 53:161-167.

Lloyd KG, Hornykiewicz O (1970) Parkinson's disease: activity of L-dopa decarboxylase in discrete brain regions. *Science* 170:1212-1213.

Lloyd KG, Hornykiewicz O (1972) Occurrence and distribution of aromatic L-amino acid (L-DOPA) decarboxylase in the human brain. *J Neurochem* 19:1549-1559.

Lloyd KG, Hornykiewicz O (1973) L-Glutamic acid decarboxylase in Parkinson's disease: effect of L-dopa therapy. *Nature* 243:521-523.

Lloyd KG, Davidson L, Hornykiewicz O (1975*a*) The neurochemistry of Parkinson's disease: effect of L-DOPA therapy. *J Pharmacol Exp Ther* 195:453-464.

Lloyd KG, Möhler H, Heitz P, Bartholini G (1975*b*) Distribution of choline acetyltransferase and glutamate decarboxylase within the substantia nigra and in other brain regions from control and parkinsonian patients. *J Neurochem* 25:789-795.

Luxen A, Guillaume M, Melega WP, Pike VW, Solin O, Wagner R (1992) Production of 6-[^{18}F]fluoro-L-DOPA and its metabolism in vivo: a critical review. [Review] *Nucl Med Biol* 19:149-158.

Mackay AVP, Davies P, Dewar AJ, Yates CM (1977) Regional distribution of enzymes associated with neurotransmission by monoamines, acetylcholine and GABA in the human brain. *J Neurochem* 30:827-839.

Martin WRW, Palmer MR, Patlak CS, Calne DB (1989) Nigrostriatal function in humans studies with positron emission tomography. *Ann Neurol* 26:535-542.

Mazziotta JC, Phelps ME, Plummer D, Kuhl DE (1981) Quantitation in positron emission computed tomography: 5. Physical-anatomical effects. *J Comput Assist Tomogr* 5:734-743.

Meguro K, Yamaguchi S, Itoh M, Fujiwara T, Yamadori A (1997) Striatal dopamine metabolism correlated with frontotemporal glucose utilization in Alzheimer's disease: a double-tracer PET study. *Neurology* 49:941-945.

Melamed E, Hefti F, Pettibone DJ, Liebman J, Wurtman RJ (1981) Aromatic L-amino acid decarboxylase in rat corpus striatum: implications for action of L-dopa in parkinsonism. *Neurology* 31:651-655.

Melamed E, Hefti F, Bitton V, Globus M (1984) Suppression of L-dopa-induced circling in rats with nigral lesions by blockade of central dopa-decarboxylase: implications for mechanism of action of L-dopa in parkinsonism. *Neurology* 34:1566-1570.

Melega WP, Perlmutter MM, Luxen A, Nissenson CHK, Grafton ST, Hunag S-C, Phelps ME, Barrio JR (1989) 4-[^{18}F]Fluoro-L-*m*-tyrosine: an L-3,4-dihydroxyphenylalanine analog for probing presynaptic dopaminergic function with positron emission tomography. *J Neurochem* 53:311-314.

Melega WP, Luxen A, Perlmutter MM, Nissenson CHK, Phelps ME, Barrio JR (1990*a*) Comparative in vivo metabolism of [^{18}F]6-fluoro-L-DOPA and [^{3}H]-L-DOPA in rats. *Biochem Pharmacol* 39:1853-1860.

Melega WP, Hoffman JM, Luxen A, Nissenson CHK, Phelps ME, Barrio JR (1990*b*) The effects of carbidopa on the metabolism of [^{18}F]6-fluoro-L-DOPA in rats, monkeys and humans. *Life Sci* 47:149-157.

Melega WP, Hoffman JM, Schneider JS, Phelps ME, Barrio JR (1991*a*) 6-[^{18}F]Fluoro-L-DOPA metabolism in MPTP-treated monkeys: assessment of tracer methodologies for positron emission tomography. *Brain Res* 543:271-276.

Melega WP, Grafton ST, Huang S-C, Satyamurthy N, Phelps ME, Barrio JR (1991*b*) L-6-[^{18}F]Fluoro-DOPA in monkeys and humans: biochemical parameters for the formulation of tracer kinetic models with positron emission tomography. *J Cereb Blood Flow Metab* 11:890-897.

Melega WP, Quintana J, Raleigh MJ, Stout DB, Yu D-C, Lin K-P, Huang S-C, Phelps ME (1996*a*) 6-[^{18}F]Fluoro-L-DOPA-PET studies show partial reversibility of long-term effects of chronic amphetamine in monkeys. *Synapse* 22:63-69.

Melega WP, Raleigh MJ, Stout DB, DeSalles AA, Cherry SR, Blurton-Jones M, Morton GG, Huang S-C, Phelps ME (1996*b*) Longitudinal behaviour and 6-[^{18}F]fluoro-L-DOPA-PET assessment in MPTP-hemiparkinsonian monkeys. *Exp Neurol* 141:318-329.

Mizoguchi K, Yokoo H, Yoshida M, Tanaka T, Tanaka M (1994) Amantadine increases the extracellular dopamine levels in the striatum by re-uptake inhibition and by *N*-methyl-D-aspartate antagonism. *Brain Res* 662:255-258.

Mizuno Y, Saitoh T, Sone N (1987*a*) Inhibition of mitochondrial NADH-ubiquinone oxidoreductase activity by 1-methyl-4-phenylpyridinium ion. *Biochem Biophys Res Commun* 143:294-299.

Mizuno Y, Suzuki K, Sone N, Saitoh T (1987*b*) Inhibition of ATP synthesis by 1-methyl-4-phenylpyridinium ion (MPP$^+$) in isolated mitochondria from mouse brains. *Neurosci Lett* 81:204-208.

Mizuno Y, Ikebe S-I, Hattori N, Mochizuki H, Nakagawa-Hattori Y, Kondo T (1997) Etiology of Parkinson's Disease. *In*: "Movement Disorders: Neurologic Principles and Practice." (Watts RL, Koller WC, Eds.), 1st ed., pp. 161-182. McGraw-Hill, New York.

Moleman P, Bruinvels J, van Valkenburg CFM (1978) Haloperidol inhibits the disappearance of acidic dopamine metabolites from rat striatum. *J Pharm Pharmacol* 30:583-585.

Morrish PK, Sawle GV, Brooks DJ (1996) An [^{18}F]dopa-PET and clinical study of the rate of progression in Parkinson's disease. *Brain* 119:585-591.

Murali D, DeJesus OT, Sunderland JJ, Nickles RJ (1992) [^{18}F]Fluoro-β-fluoromethylene-*m*-tyrosine analogs, potential PET agents for presynaptic dopamine terminals: synthesis and spectroscopic characterization. *Appl Radiat Isot* 43:969-977.

Nahmias C, Garnett ES, Firnau G, Lang A (1985) Striatal dopamine distribution in parkinsonian patients during life. *J Neurolog Sci* 69:223-230.

Nahmias C, Wahl L, Chirakal R, Firnau G, Garnett ES (1995) A probe for intracerebral aromatic amino-acid decarboxylase activity: distribution and kinetics of [^{18}F]6-fluoro-L-*m*-tyrosine in the human brain. *Move Disord* 10:298-304.

Namavari M, Satyamurthy N, Phelps ME, Barrio JR (1993) Synthesis of 6-[^{18}F] and 4-[^{18}F]fluoro-L-*m*-tyrosines via regioselective radiofluorodestannylation. *Appl Radiat Isot* 44:527-536.

Nestelbaum Z, Siris SG, Rifkin A, Klar H, Reardon GT (1986) Exacerbation of schizophrenia associated with amantadine. *Am J Psychiat* 143:1170-1171.

Netter FH (1997) Atlas of Human Anatomy, 9th ed., p. 104. Novartis, New Jersey.

Nomura T, Inoue K, Creveling CR, Komatsu F, Ohta N, Chino T, Karasawa N, Nagatsu I (1996) Immunocytochemical localization of aromatic L-amino acid decarboxylase and catechol-*O*-methyltransferase in blood vessel wall of the human dental pulp. *Brain Res* 735:314-316.

Nutt JG, Woodward WR, Anderson JL (1985) The effect of carbidopa on the pharmacokinetics of intravenously administered levodopa: the mechanism of action in the treatment of parkinsonism. *Ann Neurol* 18:537-543.

Obeso JA, Luquin MR, Vaamonde J, Grandas F, Martinez Lage JM (1987) Continuous dopaminergic stimulation in Parkinson's disease. [Review] *Can J Neurol Sci* 14:488-492.

Oldendorf WH, Szabo J (1976) Amino acid assignment to one of three blood-brain barrier amino acid carriers. *Am J Physiol* 230:94-98.

Opacka-Juffry J, Brooks DJ (1995) L-Dihydroxyphenylalanine and its decarboxylase: new ideas on their regulatory roles. [Review] *Move Disord* 10:241-249.

Ordenstein L (1867) Sur la paralysie agitante et la sclérose en plaques généralisee. [M.D. thesis] Martinet, Paris.

Owman C, Rosengren E (1967) Dopamine formation in brain capillaries: an enzymic blood-brain barrier mechanism. *J Neurochem* 14:547-550.

Paetsch P, Greenshaw AJ (1991) β-Adrenergic effects on plasma and brain large neutral amino acids are unaltered by chronic administration of antidepressants. *J Neurochem* 56:2027-2032.

Palfreyman MG, McDonald IA, Fozard JR, Mely Y, Sleight AJ, Zreika M, Wagner J, Bey P, Lewis PJ (1985) Inhibition of monoamine oxidase selectively in brain monoamine nerves using the bioprecursor (*E*)-β-fluoromethylene-*m*-tyrosine (MDL 72394), a substrate for aromatic L-amino acid decarboxylase. *J Neurochem* 45:1850-1860.

Pardridge WM and Oldendorf WH (1975) Kinetic analysis of blood-brain barrier transport of amino acids. *Biochim Biophys Acta* 401:128-136.

Parker WD Jr, Boyson SJ, Parks JK (1989) Abnormalities of the electron transport chain in idiopathic Parkinson's disease. *Ann Neurol* 26:719-723.

Pate BD, Kawamata T, Yamada T, McGeer EG, Hewitt KA, Snow BJ, Ruth TJ, Calne DB (1993) Correlation of striatal fluorodopa uptake in the MPTP monkey with dopaminergic indices. *Ann Neurol* 34:331-338.

Patlak CS, Blasberg RG, Fenstermacher JD (1983) Graphical evaluation of blood-to-brain transfer constants from multiple-time uptake data. *J Cereb Blood Flow Metab* 3:1-7.

Patlak CS, Blasberg RG (1985) Graphical evaluation of blood-to-brain transfer constants from multiple-time uptake data: generalizations. *J Cereb Blood Flow Metab* 5:584-590.

Paxinos G, Watson C (1982) The rat brain in stereotaxic coordinates. Academic Press, New York.

Perlmutter M, Satyamurthy N, Luxen A, Phelps ME, Barrio JR (1990) Synthesis of 4-[^{18}F]fluoro-L-*m*-tyrosine: a model analog for the in vivo assessment of central dopaminergic function. *Appl Radiat Isot* 41:801-807.

Perry TL, Javoy-Agid F, Agid Y, Fibiger HC (1983) Striatal GABAergic neuronal activity is not reduced in Parkinson's disease. *J Neurochem* 40:1120-1123.

Ponzio F, Achilli G, Perego C, Algeri S (1981) Differential effects of certain dopaminergic drugs on the striatal concentration of dopamine metabolites, with special reference to 3-methoxytyramine. *Neurosci Lett* 28:61-67.

Postma JU, van Tilburg W (1975) Visual hallucinations and delirium during treatment with amantadine (Symmetrel). *J Amer Geriat Soc* 23:212-215.

Pothos E, Desmond M, Sulzer D (1996) L-4,3-Dihydroxyphenylalanine increases the quantal size of exocytotic dopamine release in vivo. *J Neurochem* 66:629-636.

Rahman MK, Nagatsu T, Kato T (1980) Aromatic L-amino acid decarboxylase activity in central and peripheral tissues and serum of rats with L-DOPA and L-5-hydroxytryptophan as substrates. *Biochem Pharmacol* 30:645-649.

Reddy GN, Satyamurthy N, Barrio JR, Phelps ME (1990) Synthesis of 4-[^{18}F]fluoromethylene-*m*-tyrosine derivatives, a dual-enzyme activated inhibitor of monoamine oxidase. [Abstract] *J Nucl Med* 31:1593.

Reiffers S, Beerling-van der Molen HD, Vaalburg W, Ten Hoeve W, Paans AMJ, Korf J, Woldring MG, Wynberg H (1977) Rapid synthesis and purification of carbon-11 labelled DOPA: a potential agent for brain studies. *Int J Appl Radiat Isot* 28:955-958.

Reith J, Dyve S, Kuwabara H, Guttman M, Diksic M, Gjedde A (1990) Blood-brain transfer and metabolism of 6-[^{18}F]fluoro-L-DOPA in rat. *J Cereb Blood Flow Metab* 10:707-719.

Reith MEA, Kramer HK, Sershen H, Lajtha A (1990) D-Tartrate alters uptake of [^{3}H]dopamine into brain synaptic vesicles. *J Neurosci Methods* 31:133-136.

Reith J, Benkelfat C, Sherwin A, Yasuhara Y, Kuwabara H, Andermann F, Bachneff S, Cumming P, Diksic M, Dyve SE, Etienne P, Evans AC, Lal S, Shevell M, Savard G, Wong DF, Chouinard G, Gjedde A (1994) Elevated dopa decarboxylase activity in living brain of patients with psychosis. *Proc Natl Acad Sci USA* 91:11651-11654.

Reith J, Cumming P, Gjedde A (1998) Enhanced [^{3}H]DOPA and [^{3}H]dopamine turnover in striatum and frontal cortex in vivo linked to glutamate receptor antagonism. *J Neurochem* 70:1979-1985.

Ricaurte GA, Langston JW, DeLanney LE, Irwin I, Brooks JD (1985) Dopamine uptake blockers protect against the dopamine depleting effect of 1-methyl-4-phenyl-1,2,3,6-tetrahydropyridine (MPTP) in the mouse striatum. *Neurosci Lett* 59:259-264.

Riopelle RJ (1987) Bromocriptine and the clinical spectrum of Parkinson's disease. *Can J Neurol Sci* 14:455-459.

Rivett AJ, Francis A, Roth JA (1983) Localization of membrane-bound catechol-*O*-methyltransferase. *J Neurochem* 40:1494-1496.

Robinson DS, Sourkes TL, Nies A, Harris LS, Spector S, Bartlett DL, Kaye IS (1977) Monoamine metabolism in human brain. *Arch Gen Psychiat* 34:89-92.

Roth JA (1992) Membrane-bound catechol-*O*-methyltransferase: a reevaluation of its role in the *O*-methylation of the catecholamine neurotransmitters. [Review] *Rev Physiol Biochem Pharmacol* 120:1-28.

Rousset OG, Ma Y, Léger GC, Gjedde AH, Evans AC (1993*a*) Correction for partial volume effects in PET using MRI-based 3D simulations of individual human brain metabolism. *In*:"Quantification of Brain Function. Tracer Kinetics and Image Analysis in Brain PET." (Uemura K, Lassen NA, Jones T, Kanno I, Eds.), 1st ed., pp. 113-125. Elsevier Science Publishing, New York.

Rousset OG, Ma Y, Kamber M, Evans AC (1993*b*) 3D simulations of radiotracer uptake in deep nuclei of human brain. *Comput Med Imaging Graphics* 17:373-379.

Rousset OG, Ma Y, Marenco S, Wong DF, Evans AC (1996) In vivo correction method for partial volume effects in positron emission tomography: accuracy and precision. *In*: "Quantification of Brain Function Using PET." (Myers R, Cunningham V, Bailey D, Jones T, Eds.), 1st ed., pp. 158-165. Academic Press, New York.

Rousset OG, Ma Y, Evans AC (1998*a*) Correction for partial volume effects in PET: principle and validation. *J Nucl Med* 39:904-911.

Rousset OG, Deep P, Kuwabara H, Evans AC, Cumming P (1998*b*) The effect of partial volume correction on estimates of the influx and metabolism of [^{18}F]fluoro-L-dopa studied in normal control and Parkinson's disease subjects. *Synapse*, submitted.

Sano I, Gamo T, Kakimoto Y, Taniguchi K, Takesada M, Nishinuma K (1959) Distribution of catechol compounds in human brain. *Biochim Biophys Acta* 32:586-587.

Saura J, Kettler R, Da Prada M, Richards JG (1992) Quantitative enzyme radioautography with ^{3}H-Ro 41-1049 and ^{3}H-Ro 19-6327 in vitro: localization and abundance of MAO-A and MAO-B in rat CNS, peripheral organs, and human brain. *J Neurosci* 12:1977-1999.

Sawle GV, Colebatch JG, Shah A, Brooks DJ, Marsden CD, Frackowiak RSJ (1990) Striatal function in normal aging: implications for Parkinson's disease. *Ann Neurol* 28:799-804.

Sawle GV, Burn DJ, Morrish PK, Lammertsma AA, Snow BJ, Luthra S, Osman S, Brooks DJ (1994) The effect of entacapone (OR-611) on brain [^{18}F]-6-L-fluorodopa metabolism: implications for levodopa therapy of Parkinson's disease. *Neurology* 44:1292-1297.

Schapira AHV, Mann VM, Cooper JM, Dexter D, Daniel SE, Jenner P, Clark JB, Marsden CB (1990) Anatomic and disease specificity of NADH CoQ1 reductase (complex I) deficiency in Parkinson's disease. *J Neurochem* 55:2142-2145.

Schneider E, Jacobi P, Maxion H, Fischer P-A (1975) Neuropsychologische Untersuchungen zur Kurzzeitwirkung von Biperiden (Akineton®) beim Parkinsonsyndrom. *Arch Psychiat Nervenkr* 221:15-28.

Schwab RS, England AC Jr, Poskanzer DC, Young RR (1969) Amantadine in the treatment of Parkinson's disease. *JAMA* 208:1168-1170.

Sharman DF (1963) A fluorimetric method for the estimation of 4-hydroxy-3-methoxyphenylacetic acid (homovanillic acid) and its identification in brain tissue. *Brit J Pharmacol* 20:204-213.

Shiraishi M, Kuwabara H, Cumming P, Diksic M, Gjedde A (1996) Comparison of ratio and slope-intercept plot-based images of [^{18}F]fluoro-L-DOPA uptake in human brain. *In*: "Quantification of Brain Function Using PET." (Myers R, Cunningham V, Bailey D, Jones T, Eds.), 1st ed., pp. 237-242. Academic Press, San Diego.

Smith QR (1991) The blood-brain barrier and the regulation of amino acid uptake and availability to brain. [Review] *Adv Exp Med Biol* 291:55-71.

Snoey ER, Bessen HA (1990) Acute psychosis after amantadine overdose. *Ann Emerg Med* 19:668-670.

Snow BJ, Tooyama I, McGeer EG, Yamada T, Calne DB, Takahashi H, Kimura H (1993) Human positron emission tomographic [^{18}F]fluorodopa studies correlate with dopamine cell counts and levels. *Ann Neurol* 34:324-330.

Snyder SH, D'Amato RJ (1986) MPTP: a neurotoxin relevant to the pathophysiology of Parkinson's disease. [Review] *Neurology* 36:250-258.

Soares-da-Silva P (1987) Does brain 3,4-dihydroxyphenylacetic acid reflect dopamine release? *J Pharm Pharmacol* 39:127-129.

Soares-da-Silva P, Garrett MC (1990) A kinetic study of the rate of formation of dopamine, 3,4-dihydroxyphenylacetic acid (DOPAC) and homovanillic acid (HVA) in the brain of the rat: implications for the origin of DOPAC. *Neuropharmacology* 29:869-874.

Sokoloff L, Reivich M, Kennedy C, Des Rosiers MH, Patlak CS, Pettigrew KD, Sakurada O, Shinohara M (1977) The [^{14}C]deoxyglucose method for the measurement of local cerebral glucose utilization: theory, procedure, and normal values in the conscious and anesthetized albino rat. *J Neurochem* 28:897-916.

Somogyi P, Smith AD (1979) Projection of neostriatal spiny neurons to the substantia nigra: application of a combined Golgi-staining and horse-radish peroxidase transport procedure at both light and electron microscopic levels. *Brain Res* 178:3-15.

Spencer SE, Wooten GF (1984) Pharmacologic effects of L-dopa are not closely linked temporally to striatal dopamine concentration. *Neurology* 34:1609-1611.

Srinivasan K, Awapara J (1978) Substrate specificity and the properties of dopa decarboxylase from guinea pig kidneys. *Biochim Biophys Acta* 526:597-604.

Starr MS (1995) Glutamate/dopamine D_1/D_2 balance in the basal ganglia and its relevance to Parkinson's disease. [Review] *Synapse* 19:264-293.

Stoof JC, Booji J, Drukarch B, Wolters EC (1992) The anti-parkinsonian drug amantadine inhibits the *N*-methyl-D-aspartic acid-evoked release of acetylcholine from rat neostriatum in a non-competitive way. *Eur J Pharmacol* 213:439-443.

Strömberg U, Svennson TH, Waldeck B (1970) On the mode of action of amantadine. *J Pharm Pharmacol* 22:959-962.

Takahashi T, Yamashita H, Zhang Y-X, Nakamura S (1996) Inhibitory effect of MK-801 on amantadine-induced dopamine release in the rat striatum. *Brain Res Bull* 41:363-367.

Tedroff J, Aquilonius S-M, Hartvig P, Lundqvist H, Bjurling P, Långström B (1992*a*) Estimation of regional cerebral utilization of [^{11}C]-L-3,4-dihydroxy-phenylalanine (DOPA) in the primate by positron emission tomography. *Acta Neurol Scand* 85:166-173.

Tedroff J, Aquilonius S-M, Hartvig P, Bredberg E, Bjurling P, Långström B (1992*b*) Cerebral uptake and utilization of therapeutic [β-^{11}C]-L-DOPA in Parkinson's disease measured by positron emission tomography: relations to motor response. *Acta Neurol Scand* 85:95-102.

Tedroff J, Torstenson R, Hartvig P, Lindner KJ, Watanabe Y, Bjurling P, Westerberg G, Långström B (1997) L-DOPA modulates striatal dopaminergic function in vivo: evidence from PET investigations in nonhuman primates. *Synapse* 25:56-61.

Teräväinen H, Kaakola S, Järvinen M, Gordin A (1990) Selective COMT inhibitor, nitecapone, in Parkinson's disease. [Abstract] *Neurology* 40 (Suppl 1):271.

Thiede HM, Kehr W (1981) Endogenous dopa in rat brain: occurrence, distribution and relationship to changes in catecholamine synthesis. *Naunyn-Schmiedeberg's Arch Pharmacol* 316:299-303.

Togo Y, Hornick RB, Dawkins AT Jr (1968) Studies on induced influenza in man: I. double-blind studies designed to assess prophylactic efficacy of amantadine hydrochloride against A2/Rockville/1/65 strain. *JAMA* 203:87-92.

Torres EM, Fricker RA, Hume SP, Myers R, Opacka-Juffry J, Ashworth S, Brooks DJ, Dunnett SB (1995) Assessment of striatal graft viability in the rat in vivo using a small diameter PET scanner. *NeuroReport* 6:2017-2021.

Tsukada H, Lindner K-J, Hartvig P, Tani Y, Bjurling P, Kihlberg T, Westerberg G, Watanabe Y, Långström B (1994) Effect of 6R-L-erythro-5,6,7,8-tetrahydrobiopterin on in vivo L-[β-^{11}C]DOPA turnover in the rat striatum with infusion of L-tyrosine. *J Neural Transm (Gen Sect)* 95:1-15.

Udenfriend S, Wyngaarden JB (1956) Precursors of adrenal epinephrine and norepinephrine in vivo. *Biochim Biophys Acta* 20:48-52.

Udenfriend S, Zaltzman-Nirenberg P (1963) Norepinephrine and 3,4-dihydroxyphenylethylamine turnover in guinea pig brain in vivo. *Science* 142:394-396.

Uitti RJ, Rajput AH, Ahlskog JE, Offord KP, Schroeder DR, Ho MM, Prasad M, Rajput A, Basran P (1996) Amantadine treatment is an independent predictor of improved survival in Parkinson's disease. *Neurology* 46:1551-1556.

Ungerstedt U, Fuxe K, Goldstein M, Battista A, Ogawa M, Anagnoste B (1973) Action of *m*-tyrosine in experimental models: evidence for possible antiparkinsonian activity. *Eur J Pharmacol* 21:230-237.

Verhagen-Metman L, Del Dotto P, van den Munckhof P, Fang J, Mouradian MM, Chase TN (1998) Amantadine as treatment for dyskinesias and motor fluctuations in Parkinson's disease. *Neurology* 50:1323-1326.

Vingerhoets FJG, Schulzer M, Ruth TJ, Holden JE, Snow BJ (1996) Reproducibility and discriminating ability of fluorine-18-6-fluoro-L-DOPA PET in Parkinson's disease. *J Nucl Med* 37:421-426.

Vontobel P, Antonini A, Psylla M, Günther I, Leenders KL (1996) Evaluation of three assumptions regarding blood-brain transport of 6-[^{18}F]fluoro-dopa and *O*-methyl-dopa in healthy volunteers. *In*: "Quantification of Brain Function Using PET." (Myers R, Cunningham V, Bailey D, Jones T, Eds.), 1st ed., pp. 224-226. Academic Press, San Diego.

Wade LA, Katzman R (1975) 3-*O*-methyl-DOPA uptake and inhibition of L-DOPA at the blood-brain barrier. *Life Sci* 17:131-136.

Wahl LM, Garnett ES, Chirakal R, Firnau G, Nahmias C (1993) Quantification of dopamine metabolism in man: what is the most justifiable approach? [Abstract] *J Cereb Blood Flow Metab* 13 (Suppl 1):S722

Wahl L, Chirakal R, Firnau G, Garnett ES, Nahmias C (1994) The distribution and kinetics of [^{18}F]6-fluoro-3-*O*-methyl-L-dopa in the human brain. *J Cereb Blood Flow Metab* 14:664-670.

Wahl L, Nahmias C (1996*a*) Modelling of fluorine-18-6-fluoro-L-dopa in humans. *J Nucl Med* 37:432-437.

Wahl L, Nahmias C (1996*b*) Quantification of dopamine metabolism in man: a mathematically justifiable approach. *Phys Med Biol* 41:963-978.

Walaas I (1981) Biochemical evidence for overlapping neocortical and allocortical glutamate projections to the nucleus accumbens and rostral caudatoputamen in the rat brain. *Neuroscience* 6:399-405.

Westerink BHC, Spaan SJ (1982*a*) Estimation of the turnover of 3-methoxytyramine in the rat striatum by HPLC with electrochemical detection: implications for the sequence in the cerebral metabolism of dopamine. *J Neurochem* 38:342-347.

Westerink BHC, Spaan SJ (1982*b*) On the significance of endogenous 3-methoxytyramine for the effects of centrally acting drugs on dopamine release in the rat brain. *J Neurochem* 38:680-686.

Westerink BHC (1985) Sequence and significance of dopamine metabolism in the rat brain. [Review] *Neurochem Int* 7:221-227.

Westerink BHC, Kikkert RJ (1986) Effect of various centrally acting drugs on the efflux of dopamine metabolites from the rat brain. *J Neurochem* 46:1145-1152.

Widmann R, Sperk G (1986) Topographical distribution of amines and major amine metabolites in the rat striatum. *Brain Res* 367:244-249.

Woods RP, Mazziotta JC, Cherry SR (1993) MRI-PET registration with automated algorithm. *J Comput Assist Tomogr* 17:536-546.

Wong DF, Gjedde A, Wagner HN Jr (1986) Quantification of neuroreceptors in the living human brain. I: irreversible binding of ligands. *J Cereb Blood Flow Metab* 6:137-146.

Wooten GF, Horne MK (1982) A new autoradiographic approach for imaging forebrain dopamine distribution. *Ann Neurol* 12:163-168.

Wooten GF (1997) Neurochemistry and neuropharmacology of Parkinson's disease. *In*: "Movement Disorders: Neurologic Principles and Practice." (Watts RL, Koller WC, Eds.), 1st ed., pp. 153-160. McGraw-Hill, New York.

Wu JC, Maguire G, Riley G, Lee A, Keator D, Tang C, Fallon J, Najafi A (1997) Increased dopamine activity associated with stuttering. *NeuroReport* 8:767-770.

Wurtman RJ, Chou C, Rose C (1970) The fate of C^{14}-dihydroxyphenylalanine (C^{14}-DOPA) in the whole mouse. *J Pharm Exp Ther* 174:351-356.

Yokoi F, Rousset O, Offord SJ, Gjedde A, Evans A, Wong DF (1997) Partial volume correction for kinetic analysis of [C11]-(*S*)nicotine in normal human. [Abstract] *Society for Nuclear Medicine 44th Annual Meeting*, San Antonio, USA.

Youdim MBH, Riederer P (1997) Understanding Parkinson's disease. [Review] *Scientif Am* 726:52-59

Young EA, Neff NH, Hadjiconstantinou M (1993) Evidence for cyclic AMP-mediated increase of aromatic L-amino acid decarboxylase activity in the striatum and midbrain. *J Neurochem* 60:2331-2333.

Yu D-C, Huang S-C, Barrio JR, Melega WP, Grafton S, Mazziotta JC, Phelps ME (1990) Investigation of a 6-[F-18]fluoro-DOPA (FD) model for estimation of its kinetic parameters in human brain. [Abstract] *J Nucl Med* 31:865-866.

Zetterström T, Sharp T, Collin AK, Ungerstedt U (1988) In vivo measurement of extracellular dopamine and DOPAC in rat striatum after various dopamine-releasing drugs: implications for the origin of extracellular DOPAC. *Eur J Pharmacol* 148:327-334.

Zhu MY, Juorio AV, Paterson IA, Boulton AA (1992) Regulation of aromatic L-amino acid decarboxylase by dopamine receptors in rat brain. *J Neurochem* 58:636-641.

Zubay G (1993) Biochemistry: Catabolism and Biosynthesis, 3rd ed., pp. 523-525. Wm C Brown Publishers, Iowa.

APPENDIX #1

The following section contains the derivations of important equations and mathematical terms appearing in the two original articles presented in Chapter II (Deep et al., 1997*a*) and Chapter III (Deep et al., 1997*b*) of this thesis.

1. Simulated plasma radioactivity of radiolabelled L-dopa [$C_a^{DOPA}(T)$]

The normalized time-concentration integral of the plasma radioactivity of radiolabelled L-dopa [$\Theta(T)$] is linear with respect to tracer circulation time (T),

$$\Theta(T) = \frac{\int_0^T C_a^{DOPA}(t)dt}{C_a^{DOPA}(T)} = \alpha T \qquad (1)$$

where $C_a^{DOPA}(t)$ is the time-activity curve of plasma L-dopa, and α is a constant. From empirical observation, $C_a^{DOPA}(T)$ can be described by a series of processes that remove the tracer from the periphery,

$$C_a^{DOPA}(T) = Xe^{-\lambda_1 T} + Ye^{-\lambda_2 T} + Ze^{-\lambda_3 T} + \ldots \qquad (2)$$

where X, Y, and Z are scaling constants, and λ_1, λ_2, and λ_3 are decay constants. Eq. 2 can be approximated by,

$$C_a^{DOPA}(T) = AT^{-b} \qquad (3)$$

where A is an arbitrary constant chosen to best fit the measured plasma radioactivities, and b is a new decay constant derived from α. To evaluate b, integrate $C_a^{DOPA}(t)$ from t=0 to t=T,

$$\int_0^T C_a^{DOPA}(t)dt = \int_0^T At^{-b}dt \qquad (4)$$

$$\int_0^T C_a^{DOPA}(t)dt = \frac{A}{1-b}T^{1-b} \qquad (5)$$

Dividing Eq. 5 by Eq. 3 yields a second expression for $\Theta(T)$,

$$\Theta(T) = \frac{\int_0^T C_a^{DOPA}(t)dt}{C_a^{DOPA}(T)} = \frac{1}{1-b}T \qquad \textbf{(6)}$$

Comparison of Eq. 6 with Eq. 1 shows that,

$$\alpha = \frac{1}{1-b} \qquad \textbf{(7)}$$

Rearrange Eq. 6 to isolate b in terms of α (which is measurable as the slope of a plot of Θ as a function of T),

$$b = 1 - \frac{1}{\alpha} \qquad \textbf{(8)}$$

2. General compartmental equation

Assuming first-order kinetics and instant equilibration between the sites of tracer generation and elimination (Cumming et al., 1993), the time-activity curve of the tracer in a plasma or brain compartment $[Z_i(t)]$ changes according to,

$$\frac{d[Z_i(t)]}{dt} = \sum_1^m [k_{in}^m Z_{i-1}^m(t)] - [\sum_1^n k_{out}^n] Z_i(t) \quad \textbf{(9)}$$

where $Z_{i-1}^m(t)$ is the time-activity curve of the mth precursor compound, k_{in}^m is the kinetic constant of the process that converts the mth precursor into tracer, and k_{out}^n is the kinetic constant of the nth process that removes the tracer from the compartment.

Now rearrange Eq. 9, then multiply through by an integrating factor,

$$\frac{d[Z_i(t)]}{dt} + [\sum_1^n k_{out}^n] Z_i(t) = \sum_1^m [k_{in}^m Z_{i-1}^m(t)] \quad \textbf{(10)}$$

$$\frac{d[Z_i(t)]}{dt} \sum_1^m e^{[\sum_1^n k_{out}^n]t} + [\sum_1^n k_{out}^n] Z_i(t) \sum_1^m e^{[\sum_1^n k_{out}^n]t} = \sum_1^m [k_{in}^m Z_{i-1}^m(t) e^{[\sum_1^n k_{out}^n]t}] \quad \textbf{(11)}$$

$$\frac{d[Z_i(t) \sum_1^m e^{[\sum_1^n k_{out}^n]t}]}{dt} = \sum_1^m [k_{in}^m Z_{i-1}^m(t) e^{[\sum_1^n k_{out}^n]t}] \quad \textbf{(12)}$$

$$d[Z_i(t) \sum_1^m e^{[\sum_1^n k_{out}^n]t}] = \sum_1^m [k_{in}^m Z_{i-1}^m(t) e^{[\sum_1^n k_{out}^n]t}] dt \quad \textbf{(13)}$$

The solution to Eq. 13 is obtained by integration from t=0 to t=T,

$$\int_0^T d[Z_i(t)\sum_1^m e^{[\sum_1^n k_{out}^n]t}] = \int_0^T \sum_1^m [k_{in}^m Z_{i-1}^m(t) e^{[\sum_1^n k_{out}^n]t}]dt \quad \textbf{(14)}$$

$$Z_i(T)\sum_1^m e^{[\sum_1^n k_{out}^n]T} - Z_i(0)\sum_1^m e^0 = \sum_1^m [k_{in}^m \int_0^T Z_{i-1}^m(t) e^{[\sum_1^n k_{out}^n]t}]dt \quad \textbf{(15)}$$

$$Z_i(T)\sum_1^m e^{[\sum_1^n k_{out}^n]T} = \sum_1^m [k_{in}^m \int_0^T Z_{i-1}^m(t) e^{[\sum_1^n k_{out}^n]t}]dt \quad \textbf{(16)}$$

$$Z_i(T) = \sum_1^m e^{-[\sum_1^n k_{out}^n]T} \sum_1^m [k_{in}^m \int_0^T Z_{i-1}^m(t) e^{[\sum_1^n k_{out}^n]t}]dt \quad \textbf{(17)}$$

$$Z_i(T) = \sum_1^m [k_{in}^m \int_0^T Z_{i-1}^m(t) e^{-[\sum_1^n k_{out}^n](T-t)}]dt \quad \textbf{(18)}$$

3. Tracer distribution volume

For a tracer that is not irreversibly trapped in brain, the time-activity curve of the tracer in brain [$M(t)$] changes according to,

$$\frac{dM(t)}{dt} = K_1 C_a(t) - k_2 M(t) \qquad \textbf{(19)}$$

where $C_a(t)$ is the time-activity curve of tracer in plasma, K_1 is the unidirectional blood-brain clearance of tracer, and k_2 is the rate constant for clearance of tracer from brain to plasma. At early times, when efflux from brain is negligible,

$$\frac{dM(t)}{dt} = K_1 C_a(t) \qquad \textbf{(20)}$$

$$dM(t) = K_1 C_a(t) dt \qquad \textbf{(21)}$$

$$M(T) = K_1 \int_0^T C_a(t) + M_{vasc}(T) \qquad \textbf{(22)}$$

where $M_{vasc}(T)$ is the tracer radioactivity in the vascular compartment of brain tissue. Now divide Eq. 22 by $C_a(T)$,

$$\frac{M(T)}{C_a(T)} = K_1 \frac{\int_0^T C_a(t)}{C_a(T)} + \frac{M_{vasc}(T)}{C_a(T)} \qquad \textbf{(23)}$$

By definition, the distribution volume of tracer [$V_d(T)$] is the ratio of radioactivities in brain [$M(T)$] and plasma [$C_a(T)$],

$$V_d(T) = \frac{M(T)}{C_a(T)} \qquad \textbf{(24)}$$

Therefore, comparison of Eq. 23 and Eq. 24 yields,

$$V_d(T) = K_1 \frac{\int_0^T C_a(t)}{C_a(T)} + \frac{M_{vasc}(T)}{C_a(T)} \qquad \textbf{(25)}$$

Now substitute the expression for $\Theta(T)$ from Eq. 1 into the first term of Eq. 25,

$$V_d(T) = K_1 \Theta(T) + \frac{M_{vasc}(T)}{C_a(T)} \qquad \textbf{(26)}$$

$$V_d(T) = K_1 \Theta(T) + V_0 \qquad \textbf{(27)}$$

where V_0 is the apparent vascular volume of tracer.

4. Tracer distribution volume (equilibrium)

At equilibrium ($T=T^*$), tracer influx and efflux are equal, and so the rate of change of brain radioactivity (Eq. 19) is zero,

$$K_1 C_a(T^*) = k_2 M(T^*) \tag{28}$$

$$\frac{M(T^*)}{C_a(T^*)} = \frac{K_1}{k_2} \tag{29}$$

From Eq. 24,

$$V_d(T^*) = V_e = \frac{K_1}{k_2} \tag{30}$$

Therefore, the tracer distribution volume at equilibrium (V_e) is a constant.

5. Expression for $k_{cl}^{DA+acids}$

According to M2 (Deep et al., 1997*b*), the net efflux of radioactivity from brain [$J_{net}(T)$] is given by,

$$J_{net}(T) = k_{cl}^{DA-acids}\underline{M}^{DA-acids}(T) \quad \textbf{(31)}$$

According to M3 (Deep et al., 1997*b*), $J_{net}(T)$ is given by,

$$J_{net}(T) = k_9^{acids}\underline{M}^{acids}(T) \quad \textbf{(32)}$$

Assuming that the net efflux is the same in both models,

$$k_{cl}^{DA-acids}\underline{M}^{DA-acids}(T) = k_9^{acids}\underline{M}^{acids}(T) \quad \textbf{(33)}$$

$$k_{cl}^{DA-acids} = \frac{k_9^{acids}\underline{M}^{acids}(T)}{\underline{M}^{DA-acids}(T)} \quad \textbf{(34)}$$

Furthermore, assume that the combined radioactivity of radiolabelled dopamine and acids as a single compartment [$\underline{M}^{DA+acids}(T)$] according to M2, is equal to the sum of the individual radioactivities of radiolabelled dopamine [$\underline{M}^{DA}(T)$] and acids [$\underline{M}^{acids}(T)$] as separate compartments according to M3. The denominator of Eq. 34 then becomes,

$$k_{cl}^{DA-acids}(T) = \frac{k_9^{acids}\underline{M}^{acids}(T)}{\underline{M}^{DA}(T) + \underline{M}^{acids}(T)} \quad \textbf{(35)}$$

6. Expression for *q*

For a tracer subject to facilitated diffusion, the permeability-surface area product (*PS*) is given by,

$$PS = \frac{T_{max}}{K_t(1 + \sum C_i/K_i)} \qquad \textbf{(36)}$$

where T_{max} is the maximal transport rate of tracer into brain, K_t is the Michaelis half-saturation constant of the tracer, C_i is the concentration of a transport competitor in plasma, and K_i is the corresponding inhibitory constant.

An expression that relates *PS* to cerebral plasma flow (*F*) and tracer extraction fraction (*E*) has also been derived (Crone, 1963). The permeability (*P*) of a membrane to a given substance is the amount of tracer which passes unit area in unit time for unit concentration difference across the membrane,

$$P = \frac{dX}{dt}\frac{1}{S\Delta C} \qquad \textbf{(37)}$$

where dX/dt is the amount of tracer passing the membrane in unit time and ΔC is the average concentration difference across the capillary wall.

By definition, dX/dt is given by,

$$\frac{dX}{dt} = F E C_a \qquad \textbf{(38)}$$

where C_a is the arterial concentration of tracer.

Also by definition, *E* is given by,

$$E = \frac{C_a - C_v}{C_a} \qquad \textbf{(39)}$$

where C_v is the venous concentration of tracer. Now substitute Eq. 39 into Eq. 38.

$$\frac{dX}{dt} = F\left(\frac{C_a - C_v}{C_a}\right) C_a \tag{40}$$

$$\frac{dX}{dt} = F(C_a - C_v) \tag{41}$$

Substitute Eq. 41 into Eq. 37,

$$P = F(C_a - C_v)\frac{1}{S\Delta C} \tag{42}$$

Assume that ΔC equals the mean intracapillary concentration of tracer. Since the tracer passes through the capillary wall passively by facilitated diffusion, the tracer concentration decreases exponentially from the arterial to the venous end of the capillary. We may therefore approximate ΔC by,

$$\Delta C = \frac{C_a - C_v}{\ln(C_a) - \ln(C_v)} \tag{43}$$

$$\Delta C = \frac{C_a - C_v}{\ln\left(\frac{C_a}{C_v}\right)} \tag{44}$$

Substitute Eq. 44 into Eq. 42,

$$P = \left(\frac{F}{S}\right)(C_a - C_v)\frac{\ln\left(\frac{C_a}{C_v}\right)}{C_a - C_v} \tag{45}$$

$$P = \left(\frac{F}{S}\right) \ln\left(\frac{C_a}{C_v}\right) \quad \textbf{(46)}$$

Now rearrange Eq. 39 by subtracting both sides from unity,

$$1 - E = 1 - \frac{C_a - C_v}{C_a} \quad \textbf{(47)}$$

$$1 - E = \frac{C_v}{C_a} \quad \textbf{(48)}$$

$$\frac{1}{1 - E} = \frac{C_a}{C_v} \quad \textbf{(49)}$$

Substitute Eq. 49 into Eq. 46,

$$P = \left(\frac{F}{S}\right) \ln\left(\frac{1}{1 - E}\right) \quad \textbf{(50)}$$

$$PS = F \ln\left(\frac{1}{1 - E}\right) \quad \textbf{(51)}$$

Rearrange Eq. 51 to isolate E,

$$PS = -F \ln(1 - E) \quad \textbf{(52)}$$

$$e^{-PS} = e^{F}(1 - E) \quad \textbf{(53)}$$

$$e^{-\frac{PS}{F}} = 1 - E \quad \textbf{(54)}$$

$$E = 1 - e^{-\frac{PS}{F}} \tag{55}$$

By definition, the unidirectional blood-brain clearance of a tracer (K_1) is given by,

$$K_1 = EF \tag{56}$$

Now substitute Eq. 56 into Eq. 55,

$$\frac{K_1}{F} = 1 - e^{-\frac{PS}{F}} \tag{57}$$

$$K_1 = F(1 - e^{-\frac{PS}{F}}) \tag{58}$$

When tracer permeability into brain is low (PS is <10% of F), the magnitude of K_1 approaches PS (capillary diffusion capacity). For example, assume F=10PS,

$$K_1 = 10PS(1 - e^{-\frac{PS}{10PS}}) \tag{59}$$

$$K_1 \cong 10PS(1 - e^{-0.1}) \tag{60}$$

$$K_1 = 0.95PS \cong PS \tag{61}$$

Substitution of Eq. 61 into Eq. 36 yields,

$$K_1 \cong \frac{T_{max}}{K_t(1 + \sum C_i/K_i)} \tag{62}$$

When Eq. 62 is applied to radiolabelled *O*-methyl-L-dopa and radiolabelled L-dopa, the ratio (q) between K_1^{OMD} and K_1^{DOPA} becomes,

$$q = \frac{K_1^{OMD}}{K_1^{DOPA}} = \frac{T_{max}^{OMD}}{K_t^{OMD}(1 + \sum C_i/K_i)} \frac{K_t^{DOPA}(1 + \sum C_i/K_i)}{T_{max}^{DOPA}} \quad \textbf{(63)}$$

$$q = \frac{K_1^{OMD}}{K_1^{DOPA}} = \frac{K_t^{DOPA}}{K_t^{OMD}} \left(\frac{T_{max}^{OMD}}{T_{max}^{DOPA}}\right) \quad \textbf{(64)}$$

APPENDIX #2

The following section contains publisher reprints of the two original articles presented in Chapter II (Deep et al., 1997*a*) and Chapter III (Deep et al., 1997*b*) of this thesis.

Inclusion of these articles herein is done with the expressed written permission of the publisher (Elsevier Science Ireland Ltd.) and all co-authors (Dr. P. Cumming, Dr. A. Gjedde, and Dr. H. Kuwabara).

ELSEVIER

Journal of Neuroscience Methods 76 (1997) 157–165

JOURNAL OF NEUROSCIENCE METHODS

On the accuracy of an [^{18}F]FDOPA compartmental model: evidence for vesicular storage of [^{18}F]fluorodopamine in vivo

Paul Deep [a,*], Albert Gjedde [b], Paul Cumming [a]

[a] *Montreal Neurological Institute, McGill University, 3801 University St., Montreal, Quebec H3A 2B4, Canada*
[b] *PET Center, Aarhus University Hospital, Aarhus, Denmark*

Received 18 December 1996; received in revised form 28 April 1997; accepted 29 April 1997

Abstract

The biological accuracy of a nonlinear compartmental model describing the in vivo kinetics of L-3,4-dihydroxy-6-[^{18}F]fluorophenylalanine ([^{18}F]FDOPA) metabolism was investigated. Tissue activities for [^{18}F]FDOPA and its labeled metabolites 3-*O*-methyl-[^{18}F]FDOPA ([^{18}F]OMFD), 6-[^{18}F]fluorodopamine ([^{18}F]FDA), L-3,4-dihydroxy-6-[^{18}F]fluorophenylacetic acid ([^{18}F]FDOPAC), and 6-[^{18}F]fluorohomovanillic acid ([^{18}F]FHVA) were calculated using a plasma [^{18}F]FDOPA input function, and kinetic constants estimated previously by chromatographic fractionation of ^{18}F-labeled compounds in plasma and brain extracts from rat. Present data accurately reflected the measured radiochemical composition in rat brain for tracer circulation times past 10 min. We formulated the hypothesis that the discrepancy between calculated and measured fractions of [^{18}F]FDOPA and the deaminated metabolite [^{18}F]FDOPAC at times earlier than 10 min reflected storage of [^{18}F]FDA in vesicles without monoamine oxidase. This hypothesis explained the initially rapid appearance of [^{18}F]FDOPAC in striatum by delayed transfer of [^{18}F]FDA from cytosol into vesicles. We conclude that the simpler model of [^{18}F]FDOPA compartmentation is accurate when the cytosolic and vesicular fractions of [^{18}F]FDA are at steady-state; the approach to equilibrium has a time constant of 15–30 min. The present model is valid for positron emission tomography studies of [^{18}F]FDOPA metabolism in living brain. © 1997 Elsevier Science B.V.

Keywords: Accuracy; [^{18}F]FDOPA Compartmental model; HPLC fractionation; Kinetic constants; Positron emission tomography; Rat brain; Vesicular compartment of [^{18}F]FDA

1. Introduction

Positron emission tomography (PET) following intravenous injection of L-3,4-dihydroxy-6-[^{18}F]fluorophenylalanine ([^{18}F]FDOPA), a radiolabeled analog of the endogenous amino acid L-3,4-dihydroxyphenylalanine (L-DOPA), reveals a time-dependent and specific accumulation of radioactivity in the basal ganglia (Garnett et al., 1983a). Models of tracer uptake and metabolism are fitted to measured activity data to estimate kinetic constants of physiological processes in vivo. Assuming irreversible trapping of radioactivity in brain, a unilinear graphical method (Gjedde, 1981, 1982; Patlak et al., 1983; Patlak and Blasberg, 1985) has been used to determine the net influx of [^{18}F]FDOPA into brain (Martin et al., 1989; Sawle et al., 1990). Alternatively, multilinear or nonlinear regression methods (Gjedde et al., 1991; Huang et al., 1991; Kuwabara et al., 1993; Wahl and Nahmias, 1996) have yielded sets of blood-brain transfer coefficients for [^{18}F]FDOPA and 3-*O*-methyl-[^{18}F]FDOPA ([^{18}F]OMFD), and regional activities of L-DOPA decarboxylase (DDC; EC 4.1.1.28), the enzyme that converts [^{18}F] FDOPA to 6-[^{18}F]flurodopamine ([^{18}F]; Firnau et al., 1975).

Multilinear or nonlinear regression to [^{18}F]FDOPA activity data is computationally demanding but yields

* Corresponding author. Tel.: +1 514 3981996; fax: +1 514 3988948; e-mail: deep@pet.mni.mcgill.ca

PII S0165-0270(97)00094-0

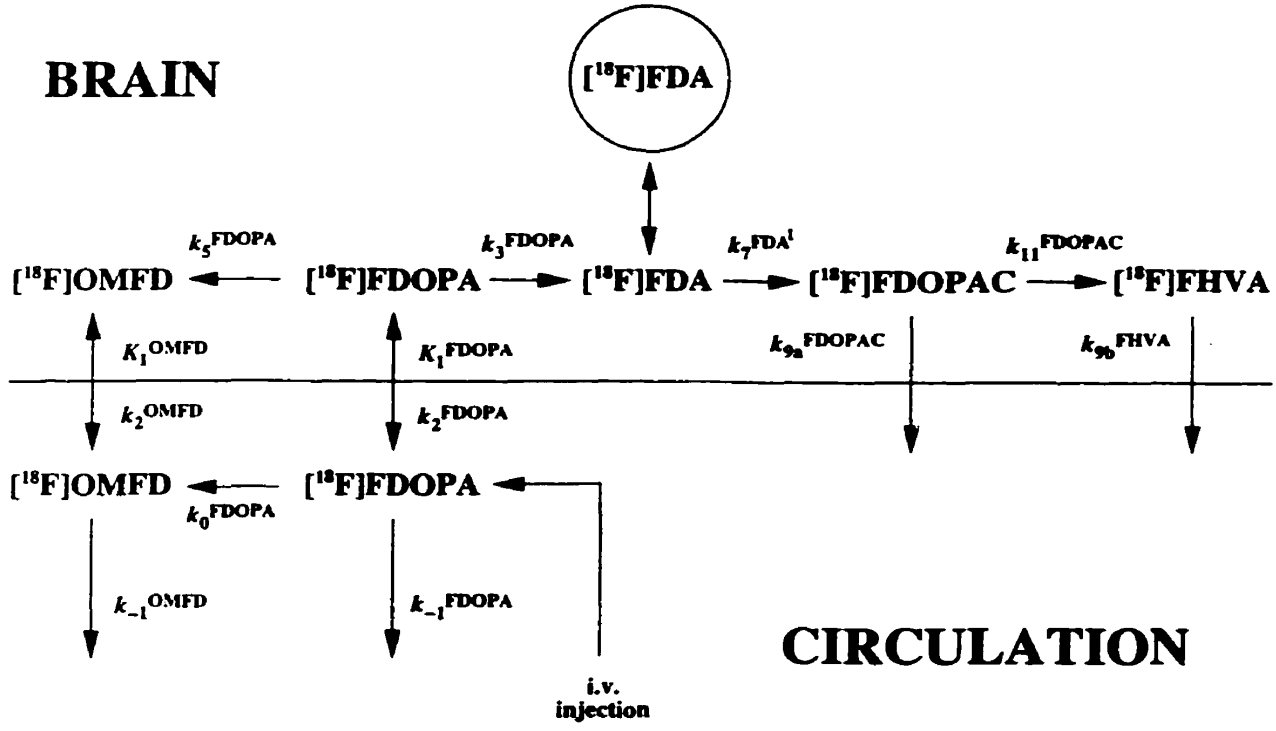

Fig. 1. Schematic summary of [^{18}F]FDOPA blood-brain transfer and metabolism, including the associated kinetic constants. [^{18}F]FDOPA injected intravenously into the circulation is *O*-methylated (k_0^{FDOPA}) by COMT to form [^{18}F]OMFD. Both tracers are subsequently cleared from circulation by renal elimination (k_{-1}^{FDOPA} and k_{-1}^{OMFD}). Both tracers are transferred into brain (K_1^{FDOPA} and K_1^{OMFD}) and out of brain (k_2^{FDOPA} and k_2^{OMFD}) by facilitated diffusion. [^{18}F]FDOPA in brain is *O*-methylated (k_5^{FDOPA}) by COMT to form [^{18}F]OMFD. In brain, [^{18}F]FDOPA is decarboxylated by DDC (k_3^{FDOPA}) to form [^{18}F]FDA, which is not cleared directly from brain. [^{18}F]FDA is sequestered in vesicles (circle) or undergoes oxidative deamination ($k_7^{FDA'}$) by MAO to form [^{18}F]FDOPAC, which is then *O*-methylated (k_{11}^{FDOPAC}) by COMT to yield [^{18}F]FHVA. Both [^{18}F]FDOPAC (k_{9a}^{FDOPAC}) and [^{18}F]FHVA (k_{9b}^{FHVA}) are cleared from brain into cerebrospinal fluid and then back into the circulation.

kinetic constants of several physiological processes. Conversely, the unilinear method is computationally simple, but valid only within certain times (~ 10–90 min) because of its unilinearity. It yields a single kinetic constant that is the composite of [^{18}F]FDOPA influx, efflux, and decarboxylation. The choice of method depends on the duration of tracer circulation and the desired kinetic information, but in all cases, the validity of the method can only be substantiated by the agreement between predicted and measured metabolite concentrations.

[^{18}F]FDOPA has metabolites analogous to those of the endogenous amino acid, as shown by high-performance liquid chromatography (HPLC) fractionation of ^{18}F-labeled compounds in plasma and brain extracts, from rat (Cumming et al., 1987a,b, 1988, 1994, 1995a; Melega et al., 1990a,b; Reith et al., 1990) and primate (Boyes et al., 1986; Firnau et al., 1987, 1988; Melega et al., 1990b, 1991a,b; Cumming et al., 1993). Therefore, [^{18}F]FDOPA is a tracer of L-DOPA in vivo, whose tissue disposition can be predicted by models which incorporate the major physiological processes responsible for L-DOPA uptake, metabolism and clearance.

The goal of this study is to test the validity of the present nonlinear compartmental model for kinetic analysis of [^{18}F]FDOPA activity data measured by PET in living brain, by demonstrating that it accurately predicts the concentrations of [^{18}F]FDOPA and its several labeled metabolites measured in vivo in rat by HPLC.

2. Materials and methods

2.1. [^{18}F]FDOPA compartmental model

The in vivo metabolic pathway for [^{18}F]FDOPA, including the associated kinetic constants, is summarized in Fig. 1. Following injection into the venous circulation, [^{18}F]FDOPA is *O*-methylated (k_0^{FDOPA}, min^{-1}) by catechol-*O*-methyltransferase (COMT; EC 2.1.1.6) to form its principal metabolite [^{18}F]OMFD. Renal elimination clears [^{18}F]FDOPA and [^{18}F]OMFD from the circulation as a first-order process (k_{-1}^{FDOPA} and k_{-1}^{OMFD}, min^{-1}). The transporter of large neutral amino acids brings both tracers into brain (K_1^{FDOPA} and K_1^{OMFD}, ml g^{-1} per min) and out of brain (k_2^{FDOPA} and k_2^{OMFD}, min^{-1}) by facilitated diffusion. In brain, [^{18}F]FDOPA is *O*-methylated by COMT (k_5^{FDOPA}, min^{-1}) to form [^{18}F]OMFD, or decarboxylated by

Table 1
Estimates of [^{18}F]FDOPA kinetic constants in rat

Kinetic constant	Definition	Units	Estimate
V_0^{FDOPA}	Vascular volume of [^{18}F]FDOPA	ml g^{-1}	0.037[a]
V_0^{OMFD}	Vascular volume of [^{18}F]OMFD	ml g^{-1}	—
k_0^{FDOPA}	Rate constant for conversion of [^{18}F]FDOPA to [^{18}F]OMFD in plasma	min^{-1}	0.055
k_{-1}^{OMFD}	Rate constant for clearance of [^{18}F]OMFD from plasma	min^{-1}	0.01
K_1^{FDOPA}	Unidirectional blood-brain clearance of [^{18}F]FDOPA	ml g^{-1} per min	0.07
K_1^{OMFD}	Unidirectional blood-brain clearance of [^{18}F]OMFD	ml g^{-1} per min	0.08
k_2^{FDOPA}	Rate constant for clearance of [^{18}F]FDOPA from brain	min^{-1}	0.10
k_2^{OMFD}	Rate constant for clearance of [^{18}F]OMFD from brain	min^{-1}	0.11
k_3^{FDOPA}	Rate constant for conversion of [^{18}F]FDOPA to [^{18}F]FDA in brain	min^{-1}	0.17
k_5^{FDOPA}	Rate constant for conversion of [^{18}F]FDOPA to [^{18}F]OMFD in brain	min^{-1}	—
k_7^{FDA}	Rate constant for conversion of [^{18}F]FDA to [^{18}F]FDOPAC in brain	min^{-1}	0.055
k_{11}^{FDOPAC}	Rate constant for conversion of [^{18}F]FDOPAC to [^{18}F]FHVA in brain	min^{-1}	0.083
k_{9a}^{FDOPAC}	Rate constant for clearance of [^{18}F]FDOPAC from brain	min^{-1}	—
k_{9b}^{FHVA}	Rate constant for clearance of [^{18}F]FHVA from brain	min^{-1}	0.12

All kinetic constants were estimated by chromatographic fractionation of ^{18}F-labeled compounds in plasma extracts and striatal tissue following bolus i.v. injection of [^{18}F]FDOPA (Cumming et al., 1994). Some estimates were unavailable (—); see Section 2 for explanations.
[a] Cumming et al., 1995a.

DDC (k_3^{FDOPA}, min^{-1}) to form [^{18}F]FDA, which is not directly cleared from brain. [^{18}F]FDA is sequestered in vesicles (circle) where it is protected from catabolism. In the cytosol, [^{18}F]FDA is deaminated (k_7^{FDA}, min^{-1}) by monoamine oxidase (MAO; EC 1.4.3.4) to yield L-3,4-dihydroxy-6-[^{18}F]fluorophenylacetic acid ([^{18}F]-FDOPAC), which is *O*-methylated by COMT (k_{11}^{FDOPAC}, min^{-1}) to form 6-[^{18}F]fluorohomovanillic acid ([^{18}F]FHVA). The acidic metabolites [^{18}F]FDOPAC (k_{9a}^{FDOPAC}, min^{-1}) and [^{18}F]FHVA (k_{9b}^{FHVA}, min^{-1}) diffuse out of brain into cerebrospinal fluid (Hammerstad et al., 1993), and back into the venous circulation.

The present model thus identifies two plasma compartments ([^{18}F]FDOPA and [^{18}F]OMFD) and five brain compartments ([^{18}F]FDOPA, [^{18}F]OMFD, [^{18}F]FDA, [^{18}F]FDOPAC, and [^{18}F]FHVA). Estimates of brain kinetic constants (Table 1; Cumming et al., 1994) were obtained from striatum, since nigrostriatal dopaminergic terminals are the primary site of L-DOPA uptake and metabolism (Hefti et al., 1981; Melamed et al., 1981).

2.2. Plasma [^{18}F]FDOPA activity

The plasma [^{18}F]FDOPA activity [$C_a^{FDOPA}(T)$; dpm μl^{-1}] served as the input function for the subsequent calculation of metabolite activities in brain (see below). It was calculated as a single power function (Matlab©, The MathWorks, Natick, MA),

$$C_a^{FDOPA}(T) = AT^{((1/\alpha)-1)} \quad (1)$$

where A is an arbitrary scaling constant (1000 dpm μl^{-1} per min), T is the tracer circulation time (min; defined as the time elapsed following tracer injection), and α is a dimensionless constant (2.2; Deep et al., 1997) obtained as the linear regression slope of a plot of pharmacokinetic circulation time versus T for a population of rats administered [^{3}H]DOPA (Cumming et al., 1995b). A straight line between zero activity at injection time and peak activity at 0.5 min described the rapid increase in plasma [^{18}F]FDOPA concentration immediately after tracer injection.

2.3. Plasma [^{18}F]OMFD and brain tissue activities

Assuming first-order kinetics and instant equilibration between the sites of metabolite formation and clearance, the plasma [^{18}F]OMFD activity [$C_a^{OMFD}(T)$; dpm μl^{-1}] and the brain tissue activities (dpm mg^{-1}) of [^{18}F]FDOPA [$M^{FDOPA}(T)$], [^{18}F]OMFD [$M^{OMFD}(T)$], [^{18}F]FDA [$M^{FDA}(T)$], [^{18}F]FDOPAC [$M^{FDOPAC}(T)$], and [^{18}F]FHVA [$M^{FHVA}(T)$], all change with time according to the general compartmental equation,

$$\frac{d[Z_i(t)]}{dt} = \sum_1^m [k_{in}^m Z_{i-1}^m(t)] - \left[\sum_1^n k_{out}^n\right] Z_i(t) \quad (2)$$

where $Z_i(t)$ is the time-activity curve of the metabolite, $Z_{i-1}^m(t)$ is the time-activity curve of the mth precursor compound, k_{in}^m is the kinetic constant of the process that converts the mth precursor into metabolite, and k_{out}^n is the kinetic constant of the nth process that removes the metabolite from the compartment. Using $C_a^{FDOPA}(T)$ (Eq. (1)) as the input function, integration of Eq. (2) for each metabolite compartment yielded the following activities

$$C_a^{OMFD}(T) = k_0^{FDOPA} \int_0^T C_a^{FDOPA}(t)\, e^{-k_{-1}^{OMFD}(T-t)}\, dt \quad (3)$$

$$M^{FDOPA}(T) = K_1^{FDOPA}\int_0^T C_a^{FDOPA}(t)\, e^{-(k_2^{FDOPA}+k_3^{FDOPA}+k_5^{FDOPA})(T-t)}dt \quad (4)$$

$$M^{OMFD}(T) = K_1^{OMFD}\int_0^T C_a^{OMFD}(t)\, e^{-k_2^{OMFD}(T-t)}\,dt + k_5^{FDOPA}\int_0^T M^{FDOPA}(t)\, e^{-k_2^{OMFD}(T-t)}\,dt \quad (5)$$

$$M^{FDA}(T) = k_3^{FDOPA}\int_0^T M^{FDOPA}(t)\, e^{-k_7^{FDA}(T-t)}\,dt \quad (6)$$

$$M^{FDOPAC}(T) = k_7^{FDA}\int_0^T M^{FDA}(t)\, e^{-(k_{9a}^{FDOPAC}+k_{9b}^{FDOPAC})(T-t)}\,dt \quad (7)$$

$$M^{FHVA}(T) = k_{11}^{FDOPAC}\int_0^T M^{FDOPAC}(t)\, e^{-k_{9b}^{FHVA}(T-t)}\,dt \quad (8)$$

Total activity in plasma $[C_a^{total}(T)]$ was calculated as the sum of Eqs. (1) and (3),

$$C_a^{total}(T) = C_a^{FDOPA}(T) + C_a^{OMFD}(T) \quad (9)$$

The omission of plasma compartments for [^{18}F]FDA, [^{18}F]FDOPAC, and [^{18}F]FHVA is consistent with the results of HPLC fractionations of ^{18}F-labeled compounds in plasma extracts from rats (Cumming et al., 1987a,b, 1988, 1994, 1995a; Melega et al., 1990a,b; Reith et al., 1990) and primates (Boyes et al., 1986; Melega et al., 1990b, 1991a,b; Cumming et al., 1993) treated with carbidopa, a peripheral DDC inhibitor, which failed to detect significant amounts of these compounds.

Total activity in striatum $[M^{total}(T)]$ was calculated as the sum of Eqs. (4)–(8),

$$M^{total}(T) = M^{FDOPA}(T) + M^{OMFD}(T) + M^{FDA}(T) + M^{FDOPAC}(T) + M^{FHVA}(T) + V_0^{FDOPA}C_a^{FDOPA}(T) + V_0^{OMFD}C_a^{OMFD}(T) \quad (10)$$

No brain compartment for 3-methoxy-6-^{18}F-labeled 3- methoxytyramine a precursor of [^{18}F]FHVA formed by *O*-methylation of [^{18}F]FDA, was included because the majority of HVA in rat brain is derived from DOPAC (Westerink and Spaan, 1982; Cumming et al., 1992). The final two terms in Eq. (10) account for the vascular components of tissue activity, where V_0^{FDOPA} and V_0^{OMFD} are the volumes of the vascular compartments of [^{18}F]FDOPA and [^{18}F]OMFD, respectively.

All metabolite activities were calculated for 120 min of tracer circulation, using the kinetic constants estimated for [^{18}F]FDOPA in rat (Cumming et al., 1994; Table 1), with the following assumptions:

- V_0^{FDOPA} and V_0^{OMFD} were set to 0, since the rat brains were assumed to be devoid of blood prior to HPLC fractionation.
- k_{9a}^{FDOPAC} was assumed to be equal to the estimate of k_{9b}^{FHVA} (0.12 min^{-1}).
- k_5^{FDOPA} was assumed to be equal to the corresponding estimate for [^{3}H]DOPA in rat (0.06 min^{-1}; Cumming et al., 1995b), which was the average of estimates from five brain regions, assuming a homogenous distribution of COMT activity throughout rat brain (Broch and Fonnum, 1972; Rivett et al., 1983; Roth, 1992).

2.4. Fractional metabolite activities

The calculated plasma metabolite activities (Eqs. (1) and (3)) were expressed as fractions of total plasma activity by division by Eq. (9); the calculated striatal metabolite activities (Eqs. (4)–(8)) were expressed as fractions of total striatal activity by division by Eq. (10). The resulting metabolite fractions facilitated comparison of present estimates with literature results. Absolute metabolite activities could not be compared because of varying amounts of injected [^{18}F]FDOPA.

3. Results

The calculated metabolite activities and fractions in plasma and striatum are shown in Fig. 2. In striatum, the activities of [^{18}F]FDOPA, [^{18}F]OMFD, [^{18}F]FDA, [^{18}F]FDOPAC, and [^{18}F]FHVA peaked at 3, 89, 21, 28, and 39 min, respectively.

The present calculations predicted ^{18}F-labeled metabolite fractions to within 10% of those measured by HPLC in 83 out of 96 comparisons with the literature (Cumming et al., 1987a,b, 1988; Melega et al., 1990a,b; Table 2). The largest discrepancies between calculated and measured data occurred at early time points: the calculations over-estimated striatal [^{18}F]FDOPA by 33% at 5 min and 14% at 10 min, and under-estimated striatal [^{18}F]FDOPAC by 29% at 5 min.

4. Discussion

4.1. Model applicability

In the compartmental model, species differences between rat and human with respect to the handling of [^{18}F]FDOPA will be reflected in the magnitudes of kinetic constant estimates (Table 1). Since [^{18}F]FDOPA follows the same in vivo metabolic pathways (Fig. 1) in rat and primate, activity data measured in the two species reflect the same compartments, albeit of differ-

ent sizes. Therefore, we propose that the present model can be used with equal accuracy in analyzing activity data from rat and human. We have confirmed this by successfully fitting the model to [^{3}H]DOPA autoradiographic data in rats (Deep et al., 1997) and [^{18}F]FDOPA/PET data in humans (Gjedde et al., 1991; Kuwabara et al., 1993).

4.2. Comparison of calculated and measured data

In general, qualitative and quantitative profiles of [^{18}F]FDOPA metabolite fractions calculated by the present model were in close agreement with those measured by HPLC analyses of labeled plasma and brain extracts in rat, for circulation times past 10 min. The relative time of the peak activity of [^{18}F]OMFD does not reflect its formation in vivo before [^{18}F]FDOPAC or [^{18}F]FHVA, since the striatal [^{18}F]OMFD activity (Eq. (4)) is the sum of two components: one originating in the transfer of plasma [^{18}F]OMFD into brain, and the other originating from COMT activity in brain. The time courses of metabolite fraction (Fig. 2) in plasma and striatum agreed excellently with corresponding measurements in rat (Cumming et al., 1987a; Melega et al., 1990a).

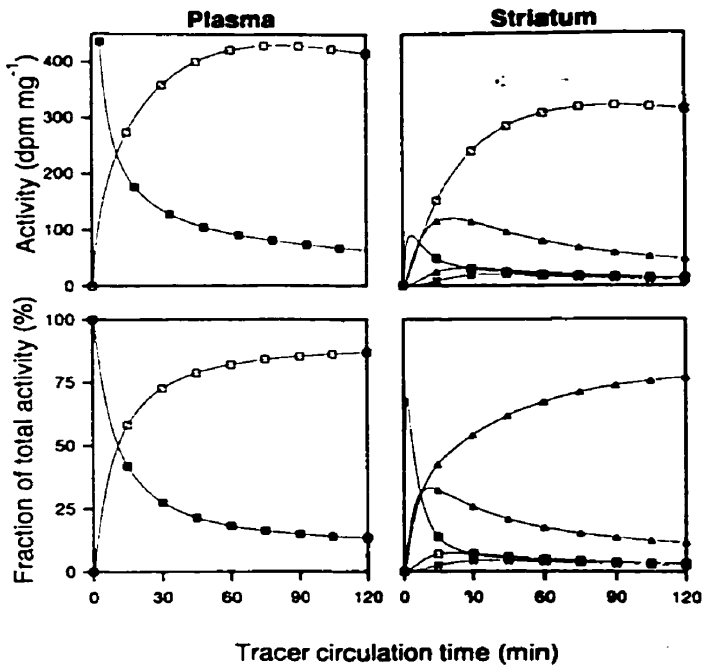

Fig. 2. Calculated activities and fractions in plasma and striatum for [^{18}F]FDOPA (■), [^{18}F]OMFD (□), [^{18}F]FDA (▲), [^{18}F]FDOPAC (△), and [^{18}F]FHVA (X) during 120 min of tracer circulation in rat. Plasma [^{18}F]FDOPA activities were calculated with a power function; all other activities were calculated by integration of first-order differential equations, with previous estimates of kinetic constants (Table 1) as inputs. Metabolite fractions were obtained by dividing calculated metabolite activities by total calculated activity.

Uncertainty about the estimate of COMT activity in brain with respect to [^{18}F]FDOPA (k_5^{FDOPA}), which was set equal to the corresponding estimate for [^{3}H]DOPA (0.06 min^{-1}; Cumming et al., 1995b), may explain the consistent over-estimation of the calculated striatal [^{18}F]OMFD activities (Table 2). Fluorination of L-DOPA significantly reduces its affinity for COMT in vitro (Creveling and Kirk, 1985; Firnau et al., 1988), so k_5^{FDOPA} may be lower for [^{18}F]FDOPA than [^{3}H]DOPA. Other significant discrepancies (> 10%) between calculated and measured metabolite fractions likely reflect the simplicity of the biological model, compared with real brain. The present model excludes two known brain compartments, corresponding to (i) [^{18}F]FDA-sulfate, which has been detected at concentrations comparable to those of [^{18}F]FDOPAC and [^{18}F]FHVA in both rat (Melega et al., 1990a,b) and primate (Melega et al., 1990b, 1991a,b), and (ii) the vesicular fraction of [^{18}F]FDA. There is considerable evidence to suggest that [^{18}F]FDA, like endogenous dopamine (Leviel et al., 1989; Pothos et al., 1996) and perhaps L-DOPA (Opacka-Juffry and Brooks, 1995), is stored in vesicles. An ^{19}F nuclear magnetic resonance examination of nerve-ending microsacs, isolated from guinea pig striatum and incubated with fluorinated amines, detected a strong signal corresponding to [^{18}F]FDA, with a minor signal corresponding to [^{18}F]FDOPAC (Diffley et al., 1983). [^{18}F]FDA is released from dopaminergic nerve terminals along with dopamine following depolarization by potassium (Chiueh et al., 1983). Furthermore, depletion of striatal activity was observed by [^{18}F]FDOPA/PET in monkeys treated with reserpine (Garnett et al., 1983b), a drug known to discharge dopamine from pre-synaptic storage vesicles. We therefore attempted to model the vesicular fraction of [^{18}F]FDA in vivo.

4.3. Modelling the vesicular fraction of [^{18}F]FDA

By definition, the apparent MAO activity measured in vivo assuming a homogeneous distribution of [^{18}F]FDA in brain [$k_7^{FDA'}(T)$] is proportional to the fraction of [^{18}F]FDA in the cytosol (Cumming et al., 1995b),

$$k_7^{FDA'}(T) = \left[\frac{M_{cyt}^{FDA}(T)}{M_{cyt}^{FDA}(T) + M_{ves}^{FDA}(T)}\right] k_7^{FDA} \qquad (11)$$

where $M_{cyt}^{FDA}(T)$ is the concentration of [^{18}F]FDA in the cytosolic compartment, $M_{ves}^{FDA}(T)$ is the concentration of [^{18}F]FDA in the vesicular compartment, and k_7^{FDA} is the true MAO activity in vivo assuming a homogenous distribution of [^{18}F]FDA within the compartment containing MAO. Eq. (11) predicts that apparent MAO activity is not constant during a tracer experiment: at early times prior to vesicular trapping of [^{18}F]FDA, $k_7^{FDA'}(T)$ equals k_7^{FDA}. The magnitude of $k_7^{FDA'}(T)$ then

Table 2
[^{18}F]FDOPA metabolite fractions in plasma and striatum of rat

Metabolite	Reference	Time (min)											
		2.5	5	10	15	20	25	30	45	60	75	90	120
Plasma [^{18}F]FDOPA	Present study	84	70	52	42	35	31	27	21	18	16	15	13
	Cumming et al., 1988	—	—	37	—	—	—	—	—	9	—	—	—
	Melega et al., 1990a	80	—	62	42	—	—	24	—	14	—	—	—
	Melega et al., 1990b	—	—	—	—	—	—	24	—	—	—	—	—
Plasma [^{18}F]OMFD	Present study	16	30	48	58	65	69	73	79	82	84	85	87
	Cumming et al., 1988	—	—	45	—	—	—	—	—	72	—	—	—
	Melega et al., 1990a	20	—	38	58	—	—	72	—	81	—	—	—
	Melega et al., 1990b	—	—	—	—	—	—	70	—	—	—	—	—
Striatal [^{18}F]FDOPA	Present study	62	42	22	14	10	8	7	5	4	4	4	3
	Cumming et al., 1987a	—	11	8	10	5	6	3	7	5	1	4	3
	Cumming et al., 1987b	—	—	—	—	—	—	4	—	4	—	4	—
	Cumming et al., 1988	—	—	12	—	—	—	—	—	3	—	—	—
	Melega et al., 1990a	—	—	—	7	—	—	2	—	2	—	—	—
	Melega et al., 1990b	—	—	—	—	—	—	2	—	—	—	—	—
Striatal [^{18}F]OMFD	Present study	12	23	36	42	47	51	54	62	67	71	74	77
	Cumming et al., 1987a	—	18	32	37	36	41	45	50	50	49	58	69
	Cumming et al., 1987b	—	—	—	—	—	—	50	—	53	—	73	—
	Cumming et al., 1988	—	—	31	—	—	—	—	—	52	—	—	—
	Melega et al., 1990a		—	—	40	—	—	50	—	51	—	—	—
	Melega et al., 1990b	—	—	—	—	—	—	49	—	—	—	—	—
Striatal [^{18}F]FDA	Present study	16	26	33	32	30	27	25	21	17	15	14	12
	Cumming et al., 1987a	—	23	24	25	20	19	21	18	21	17	15	7
	Cumming et al., 1987b	—	—	—	—	—	—	20	—	18	—	11	—
	Melega et al., 1990a	—	—	—	37	—	—	33	—	36	—	—	—
	Melega et al., 1990b	—	—	—	—	—	—	29	—	—	—	—	—
Striatal [^{18}F]FDOPAC	Present study	1	2	5	7	7	7	7	6	5	4	4	3
	Cumming et al., 1987a	—	31	10	10	8	9	8	11	6	5	5	3
	Cumming et al., 1987b	—	—	—	—	—	—	6	—	5	—	4	—
	Melega et al., 1990a	—	—	—	5	—	—	5	—	4	—	—	—
	Melega et al., 1990b	—	—	—	—	—	—	7	—	—	—	—	—
Striatal [^{18}F]FHVA	Present study	0	0	1	2	3	4	4	4	4	3	3	2
	Melega et al., 1990a	—	—	—	2	—	—	5	—	2	—	—	—
	Melega et al., 1990b	—	—	—	—	—	—	7	—	—	—	—	—

All results are percentages, determined as [([^{18}F]metabolite activity)/(total regional [^{18}F]activity) × 100].
A dash (—) indicates that the metabolite fraction was not given or could not be calculated with the given data at that time point.

declines as [^{18}F]FDA is sequestered in vesicles, until equilibrium between the cytosolic and vesicular compartments is reached.

According to Eq. (2), the activities of the cytosolic and vesicular [^{18}F]FDA compartments are given by,

$$\frac{d[M_{cyt}^{FDA}(t)]}{dt} = k_3^{FDOPA} M^{FDOPA} + k_{out}^{FDA} M_{ves}^{FDA} - (k_7^{FDA} + k_{in}^{FDA}) M_{cyt}^{FDA} \quad (12)$$

$$\frac{d[M_{ves}^{FDA}(t)]}{dt} = k_{in}^{FDA} M_{cyt}^{FDA} - k_{out}^{FDA} M_{ves}^{FDA} \quad (13)$$

where k_{in}^{FDA} is the rate constant for transfer of [^{18}F]FDA into vesicles, and k_{out}^{FDA} is the rate constant for release of [^{18}F]FDA from vesicles back into the cytosolic compartment. At late tracer circulation times, [^{18}F]FDA synthesis declines toward zero and the system approaches equilibrium ($T = T_{eq}$), in which case Eq. (13) reduces to,

$$\frac{k_{in}^{FDA}}{k_{out}^{FDA}} = \frac{M_{ves}^{FDA}(T_{eq})}{M_{cyt}^{FDA}(T_{eq})} \quad (14)$$

The magnitudes of k_{in}^{FDA} and k_{out}^{FDA} therefore determine the relative proportions of [^{18}F]FDA in the cytosolic and vesicular compartments in vivo at equilibrium. To our knowledge the only measurement of this ratio to date was made in vitro by Chien et al., 1990 in a giant dopamine neuron of the snail *Planorbis corneus*; voltammetric techniques detected that at least 98% of intracellular dopamine is bound and not directly exchangeable with dopamine in the cytoplasm at equilibrium. It is currently unknown if a similar distribution occurs in dopamine neurons of the rat.

To obtain the first in vivo estimates of k_{in}^{FDA} and k_{out}^{FDA}, we integrated Eqs. (12) and (13),

$$M_{cyt}^{FDA}(T) = k_3^{FDOPA}\int_0^T M^{FDOPA}(t)\, e^{-(k_7^{FDA}+k_{in}^{FDA})(T-t)}\, dt + k_{out}^{FDA}\int_0^T M_{ves}^{FDA}(t)\, e^{-(k_7^{FDA}+k_{in}^{FDA})(T-t)}\, dt \quad (15)$$

$$M_{ves}^{FDA}(T) = k_{in}^{FDA}\int_0^T M_{cyt}^{FDA}(t)\, e^{-k_{out}^{FDA}(T-t)}\, dt \quad (16)$$

The sum of Eqs. (15) and (16), equal to total [^{18}F]FDA activity in brain, was fitted by least-squares nonlinear regression to [^{18}F]FDA activities measured in rat striatum (Cumming et al., 1987a; Table 2), with the striatal [^{18}F]FDOPA curve as the input function. To solve for k_3^{FDOPA}, k_{in}^{FDA}, and k_{out}^{FDA}, it was necessary to fix the magnitude of k_7^{FDA} to reduce parameterization. However, the magnitude of k_7^{FDA} in vivo in striatal dopamine neurons is unknown, so we varied k_7^{FDA} over a range of fixed input values. At $k_7^{FDA} > 0.6$ min^{-1}, fits did not converge; complete results of these analyses are summarized in Table 3.

Present estimates of k_{out}^{FDA} were not significantly different from zero. But transfer of dopamine from cytosol to vesicles in vivo is not irreversible (Leviel et al., 1989), so k_{out}^{FDA} must have a small positive value. With fixed k_7^{FDA} values between 0.1–0.4 min^{-1}, inclusion of the vesicular compartment accounted for the large discrepancies between measured and calculated data at early times. In this range, estimates of DDC activity (k_3^{FDOPA}) were increased by 12–35%, relative to the HPLC estimate (0.17 min^{-1}; Cumming et al., 1994). By under-estimating k_3^{FDOPA}, the exclusion of vesicular storage of [^{18}F]FDA from the present model may contribute to the over-estimation of [^{18}F]FDOPA concentrations in striatum at early times (Table 2). The magnitude of k_{in}^{FDA} suggests that newly-formed [^{18}F]FDA is transferred to the vesicular compartment with a half-life of 12–34 min (calculated as $0.693/k_{in}^{FDA}$). Therefore at early times, the majority of [^{18}F]FDA is in the cytosolic compartment and so unprotected from metabolism by MAO, accounting for the high proportion of [^{18}F]FDOPAC measured at 5 min (31%, Table 2). Previous estimates of apparent MAO activity (Table 1) are several-fold lower than the valid range of k_7^{FDA} input values, consistent with the initial under-estimation of [^{18}F]FDOPAC concentrations, which became insignificant at times after 10 min (Table 2).

Table 3
Estimates of rate constants (min^{-1}) for the distribution of cerebral [^{18}F]FDA between cytosolic and vesicular compartments, as a function of MAO activity (k_7^{FDA})

k_7^{FDA}	k_3^{FDOPA}	k_{in}^{FDA}	k_{out}^{FDA}
0.1	0.19 ± 0.01	0.02 ± 0.01	0.06 ± 0.07
0.2	0.24 ± 0.02	0.04 ± 0.02	0.05 ± 0.07
0.3	0.23 ± 0.03	0.05 ± 0.02	0.04 ± 0.05
0.4	0.20 ± 0.04	0.06 ± 0.02	0.03 ± 0.04
0.5	0.17 ± 0.04	0.07 ± 0.02	0.02 ± 0.03
0.6	0.14 ± 0.04	0.08 ± 0.02	0.01 ± 0.02
0.7	—	—	—

Results are best estimates ± 95% C.I., obtained by nonlinear regression of the sum of Eqs. (15) and (16) to [^{18}F]FDA activities measured in rat striatum (Cumming et al., 1987a).
To reduce model paramterization, the value of k_7^{FDA} was fixed as an input constant.
Analyses were performed over a range of k_7^{FDA} values; fits did not converge for all $k_7^{FDA} > 0.6$ min^{-1}.

5. Conclusion

The present study compared the time courses of [^{18}F]FDOPA metabolite fractions calculated by a compartmental model of [^{18}F]FDOPA blood-brain transfer and metabolism, with those measured in vivo by chromatographic fractionation of ^{18}F-labeled compounds in plasma and striatal tissue extracts in rat. Based on the general agreement between calculated and measured data, we conclude that the model is biologically accurate and therefore valid for analysis of [^{18}F]FDOPA activity measured in living brain by PET. The large discrepancies between calculated and measured data at early times (< 10 min) could be explained by incorporation of a vesicular compartment for [^{18}F]FDA into the model thereby providing indirect evidence for vesicular storage of [^{18}F]FDA in vivo. Present data and methods were insufficient to independently estimate all kinetic constants associated with the distribution of [^{18}F]FDA between the cytolsol and vesicles. However, it is likely that the exclusion of vesicular storage from the present model does not greatly alter the magnitudes of kinetic constants estimated by regression analysis of PET data, because the long duration of PET studies permits near-equilibration of cytosolic and vesicular [^{18}F]FDA.

Acknowledgements

This work was supported by grant SP-30 from the Medical Research Council (MRC) of Canada. PD is a recipient of the Jeanne Timmins Costello Student Fellowship of the Montreal Neurological Institute, and a fellowship from the Fonds pour la Formation de Chercheurs et l'Aide à la Recherche (FCAR).

References

Boyes BE, Cumming P, Martin WRW, McGeer EG. Determination of plasma [^{18}F]-6-fluorodopa during positron emission tomography: elimination and metabolism in carbidopa treated subjects. Life Sci 1986;39:2243–52.

Broch OJ, Fonnum F. The regional and subcellular distribution of catechol-*O*-methyl transferase in the rat brain. J Neurochem 1972;19:2049–55.

Chien JB, Wallingford RA, Ewing AG. Estimation of free dopamine in the cytoplasm of the giant dopamine cell of *Planorbis corneus* by voltammetry and capillary electrophoresis. J Neurochem 1990;54:633–8.

Chiueh CC, Zukowska-Grojec Z, Kirk KL, Kopin IJ. 6-Fluorocatecholamines as false adrenergic neurotransmitters. J Pharmacol Exp Ther 1983;225:529–33.

Creveling CR, Kirk KL. The effect of ring-fluorination on the rate of *O*-methylation of dopa by catechol-*O*-methyltransferase: significance in the development of [^{18}F]PETT scanning agents. Biochem Biophys Res Commun 1985;130:1123–31.

Cumming P, Boyes BE, Martin WRW, Adam MJ, Grierson J, Ruth TJ, McGeer EG. The metabolism of [^{18}F]6-fluoro-L-3,4-dihydroxyphenylalanine in the hooded rat. J Neurochem 1987a;48:601–8.

Cumming P, Boyes BE, Martin WRW, Adam MJ, Ruth TJ, McGeer EG. Altered metabolism of [^{18}F]6-fluorodopa in the hooded rat following inhibition of catechol-*O*-methyltransferase with U-0521. Biochem Pharmacol 1987b;36:2527–31.

Cumming P, Hausser M, Martin WRW, Grierson J, Adam MJ, Ruth TJ, McGeer ED. Kinetics of in vitro decarboxylation and the in vivo metabolism of 2-^{18}F and 6-^{18}F-fluorodopa in the hooded rat. Biochem Pharmacol 1988;37:247–50.

Cumming P, Brown E, Damsma G, Fibiger H. Formation and clearance of interstitial metabolites of dopamine and serotonin in the rat striatum: an in vivo microdialysis study. J Neurochem 1992;59:1905–14.

Cumming P, Léger GC, Kuwabara H, Gjedde A. Pharmacokinetics of plasma 6-[^{18}F]fluoro-L-3,4-dihydroxyphenylalanine ([^{18}F]FDOPA) in humans. J Cereb Blood Flow Metab 1993;13:668–75.

Cumming P, Kuwabara H, Gjedde A. A kinetic analysis of 6-[^{18}F]fluoro-L-dihydroxyphenylalanine metabolism in the rat. J Neurochem 1994;63:1675–82.

Cumming P, Ase A, Diksic M, Harrison J, Jolly D, Kuwabara H, Laliberté C, Gjedde AH. Metabolism and blood-brain clearance of L-3,4-dihydroxy-[^{3}H]phenylalanine ([^{3}H]DOPA) and 6-[^{18}F]fluoro-L-DOPA in the rat. Biochem Pharmacol 1995a;50:943–6.

Cumming P, Kuwabara H, Ase A, Gjedde A. Regulation of DOPA decarboxylase activity in brain of living rat. J Neurochem 1995b;65:1381–90.

Deep P, Kuwabara H, Gjedde A, Cumming P. The cerebral kinetics of [^{3}H]DOPA in rat investigated by compartmental modelling of autoradiograms. J. Neurosci. Meth 1997 (submitted).

Diffley DM, Costa JL, Sokoloski EA, Chiueh CC, Kirk KL, Creveling CR. Direct observation of 6-fluorodopamine in guinea pig nerve microsacs by F-19 NMR. Biochem Biophys Res Commun 1983;110:740–5.

Firnau G, Garnett ES, Sourkes TL, Missala K. [^{18}F]Fluoro-dopa: a unique gamma emitting substrate for dopa decarboxylase. Experimentia 1975;31:1254–5.

Firnau G, Sood S, Chirakal R, Nahmias C, Garnett ES. Cerebral metabolism of 6-[^{18}F]fluoro-L-3,4-dihydroxyphenylalanine in the primate. J Neurochem 1987;48:1077–82.

Firnau G, Sood S, Chirakal R, Nahmias C, Garnett ES. Metabolites of 6-[^{18}F]fluoro-L-dopa in human blood. J Nucl Med 1988;29:363–9.

Garnett ES, Firnau G, Nahmias C. Dopamine visualized in the basal ganglia of living man. Nature (London) 1983a;305:137–8.

Garnett ES, Firnau G, Nahmias C, Chirakal R. Striatal dopamine metabolism in living monkeys examined by positron emission tomography. Brain Res 1983b;280:169–71.

Gjedde A. High-and low-affinity transport of D-glucose from blood to brain. J Neurochem 1981;36:1463–71.

Gjedde A. Calculation of glucose phosphorylation from brain uptake of glucose analogs in vivo: a re-examination. Brain Res Rev 1982;4:237–74.

Gjedde A, Reith J, Dyve S, Léger G, Guttman M, Diksic M, Evans A, Kuwabara H. Dopa decarboxylase activity of the living human brain. Proc Natl Acad Sci USA 1991;88:2721–5.

Hammerstad JP, Pate BD, Hewitt KA, Chan GL-Y, Ruth TJ, Calne DB. The transport of L-6-fluorodopa and its metabolites from blood to cerebrospinal fluid and brain. Ann Neurol 1993;34:604–8.

Hefti F, Melamed E, Wurtman RJ. The site of dopamine formation in rat striatum after L-dopa administration. J Pharmacol Exp Ther 1981;217:189–97.

Huang S-C, Yu D-C, Barrio JR, Grafton S, Melega WP, Hoffman JM, Satyamurthy N, Mazziotta JC, Phelps ME. Kinetics and modelling of L-6-[^{18}F]fluoro-DOPA in human positron emission tomographic studies. J Cereb Blood Flow Metab 1991;11:898–913.

Kuwabara H, Cumming P, Reith J, Léger G, Diksic M, Evans AC, Gjedde A. Human striatal L-DOPA decarboxylase activity estimated in vivo using 6-[^{18}F]fluoro-DOPA and positron emission tomography: error analysis and application to normal subjects. J Cereb Blood Flow Metab 1993;13:43–56.

Leviel V, Gobert A, Guilbert B. Direct observation of dopamine compartmentation in striatal nerve terminal by 'in vivo' measurement of the specific activity of released dopamine. Brain Res 1989;499:205–13.

Martin WRW, Palmer MR, Patlak CS, Calne DB. Nigrostriatal function in human studies with positron emission tomography. Ann Neurol 1989;26:535–42.

Melamed E, Hefti F, Pettibone DJ, Liebman J, Wurtman RJ. Aromatic L-amino acid decarboxylase in rat corpus striatum: implications for action of L-dopa in parkinsonism. Neurology 1981;31:651–5.

Melega WP, Luxen A, Perlmutter MM, Nissenson CHK, Phelps ME, Barrio JR. Comparative in vivo metabolism of [^{18}F]6-fluoro-L-DOPA and [^{3}H]-L-DOPA in rats. Biochem Pharamcol 1990a;39:1853–60.

Melega WP, Hoffman JM, Luxen A, Nissenson CHK, Phelps ME, Barrio JR. The effects of carbidopa on the metabolism of [^{18}F]6-fluoro-L-DOPA in rats, monkeys, and humans. Life Sci 1990b;47:149–57.

Melega WP, Hoffman JM, Schneider JS, Phelps ME, Barrio JR. 6-[^{18}F]Fluoro-L-DOPA metabolism in MPTP-treated monkeys: assessment of tracer methodologies for positron emission tomography. Brain Res 1991a;543:271–6.

Melega WP, Grafton ST, Huang S-C, Satyamurthy N, Phelps ME, Barrio JR. L-6-[^{18}F]Fluoro-DOPA in monkeys and humans: bilochemical parameters for the formulation of tracer kinetic models with positron emission tomography. J Cereb Blood Flow Metab 1991b;11:890–7.

Opacka-Juffry J, Brooks DJ. L-Dihydroxyphenylalanine and its decarboxylase: new ideas on their regulatory roles. Move Disord 1995;10:241–9.

Patlak CS, Blasberg RG, Fenstermacher JD. Graphical evaluation of blood-to-brain transfer constants from multiple-time uptake data. J Cereb Blood Flow Metab 1983;3:1–7.

Patlak CS, Blasberg RG. Graphical evaluation of blood-to-brain transfer constants from multiple-time uptake data: generalizations. J Cereb Blood Flow Metab 1985;5:584–90.

Pothos E, Desmond M, Sulzer D. L-3,4-Dihydroxyphenylalanine increases the quantal size of exocytotic dopamine release in vitro. J Neurochem 1996;66:629–36.

Reith J, Dyve S, Kuwabara H, Guttman M, Diksic M, Gjedde A. Blood-brain transfer and metabolism of 6-[^{18}F]fluoro-L-DOPA in rat. J Cereb Blood Flow Metab 1990;10:707–19.

Rivett AJ, Francis A, Roth JA. Localization of membrane-bound catechol-*O*-methyltransferase. J Neurochem 1983;40:1494–6.

Roth JA. Membrane-bound catechol-*O*-methyltransferase: a reevaluation of its role in the *O*-methylation of the catecholamine neurotransmitters. Rev Physiol Biochem Pharmacol 1992;120:1–28.

Sawle GV, Colebatch JG, Shah A, Brooks DJ, Marsden CD, Frackowiak RS. Striatal function in normal agin: inplications for Parkinson's disease. Ann Neurol 1990;28:799–804.

Wahl L, Nahmias C. Modelling of fluorine-18-6-fluoro-L-DOPA in humans. J Nucl Med 1996;37:432–7.

Westerink BHC, Spaan SJ. Estimation of the turnover of 3-methoxytyramine in the rat striatum by HPLC with electrochemical detection: implications for the sequence in the cerebral metabolism of dopamine. J Neurochem 1982;38:342–7.

ELSEVIER

Journal of Neuroscience Methods 78 (1997) 157–168

JOURNAL OF NEUROSCIENCE METHODS

The kinetic behaviour of [^{3}H]DOPA in living rat brain investigated by compartmental modelling of static autoradiograms

Paul Deep [a,*], Hiroto Kuwabara [b], Albert Gjedde [c], Paul Cumming [a]

[a] *Montreal Neurological Institute, McGill University, 3801 University St., Montreal, Quebec H3A 2B4, Canada*
[b] *Department of Neurosurgery, West Virginia University, Morgantown, WV, USA*
[c] *PET Center, Aarhus University Hospital, Aarhus, Denmark*

Received 23 June 1997; received in revised form 28 August 1997; accepted 1 September 1997

Abstract

The kinetic behaviour of [^{3}H]DOPA in living rat brain was investigated by compartmental modelling of measured activities from combined metabolite pools in a time-series (180 min) of static autoradiograms from right cerebral hemispheres. Two models of [^{3}H]DOPA uptake and metabolism that incorporated the removal of the decarboxylation product, [^{3}H]dopamine, from brain were significantly more accurate than a model in which [^{3}H]dopamine accumulated irreversibly in situ. Present estimates of [^{3}H]DOPA kinetic constants were compared to previously published results based on the analysis of measured activities from individual metabolite pools separated by chromatographic fractionation of [^{3}H]DOPA metabolites in the left cerebral hemispheres of the same rats. Autoradiographic estimates of DOPA decarboxylase activity with respect to [^{3}H]DOPA in brain (k_3^{DOPA}) were under-estimated several-fold relative to chromatographic estimates; this discrepancy is explained by post-mortem enzyme activity and omission of biological compartments from the models. However, autoradiographic estimates of the unidirectional blood–brain clearance of [^{3}H]DOPA (K_1^{DOPA}) and monoamine oxidase activity with respect to [^{3}H]dopamine in brain ($k_7^{DA'}$) agreed with chromatographic estimates. This concordance represents the first empirical validation of compartmental modelling of autoradiographic data as a method for quantitatively investigating the kinetic behaviour of radiolabelled L-DOPA in living mammalian brain. © 1997 Elsevier Science B.V.

Keywords: Blood–brain clearance; Chromatographic fractionation; Compartmental model; DOPA decarboxylase activity; [^{3}H]DOPA autoradiography; [^{3}H]Dopamine; Kinetic constants; Rat brain

1. Introduction

Static autoradiograms made from cryostat sections of brain have revealed that the cerebral accumulation of radioactivity in living rats following intravenous injection of [^{3}H]DOPA (Liskowsky and Potter, 1985; Cumming et al., 1995a, 1997a) and [^{14}C]DOPA (Horne et al., 1984) is greater in the basal ganglia than in structures containing little activity of DOPA decarboxylase (EC 4.1.1.28), the ultimate enzyme in dopamine synthesis. The trapping of labelled decarboxylated metabolites in catecholamine fibres (Deep et al., 1997a) is the basis for similar qualitative results in living human brain, first observed by dynamic positron emission tomography with the exogenous DOPA decarboxylase substrate L-6-[^{18}F]fluoro-DOPA ([^{18}F]fluoro-DOPA; Garnett et al., 1983). With these autoradiographic techniques, the cerebral concentrations of individual radiolabelled metabolites cannot be measured directly, but are calculated by fitting compartmental models of tracer uptake and metabolism to a time-series of total observed cerebral activities.

Compartmental modelling of brain tissue activities measured by positron emission tomography in humans administered [^{18}F]fluoro-DOPA (Gjedde et al., 1991;

* Corresponding author. Tel.: +1 514 3981996; fax: +1 514 3988948; e-mail: deep@pet.mni.mcgill.ca

PII S0165-0270(97)00147-7

Kuwabara et al., 1993; Dhawan et al., 1996; Ishikawa et al., 1996; Wahl and Nahmias, 1996a,b) has yielded in vivo estimates of equilibrium distribution volumes and blood–brain transfer coefficients for the tracer and its *O*-methylated derivative, and regional activities of DOPA decarboxylase. In living rat, these same kinetic constants have been calculated for [^{3}H]DOPA (Cumming et al., 1995a,b) and [^{18}F]fluoro-DOPA (Cumming et al., 1994a, 1995b) from the temporal changes in the concentrations of product and precursor pools measured by chromatographic fractionation of labelled metabolites in brain tissue extracts. However, this chromatographic DOPA decarboxylase assay has not hitherto been systematically compared with the corresponding assay based on compartmental modelling of total cerebral activities in labeled L-DOPA autoradiograms.

The major metabolite of [^{3}H]DOPA in the circulation and the brain is *O*-methyl-[^{3}H]DOPA (Melega et al., 1990; Cumming et al., 1995a,b), generated by catechol-*O*-methyltransferase (EC 2.1.1.6). [^{3}H]DOPA in brain is decarboxylated by DOPA decarboxylase to form [^{3}H]dopamine, which is stored in synaptic vesicles (Descarries et al., 1980). Monoamine oxidase (EC 1.4.3.4) further metabolizes [^{3}H]dopamine in the cytosol to yield 3,4-dihydroxy-[^{3}H]phenylacetic acid ([^{3}H]DOPAC), which is then *O*-methylated by catechol-*O*-methyltransferase to form [^{3}H]homovanillic acid. Whereas no transport mechanism is known to clear [^{3}H]dopamine directly from brain, the acidic metabolites [^{3}H]DOPAC and [^{3}H]homovanillic acid (collectively called [^{3}H]acids) are freely diffusible into cerebrospinal fluid. The total activity measured by [^{3}H]DOPA autoradiography reflects the sum of all these physiological processes.

In the present study, we estimate [^{3}H]DOPA kinetic constants in living rat brain by compartmental modelling of measured activities from combined metabolite pools in static autoradiograms from right cerebral hemispheres. To validate compartmental modelling of autoradiographic data as a method for investigating the kinetic behaviour of radiolabelled L-DOPA in living mammalian brain, the present results are compared with previously published results based on the analysis of measured activities from individual metabolite pools separated by chromatographic fractionation of [^{3}H]DOPA metabolites in the left cerebral hemispheres of the same rats (Cumming et al., 1995a). The compartmental models of [^{3}H]DOPA blood–brain clearance and metabolism described herein are based on the several distinct compartmental models used for the analysis of positron emission tomography studies with [^{18}F]fluoro-DOPA in primates (for reviews, see Cumming and Gjedde, 1997; Cumming et al., 1997b). Therefore, we also test the influence of model choice on the estimation of [^{3}H]DOPA kinetic constants previously defined by analytic methods.

2. Materials and methods

2.1. Autoradiography

In vivo studies were conducted in accordance with the requirements of the McGill Animal Ethics Committee, as described in detail previously (Cumming et al., 1995a). Briefly, male Wistar rats (Charles River, $n = 13$) received polyethylene catheters (Clay Adams, 0.965 mm o.d.; Becton Dickenson, Sparks, MD, USA) in the left femoral artery and vein. Rats were immobilized in a plaster body cast, and then administered carbidopa (5 mg kg^{-1}, i.p.; MS and D, Kirkland, Quebec, Canada) 30 min prior to bolus injection (200 μCi per animal, i.v.) of L-3,4-dihydroxy-[*ring*-2,5,6-^{3}H]phenylalanine ([^{3}H]DOPA, 80 Ci mmol^{-1}; New England Nuclear, Boston, MA, USA) to inhibit peripheral decarboxylation of tracer. Rats were decapitated at specific times after tracer injection (5, 10, 15, 30, 45, 60, 90, 120, 150 and 180 min); three rats were sacrificed at 30 min, two at 180 min, and one at all other times. Brains were removed and bisected; left cerebral hemispheres were further dissected and then fractionated by high-performance liquid chromatography to determine the radiochemical composition (Cumming et al., 1995a).

Right cerebral hemispheres were frozen, mounted with embedding matrix (Lipshaw, Pittsburgh, PA, USA), slowly warmed to −20°C in a refrigerated cryostat (HM 500 M, Zeiss), and then cut into a series of 20-μm-thick frontal sections. Each eighth section was placed on a glass coverslip. Tritium-sensitive film (Hyperfilm, Amersham, Oakville, Ontario, Canada) was exposed to these sections along with autoradiographic standards (Amersham) for 6 weeks before development by conventional means. Total regional activity was measured by quantitative densitometry (Imaging Systems, St. Catherines, Ontario, Canada) in (n) sections from the following nine regions of rat brain: dorsal–medial caudate (10), central caudate (13), nucleus accumbens shell (5), nucleus accumbens body (5), olfactory tubercle (7), amygdala (4), hypothalamus (6), dorsal hippocampus (7), and ventral hippocampus (4). Boundaries between adjacent regions were determined by visual inspection. The regions of interest were circles approximately 2 mm in diameter. Anatomical coordinates of brain sections in the anterior–posterior axis were recorded relative to bregma (Paxinos and Watson, 1982).

To recalibrate the autoradiographic standards (nCi mg^{-1}) relative to plasma activity (dpm μl^{-1}), we measured the autoradiographic density in a reference region (occipital cortex). A portion of adjacent occipital cortex (30 mg) was then dissolved overnight in organic base (1 ml; NSC II, Amersham) and the radioactivity measured (dpm mg^{-1}) by scintillation spectroscopy following addition of scintillation fluid (10 ml; BCS, Amersham).

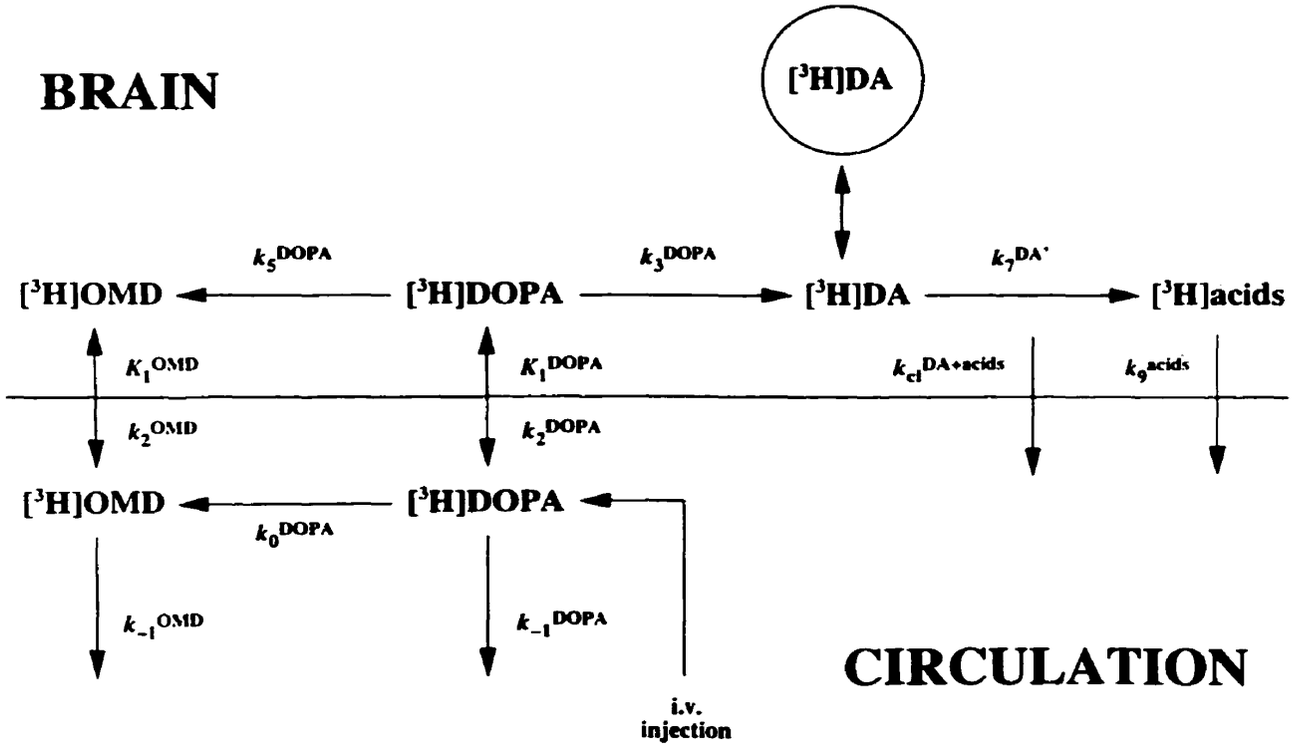

Fig. 1. Schematic summary of [^{3}H]DOPA blood–brain transfer and metabolism, according to three different compartmental models. [^{3}H]DOPA in circulation is *O*-methylated (k_0^{DOPA}) by catechol-*O*-methyltransferase to form *O*-methyl-[^{3}H]DOPA. Both tracers are subsequently cleared from circulation by renal elimination (k_{-1}^{DOPA} and k_{-1}^{OMD}). Both tracers are transferred into the brain (K_1^{DOPA} and K_1^{OMD}) and out of the brain (k_2^{DOPA} and k_2^{OMD}) by facilitated diffusion. [^{3}H]DOPA in the brain is *O*-methylated (k_5^{DOPA}) by catechol-*O*-methyltransferase to form *O*-methyl-[^{3}H]DOPA. In brain regions containing DOPA decarboxylase, [^{3}H]DOPA is decarboxylated (k_3^{DOPA}) to form [^{3}H]dopamine ([^{3}H]DA), most of which is rapidly sequestered in vesicles (circle) and so protected from deamination by monoamine oxidase. For M1, [^{3}H]DA is not metabolized or otherwise cleared from the brain. For M2, [^{3}H]DA and [^{3}H]acids occupy the same compartment and are together cleared from the brain ($k_{cl}^{DA+acids}$). For M3, [^{3}H]DA is not cleared from the brain but is metabolized to form [^{3}H]acids ($k_7^{DA^*}$), which are subsequently cleared from the brain into cerebrospinal fluid (k_9^{acids}) and back into the venous circulation.

A perchloric acid extract of another portion of occipital cortex was fractionated to determine the fraction of radioactivity due to [^{3}H]H_2O (10–20%). After correction for the presence of [^{3}H]H_2O (which evaporated from the cryostat sections), the ratio of the activity measured by scintillation spectroscopy to the activity measured by autoradiography in the reference region gave a linear tissue cross-calibration factor ($\sim$ 1000 dpm nCi^{-1}). All autoradiographic densities were then multiplied by this factor to convert to dpm mg^{-1}, thus permitting the use of arterial activities (dpm μl^{-1}) as input functions for the calculation of brain tissue activities (dpm mg^{-1}).

Areas under the measured arterial [^{3}H]DOPA curves were calculated for each rat. Corresponding areas under the common simulated arterial [^{3}H]DOPA curve (Eq. (1), see below) were divided by the measured integrals to produce a linear plasma correction factor for each rat. Tissue activities in each rat were then multiplied by its respective factor. This normalization allowed the use of common arterial input curves for all rats, in order to (i) correct for scatter in measured data attributable to variations in the individual arterial curves, and (ii) approximate better the methodology of a positron emission tomography scan, in which all data points are measured from the same subject.

2.2. [^{3}H]DOPA compartmental models

The biological pathways traced by [^{3}H]DOPA in circulation and brain tissue, including the associated kinetic constants, are illustrated in Fig. 1. In brain regions assumed to have low DOPA decarboxylase activity, we used a two-parameter two-compartment model (M0) described by the unidirectional blood–brain clearance of [^{3}H]DOPA (K_1^{DOPA}, ml g^{-1} min^{-1}) and the equilibrium distribution volume of [^{3}H]DOPA (V_e^{DOPA}, ml g^{-1}). In brain regions assumed to have high DOPA decarboxylase activity, we present three models extended to incorporate the presence of additional compartments. The first model (M1) is a two-parameter three-compartment model (Gjedde et al., 1991; Wahl and Nahmias, 1996a,b) described by K_1^{DOPA}, and the activity of DOPA decarboxylase with

respect to [^{3}H]DOPA in the brain (k_3^{DOPA}, min^{-1}); [^{3}H]dopamine is not metabolized or otherwise cleared from the brain. The second model (M2) is a three-parameter three-compartment model described by K_1^{DOPA}, k_3^{DOPA}, and the rate constant for the efflux of activity from the brain ($k_{cl}^{DA+acids}$, min^{-1}); [^{3}H]dopamine and [^{3}H]acids are together cleared from the brain into cerebrospinal fluid as a single compartment. The third model (M3) is a three-parameter four-compartment model (Kuwabara et al., 1993) described by K_1^{DOPA}, k_3^{DOPA}, and the rate constant for the conversion of cerebral [^{3}H]dopamine to [^{3}H]acids by monoamine oxidase ($k_7^{DA'}$, min^{-1}); [^{3}H]dopamine and [^{3}H]acids are in separate compartments, and only [^{3}H]acids are cleared from the brain into cerebrospinal fluid. M1 was fitted to 60 min ($M1_{60}$) and 180 min ($M1_{180}$) of activity data; M2 and M3 were fitted to 180 min of activity data.

The model equations that define the individual metabolite compartments in arterial plasma and brain have been presented elsewhere (Cumming et al., 1995a; Deep et al., 1997a). Briefly, values of the normalized integral of plasma activity (Θ, min; Gjedde, 1981, 1982; Patlak et al., 1983) for [^{3}H]DOPA were calculated for each rat. The linear regression slope of a plot of Θ versus tracer circulation time, defined as the dimensionless constant α (Wong et al., 1986), was then used to calculate the activity of arterial [^{3}H]DOPA [$C_a^{DOPA}(T)$] as the single power function (Cumming et al., 1997c,d; Deep et al., 1997a):

$$C_a^{DOPA}(T) = AT^{((1/\alpha)-1)} \quad (1)$$

where A is an arbitrary scaling constant (dpm μl^{-1} min^{-1}), and T is the tracer circulation time (min). Using $C_a^{DOPA}(T)$ as the input function, the activities of arterial O-methyl-[^{3}H]DOPA (dpm μl^{-1}) and all brain metabolites (dpm mg^{-1}) were calculated by the general compartmental equation:

$$Z_i(T) = \sum_1^m \left[k_{in}^m \int_0^T Z_{i-1}^m(t) \exp\left(-\sum_1^n k_{out}^n (T-t) \right) \right] dt \quad (2)$$

where $Z_i(T)$ is the instantaneous activity of the metabolite, $Z_{i-1}^m(t)$ is the time–activity curve of the m-th precursor compound, k_{in}^m is the kinetic constant of the process that converts the m-th precursor into metabolite, and k_{out}^n is the kinetic constant of the n-th process that removes the metabolite from the compartment. Therefore, total brain activity was the sum of Eq. (2) for each metabolite compartment.

2.3. Constraints and assumptions

We applied the following assumptions and physiological constraints to the models to reduce parameterization:

(1) Population means estimated previously from the same rats (Cumming et al., 1995a) for the rate constants for O-methylation of arterial [^{3}H]DOPA (k_0^{DOPA}, 0.015 min^{-1}) and the elimination of arterial O-methyl-[^{3}H]DOPA (k_{-1}^{OMD}, 0.013 min^{-1}) were used to calculate the activity of arterial O-methyl-[^{3}H]DOPA.

(2) By definition, V_e^{DOPA} is equal to the ratio K_1^{DOPA}/k_2^{DOPA}, thus eliminating k_2^{DOPA}, the rate constant for clearance of [^{3}H]DOPA from brain to plasma.

(3) The magnitude of V_e^{DOPA} was estimated in the posterior cingulate cortex and then assumed to be uniform throughout the rat brain (Gjedde et al., 1991).

(4) The constant of proportionality (q; Reith et al., 1990) between the unidirectional blood–brain clearances of O-methyl-[^{3}H]DOPA and [^{3}H]DOPA (K_1^{OMD}/K_1^{DOPA}), also equal to the ratio of the rate constants of clearance from the brain of O-methyl-[^{3}H]DOPA and [^{3}H]DOPA (k_2^{OMD}/k_2^{DOPA}), was fixed at a value of 1.5 based on previous measurements in the rat (Cumming et al., 1995a). Knowledge of this constant thus eliminates K_1^{OMD} and k_2^{OMD} from the models.

(5) Cerebral O-methyl-[^{3}H]DOPA originates from two sources: transfer of arterial O-methyl-[^{3}H]DOPA into the brain, and conversion of [^{3}H]DOPA in the brain to O-methyl-[^{3}H]DOPA. However, the rate constant for O-methylation of [^{3}H]DOPA in brain (k_5^{DOPA}) was set to zero (Gjedde et al., 1991). Therefore, arterial O-methyl-[^{3}H]DOPA was assumed to be the only source of O-methyl-[^{3}H]DOPA in the brain.

(6) No plasma compartments were defined for [^{3}H]dopamine or [^{3}H]acids, based on chromatographic studies in carbidopa-treated rats which failed to detect these compounds in plasma following injection of [^{3}H]DOPA (Melega et al., 1990; Cumming et al., 1995a).

(7) The formation of homovanillic acid in rat brain proceeds by two pathways: O-methylation of DOPAC, and oxidative deamination of 3-methoxytyramine. However, the concentration of 3-methoxytyramine in striatum is low (Cheng and Wooten, 1982) and the majority of homovanillic acid is derived from DOPAC (Westerink and Spaan, 1982; Cumming et al., 1992), so the contribution of the labelled 3-methoxytyramine compartment to total activity in the autoradiograms was considered negligible.

(8) In M3, [^{3}H]DOPAC and [^{3}H]homovanillic acid were assumed to occupy the same compartment in the brain ([^{3}H]acids), thus eliminating one compartment and two rate constants from the model.

(9) The rate constant $k_7^{DA'}$ indicates the apparent monoamine oxidase activity measured in vivo assuming a homogeneous distribution of [^{3}H]dopamine in the brain. It is reduced relative to the true monoamine oxidase activity in vivo assuming a homogenous distribution of [^{3}H]dopamine within the compartment containing monoamine oxidase (k_7^{DA}), in proportion to the

unknown ratio of cytosolic [^{3}H]dopamine to whole tissue [^{3}H]dopamine (Cumming et al., 1995a; Deep et al., 1997a).

(10) The rate constants for the formation ($k_7^{DA'}$) and clearance (k_9^{acids}) of [^{3}H]acids were fixed at a ratio of unity (Kuwabara et al., 1993), thus eliminating k_9^{acids} from M3.

(11) The vascular component of brain tissue activity was omitted, since the rat brain sections were assumed to be devoid of significant plasma radioactivity during exposure to autoradiographic film.

2.4. Data analysis

Analyses were performed by least-squares nonlinear regression of compartmental models to the measured data (Matlab, © The MathWorks, Natick, MA, USA). We first estimated V_c^{DOPA} according to M0 in a section of posterior cingulate cortex, a brain region assumed to have negligible DOPA decarboxylase activity. This value of V_c^{DOPA} was then used as a fixed input to estimate other kinetic constants in sections of brain regions with high DOPA decarboxylase activity according to M1, M2 and M3.

The accuracy of a nonlinear regression fit to measured data was evaluated by the magnitude of the residual sum of squares. The mean value of multiple determinations was calculated for kinetic constant estimates in each brain region, and results were expressed as mean ± SD. One-factor analysis of variance (ANOVA) tests were used for comparisons of mean regional values of residuals, K_1^{DOPA} and k_3^{DOPA}, to identify a significant main effect of compartmental model. [^{3}H]Dopamine clearance rate constants ($k_{cl}^{DA+acids}$ and $k_7^{DA'}$) were not compared statistically since they have different biological definitions. Tukey's test was used for post hoc comparisons to identify specific differences in mean values between the models. The correlation between kinetic constant estimates and position along the anterior–posterior axis in each brain region was evaluated by linear regression analysis; the presence of a significant linear correlation was interpreted as signifying a regional gradient in the magnitude of that constant. For all tests, a probability value of $p < 0.05$ was considered significant.

3. Results

Linear regression of the normalized integral of plasma [^{3}H]DOPA activity [$\Theta = \int C_a^{DOPA}(t)\,dt / C_a^{DOPA}(T)$] versus tracer circulation time for the population of rats ($r = 0.99$, $p < 0.05$; Fig. 2) yielded a slope $\alpha = 2.2$. The close agreement between the common simulated activities for arterial [^{3}H]DOPA and *O*-methyl-[^{3}H]DOPA, and measured activities of these compounds in arterial plasma of a carbidopa-treated rat following [^{3}H]DOPA injection, is shown in Fig. 3. The fit of M0 to data measured in a section of posterior cingulate cortex (Fig. 4) yielded an estimate of V_c^{DOPA} of 0.75 ml g^{-1}. In Fig. 5 are plotted the fits of M1, M2 and M3 to data measured in a section of nucleus accumbens body. Tissue activities measured from autoradiograms clearly illustrate that regions of rat brain containing relatively high levels of DOPA decarboxylase activity such as the basal ganglia (Fig. 5) retained more radioactivity following [^{3}H]DOPA injection than regions with little or no DOPA decarboxylase activity such as the posterior cingulate cortex (Fig. 4).

In all brain regions, the mean residuals (data not shown) for fits with M2 and M3 were significantly lower than those for fits with $M1_{180}$; the mean residuals for M2 and M3 were equal. Estimates of the unidirectional blood–brain clearance of [^{3}H]DOPA (K_1^{DOPA}; Table 1) ranged from 0.05 to 0.08 ml g^{-1} min^{-1}, and displayed little variation between the different models. Estimates of DOPA decarboxylase activity with respect to [^{3}H]DOPA in brain (k_3^{DOPA}; Table 2) ranged from 0.01 to 0.09 min^{-1}, with the largest values in the basal ganglia. Estimates of k_3^{DOPA} for fits with $M1_{180}$ were significantly lower than those with all other models; k_3^{DOPA} estimates were not significantly different between $M1_{60}$ and M3. Estimates of the [^{3}H]dopamine clearance rate constants ($k_{cl}^{DA+acids}$ and $k_7^{DA'}$; Table 3) ranged from 0.02 to 0.04 min^{-1}. Results of post hoc comparisons for mean estimates of K_1^{DOPA} and k_3^{DOPA} are summarized in Table 4.

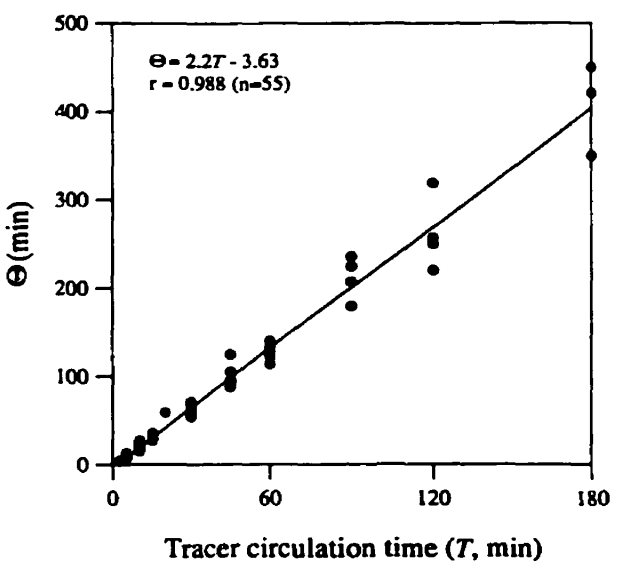

Fig. 2. Values of the normalized integral of plasma [^{3}H]DOPA activity [$\Theta = \int C_a^{DOPA}(t)\,dt / C_a^{DOPA}(T)$; $n = 55$] vs. tracer circulation time in rat. A significant linear relationship is demonstrated by the line of regression ($r = 0.99$, $p < 0.05$) to the measured data (●). The regression slope α (2.2) was used to calculate the activity of arterial [^{3}H]DOPA.

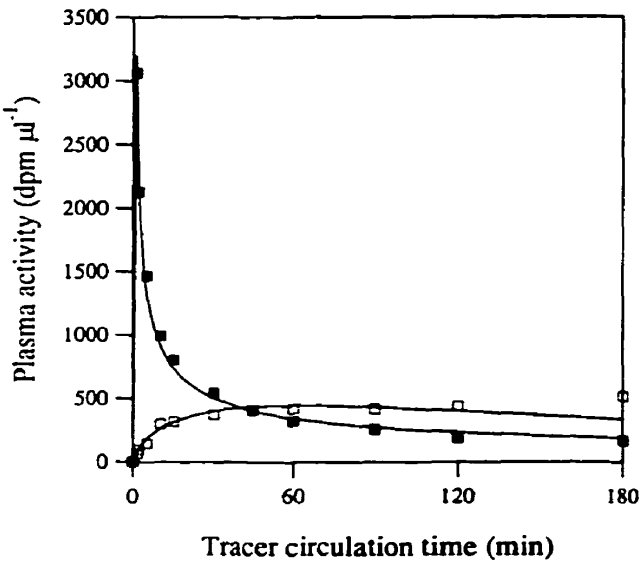

Fig. 3. Measured activities of [^{3}H]DOPA (■) and *O*-methyl-[^{3}H]DOPA (□) in arterial plasma of a single carbidopa-treated rat as a function of tracer circulation time following the injection of [^{3}H]DOPA (200 μCi, i.v.; Cumming et al., 1995a). The smooth lines represent the calculated arterial activities of [^{3}H]DOPA and *O*-methyl-[^{3}H]DOPA. The arterial [^{3}H]DOPA activities were calculated using a power function defined relative to the normalized arterial integral of [^{3}H]DOPA. The arterial *O*-methyl-[^{3}H]DOPA activities were calculated using population means for the rate constants for *O*-methylation of arterial [^{3}H]DOPA (k_0^{DOPA}, 0.015 min^{-1}) and the elimination of arterial *O*-methyl-[^{3}H]DOPA (k_1^{OMD}, 0.013 min^{-1}), estimated previously in the same rats (Cumming et al., 1995a).

Increasing posterior–anterior gradients were found for the magnitudes of K_1^{DOPA} in dorsal–medial caudate and hypothalamus, and [^{3}H]dopamine clearance rate constants ($k_{cl}^{DA+acids}$ and k_7^{DA}) in nucleus accumbens body. Similar gradients for k_3^{DOPA} were observed in the dorsal–medial caudate, olfactory tubercle, hypothalamus, dorsal hippocampus, and nucleus accumbens. Estimates of kinetic constant as functions of anatomical position in dorsal–medial caudate are plotted in Fig. 6.

4. Discussion

4.1. Estimates of [^{3}H]DOPA kinetic constants

This study represents the first assay of [^{3}H]DOPA kinetics in living rat brain by compartmental modelling of activities measured with quantitative autoradiography; the present technique is analogous to that of Sokoloff et al. (1977), who modelled cerebral glucose consumption in rats using [^{14}C]deoxyglucose autoradiograms. To validate compartmental modelling of autoradiographic data as a method for investigating the kinetic behaviour of radiolabelled L-DOPA in living mammalian brain, we compared estimates of [^{3}H]DOPA kinetic constants based on compartmental modelling of total cerebral activities from combined metabolite pools in a time-series of static autoradiograms from the right cerebral hemispheres of rats, with corresponding estimates based on the analysis of measured activities from individual metabolite pools separated by chromatographic fractionation of [^{3}H]DOPA metabolites in the left cerebral hemispheres of the same rats (Cumming et al., 1995a).

The present autoradiographic estimate of the equilibrium distribution volume of [^{3}H]DOPA (V_e^{DOPA}) matched the corresponding chromatographic result in the cortex (0.71 ml g^{-1}; Cumming et al., 1995a). Large neutral amino acids such as L-DOPA are water-soluble, and are passively transferred from blood to brain by facilitated diffusion (Wade and Katzman, 1975; Oldendorf and Szabo, 1976; Smith, 1991); the same mechanism applies to [^{3}H]DOPA. The fact that this transport process requires no energy indicates that the distribution volumes of large neutral amino acids cannot in general exceed the ratio of water contents between brain tissue and plasma (0.92 ml g^{-1}; Gjedde and Bodsch, 1987); amino acid concentrations measured in the rat clearly confirm this principle (Gjedde and Bodsch, 1987; Paetsch and Greenshaw, 1991). Indeed, the present autoradiographic estimate of V_e^{DOPA} is consistent with this postulate. Thus, there exists no gradient for the accumulation of [^{3}H]DOPA in a specific region of brain, which is the basis of our assumption of a uniform distribution of [^{3}H]DOPA throughout the rat brain at equilibrium.

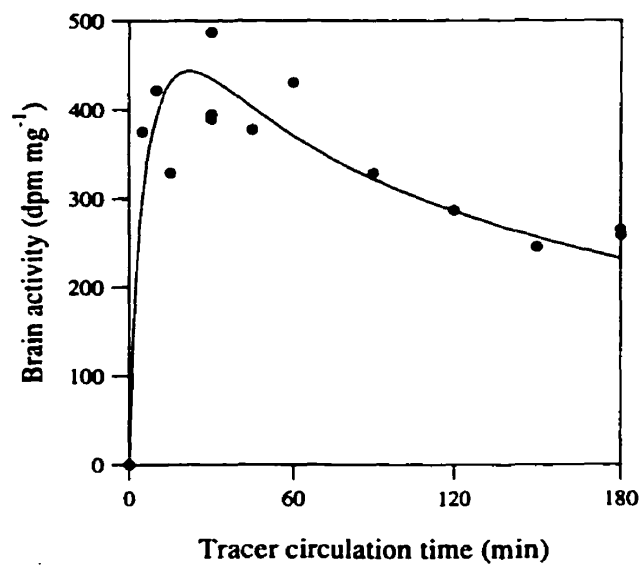

Fig. 4. Total activity measured in a section of posterior cingulate cortex during 180 min of [^{3}H]DOPA circulation in rat (n = 13). Tissue activities were scaled to common simulated [^{3}H]DOPA and *O*-methyl-[^{3}H]DOPA arterial curves. The smooth line is defined by least-squares nonlinear regression of a two-parameter two-compartment model (M0), in which [^{3}H]DOPA is not decarboxylated to [^{3}H]dopamine, to the measured data (●). Each data point was measured in one rat.

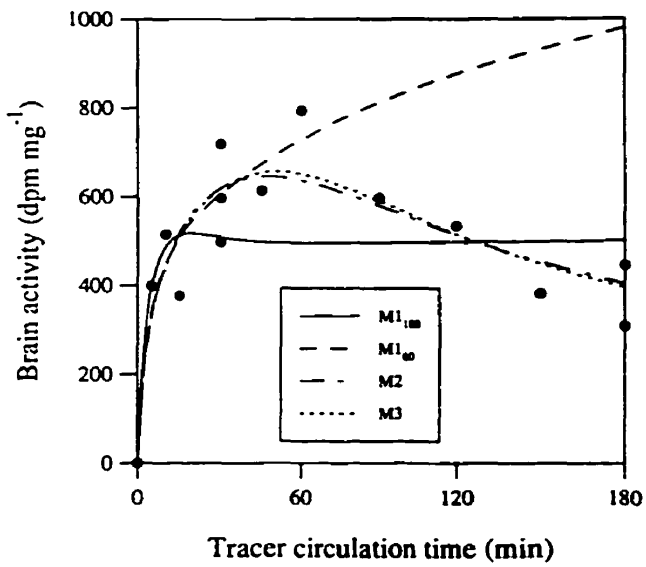

Fig. 5. Total activity measured in a section of nucleus accumbens body during 180 min of [^{3}H]DOPA circulation in rat ($n = 13$). Tissue activities were scaled to common simulated [^{3}H]DOPA and *O*-methyl-[^{3}H]DOPA arterial curves. The smooth lines are defined by least-squares nonlinear regression to the measured data (●) of a two-parameter three-compartment model (M1) in which [^{3}H]dopamine accumulates irreversibly in brain, a three-parameter three-compartment model (M2) in which [^{3}H]dopamine is cleared from the brain with [^{3}H]acids as a single compartment, and a three-parameter four-compartment model (M3) in which [^{3}H]dopamine and [^{3}H]acids are assumed to occupy separate compartments. Model M1 was fitted to 60 min ($M1_{60}$) and 180 min ($M1_{180}$) of measured data; the curve fitted to 60 min has been extrapolated to 180 min. Each data point was measured in one rat.

Autoradiographic estimates of the unidirectional blood–brain clearance of [^{3}H]DOPA (K_1^{DOPA}; Table 1) showed excellent quantitative agreement with corresponding chromatographic results (0.04–0.06 ml g^{-1} min^{-1}; Cumming et al., 1995a). The small regional variation in brain uptake measured for [^{3}H]DOPA, [^{18}F]fluoro-DOPA (Cumming et al., 1994a), and [^{3}H]tyrosine (Cumming et al., 1994b), together suggest a relatively homogeneous concentration of the transporter of large neutral amino acids throughout the cerebral vasculature of rat forebrain.

Autoradiographic estimates of apparent monoamine oxidase activity with respect to [^{3}H]dopamine in the brain ($k_7^{DA'}$; Table 3) agreed within the range of corresponding chromatographic results (0.01–0.15 min^{-1}; Cumming et al., 1995a). However, autoradiographic estimates of DOPA decarboxylase activity with respect to [^{3}H]DOPA in the brain (k_3^{DOPA}; Table 2) were several-fold lower than chromatographic estimates, especially in the striatum (0.26 min^{-1}; Cumming et al., 1995a). Several possible factors contributed to this discrepancy. First, analysis by chromatography could lead to systematic overestimation of k_3^{DOPA} if DOPA decarboxylase continued to consume cerebral [^{3}H]DOPA in the post mortem period: several minutes transpired between decapitation and extraction of brain samples in perchloric acid, such that the true activity of [^{3}H]DOPA at the time of death would be underestimated. Indeed, the concentration of endogenous L-DOPA in the brain of rats killed by decapitation was over 2.5 times smaller than that measured in rats killed by microwave irradiation (Thiede and Kehr, 1981). Such irradiation causes thermal denaturation of enzymes, including DOPA decarboxylase, and therefore prevents the rapid post mortem degradation of L-DOPA. Second, the omission of catechol-*O*-methyltransferase activity with respect to [^{3}H]DOPA in brain (k_5^{DOPA}) from the present models overestimated the amount of [^{3}H]DOPA available for decarboxylation, thus underestimating k_3^{DOPA}. Third, we have recently shown that the omission of the vesicular compartment of labelled dopamine further underestimates k_3^{DOPA} (Deep et al., 1997a). Fourth, estimates of k_3^{DOPA} in rat decline rapidly with increasing V_e^{DOPA} (Deep et al., 1997b); if the magnitude of V_e^{DOPA} estimated in the cortex was higher than the true magnitude in non-cortical regions, present estimates of k_3^{DOPA} would be further reduced relative to chromatographic estimates. The choice of q did not contribute to the discrepancy between present and chromatographic results. Values of k_3^{DOPA} previously estimated from this data set were relatively unaffected by input values of q between 0.5 and 3.0 (Deep et al., 1997b).

The regional distributions of enzyme activities measured in vivo by autoradiography (Tables 2 and 3) are consistent with those of DOPA decarboxylase (Rahman et al., 1980) and monoamine oxidase (Saura et al., 1982) assayed in vitro in rat brain. Furthermore, we report gradients in the magnitudes of [^{3}H]DOPA kinetic constant estimates within structures of the rat basal ganglia (Fig. 6), indicating that the striatum is chemically heterogeneous. A rostrocaudal gradient for DOPA decarboxylase activity has been observed in vivo in the human striatum (Garnett et al., 1987). Present estimates of the activities of DOPA decarboxylase in the caudate nucleus and monoamine oxidase in the nucleus accumbens also increased from posterior to anterior, in agreement with the distribution of endogenous dopamine, DOPAC, and homovanillic acid in divisions of rat striatum (Widmann and Sperk, 1986).

4.2. Comparison of compartmental models

The present modelling approach, in which a simulated arterial [^{3}H]DOPA curve is used as the input function, has been previously derived (Deep et al., 1997a). We now compare three different compartmental models of [^{3}H]DOPA blood–brain clearance and metabolism (Fig. 1), each reflecting a different possible metabolic route available to [^{3}H]dopamine formed in brain. The present models are identical to those used

Table 1
Estimates of the unidirectional blood–brain clearance of [^{3}H]DOPA (K_1^{DOPA}, ml g^{-1} min^{-1})

Brain region	$M1_{180}$	$M1_{60}$	M2	M3
Dorsal-medial caudate (n = 10)	0.060 ± 0.010	0.050 ± 0.010	0.052 ± 0.009	0.050 ± 0.010
Central caudate (n = 13)	0.065 ± 0.005	0.056 ± 0.003	0.054 ± 0.003	0.054 ± 0.004*
Nucleus accumbens shell (n = 5)	0.075 ± 0.007	0.063 ± 0.007	0.061 ± 0.007	0.061 ± 0.008*
Nucleus accumbens body (n = 5)	0.073 ± 0.004	0.060 ± 0.004	0.057 ± 0.004	0.057 ± 0.004*
Olfactory tubercle (n = 7)	0.076 ± 0.006	0.067 ± 0.005	0.064 ± 0.004	0.065 ± 0.004*
Amygdala (n = 4)	0.053 ± 0.002	0.050 ± 0.004	0.052 ± 0.003	0.050 ± 0.004
Hypothalamus (n = 6)	0.072 ± 0.006	0.069 ± 0.006	0.068 ± 0.005	0.068 ± 0.005
Dorsal hippocampus (n = 7)	0.048 ± 0.002	0.046 ± 0.002	0.046 ± 0.002	0.046 ± 0.002*
Ventral hippocampus (n = 4)	0.059 ± 0.002	0.056 ± 0.002	0.055 ± 0.002	0.055 ± 0.002*

Results are mean ± SD values of separate determinations in (n) sections of rat brain region, obtained by nonlinear regression of compartmental models M1, M2 and M3 to total cerebral activities measured from a time-series (180 min) of autoradiograms from right cerebral hemishperes, obtained following i.v. injection of [^{3}H]DOPA. One-factor ANOVA tests were performed on mean K_1^{DOPA} estimates.
* Indicates a significant main effect of compartmental model ($p<0.05$).

for analysis of positron emission tomography studies with [^{18}F]fluoro-DOPA in primates. M1 stipulates that [^{3}H]dopamine accumulates irreversibly in brain. Extrapolation of M1 fitted to 60 min of measured data (Fig. 5) predicted that activity would increase continuously in brain regions of non-zero DOPA decarboxylase activity, due to accumulation of [^{3}H]dopamine in situ. Fits of M1 to 180 min of measured data greatly underestimated brain activity past 60 min. The absence of [^{3}H]acids in M1 indicates that all brain activity past 60 min (not including that due to [^{3}H]DOPA and *O*-methyl-[^{3}H]DOPA) must be due solely to [^{3}H]dopamine. The activity of [^{3}H]dopamine in M1 is therefore underestimated, which leads to a consequent overestimation of precursor [^{3}H]DOPA, resulting in underestimation of DOPA decarboxylase activity. The omission of [^{3}H]dopamine clearance from compartmental models therefore explains the significant reductions in (i) accuracy and (ii) the magnitude of k_3^{DOPA} estimates, in fits with M1 compared to fits with M2 and M3 (Table 2).

No difference was observed in kinetic constant estimates according to $M1_{60}$ and M3 (Table 4), indicating that significant clearance of [^{3}H]dopamine occurred only after 60 min of tracer circulation. This conclusion is consistent with the results of chromatographic assays of striatal tissue from rats administered [^{3}H]DOPA (Melega et al., 1990; Cumming et al., 1995a), and monkeys administered [^{18}F]fluoro-DOPA (Firnau et al., 1987), in which labelled dopamine accounted for the majority of striatal activity during the first hour following tracer injection.

Several studies have omitted the clearance of ^{18}F-labelled dopamine from compartmental models of [^{18}F]fluoro-DOPA metabolism in primate brain (Gjedde et al., 1991; Barrio et al., 1996; Dhawan et al., 1996; Ishikawa et al., 1996; Wahl and Nahmias, 1996a,b). However, there is considerable evidence to suggest that, for extended tracer studies (>1 h), the clearance of labelled dopamine from the brain cannot be ignored without prejudicing the results of model fits. Assuming that labelled dopamine accumulated irreversibly in the brain produced inaccurate fits to measured data (M1; Fig. 5), and influenced the magnitudes of kinetic constant estimates by 10–100%. Furthermore, independant estimates of the rate constants for the elimination of endogenous (Moleman et al., 1978; Dedek et al., 1979; Soares-da-Silva and Garrett, 1990; Cumming et al., 1992) and labelled (Cumming et al., 1994a, 1995a) acidic metabolites from the brain of living rat are all in the range 0.04–0.10 min^{-1}. Therefore, most of the labelled acids formed during the first hour following tracer injection have been cleared into cerebrospinal fluid by the third hour, indicating that this process contributes significantly to activity signals measured during extended tracer studies.

Two of the compartmental models presented here account for the clearance of [^{3}H]dopamine from the brain, either by direct transport into cerebrospinal fluid with [^{3}H]acids (M2, $k_{cl}^{DA+acids}$) or oxidative deamination by monoamine oxidase (M3, $k_7^{DA'}$). Assuming that the net efflux of radioactivity from the brain is the same for both models, then it may be shown that:

$$k_{cl}^{DA+acids}(T) = \frac{k_9^{acids} M^{acids}(T)}{M^{DA}(T) + M^{acids}(T)} \quad (3)$$

Previous estimates of [^{3}H]DOPA kinetic constants from four regions of rat brain (Cumming et al., 1995a) were used to calculate activities of [^{3}H]dopamine [$M^{DA}(T)$] and [^{3}H]acids [$M^{acids}(T)$] in brain according to Eq. (2), which were then substituted into Eq. (3). In all regions so simulated, the magnitude of $k_{cl}^{DA+acids}$ increased from nil at injection when the activity of [^{3}H]acids is nil, to a peak between 60 and 120 min when clearance of [^{3}H]acids from the brain is well established (Fig. 7). During the rising portions of the curves, the apparent rate of formation of [^{3}H]acids is much greater than the apparent rate of clearance of [^{3}H]acids from the brain.

Table 2
Estimates of DOPA decarboxylase activity with respect to [^{3}H]DOPA in brain (k_3^{DOPA}, min^{-1})

Brain region	$M1_{180}$	$M1_{60}$	M2	M3
Dorsal–medial caudate ($n = 10$)	0.007 ± 0.003	0.018 ± 0.007	0.030 ± 0.010	0.023 ± 0.009*
Central caudate nucleus ($n = 13$)	0.009 ± 0.002	0.025 ± 0.006	0.060 ± 0.020	0.033 ± 0.009*
Nucleus accumbens shell ($n = 5$)	0.008 ± 0.001	0.029 ± 0.002	0.070 ± 0.010	0.042 ± 0.006*
Nucleus accumbens body ($n = 5$)	0.009 ± 0.001	0.032 ± 0.003	0.090 ± 0.010	0.050 ± 0.006*
Olfactory tubercle ($n = 7$)	0.006 ± 0.001	0.025 ± 0.005	0.060 ± 0.020	0.040 ± 0.010*
Amygdala ($n = 4$)	0.002 ± 0.001	0.010 ± 0.004	0.020 ± 0.010	0.013 ± 0.006*
Hypothalamus ($n = 6$)	0.002 ± 0.001	0.010 ± 0.003	0.021 ± 0.009	0.013 ± 0.006*
Dorsal hippocampus ($n = 7$)	0.002 ± 0.001	0.008 ± 0.001	0.017 ± 0.003	0.009 ± 0.002*
Ventral hippocampus ($n = 4$)	0.003 ± 0.001	0.012 ± 0.002	0.028 ± 0.008	0.016 ± 0.003*

Results are mean ± SD values of separate determinations in (n) sections of rat brain region, obtained by nonlinear regression of compartmental models M1, M2 and M3 to total cerebral activities measured from a time-series (180 min) of autoradiograms from right cerebral hemishperes, obtained following i.v. injection of [^{3}H]DOPA. One-factor ANOVA tests were performed on mean k_3^{DOPA} estimates.
* Indicates a significant main effect of compartmental model ($p < 0.05$).

The plateau after 60 min thus corresponds to a state of transient equilibrium between the rates of these two processes. Therefore, in non-steady state, the magnitude of $k_{cl}^{DA+acids}$ (Huang et al., 1991) is time-dependent.

5. Conclusion

Excluding efflux of [^{3}H]DOPA and *O*-methyl-[^{3}H]DOPA, no significant elimination of activity from brain was detected by autoradiography before 60 min of tracer circulation. However, trapping of [^{3}H]dopamine is not irreversible; at circulation times greater than 60 min after tracer injection, compartmental modelling of autoradiograms failed to account for measured tissue activities unless the clearance of [^{3}H]dopamine from brain was included in the models.

The present autoradiographic method permits the analysis of discrete brain regions too small to be resolved by other in vivo techniques such as chromatography or positron emission tomography; small regions also better satisfy the compartmental definition of spatial homogeneity. Furthermore, unlike positron emission tomography, the present method is not influenced by partial volume effects (Mazziotta et al., 1981), which can significantly affect kinetic constant estimates. A disadvantage of the present autoradiographic method is the requirement of multiple subjects; in positron emission tomography studies all data are measured from a single subject. Notwithstanding efforts to normalize all animals to common arterial input curves, inter-subject variability contributed to the scatter observed in present data.

The general agreement of present autoradiographic estimates of [^{3}H]DOPA kinetic constants based on compartmental modelling of total cerebral activities from combined metabolite pools in a time-series of static autoradiograms from the right cerebral hemispheres of rats, with corresponding estimates based on the analysis of measured activities from individual metabolite pools separated by chromatographic fractionation of [^{3}H]DOPA metabolites in the left cerebral hemispheres of the same rats (Cumming et al., 1995a),

Table 3
Estimates of rate constants (min^{-1}) for the clearance of cerebral [^{3}H]dopamine, either by direct removal from brain with [^{3}H]acids ($k_{cl}^{DA+acids}$) or oxidative deamination ($k_7^{DA'}$)

Brain region	M2, $k_{cl}^{DA+acids}$	M3, $k_7^{DA'}$
Dorsal–medial caudate ($n = 10$)	0.015 ± 0.003	0.025 ± 0.004
Central caudate ($n = 13$)	0.017 ± 0.003	0.029 ± 0.004
Nucleus accumbens shell ($n = 5$)	0.023 ± 0.002	0.036 ± 0.002
Nucleus accumbens body ($n = 5$)	0.023 ± 0.002	0.036 ± 0.002
Olfactory tubercle ($n = 7$)	0.025 ± 0.003	0.039 ± 0.004
Amygdala ($n = 4$)	0.023 ± 0.006	0.040 ± 0.010
Hypothalamus ($n = 6$)	0.029 ± 0.004	0.043 ± 0.006
Dorsal hippocampus ($n = 7$)	0.024 ± 0.004	0.037 ± 0.005
Ventral hippocampus ($n = 4$)	0.027 ± 0.005	0.040 ± 0.007

[^{3}H]Dopamine clearance rate constants were explicitly set to 0 in M1. Results are mean ± SD values of separate determinations in (n) sections of rat brain region, obtained by nonlinear regression of compartmental models M2 and M3 to total cerebral activities measured from a time-series (180 min) of autoradiograms from right cerebral hemishperes, obtained following i.v. injection of [^{3}H]DOPA.

Table 4
Summary of post hoc comparisons for estimates of the unidirectional blood–brain clearance of [^{3}H]DOPA (K_1^{DOPA}) and DOPA decarboxylase activity with respect to [^{3}H]DOPA in brain (k_3^{DOPA})

	$M1_{60}$	$M1_{180}$	M2	M3
$M1_{60}$	—	3	0	0
$M1_{180}$	6	—	4	4
M2	8	9	—	0
M3	1	9	8	—

Results are number of brain regions (out of nine) in which a significant difference between compartmental models was found in mean estimates of K_1^{DOPA} (above the diagonal) and k_3^{DOPA} (below the diagonal), according to one-factor ANOVA followed by post hoc comparison with Tukey's test.

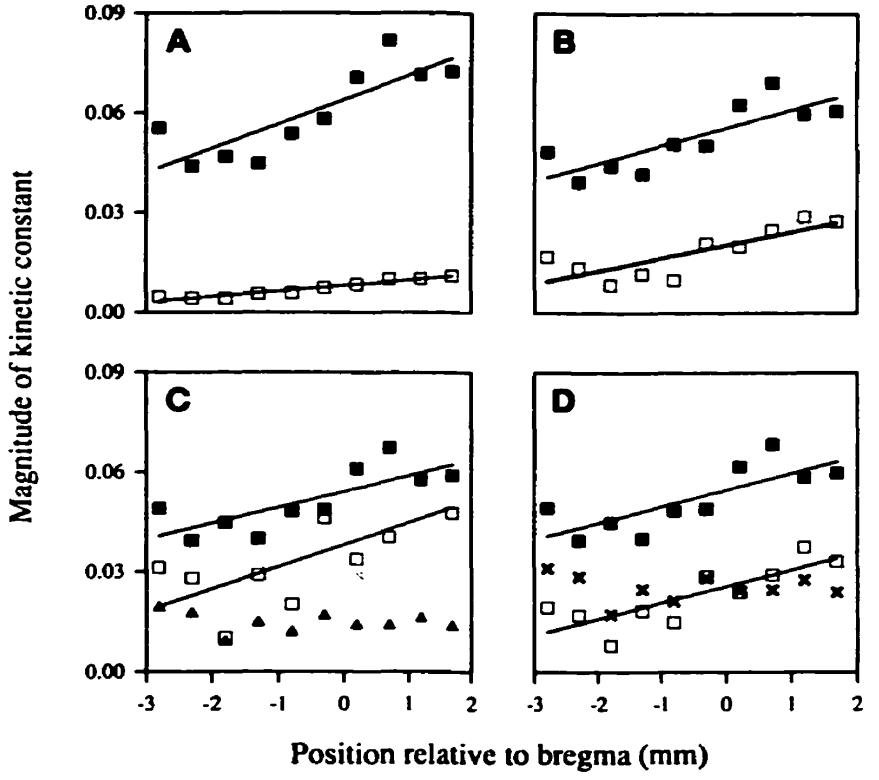

Fig. 6. Estimates of K_1^{DOPA} (■, ml g^{-1} min^{-1}), k_3^{DOPA} (□, min^{-1}), $k_{cl}^{DA+acids}$ (▲, min^{-1}), and k_7^{DA} (×, min^{-1}) as a function of anatomical position along the anterior–posterior axis of the rat dorsal–medial caudate, according to models $M1_{180}$ (A), $M1_{60}$ (B), M2 (C) and M3 (D). Positive abscissa points indicate positions anterior to bregma (recorded as 0 mm). Significant linear correlations ($p < 0.05$), indicated by the lines of regression, between kinetic constant and position were found for K_1^{DOPA} ($M1_{180}$, $r = 0.83$; $M1_{60}$, $r = 0.82$; M2, $r = 0.77$; M3, $r = 0.78$), and k_3^{DOPA} ($M1_{180}$, $r = 0.93$; $M1_{60}$, $r = 0.80$; M2, $r = 0.72$; M3, $r = 0.82$).

represents the first empirical validation of compartmental modelling of autoradiographic data as a method for quantitatively investigating the kinetic behaviour of radiolabelled L-DOPA in living mammalian brain.

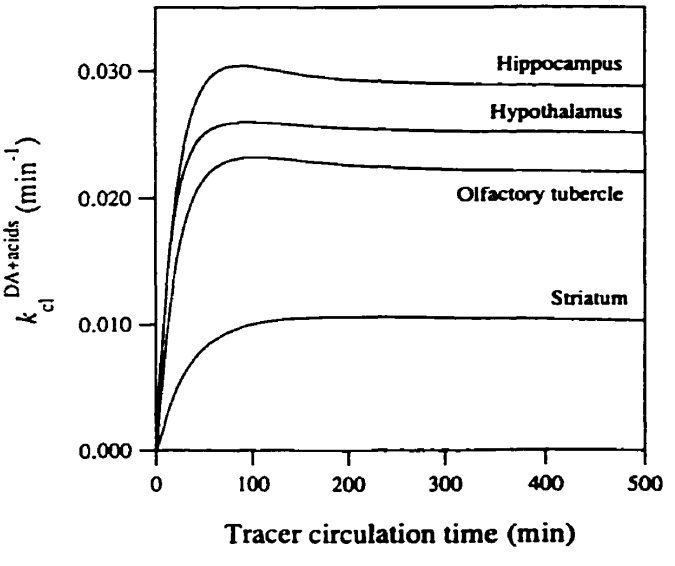

Fig. 7. The magnitude of $k_{cl}^{DA+acids}$ as a function of tracer circulation time, calculated in four regions of the rat brain.

Acknowledgements

This research was supported by grant SP-30 from the Medical Research Council (MRC) of Canada. PD is a recipient of the Jeanne Timmins Costello Student Fellowship of the Montreal Neurological Institute, and a fellowship from the Fonds pour la Formation de Chercheurs et l'Aide à la Recherche (FAR). The authors thank Ms. Christine Laliberté for expert technical assistance. This work is dedicated to Doris (Sept. 27, 1979–Feb. 13, 1997), cherished friend of PD: she is gone, but never forgotten.

References

Barrio JR, Huang S-C, Yu D-C, Melega WP, Quintana J, Cherry SR, Jacobson A, Namavari M, Satyamurthy N, Phelps ME. Radiofluorinated L-*m*-tyrosines: new in vivo probes for central dopamine biochemistry. J Cereb Blood Flow Metab 1996;16:667–78.

Cheng CH, Wooten GF. Dopamine turnover estimated by simultaneous LCEC assay of dopamine and dopamine metabolites. J Pharmacol Meth 1982;8:123–33.

Cumming P, Gjedde A. Compartmental analysis of dopa decarboxylation in living brain from dynamic positron emission tomograms. Synapse 1997, in press.

Cumming P, Brown E, Damsma G, Fibiger H. Formation and clearance of interstitial metabolites of dopamine and serotonin in the rat striatum: an in vivo microdialysis study. J Neurochem 1992;59:1905–14.

Cumming P, Kuwabara H, Gjedde A. A kinetic analysis of 6-[^{18}F]fluoro-L-dihydroxyphenylalanine metabolism in the rat. J Neurochem 1994a;63:1675–82.

Cumming P, Venkatachalam TK, Rajagopal S, Diksic M, Gjedde A. Brain uptake of α-[^{14}C]methyl-*para*-tyrosine in the rat. Synapse 1994b;17:125–8.

Cumming P, Kuwabara H, Ase A, Gjedde A. Regulation of DOPA decarboxylase activity in brain of living rat. J Neurochem 1995a;65:1381–90.

Cumming P, Ase A, Diksic M, Harrison J, Jolly D, Kuwabara H, Laliberté C, Gjedde A. Metabolism and blood–brain clearance of L-3,4-dihydroxy-[^{3}H]phenylalanine ([^{3}H]DOPA) and 6-[^{18}F]fluoro-L-DOPA in the rat. Biochem Pharmacol 1995b;50:943–6.

Cumming P, Ljubic-Thibal V, Laliberté C, Diksic M. The effect of unilateral neurotoxic lesions to serotonin fibres in the medial forebrain bundle on the metabolism of [^{3}H]DOPA in the telencephalon of the living rat. Brain Res 1997a;747:60–9.

Cumming P, Deep P, Rousset O, Evans A, Gjedde A. On the rate of decarboxylation of dopa to dopamine in living mammalian brain. In: Reis DJ, Posner J, editors. Frontiers of Neurology. New York: New York Academy of Sciences Press, 1997b, in press.

Cumming P, Ase A, Laliberté C, Kuwabara H, Gjedde A. In vivo regulation of DOPA decarboxylase by dopamine receptors in rat brain. J Cereb Blood Flow Metab 1997c, in press.

Cumming P, Ase A, Kuwabara H, Gjedde A. [^{3}H]DOPA formed from [^{3}H]tyrosine in living rat brain is not committed to dopamine synthesis. J Cereb Blood Flow Metab 1997d, in press.

Dedek J, Baumes R, Tien-Duc N, Gomeni R, Korf J. Turnover of free and conjugated (sulphonyloxy)-dihydroxyphenylacetic acid and homovanillic acid in rat striatum. J Neurochem 1979;33:687–95.

Deep P, Gjedde A, Cumming P. On the accuracy of an [^{18}F]FDOPA compartmental model: evidence for vesicular storage of [^{18}F]fluorodopamine in vivo. J Neurosci Methods, 1997;76:157–65.

Deep P, Kuwabara H, Gjedde A, Cumming P. Modelling the cerebral kinetics of [^{3}H]DOPA. Neuroimage 1997b;5:A24.

Descarries L, Bosler O, Berthelet F, Des Rosiers MH. Dopaminergic nerve endings visualized by high-resolution autoradiography in adult rat neostriatum. Nature 1980;284:620–2.

Dhawan V, Ishikawa T, Patlak C, Chaly T, Robeson W, Abdelfatihe B, Margouleff C, Mandel F, Eidelberg D. Combined FDOPA and 3OMFD PET studies in Parkinson's disease. J Nucl Med 1996;37:209–16.

Firnau G, Sood S, Chirakal R, Nahmias C, Garnett ES. Cerebral metabolism of 6-[^{18}F]fluoro-L-3,4-dihydroxyphenylalanine in the primate. J Neurochem 1987;48:1077–82.

Garnett ES, Firnau G, Nahmias C. Dopamine visualized in the basal ganglia of living man. Nature 1983;305:137–8.

Garnett ES, Lang AE, Chirakal R, Firnau G, Nahmias C. A rostrocaudal gradient for aromatic acid decarboxylase in the human striatum. Can J Neurol Sci 1987;14:444–7.

Gjedde A. High- and low-affinity transport of D-glucose from blood to brain. J Neurochem 1981;36:1463–71.

Gjedde A. Calculation of glucose phosphorylation from brain uptake of glucose analogs in vivo: a re-examination. Brain Res Rev 1982;4:237–74.

Gjedde A, Bodsch W. Facilitated diffusion across the blood–brain barrier: interactions between receptors and transporters. Wissenschaftl Z Karl Marx Univ (Leipzig) 1987;36:67–71.

Gjedde A, Reith J, Dyve S, Léger G, Guttman M, Diksic M, Evans A, Kuwabara H. Dopa decarboxylase activity of the living human brain. Proc Natl Acad Sci USA 1991;88:2721–5.

Horne MK, Cheng CH, Wooten GF. The cerebral metabolism of L-dihydroxyphenylalanine. Pharmacology 1984;28:12–26.

Huang S-C, Yu D-C, Barrio JR, Grafton S, Melega WP, Hoffman JM, Sabyamurthy N, Mazziotta JC, Phelps ME. Kinetics and modelling of L-6-[^{18}F]fluoro-DOPA in human positron emission tomographic studies. J Cereb Blood Flow Metals 1991;11:898–913.

Ishikawa T, Dhawan V, Chaly T, Robeson W, Belakhlef A, Mandel F, Dahl R, Margouleff C, Eidelberg D. Fluorodopa positron emission tomography with an inhibitor of catechol-*O*-methyltransferase: effect of the plasma 3-*O*-methyldopa fraction on data analysis. J Cereb Blood Flow Metab 1996;16:854–63.

Kuwabara H, Cumming P, Reith J, Léger G, Diksic M, Evans AC, Gjedde A. Human striatal L-DOPA decarboxylase activity estimated in vivo using 6-[^{18}F]fluoro-DOPA and positron emission tomography: error analysis and application to normal subjects. J Cereb Blood Flow Metab 1993;13:43–56.

Liskowsky DR, Potter LT. A pre-positron emission tomography study of L-3,4-dihydroxy-[^{3}H]phenylalanine distribution in the rat. Neurosci Lett 1985;53:161–7.

Mazziotta JC, Phelps ME, Plummer D, Kuhl DE. Quantitation in positron emission computed tomography: 5. Physical–anatomical effects. J Comput Assist Tomogr 1981;5:734–43.

Melega WP, Luxen A, Perlmutter MM, Nissenson CHK, Phelps ME, Barrio JR. Comparative in vivo metabolism of [^{18}F]6-fluoro-L-DOPA and [^{3}H]-L-DOPA in rats. Biochem Pharamcol 1990;39:1853–60.

Moleman P, Bruinvels J, Cornelis FM van Valkenburg. Haloperidol inhibits the disappearance of acidic dopamine metabolites from rat striatum. J Pharm Pharmacol 1978;30:583–585.

Oldendorf WH, Szabo J. Amino acid assignment to one of three blood–brain barrier amino acid carriers. Am J Physiol 1976;230:94–8.

Paetsch P, Greenshaw AJ. β-Adrenergic effects on plasma and brain large neutral amino acids are unaltered by chronic administration of antidepressants. J Neurochem 1991;56:2027–32.

Patlak CS, Blasberg RG, Fenstermacher JD. Graphical evaluation of blood-to-brain transfer constants from multiple-time uptake data. J Cereb Blood Flow Metab 1983;3:1–7.

Paxinos G, Watson C. The Rat Brain in Stereotaxic Coordinates. New York: Academic Press, 1982.

Rahman MK, Nagatsu T, Kato T. Aromatic L-amino acid decarboxylase activity in central and peripheral tissues and serum of rats with L-DOPA and L-5-hydroxytryptophan as substrates. Biochem Pharmacol 1980;30:645–9.

Reith J, Dyve S, Kuwabara H, Guttman M, Diksic M, Gjedde A. Blood–brain transfer and metabolism of 6-[^{18}F]fluoro-L-DOPA in rat. J Cereb Blood Flow Metab 1990;10:707–19.

Rousset OG, Ma Y, Léger GC, Gjedde AH, Evans AC. Correction for partial volume effects in PET using MRI-based 3D simulations of individual human brain metabolism. In: Uemura K, Lassen NA, Jones T, Kanno I, editors. Quantification of Brain Function: Tracer Kinetics and Image Analysis in Brain PET. Amsterdam: Elsevier Science, 1993:113–125.

Saura J, Kettler R, Da Prada M, Richards JG. Quantitative enzyme radioautography with ^{3}H-Ro 41-1049 and ^{3}H-Ro 19-6327 in vitro: localization and abundance of MAO-A and MAO-B in rat CNS, peripheral organs, and human brain. J Neurosci 1992;12:1977–99.

Smith QR. The blood–brain barrier and the regulation of amino acid uptake and availability to brain. Adv Exp Med Biol 1991;291:55–71.

Soares-da-Silva P, Garrett MC. A kinetic study of the rate of formation of dopamine, 3,4-dihydroxyphenylacetic acid (DOPAC) and homovanillic acid (HVA) in the brain of the rat:

implications for the origin of DOPAC. Neuropharmacology 1990;29:869–74.

Sokoloff L, Reivich M, Kennedy C, Des Rosiers MH, Patlak CS, Pettigrew KD, Sakurada O, Shinohara M. The [^{14}C]deoxyglucose method for the measurement of local cerebral glucose utilization: theory, procedure, and normal values in the conscious and anesthetized albino rat. J Neurochem 1977;28:897–916.

Thiede HM, Kehr W. Endogenous dopa in rat brain: occurrence, distribution and relationship to changes in catecholamine synthesis. Naunyn-Schmiedeberg's Arch Pharmacol 1981;316:299–303.

Wade LA, Katzman R. 3-*O*-Methyl-DOPA uptake and inhibition of L-DOPA at the blood–brain barrier. Life Sci 1975;17:131–6.

Wahl L, Nahmias C. Modelling of fluorine-18-6-fluoro-L-dopa in humans. J Nucl Med 1996a;37:432–7.

Wahl L, Nahmias C. Quantification of dopamine metabolism in man: a mathematically justifiable approach. Phys Med Biol 1996b;41:963–78.

Westerink BHC, Spaan SJ. Estimation of the turnover of 3-methoxytyramine in the rat striatum by HPLC with electrochemical detection: implications for the sequence in the cerebral metabolism of dopamine. J Neurochem 1982;38:342–7.

Widmann R, Sperk G. Topographical distribution of amines and major amine metabolites in the rat striatum. Brain Res 1986;367:244–9.

Wong DF, Gjedde A, Wagner HN Jr. Quantification of neuroreceptors in the living human brain. I: Irreversible binding of ligands. J Cereb Blood Flow Metab 1986;6:137–46.